

Design, synthesis and bio-evaluation of piperidines and CGRP peptides; Synthesis of substituted 6-(dimethylamino)-2-phenylisoindolin-1-ones for the inhibition of luciferase.

by

Medha Jaimini Gunaratna Anhettigama Gamaralalage

B.S., University of Colombo, 2011

AN ABSTRACT OF A DISSERTATION

submitted in partial fulfillment of the requirements for the degree

DOCTOR OF PHILOSOPHY

Department of Chemistry
College of Arts and Sciences

KANSAS STATE UNIVERSITY
Manhattan, Kansas

2017

Abstract

Three research projects are described in this dissertation, and they are: (i) discovery of piperidine derivatives as T-type calcium channel inhibitors for the treatment of epilepsy and neuropathic pain and as protein disulfide isomerase inhibitors for the treatment of influenza viral infection; (ii) discovery of peptide-based calcitonin gene-related peptide receptor antagonists for the treatment of inflammatory pain; and (iii) synthesis of substituted 6-(dimethylamino)-2-phenylisoindolin-1-ones for the inhibition of luciferase.

T-type calcium channels are important regulators of nervous system, and upregulated T-type calcium channel activities have been found to link to various types of neurological disorders, such as epilepsy and neuropathic pain. To discover novel T-type calcium channel blockers, a series of 1,4-disubstituted piperidine derivatives were designed and synthesized. Among them, compound **1-4** was found to be a good T-type calcium channel inhibitor with an IC_{50} of 1 nM for $Ca_v3.2$ inhibition. It also showed 86% suppression of seizure induced death in mice and good *in vivo* analgesic effects on both thermal and mechanical pain thresholds in Spared Nerve Injury rat models. Therefore **1-4** can potentially be used as a T-type calcium channel blocker in the treatment of epilepsy and neuropathic pain.

Influenza is a respiratory viral infection. Since viruses rely on host cell proteins for their entry, survival and replication, development of drugs targeting host cell proteins has identified as an effective strategy in controlling viral infections. We synthesized a series of 1,4-disubstituted piperidine derivatives for the inhibition of protein disulfide isomerase enzyme and influenza. Among them, **1-29** was found to possess strong anti-influenza activity ($EC_{50} = 2.5 \mu M$). This suggests the potential use of piperidine scaffold in designing anti-influenza drugs in future.

Calcitonin gene related peptide (CGRP) receptor antagonism has been identified as a successful approach for the treatment of inflammatory pain. Therefore, a novel class of peptide antagonists of CGRP receptor was synthesized and screened for their binding affinities to the CGRP receptor and their analgesic effects on inflammatory-induced pain in rats. Among them,

peptide **2-3** showed a higher binding affinity towards the CGRP receptor than previously reported peptide antagonists and exhibited analgesic effects up to 2 h in both A δ and c-fiber pain tests. Therefore **2-3** indicates its potential use as a CGRP receptor antagonist in the treatment of inflammatory pain.

Firefly luciferase is commonly used as a reporter in cells expressing a luciferase gene or its enzymatic activity under the control of a promoter of interest to assess its transcriptional activity. It has been found that some molecules such as molecules with carboxylic acid moiety can directly inhibit luciferase activity in cells. However, it is suggested that carboxylic acid moiety of the compounds may also be associated with side reactions in cells. Therefore, to study whether carboxylic acid moiety causes side effects, we designed two probe molecules, **3-1** and **3-2**. Synthesis of probe molecule **3-2** is discussed. Synthesis of probe molecule **3-1** and further investigation of its luciferase inhibition will therefore be useful to understand the toxicity of carboxylic acid containing drugs in future.

Design, synthesis and bio-evaluation of piperidines and CGRP peptides; Synthesis of substituted 6-(dimethylamino)-2-phenylisoindolin-1-ones for the inhibition of luciferase.

by

Medha Jaimini Gunaratna Anhettigama Gamaralalage

B.S., University of Colombo, 2011

A DISSERTATION

submitted in partial fulfillment of the requirements for the degree

DOCTOR OF PHILOSOPHY

Department of Chemistry
College of Arts and Sciences

KANSAS STATE UNIVERSITY
Manhattan, Kansas

2017

Approved by:

Major Professor
Duy H. Hua

Copyright

© Medha Jaimini Gunaratna Anhettigama Gamaralalage 2017.

Abstract

Three research projects are described in this dissertation, and they are: (i) discovery of piperidine derivatives as T-type calcium channel inhibitors for the treatment of epilepsy and neuropathic pain and as protein disulfide isomerase inhibitors for the treatment of influenza viral infection; (ii) discovery of peptide-based calcitonin gene-related peptide receptor antagonists for the treatment of inflammatory pain; and (iii) synthesis of substituted 6-(dimethylamino)-2-phenylisoindolin-1-ones for the inhibition of luciferase.

T-type calcium channels are important regulators of nervous system, and upregulated T-type calcium channel activities have been found to link to various types of neurological disorders, such as epilepsy and neuropathic pain. To discover novel T-type calcium channel blockers, a series of 1,4-disubstituted piperidine derivatives were designed and synthesized. Among them, compound **1-4** was found to be a good T-type calcium channel inhibitor with an IC_{50} of 1 nM for $Ca_v3.2$ inhibition. It also showed 86% suppression of seizure induced death in mice and good *in vivo* analgesic effects on both thermal and mechanical pain thresholds in Spared Nerve Injury rat models. Therefore **1-4** can potentially be used as a T-type calcium channel blocker in the treatment of epilepsy and neuropathic pain.

Influenza is a respiratory viral infection. Since viruses rely on host cell proteins for their entry, survival and replication, development of drugs targeting host cell proteins has identified as an effective strategy in controlling viral infections. We synthesized a series of 1,4-disubstituted piperidine derivatives for the inhibition of protein disulfide isomerase enzyme and influenza. Among them, **1-29** was found to possess strong anti-influenza activity ($EC_{50} = 2.5 \mu M$). This suggests the potential use of piperidine scaffold in designing anti-influenza drugs in future.

Calcitonin gene related peptide (CGRP) receptor antagonism has been identified as a successful approach for the treatment of inflammatory pain. Therefore, a novel class of peptide antagonists of CGRP receptor was synthesized and screened for their binding affinities to the CGRP receptor and their analgesic effects on inflammatory-induced pain in rats. Among them,

peptide **2-3** showed a higher binding affinity towards the CGRP receptor than previously reported peptide antagonists and exhibited analgesic effects up to 2 h in both A δ and c-fiber pain tests. Therefore **2-3** indicates its potential use as a CGRP receptor antagonist in the treatment of inflammatory pain.

Firefly luciferase is commonly used as a reporter in cells expressing a luciferase gene or its enzymatic activity under the control of a promoter of interest to assess its transcriptional activity. It has been found that some molecules such as molecules with carboxylic acid moiety can directly inhibit luciferase activity in cells. However, it is suggested that carboxylic acid moiety of the compounds may also be associated with side reactions in cells. Therefore, to study whether carboxylic acid moiety causes side effects, we designed two probe molecules, **3-1** and **3-2**. Synthesis of probe molecule **3-2** is discussed. Synthesis of probe molecule **3-1** and further investigation of its luciferase inhibition will therefore be useful to understand the toxicity of carboxylic acid containing drugs in future.

Table of Contents

List of Figures	xi
List of Tables	xiii
List of Schemes	xiv
List of Symbols	xv
List of Abbreviations	xvi
Acknowledgements	xix
Dedication	xxi
Chapter 1 - Design, synthesis and bio-evaluation of novel 1,4-substituted piperidine derivatives	1
1.1 Introduction	1
1.2 Background	3
1.2.1 T-type calcium channels	3
1.2.2 T-type calcium channels in epilepsy	4
1.2.3 T-type calcium channels in neuropathic pain	5
1.2.4 Reported T-type calcium channel blockers	6
1.2.5 Reported piperidine derivatives as T-type Ca ²⁺ channel inhibitors	7
1.2.6 Inhibition of epilepsy and neuropathic pain by reported T-type calcium channel blockers	8
1.2.7 Influenza virus	9
1.2.8 Anti-influenza treatment strategies	10
1.2.9 Protein disulfide isomerase (PDI) – a potential target against influenza	11
1.2.10 Inhibition of PDI activity	13
1.3 Molecular design, synthetic routes and bio-evaluation methods	15
1.3.1 Novel T-type calcium channel blockers	15
1.3.1.1 Molecular design of the novel T-type calcium channel blockers	15
1.3.1.2 Synthetic routes	18
1.3.1.3 Bio-evaluation methods	23
1.3.1.3.1 Preparation of HEK293 cell expressing Cav3.2 channels and DRG neurons ...	23
1.3.1.3.2 Patch clamp recordings	23
1.3.1.3.4 Seizure models	24

1.3.1.3.5 In vivo analgesic effects in spared nerve injury (SNI) pain models	24
1.3.2 Novel PDI inhibitors as anti-influenza agents	25
1.3.2.1 Molecular design of novel PDI inhibitors.....	25
1.3.2.2 Synthetic routes.....	28
1.3.2.3 Bio-evaluation methods	29
1.3.2.3.2 The screening of compounds 1-29 to 1-32 and 1-2 for PDI inhibition.....	29
1.3.2.3.2 The screening of compounds 1-29 to 1-32 and 1-2 for anti-influenza virus activity.....	30
1.4 Results and Discussion	30
1.4.1 Mouse DRG neurons inhibition (%) of T- type calcium ion channel and inhibition of seizure induced death by the synthesized piperidine compounds.....	30
1.4.2 Structure activity relationship of synthesized piperidine compounds	32
1.4.3 PDI inhibition and anti-influenza activity of compounds.....	36
1.4.4 Structure activity relationship of synthesized piperidine compounds	36
1.5 Conclusion	37
1.6 Experimental section.....	38
1.6.1 General experimental procedures.....	38
1.7 References.....	55
Chapter 2 - Design, synthesis and bio-evaluation of novel peptide-based calcitonin gene-related peptide receptor antagonists for the treatment of inflammatory pain.....	61
2.1 Introduction.....	61
2.2 Background.....	61
2.2.1 Calcitonin gene-related peptide (CGRP)	62
2.2.2 The calcitonin gene related peptide receptor	64
2.2.3 The role of CGRP and CGRP receptors in the induction and maintenance of pain	67
2.2.4 Pain inhibition by CGRP antagonists	68
2.2.5 Reported peptide based CGRP receptor antagonists.....	68
2.3 Molecular design, synthetic routes and bio-evaluation methods	69
2.3.1 Molecular design.....	69
2.3.2 Peptide synthesis	72
2.3.3 Bio-evaluation.....	74

2.3.3.1 Binding assay	74
2.3.3.2 Effects of peptide 2-3 and 2-4 on rats' facial pain.....	74
2.4 Results and Discussion	75
2.4.1 Binding affinity results of CGRP peptide fragments and peptide 2-3 on human CGRP receptor membranes	75
2.4.2 Synthesized CGRP peptide effects on rats' facial pain	76
2.4.2.1 A δ thermal pain test	76
2.4.2.2 C-fiber thermal pain test	77
2.5 Conclusion	78
2.6 Experimental section.....	78
2.6.1 General experimental procedures.....	78
2.7 References.....	80
Chapter 3 - Synthesis of substituted 6-(dimethylamino)-2-phenylisoindolin-1-ones for the inhibition of luciferase	84
3.1 Introduction.....	84
3.1.1 Firefly luciferase enzyme.....	85
3.1.2 Inhibitors of firefly luciferase	87
3.1.3 Potential toxicological effects of carboxylic acid moiety	89
3.2 Molecular design and synthetic routes.....	91
3.2.1 Molecular design of substituted 6-(dimethylamino)-2-phenylisoindolin-1-ones	91
3.2.2 Synthetic routes.....	95
3.4 Future work.....	97
3.5 Conclusion	103
3.6 Experimental section.....	103
3.6.1 General experimental procedures.....	103
3.7 References.....	110
Appendix A - Supplemental data.....	113

List of Figures

Figure 1.1 Structures of some of piperidine-based drugs.	2
Figure 1.2 T-type Ca^{2+} channels in the neuropathic pain pathway.	5
Figure 1.3 First generation T-type calcium channel inhibitors.	6
Figure 1.4 Representative examples of T-Type calcium channel blockers TTA-A, TTA-Q and oxadiazole. ²¹	7
Figure 1.5 Reported piperidine derivatives as T-type calcium channel inhibitors.	8
Figure 1.6 a. Domain composition of human PDI ⁶² ; b. Crystal Structure of oxidized human PDI (PDB code: 4EL1).....	12
Figure 1.7 Reported PDI inhibitors.....	13
Figure 1.8 Designed 1,4-substituted piperidine compounds as T-type calcium channel inhibitors.	16
Figure 1.9 Designed 1,4-substituted piperidine compounds as PDI inhibitors.....	26
Figure 1.10 Minimum energy conformations of compounds 1-29 to 1-32 and 1-2 with their calculated PSA (polar surface area) values.....	27
Figure 1.11 Spared Nerve Injury (SNI) rats' left hindpaw withdrawal latencies in response to thermal stimulation (Hargreaves test).	35
Figure 1.12 Mechanical pain threshold assessment (von Frey monofilament test) of SNI rats' left hind paws.	35
Figure 2.1 Schematic diagram of trigeminothalamic pain signaling pathway. ¹²	62
Figure 2.2 Amino acid sequences of human α - CGRP and β - CGRP. ¹⁷	63
Figure 2.3 Proposed functional regions of the primary structure of human α CGRP (CGRP ₁₋₃₇). 64	
Figure 2.4 Representative cartoon structure of CGRP receptor. ²⁹	65
Figure 2.5 The expanded portion shows the crystal structure of the human RAMP1 N-terminus (RAMP1 ₂₇₋₁₀₇). PDB code: 2YX8 ³²	66
Figure 2.6 Role of CGRP in the central sensitization.	67
Figure 2.7 Synthesized CGRP receptor antagonists, 2-1 to 2-5	71
Figure 2.8 A δ thermal pain threshold assessment of rats' depilated left cheeks.	76
Figure 2.9 C-fiber thermal pain threshold assessment of rats' depilated left cheeks.	77

Figure 3.1 Surface view of (a) firefly luciferase (Protein Data Bank accession number 1LCI) without its substrate ¹⁰ (b) firefly luciferase in complex with bromoform (Protein Data Bank accession number 1ba3). ¹²	85
Figure 3.2 Reported firefly luciferase inhibitors.....	87
Figure 3.3 An illustration of how firefly luciferase activity is increased by PTC124 inhibitor. ..	88
Figure 3.4 Glucuronidation and protein conjugation of carboxylic acid containing drugs. ²⁸	90
Figure 3.5 CoA conjugation and protein conjugation of carboxylic acid containing drugs. ²⁸	90
Figure 3.6 Chemical structures of compounds F-53 , 3-1 and 3-2	91
Figure 3.7(a) surface view of conformation #1 of PTC124-AMP complexed with firefly luciferase 3IES structure. (b) zoomed surface view of conformation #1 of PTC124-AMP bound to the active site of firefly luciferase 3IES structure. (c) Chemical structure of PTC124-AMP. (d) overlay of the docking conformation of PTC124-AMP (in purple) and the crystal structure of PTC124-AMP at the active site of firefly luciferase 3IES structure.	93
Figure 3.8 Surface view of docking conformation #1 of compound 3-1-AMP complexed with Firefly luciferase (protein pdb code: 3IES).....	93
Figure 3.9 Close-up structure of docking conformation #1 of compound 3-1-AMP with firefly luciferase (protein pdb code: 3IES) showing hydrogen bond and hydrophobic interactions between 3-1-AMP and the protein. Bonding distances are given in Å.	94
Figure 3.10 Schematic representation of activity-based protein profiling using click chemistry.	98

List of Tables

Table 1.1 Calculated molecular weights and Log P values (lipophilicity) of synthesized piperidine compounds using Molinspiration Predictor.	17
Table 1.2 Calculated Log P values (lipophilicity) of synthesized piperidine compounds using Molinspiration Predictor.	26
Table 1.3 In vitro and in vivo bioactivities of synthesized piperidine derivatives. (NT: not tested)	31
Table 1.4 Comparison of inhibitory activity of compounds 1-1 to 1-4 (changing part A) against T-type calcium channels and seizure induced deaths.	32
Table 1.5 Comparison of inhibitory activity of compounds 1-1 , 1-5 , and 1-6 (changing part B) against T-type calcium channels and seizure induced deaths.	33
Table 1.6 Comparison of inhibitory activity of compounds 1-1 and 1-8 (changing part C) against T-type calcium channels and seizure induced deaths.	34
Table 1.7 PDI inhibition and anti-influenza activity data.	36
Table 2.1 Binding affinity of peptides on hCGRP receptor.	75

List of Schemes

Scheme 1.1 Synthesis of compounds 1-1 to 1-4	19
Scheme 1.2 Mechanism for CDI assisted amide bond formation and silyl deprotection to obtain compound 1-2	20
Scheme 1.3 Synthesis of compound 1-5	21
Scheme 1.4 Synthesis of compounds 1-6 , 1-7 and 1-9 , 1-10	22
Scheme 1.5 Synthesis of compound 1-8	23
Scheme 1.6 Synthesis of compounds 1-29 , 1-30 , 1-31 , 1-32	28
Scheme 2.1 A representative synthesis of CGRP receptor antagonist, 2-3	73
Scheme 2.2 Mechanism of deprotection of Fmoc-protected Rink amide resin.....	73
Scheme 3.1 Luciferase catalyzed reactions (1) in the presence of D-luciferin D-LH ₂ (2) in the presence of long chain fatty acids. ¹³	88
Scheme 3.2 Synthesis of molecule 3-2	97
Scheme 3.3 Schematic representation for 3-1-S-CoA synthesis by firefly luciferase.....	99
Scheme 3.4 Proposed mechanism for the reaction of 3-1-CoA with firefly luciferase.	100
Scheme 3.5 Proposed synthesis of compound 3-1	102

List of Symbols

EC_{50}	half maximal effective concentration
IC_{50}	half maximal inhibitory concentration
δ	delta, chemical shift
$t_{1/2}$	half time

List of Abbreviations

AM	adrenomedullin
AMP	adenosine monophosphate
Aib	aminoisobutyric acid
Arg	arginine
Asn	asparagine
Asp	aspartic acid
ATP	adenosine triphosphate
BF ₃ ·OEt ₂	boron trifluoride diethyl ether complex
Boc ₂ O	di- <i>tert</i> -butyl dicarbonate
CH ₂ Cl ₂	methylene chloride
CGRP	calcitonin gene-related peptide
CLR	calcitonin-like receptor
CoCl ₂ ·6H ₂ O	cobalt (II) chloride hexahydrate
CoA	coenzyme A
DTT	dithiothreitol
DMAP	4-(dimethylamino)pyridine
DMF	<i>N,N</i> -dimethyl formamide
DRG	dorsal root ganglion
EDC	<i>N</i> -(3-dimethylaminopropyl)- <i>N'</i> -ethylcarbodiimide hydrochloride
ESI	electrospray ionization
EtOH	ethanol
Et ₃ N	triethylamine
Gln	glutamine
Glu	glutamic acid
Gly	glycine
HCl	hydrochloric acid
HRMS	high-resolution mass spectrometry
HPLC	high pressure liquid chromatography

HSE	heat shock element
HPC	hydroxypropyl cellulose
H ₂ SO ₄	sulfuric acid
I.N.	intranasal
I.P.	intraperitoneally
K ₂ CO ₃	potassium carbonate
KNO ₃	potassium nitrate
K _i	binding affinity
LDA	lithium diisopropylamide
Leu	leucine
Luc	luciferase
Lys	lysine
MDCK	Madin-Darby canine kidney
MES	maximal electroshock seizure
MeOH	methanol
mRNA	messenger RNA
MS	mass spectrometry
MsCl	methanesulfonyl chloride
NaCl	sodium chloride
NaHCO ₃	sodium bicarbonate
Na ₂ SO ₄	sodium sulfate
NH ₄ Cl	ammonium chloride
NMR	nuclear magnetic resonance
NO ²⁺	nitronium ion
NSAIDs	nonsteroidal anti-inflammatory drugs
pK _a	-log K _a , (K _a : acid dissociation constant)
PDI	protein disulfide isomerase
Phe	phenylalanine
Pro	proline
PDB	protein data bank
PSA	polar surface area

PTZ	pentylenetetrazole
PPi	pyrophosphate
RAMP1	receptor activity modifying protein 1
RCP	receptor component protein
Rf	retention factor
Ser	serine
siRNA	small (or short) interfering RNA
SNI	spared nerve injury
SOCl ₂	thionyl chloride
THF	tetrahydrofuran
TFA	trifluoroacetic acid
Trp	tryptophan
Tyr	tyrosine
Val	valine

Acknowledgements

I would like to express my sincere gratitude to my research advisor Dr. Duy H. Hua for his invaluable guidance, patience and support throughout my research and during my stay at Kansas State University. It's an honor for me to have the opportunity to work in Dr. Hua's research group. I am very grateful to Dr. Hua for accepting me for his research group.

I would like to thank all my committee members, Dr. Jun Li, Dr. Ping Li and Dr. Kun Yan Zhu for their valuable time, suggestions, helps and dedications during my Ph. D. study. I am thankful to Dr. Weiqun (George) Wang for his valuable time to serve as my outside chairperson for the committee.

I also want to thank collaborators, the Xie group from AfaSci Research Laboratory, Dr. Yunjeong Kim and Dr. Kyeong-Ok Chang in the College of Veterinary Medicine, Kansas State University for their dedication in the bio-evaluation work.

My special thanks goes to K-State Chemistry Department for providing me a great opportunity to pursue my PhD degree. I want to thank the department staff, Dr. Leila Maurmann, Dr. Louis Wojcinski, Dr. Tingting Liu, Mr. Tobe Eggers, Mr. Ron Jackson, Mr. Jim Hodgson, Ms. Mary Dooley and Ms. Kimberly Ross and others for their kind help.

Big thanks must be given to Mrs. Sadami Hua and Hua group past and present members, Dr. Allan M. Prior, Dr. Sahani Weerasekara, Dr. Man Zhang, Dr. Jianyu Lu, Dr. Thi Nguyen, Mr. Bo Hao and Mr. Serkan Koldas for their friendship, encouragement and excellent cooperation. I would like to thank Ms. Kaimin Jia in Dr. Li's laboratory at the Chemistry Department, K-State for the help in HRMS analysis of compound CGRP peptides.

My sincere thanks goes to Dr. Amendra Fernando, Dr. Tharanga Wijethunga, Dr. Madumali Kalubowila, Ms. Ravithree Senanayake, Ms. Chamitha Weeramange, Mr. Janaka Gamekkanda and Ms. Dimuthu Weerawardene for their continuous friendship and for everything they have done for me over the last five years. I feel very lucky to have such wonderful friends in my life. I am grateful to all my friends in Manhattan, for their friendship during my stay at Kansas State University.

Finally, I would like to thank my parents, sister, brother other family members and friends in Sri Lanka for their love, support and encouragements.

Dedication

To my beloved parents, Mr. A.G. Gunaratna and Mrs. I.K.S.R. Kalyani.

Chapter 1 - Design, synthesis and bio-evaluation of novel 1,4-substituted piperidine derivatives

1.1 Introduction

Heterocyclic chemistry offers diverse biological activity, due to the heteroatom-containing ring compounds' ability to mimic the structure of natural ligands and to bind reversibly to the target proteins.¹ Among various reported heterocyclic systems, derivatives containing piperidine ring scaffold demonstrate a large variety of pharmacological activities such as antihistaminic, anticholinergic, antipsychotic, anti-estrogenic and anticonvulsant activities.²⁻⁹ Piperidine is a saturated, six-membered amine compound which occurs as either as mono-substituted or multi-substituted derivatives in biologically active compounds.^{9,10} Among them, 1,4-disubstituted piperidine derivatives have attracted increasing interest due to their potent biological activities and ease of synthesis.¹⁰ Diphenylpyraline (an antihistaminic agent), propiverine (an anticholinergic agent), donepezil (a cholinesterase inhibitor), fentanyl (a μ -opioid receptor agonist), and risperidone (an antipsychotic drugs) are few examples for drugs containing 1,4-disubstituted piperidine scaffold.²⁻⁷

Due to the broader scope of potential therapeutic use of 1,4-disubstituted piperidines, this chapter describes my efforts for the design, synthesis, and optimization of novel small molecule 1,4-disubstituted piperidine derivatives and bioevaluation results as T-type calcium channels inhibitors for the treatment of epilepsy, neuropathic pain and as protein disulfide isomerase (PDI) enzyme inhibitors for the treatment against influenza virus.

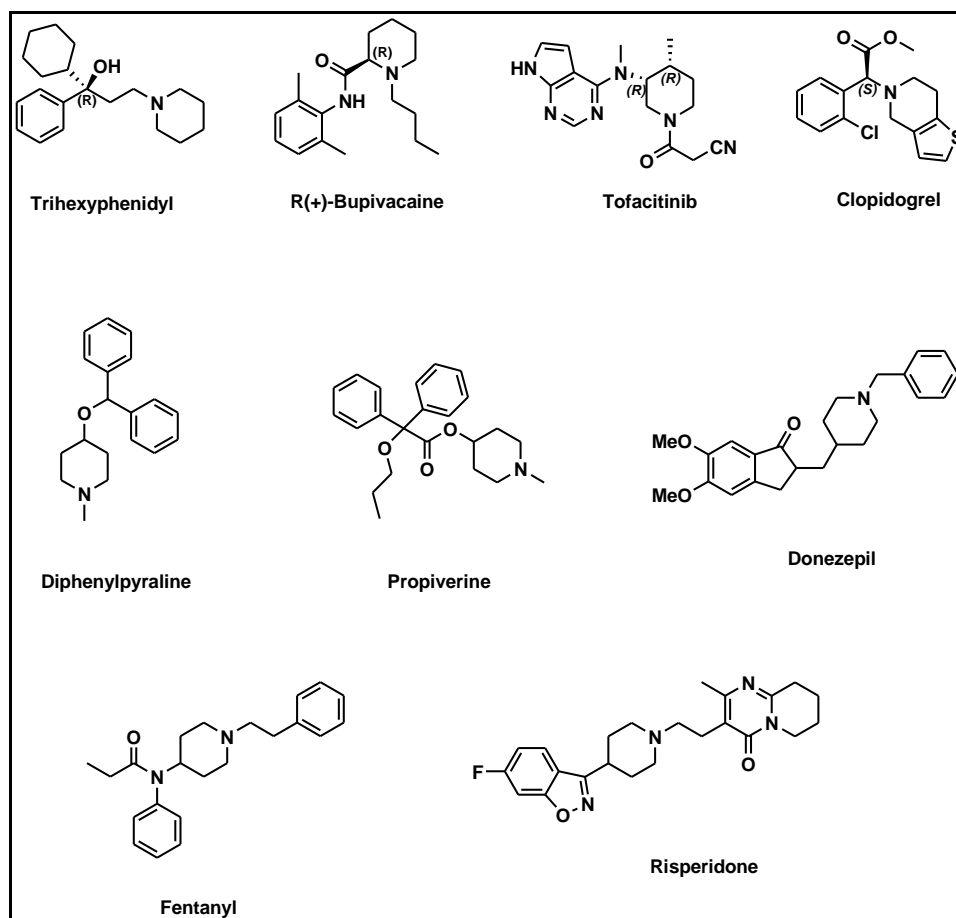


Figure 1.1 Structures of some of piperidine-based drugs.

T-type calcium channels have been identified as important regulators of nervous system, heart, and muscles. Therefore, dysfunction of T-type calcium channels has been found to cause various pathophysiological conditions such as cardiovascular disorders and neurophysiological conditions such as epilepsy, pain and hypertension.¹¹ Epilepsy is a neurological disorder which is occurred by abnormal hyperactivity of neurons.¹² According to the reported data, there are about 50 million people affected by epilepsy and approximately 30% of patients do not get an adequate seizure control with currently available anti-epileptic drugs.¹³ Neuropathic pain is a dysfunction of central and peripheral nervous system, resulted from nerve injury, inflammation, viral infection, diabetes or other factors.¹¹ About 6%–8% of the world's population found to be affected by the neuropathic pain.¹⁴ Despite various drugs available to treat neuropathic pain, they are either lack of effectiveness or are associated with side effects.¹⁵ Therefore, our first effort

was to develop a series of piperidine derivatives as potent T- calcium channel blockers for the treatment of epilepsy and neuropathic pain.

Our second effort was to develop a series of piperidine derivatives as potent anti-influenza drugs targeting host cell protein function. Influenza is a highly contagious viral infection.¹⁶ It is a serious threat to public health and causes significant loss of workforce productivity, high number of hospitalizations, and deaths annually. The US Centers for Disease Control and Prevention (CDC) estimates that seasonal influenza virus is responsible for a number between 140,000 - 710,000 hospitalizations and a number between 12,000 - 56,000 deaths annually since 2010.¹⁷ Currently, there are two strategies to fight against influenza infections.¹⁸ They are designed either to target at viral proteins or host cellular proteins.¹⁸ Though, there are numerous vaccinations and antiviral drug treatments are available against influenza infections, development of strains' resistance to current anti-influenza drugs has become a major problem.¹⁸ Thus, there is an urgent need of discovering more effective drugs against influenza virus infection, which are importantly less prone to resistance.

1.2 Background

1.2.1 T-type calcium channels

Intracellular calcium concentrations play vital roles in important biological processes such as signal transduction pathways, neuronal functions, muscular contraction, hormone secretion, gene expression, cell growth and division.¹⁹⁻²¹ Control of calcium entry into cells through the cell membrane is partly regulated by a family of transmembrane proteins called voltage-gated calcium channels.^{20,21} Voltage-gated calcium channels modulate the entry of extracellular calcium ions into cells in response to the changes in electrical potential difference across the cell membrane.^{19,21} Depending on the membrane potential required for activation, voltage gated calcium channels are divided into two types.^{19,22} They are called low voltage-activated channels (T-type) and high voltage-activated channels (L-, N-, P/Q-, and R-types).^{19,22} Low-voltage activated channels are activated by much smaller membrane depolarization potentials (from about -40 mV to -50 mV) and have a fast voltage-dependent inactivation.^{19,20} Therefore, they produce transient currents.^{19,20} The high-voltage activated channels are activated

by much positive membrane depolarization potentials (from about -35 mV to +15 mV).²³ Voltage gated calcium channels are divided into three main channel families called Ca_v1 (L-type), Ca_v2 (P/Q, N, and R-types) and Ca_v3 (T-type). Based on the sequence of their membrane pore-forming $\alpha1$ subunit, each channel family is further classified into subtypes such as $\text{Ca}_v1.1$ - $\text{Ca}_v1.4$, $\text{Ca}_v2.1$ - $\text{Ca}_v2.3$, $\text{Ca}_v3.1$ - $\text{Ca}_v3.3$.¹⁹ L-type calcium channels are mainly distributed in skeletal, cardiac, smooth muscle and endocrine cells and P/Q-, N- and R- type channels are expressed in neuronal presynaptic terminals.²³ T type calcium channel $\text{Ca}_v3.1$ is mainly expressed in the brain, peripheral nervous tissues (dorsal root ganglia and autonomic ganglia) and peripheral tissues such as heart, smooth muscle, bone and endocrine cells.²⁴ $\text{Ca}_v3.2$ can be found in central nervous system (thalamus, cerebellum, and other parts of the brain) and peripheral tissues such as heart, liver, kidney, endocrine cells, skeletal muscle and smooth muscle and $\text{Ca}_v3.3$ is mainly expressed in the brain and peripheral nerve tissues such as dorsal root ganglia and autonomic ganglia.^{19,24}

Due to their widespread distribution throughout the body, T-type calcium channels are involved in many biological processes.^{13,20,21} In the central nervous system, they are involved in controlling neuron excitability and burst firing.²⁰ In the cardiovascular system, they are involved in cardiac pace making, blood pressure regulation and vascular smooth muscle contraction regulation.^{25,26} Therefore, dysregulation of these processes have been proposed to link to various types of neurological disorders, including hypertension, absence seizures, neuropathic pain and cardiovascular diseases such as angina pectoris, atrial fibrillation and heart failure.^{13,20}

1.2.2 T-type calcium channels in epilepsy

Epilepsy can be divided into two categories such as genetic and structural/metabolic epilepsy.^{12,13} The structural/metabolic epilepsy is caused by various factors such as head trauma, stroke, infectious diseases (such as meningitis), tremor (Parkinson's disease), hypoxia, and metabolic disorders.¹³ The genetic epilepsy is caused by mutations in function and expression of human CACNA1G ($\text{Ca}_v3.1$) and CACNA1H ($\text{Ca}_v3.2$) genes.^{12,13,27} Patients with epilepsy experience absence seizures or blank out which are characterized by sudden, brief lapse of consciousness with 3–6 Hz spike-and-wave discharges (SWDs) on an

electroencephalogram.^{12,13,20,27} Although the molecular mechanisms underlying the development of epilepsy are poorly understood, voltage gated ion channels are likely to have a crucial role in the seizure generation and propagation.²⁸ Rat models of absence seizures have shown increased T-type calcium currents in thalamic neurons.^{11,28,29} It is suggested that T-type channels in the thalamus and cortex generate low-threshold spike, leading to both burst firing and oscillatory behaviors.^{11,28,29} However, it is not known how burst firing and oscillatory behaviors cause seizures.^{12,28}

1.2.3 T-type calcium channels in neuropathic pain

It has been found that T-type calcium channels are up-regulated in sensory neurons in rat models of neuropathic pain.³⁰ Further, antisense knock-down of Cav3.2 T-type channel in mice models also have shown hyposensitivity to thermal, mechanical and chemical pain.³¹ In addition, antisense knockdown of Cav3.2 have shown attenuated response to chronic mechanical hyperalgesia.³²

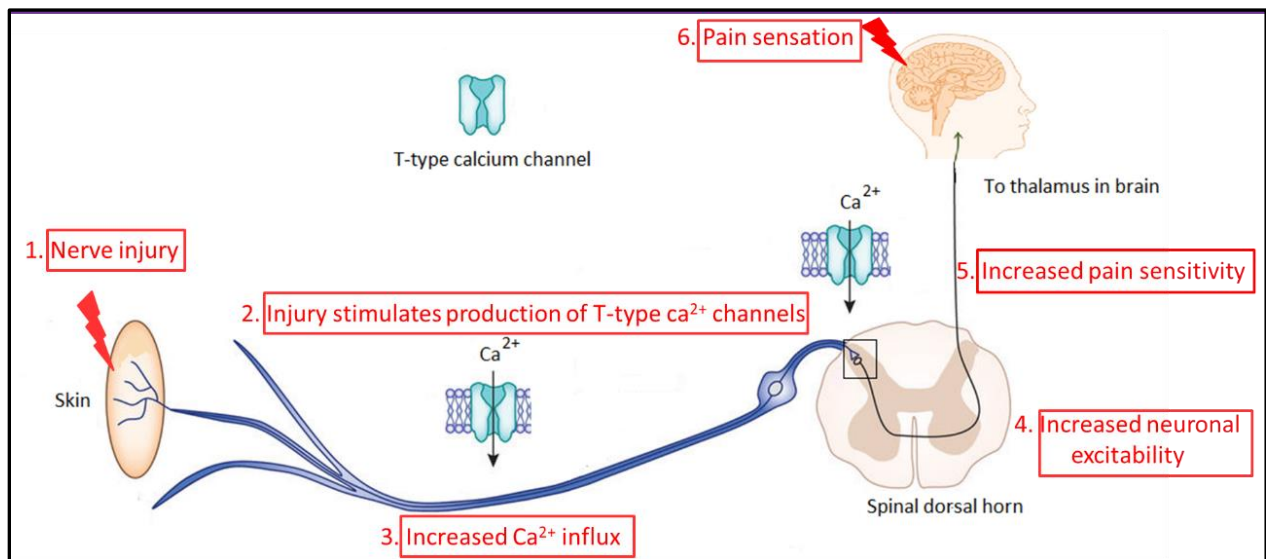


Figure 1.2 T-type Ca^{2+} channels in the neuropathic pain pathway.

1.2.4 Reported T-type calcium channel blockers

There are several structurally different T-type calcium channel blockers have been reported in last 20 years. The first generation of T-type calcium channel blockers was discovered based on drugs that were already developed for other therapeutic purposes.^{21,22} Antiepileptic drugs such as zonisamide and ethosuximide ($IC_{50} = >5 \mu M$ (evaluated using a high-throughput cell-based calcium flux assay, FLIPR=Fluorescence Imaging Plate Reader)), antihypertensive agents such as mibefradil ($IC_{50} = 0.89 \mu M$) and efonidipine ($IC_{50} = 0.43 \mu M$), a neuroleptic agent, flunarizine ($IC_{50} = 5 \mu M$) and an antipsychotic agent, pimozide ($IC_{50} = 0.5 \mu M$) are some of them that were found to inhibit T-type channel at therapeutic concentrations.^{21,22,33,34} Zonisamide, has shown anticonvulsant effective against maximal electroshock (MES) seizures in mice with a mean percentage of reduction of $59.5 \pm 7.2\%$ at $500 \mu M$.³⁵ However, these first-generation T-type channel blockers were found to be less potent and selective since they were originally designed for other targets. Moreover, mibefradil was withdrawn from the market due to its potent inhibitory activity at CYP3A4 and CYP2D6 enzymes.²¹ And, flunarizine and pimozide were also found to be potent against biogenic amine targets.²²

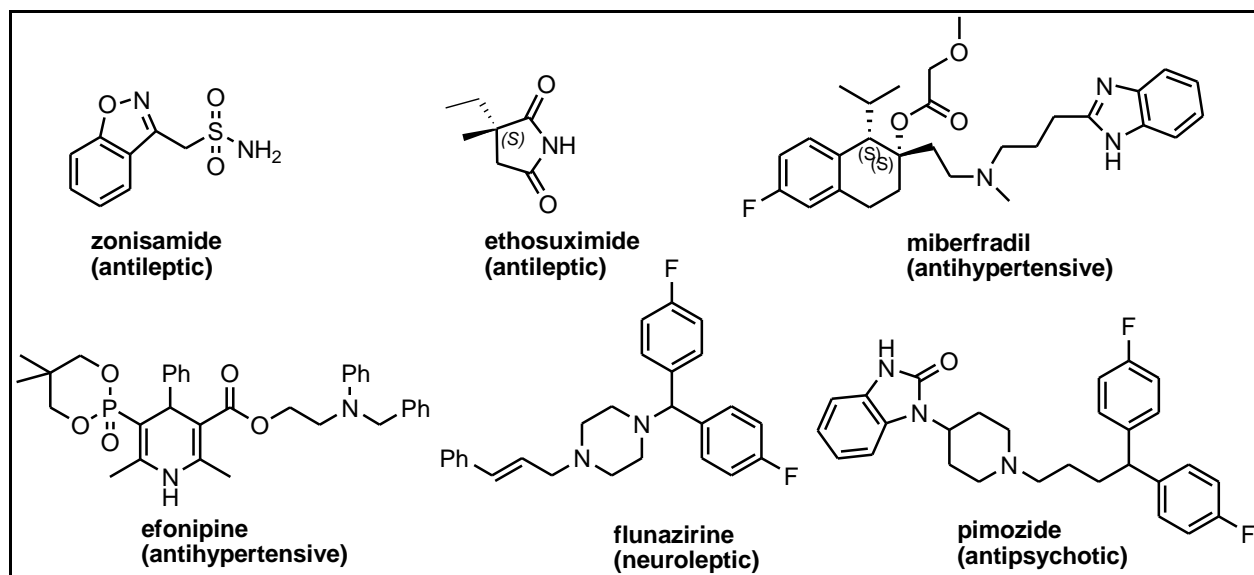


Figure 1.3 First generation T-type calcium channel inhibitors.

Therefore, later, T-type channel blockers were discovered by either rational design or unbiased library screening.²¹ In 2004, Merck reported a series of 4,4-disubstituted quinazoline-2-one compounds (TTA-Q) with good *in vitro* potencies and *in vivo* efficacies against the T-type calcium channel.^{19,21} However, they were also unsuccessful due to drug-drug interactions.²¹ Later, Merck introduced another series of potent T-type calcium channel inhibitors with pyridyl and phenylacetamide moieties called TTA-A.^{19,21} Pfizer reported another series of T-type calcium channel blockers using oxadiazole pharmacophore to treat pain, hypertension, congestive heart failure, stroke, ischemic heart disease and angina pectoris.²¹

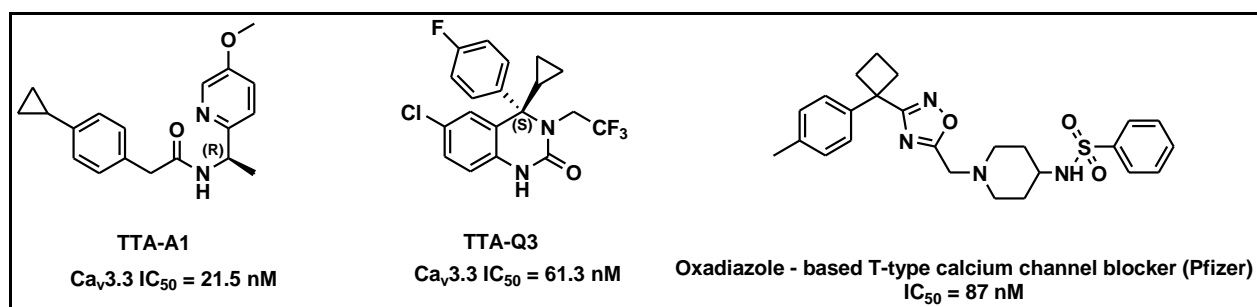


Figure 1.4 Representative examples of T-Type calcium channel blockers TTA-A, TTA-Q and oxadiazole.²¹

1.2.5 Reported piperidine derivatives as T-type Ca²⁺ channel inhibitors

Merck has reported another series of T-type calcium channel blockers with 1,4 substituted piperidine scaffold called TTA-P.^{19,21} Among them, compounds TTA-P1 (IC₅₀ = 32 nM (FLIPR)) and TTA-P2 (IC₅₀ = 180 nM (FLIPR)) have shown greater potency at T-type calcium channels over other ion channels.²¹ They attached fluorine into the piperidine ring of TTA-P1 and TTA-P2 to reduce the basicity of the ring nitrogen atom and enhance the metabolic stability. Recently, Zalicus Inc. reported Z944, which is a *N*-piperidinyl acetamide derivative with potent T-type calcium channel inhibitory activity (IC₅₀ = 61 nM (FLIPR)).

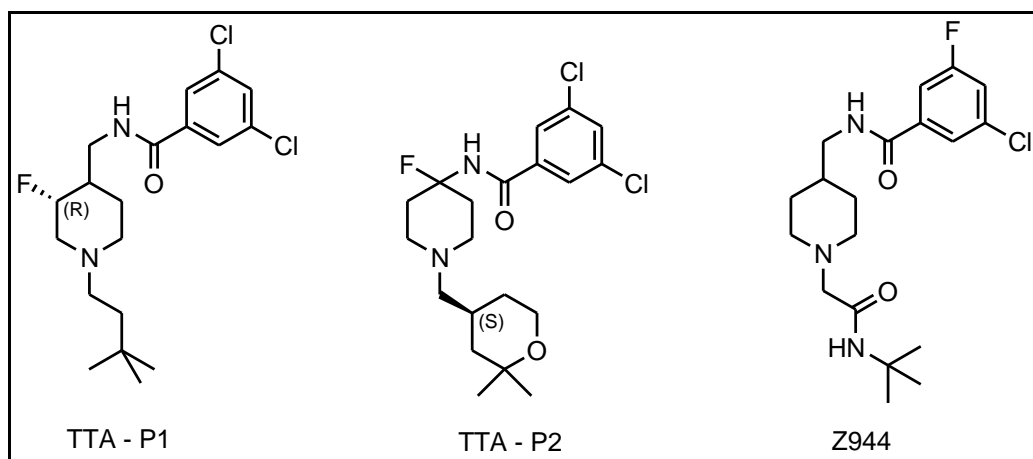


Figure 1.5 Reported piperidine derivatives as T-type calcium channel inhibitors.

1.2.6 Inhibition of epilepsy and neuropathic pain by reported T-type calcium channel blockers

Zonisamide is an antiepileptic drug which is found to have its antiepileptic activity through T-type calcium channel inhibition.³⁶ It has been found that zonisamide shifts T-type calcium channel population toward the inactivation state, allowing fewer channels to open during membrane depolarization.³⁷ This increases the threshold for the generation of an action potential and stabilizes neuronal membranes, thereby suppress the progression of seizures.^{13,36} Another antiepileptic drug, Valproic acid has also been shown to block T-type calcium currents via same mechanism in rat models of absence epilepsy.^{11,13} Piperidine based T-type calcium channel blockers Z944, TTA-P1 and TTA-P2 are also found to suppress seizures in the rat models of absence epilepsy.^{11,28} Antihypertensive drug and a T-type calcium channel blocker, Mibefradil has shown suppressed absence seizures and reduced mechanical and thermal hyperalgesia in the neuropathic pain corresponding rat models.^{13,38} Another study has shown that TTA-A2 inhibits presynaptic T-type Ca^{2+} channels in the dorsal horn in rats with diabetic neuropathy, thereby suppressed excitatory synaptic transmission.³⁹

Although there are some T-type calcium channel inhibitors used for the treatment of seizure and neuropathic pain, there is no potent and truly selective T-type calcium channel

blocker available for clinical use until now. Therefore, there is a high demand for the development of novel, potent T-type channel specific inhibitors.

1.2.7 Influenza virus

Influenza viruses are enveloped, segmented, single-stranded, negative-sense RNA genome, which belong to the family *Orthomyxoviridae*.^{40,41} Influenza virus particles are enclosed by a lipid bilayer envelope, which is derived from the host cellular membrane. This virus envelope is decorated with three surface glycoproteins called hemagglutinin (HA) and neuraminidase (NA) and the M2 ion channel protein.^{18,41,42} Center of the influenza virus contains RNA genomic segments, each of which is associated with the trimeric viral RNA polymerase (PB1, PB2, PA) and coated with multiple nucleoproteins (NPs) to form the viral ribonucleoproteins (vRNPs).⁴³ There are four genera have been identified in the family *Orthomyxoviridae*, known as influenza virus A, influenza virus B, and influenza virus C.⁴⁰⁻⁴² The three virus types differ in host range and pathogenicity.⁴⁴ Influenza A viruses can infect humans, birds, swine, horses and other mammals.^{42,45} Influenza B viruses have been isolated only from humans and seals, and influenza C viruses have been isolated from humans, dogs and swine.^{42,46,47} Influenza A and B viruses contain eight single-stranded, negative-sense RNA segments that encode at least ten polypeptides, of which eight are structural viral proteins, and two are found in infected cells.

The life cycle of influenza virus can be divided into the following steps: 1. attachment of the virus to the host cell; 2. entry into the host cell by endocytosis; 3. pH-dependent fusion of viral and endosomal membranes; 4. uncoating and release of viral contents to the cytoplasm; 5. entry of vRNPs into the nucleus; 6. transcription of viral mRNA; 7. export of the viral mRNA from the nucleus; 8. post-translational processing and trafficking toward the cell membrane; 9. assembly and budding; and 11.release from the host cell membrane. Viral infection is initiated when the viral surface glycoprotein HA binds to sialylated glycoprotein receptors on the host cell-surface.^{43,48} The virus enters the host cell via endocytosis.⁴⁸ Then the virus is fused with an endosome using a conformational change in the HA protein caused by low endosomal pH.^{43,48,49}

Further, the low endosomal pH results influx of protons from endosome to the virus through M2 ion channel protein, which disrupt the interaction between vRNP proteins and M1 proteins.^{48,49} The vRNPs are then released into the cytoplasm and are transported into the nucleus.^{48,49} Viral mRNA are synthesized in the nucleus with use of viral RNA polymerases.^{48,49} Newly synthesized viral mRNAs are then transported to the cytoplasm for translation into viral proteins.^{48,49} After being translated, viral proteins are transported to the endoplasmic reticulum (ER) for processing.^{48,49} Then, the proteins are transported to the Golgi apparatus for further modifications such as glycosylation of HA and NA, palmitoylation of HA and M2 and phosphorylation of NS1.⁴⁸ Viral proteins are then transported to the cell membrane.^{48,49} Then the viral proteins are assembled and enclosed by the cell membrane to form a enveloped viral bud.^{48,49} Finally, the terminal sialic acid residues are removed from virus cell surface by the neuraminidase activity of the NA protein, thereby releasing the virus from the host cell.^{48,49}

1.2.8 Anti-influenza treatment strategies

There are two main strategies used in the anti-influenza treatment depending on the stage of infection. Influenza vaccines are designed to induce a protective immune response in the body against the viruses represented in the vaccine, thereby prevent or mitigate infections.⁵⁰ More importantly, vaccination also leads to the induction of a specific immunological memory against the viruses represented in the vaccine, which readily fight against the infection even exposure to the virus at a later stage.⁵⁰ However, vaccine development is a long, complex process which usually requires at least six months to develop a vaccine against a viral infection.¹⁸ The second strategy used in the anti-influenza treatment is the use of anti-influenza drugs. Anti-influenza drugs target either essential viral structures or host factors that are involved in the virus life cycle.¹⁸ There are several classes of anti-influenza drugs targeting functionally conserved domains of viral proteins, which play critical roles during the viral replication cycle. They are matrix protein 2 (M2) ion channel blockers such as amantadine, neuraminidase (NA) inhibitors such as zanamivir and oseltamivir, and influenza viral RNA-dependent RNA polymerase inhibitors such as flutamide.^{18,51} But the continued emergence of resistance to current anti-influenza drugs lowers their effectiveness against influenza. Therefore, development of anti-influenza drugs with new mechanisms of action are highly required.

1.2.9 Protein disulfide isomerase (PDI) – a potential target against influenza

Viruses often rely on host cell components and proteins for entry, survival and replication. Among them, protein disulfide isomerase (PDI) has found to play important roles in the virus replication such as facilitating virus attachment, internalization, ER mediated viral protein folding.⁵² Angelo Gallina and coworkers proposed that cell surface PDI associates with the cell surface HIV receptor called CD4 and through PDI·CD4 association at the cell surface facilitates the virus to reach and reduce disulfide bonds in the viral envelope glycoprotein, gp120 that binds to CD4.⁵³ This results conformational changes in the gp120 which is proposed to cause virus-cell fusion and internalization.⁵³ Proper folding of newly synthesized viral proteins into their native three-dimensional structures is crucial for virus replication. Chaperone proteins within the ER are found to assist in folding polypeptide chains into their three-dimensional structures.⁵⁴ Further, polypeptide chains undergo modifications such as disulfide bridge formation before exported to the plasma membrane through the Golgi apparatus.⁵⁵

Protein disulfide isomerase (PDI) is an enzyme which belongs to the family of oxidoreductases.^{52,56,57} PDI has the ability of catalyzing the formation, isomerization, and reduction of disulfide bonds. It has been found that PDI exhibits a redox-dependent chaperone activity (inhibits the aggregation of unfolded proteins) at high concentrations, but anti-chaperone activity at low concentrations.^{52,56,58} PDI is mainly expressed in the endoplasmic reticulum of eukaryotic cells but also found in the nucleus, cytosol, endosomes, cell surface, and extracellularly as well.^{52,59,60}

PDI contains two catalytically active domains called a and a' which show sequence and structural homology to thioredoxin (Trx).^{52,59} They both contain the active thioredoxin motif (WCGHCK) which provides catalytic sites to catalyze the reduction and isomerization of disulfide bonds and the oxidation of thiols.^{52,59} PDI also contains two redox-inactive thioredoxin structural domains called b and b' domains, which do not have cysteines in the active site.^{52,59,61} The crystal structure of yeast PDI demonstrates that these four domains are attached in an U-shaped structure.^{57,62} The catalytically active domains are found to located at the top of the U facing each other, and the two noncatalytic domains are localized to the inside surface of the U-

shape structure.^{57,62} PDI has another region called “c region” and a KDEL sequence at the carboxyl-terminus for ER-localization.^{61,63}

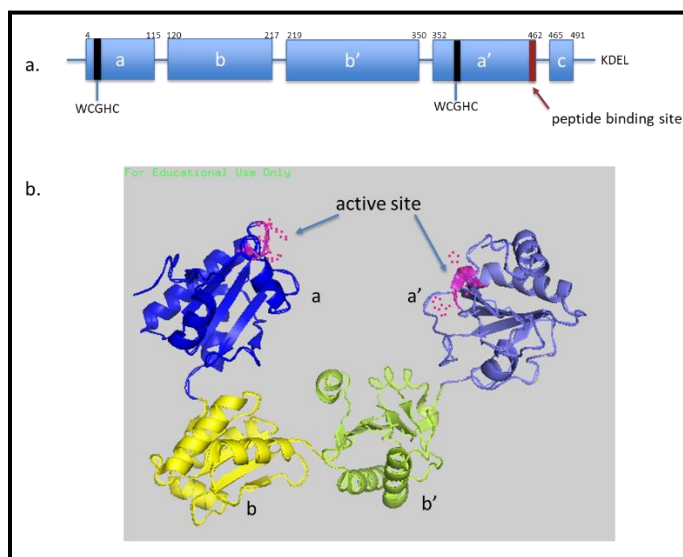


Figure 1.6 a. Domain composition of human PDI⁶³; b. Crystal Structure of oxidized human PDI (PDB code: 4EL1).

In the endoplasmic reticulum PDI catalyzes both the oxidation and isomerization of disulfides on nascent polypeptides due to its oxidizing environment.⁶³ The redox activity of the PDI enzymes is governed by the CGHC active site and the glycine and histidine amino acid residues which lying in between the two cysteine residues are found to be important in maintaining its redox potential.⁶¹ During oxidation, the active site disulfide of PDI is transferred to the dithiol substrate proteins, thereby the active site itself becomes reduced.⁶¹ Under the reducing condition of the cytoplasm, endosomes and plasma membrane of several cell types such as platelets, PDI catalyzes the reduction of protein disulfides.⁶³ During reduction, PDI with a cysteinyl dithiol motif reduces the substrate disulfides, thereby resulting active site in the oxidized state.⁶¹ In addition to peptides and proteins, PDI also binds the hormones.⁶⁴ Todd and coworkers have revealed that there are two different hormone binding sites of PDI which are distinct from the peptide/protein binding sites.⁶⁴ Therefore, they suggested the hormone binding capacity of PDI as a discrete function of PDI which is not coupled to its catalytic activity in disulfide isomerization.⁶⁴ Chaperone activity of PDI was found to promote proper folding even in substrate proteins that do not contain any disulfide bonds.⁶⁵ With use of NMR and x-ray

crystallography, b' domain has been identified as the chaperone domain.⁵⁹ Though the -CGHC- active site is found to be necessary for PDI isomerase activity, chaperone activity of PDI was found to be independent from the active site.⁶⁶

1.2.10 Inhibition of PDI activity

Since PDI is multifunctional protein, which expresses ubiquitously throughout the body, it is difficult to target a specific function of the enzyme. However, a recent study has shown inhibited PDI isomerase activity by alkylation of the redox active site cysteine residues, with no effect on the chaperone activity.⁶⁶ Later, Yong Dai and Chih-chen Wang have shown inhibited PDI chaperone activity by truncation of the C-terminal amino acid residues.⁶⁷ It is assumed that, a peptide binding site located at the interface of the a' and c domains is essential to its chaperone activity.⁶⁷ Further experimental data suggest that this peptide binding site is located between residues 452-461 in the a' domain of PDI.^{63,68} Various agents such as antibiotics, estrogenic steroids, natural and synthetic compounds have been used as PDI inhibitors.

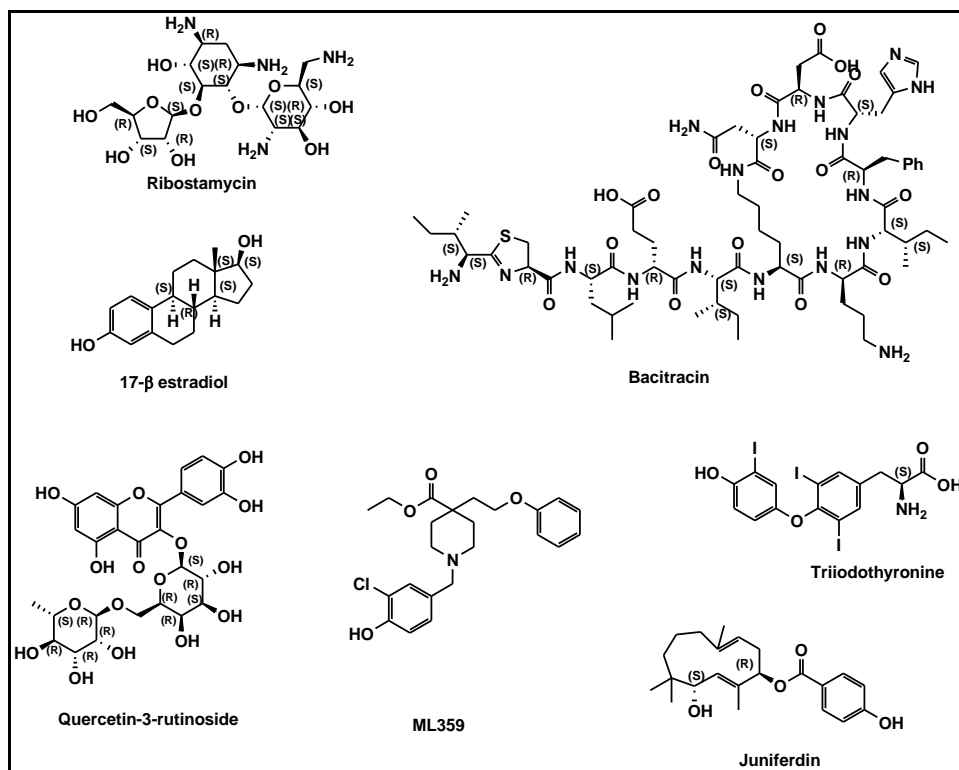


Figure 1.7 Reported PDI inhibitors.

The first reported inhibitor of the chaperone activity of PDI is ribostamycin, which has a binding affinity (K_d) of 319 μ M to bovine protein disulfide isomerase (PDI).⁶⁹ Since, ribostamycin inhibits only the chaperone activity of bovine PDI (not its isomerase activity), it is suggested that ribostamycin binds to region distinct from the CGHC motif of PDI.⁶⁹

Thyroid hormone, which is also known as triiodothyronine (T3) has shown inhibition of the isomerase activity of PDI.⁶⁴ Binding affinity studies of T3 with PDI have further revealed that there are two hormone binding sites ($K_d = 21$ nM and 100 μ M) on PDI.⁷⁰ An estrogenic steroid, 17 β -estradiol have shown 40-60% suppression of reductase activity of PDI at 1 μ M without affecting its oxidase or isomerase activity.⁷¹ But neither T3 nor estradiol found to inhibit the chaperone activity of PDI.⁶⁴ In addition, a cyclic polypeptide peptide like antibiotic, bacitracin has been reported to inhibit the reductive activity of PDI, but no significant effect on the oxidative, isomerization or the chaperone activity of PDI.^{72,73} But bacitracin's clinical use is limited by its non-specificity, nephrotoxicity, and poor membrane permeability.^{72,74,75} Dickerhof and coworkers have proposed that bacitracin binds to the hydrophobic surface of the substrate-binding region of PDI, allowing subsequent disulfide bond formation between an open thiol form of the bacitracin thiazoline ring and the free cysteines Cys314 and Cys345 cysteines in the substrate-binding domain, thereby blocking the binding of the natural substrate insulin and its reduction.⁷⁶ Since bacitracin acts on free cysteines, it is a non-specific inhibitor of proteins containing free thiols.

A flavanol, quercetin-3-rutinoside was reported to inhibit PDI with an IC_{50} of 6.1 μ M and a K_d of 2.8 μ M.⁷⁷ Further studies have shown that quercetin-3-rutinoside acts as an inhibitor of PDI reductase activity *in vitro* and blocks thrombus formation *in vivo* by inhibiting PDI.⁷⁷ A natural sesquiterpene ester, juniferdin and has been identified as a potent inhibitor of PDI-catalyzed reductase activity with IC_{50} of 0.16 μ M.⁷⁸ However, juniferdin was found to be cytotoxic in a cell based assay.⁷⁸ Further SAR studies have revealed that the juniferdin derivative with a sesquiterpene ring 9,10-monoepoxide has a similar potency with reduced cytotoxicity.⁷⁸

A piperidine based small molecule, ML359 has been identified as PDI inhibitor that selectively blocks reductase activity of PDI.^{79,80} It has shown inhibitory activity against the reductase activity of PDI in the insulin turbidometric assay with an IC₅₀ of 0.3-0.6 μ M with no inhibition against reductase activity of other thiol isomerases such as ERp5, ERp57, ERP72, thioredoxin and thioredoxin.⁷⁹ Further it has been found that the inhibition of PDI by the ML359 was reversible and has no cytotoxicity in a cell based (HeLa) cell assay.⁷⁹

To date, no PDI inhibitor for anti-influenza has been reported. Recently, our collaborator Dr. Yunjeong Kim in College of Veterinary Medicine, Kansas State University has found that PDIs are involved in the replication of influenza A and B virus (unpublished data). Using a siRNA knockdown assay, they have demonstrated that siRNAs for PDI significantly reduced the replication of influenza A and B viruses in cells. Therefore, small molecule PDI inhibitors are expected interfere with the replication of influenza and thereby to reduce disease progression and influenza virus transmission.

1.3 Molecular design, synthetic routes and bio-evaluation methods

1.3.1 Novel T-type calcium channel blockers

1.3.1.1 Molecular design of the novel T-type calcium channel blockers

Reported data show that T-type channel blockers with a piperidine scaffold have good potencies with minimal effects on L-type Ca²⁺, K⁺ and human ether-a-go-go related gene (hERG) channels and other off-targets.⁸¹ hERG is a gene that codes a protein known as K_v11.1, the α subunit of a potassium ion channel in the heart that coordinates the beating of the heart. Therefore, inhibition of hERG channel is detrimental. We chose a piperidine based reported T-type calcium channel modulator, Z944 and optimized its structure to synthesize a series of 1,4-substituted piperidine molecules using a structure-activity relationship (SAR) approach. We designed a series of molecules by changing substituents independently in three regions (A, B, or

C) of the 1,4- substituted piperidine core (Figure 1.3) with their corresponding bioisosteres. Modification in part A focused on the substitution of different aromatic ring equivalents while modifications in part B were focused on replacement of hydrogen with methyl or hydroxymethyl groups. Modification in part C focused on replacement of benzoic amide with a tertiary butyl amide. These structural modifications were expected to change the lipophilicity, rigidity, planarity, steric hindrance, and other factors of each molecule, which may improve their potency and selectivity.

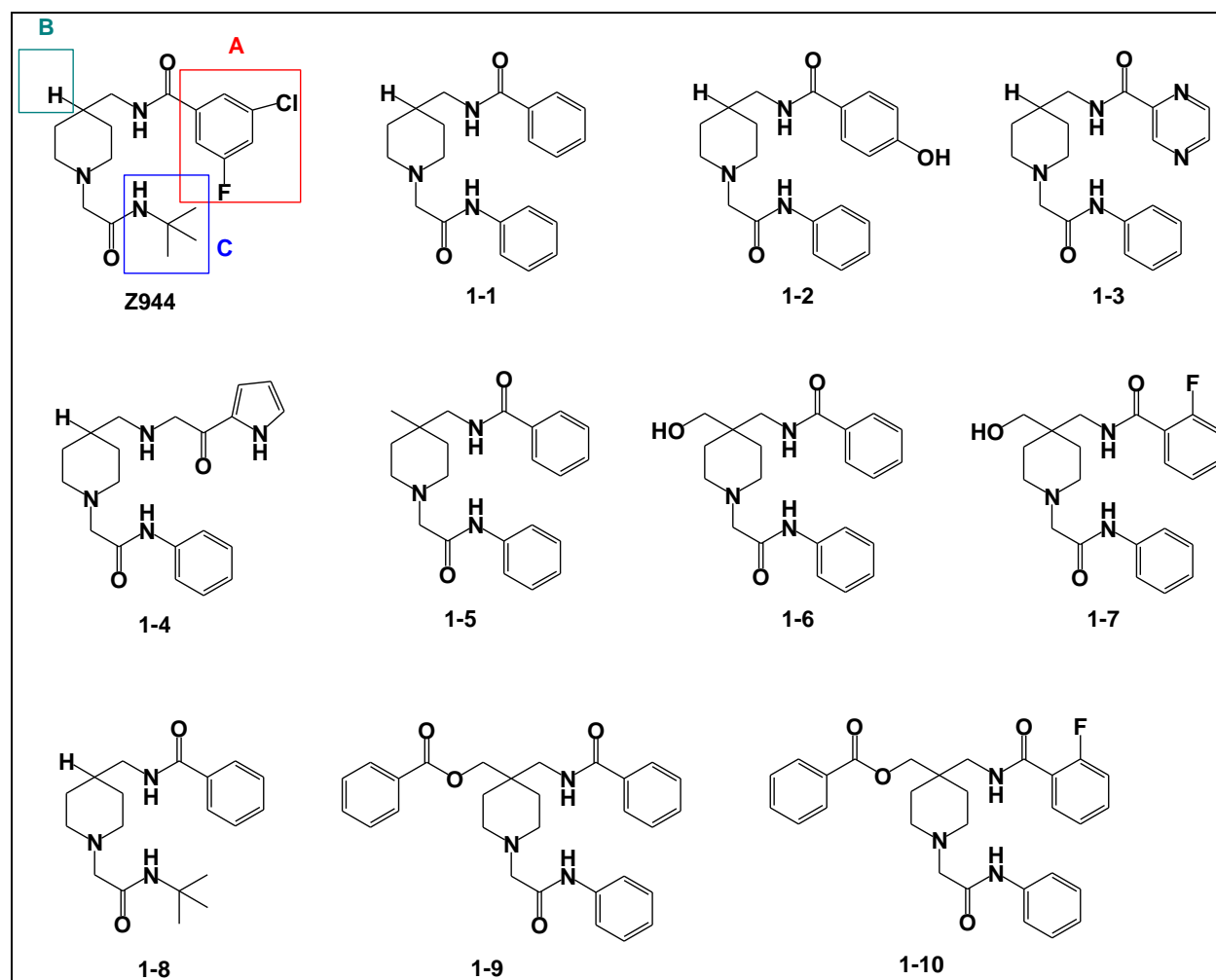


Figure 1.8 Designed 1,4-substituted piperidine compounds as T-type calcium channel inhibitors.

The above novel T-type calcium channel inhibitors were designed following Lipinski's rule of five. According to the Lipinski's rule of five, drug candidates have poor absorption or

permeability when their Log P is greater 5; molecular mass is greater than 500; the number of hydrogen bond donors (OH and NH) is greater than 5; and the number of hydrogen bond acceptors (O and N atoms) is greater than 10. For a drug candidate, lipophilicity is an important factor, as it influences ligand–target binding interactions, solubility, absorption, distribution, metabolism, elimination and toxicity properties.^{82,83} Lipophilicity of a molecule can be expressed in a Log P value, which is defined as partition coefficient of a molecule between octanol (lipophilic phase) and water (hydrophilic phase).⁸² Calculated molecular weights and Log P values (lipophilicity) of synthesized piperidine compounds using Molinspiration Predictor are listed in **Table 1.1**.

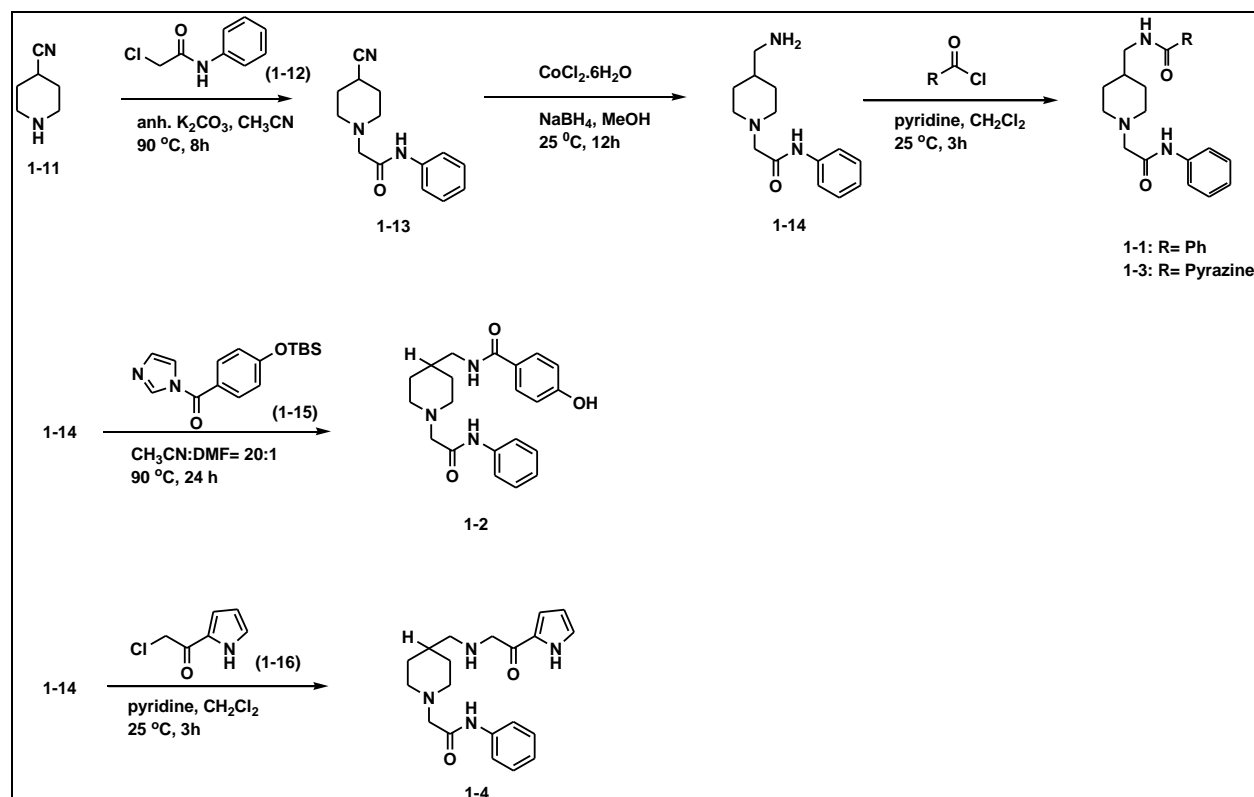
Table 1.1 Calculated molecular weights and Log P values (lipophilicity) of synthesized piperidine compounds using Molinspiration Predictor.

Code name	Molecular Weight	log P value
1-1	351.45	3.10
1-2	367.45	2.63
1-3	353.43	1.64
1-4	354.45	2.02
1-5	365.48	3.35
1-6	381.48	2.17
1-7	331.46	2.73
1-8	399.47	2.29
1-9	485.58	4.60
1-10	503.57	4.72

Designed compounds **1-1** to **1-9** obeyed “Lipinski’s rule of five”. Compound **1-10** was also satisfied four criteria out of five (except the molecular weight). Therefore, designed compounds were expected to have good “drug-like” properties.

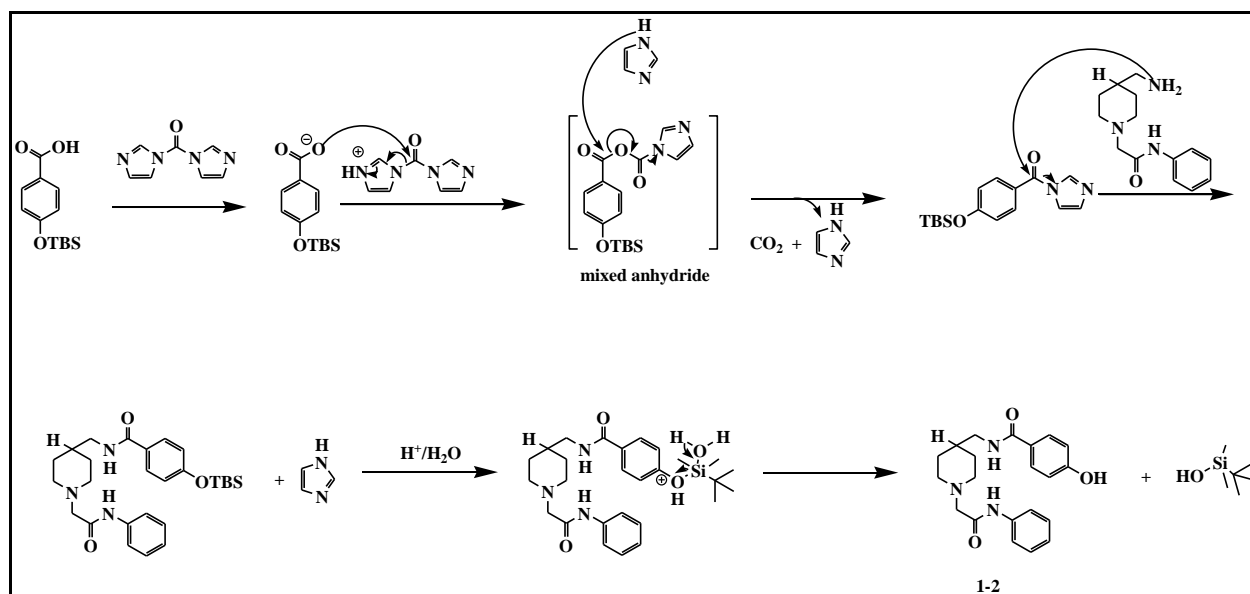
1.3.1.2 Synthetic routes

The synthetic work was collaborated with Dr. Thi Nguyen, Dr. Sahani Weerasekara, and Dr. Man Zhang in Prof. Duy Hua's laboratory. The synthetic routes of compounds **1-1**, **1-2**, **1-3**, **1-4**, **1-5**, **1-6**, **1-7**, **1-8**, **1-9** and **1-10** are shown in **Scheme 1.1** - **Scheme 1.5**. Chemistry for synthesis of these molecules was straightforward. In the synthesis of **1-1** and **1-3**, the *N*-alkylation of piperidine ring was done by *N*-phenylaminocarbonylmethyl group. Treatment of 4-cyano piperidine with *N*-phenyl-2-chloroacetamide under basic conditions yielded compound **1-13**. Then the cyanide reduction of compound **1-13** using cobalt(II) chloride hexahydrate/sodium borohydride yielded the corresponding amine compound **1-14**. Benzoic acid and pyrazinoic acid were activated to their corresponding acid chlorides (benzoyl chloride and pyrazinoyl chloride respectively) and subsequently reacted with the amine **1-14** under anhydrous conditions to obtain compounds **1-1** and **1-3** respectively. Pyridine was used to neutralized the byproduct HCl formed during the reaction.



Scheme 1.1 Synthesis of compounds **1-1** to **1-4**.

The amide coupling of compound **1-14** and *p*-hydroxybenzoic acid via activation of the acid with 1-ethyl-3-(3'-dimethylaminopropyl)-carbodiimide hydrochloride (EDC) in the presence of a catalytic amount of *N,N'*-dimethylaminopyridine (DMAP) with a prolonged reaction time (24 h) gave a very low yield. We tried several different coupling reagents and reaction conditions. Finally the amide coupling was accomplished via activation of 4-((tert-butyldimethylsilyl)oxy)benzoic acid using 1,1'-carbonyldiimidazole (CDI) followed by reaction with the amine **1-14** in a solvent mixture of acetonitrile:DMF (20:1). The reaction of 4-((tert-butyldimethylsilyl)oxy)benzoic acid with CDI forms a transient mixed anhydride that rearranges to a carbonyl imidazolide (**Scheme 1.2**). This forms one equivalent of CO_2 and imidazole which serve as a catalyst and as a base respectively in the subsequent amide coupling.⁸⁴ Finally the imidazole and *tert*-butyldimethylsilanol byproducts were easily removed by an aqueous workup.

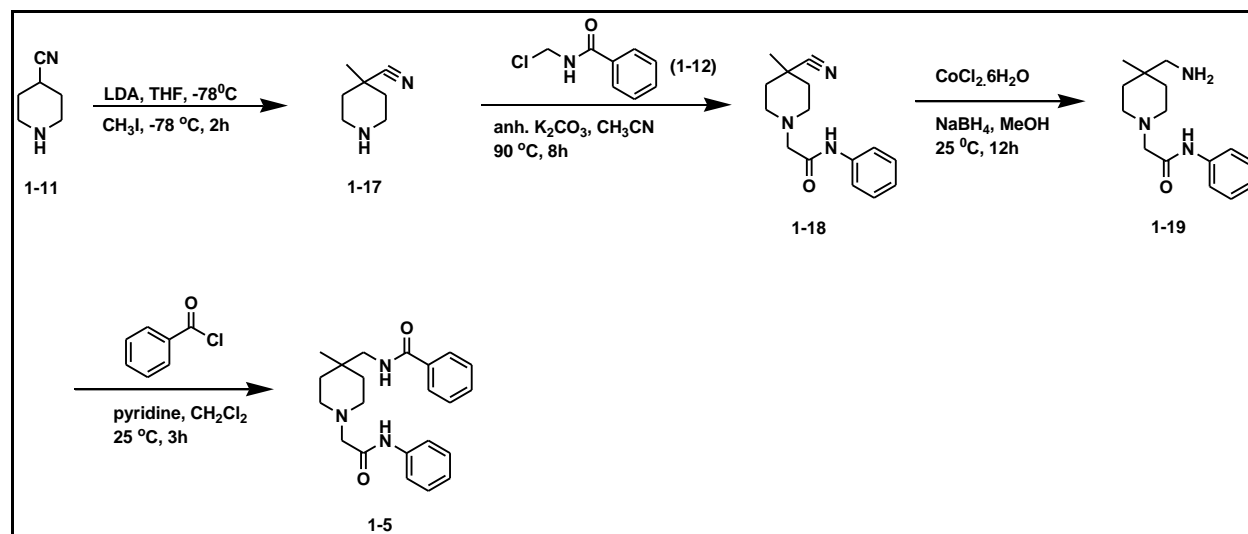


Scheme 1.2 Mechanism for CDI assisted amide bond formation and silyl deprotection to obtain compound **1-2**.

The amine **1-14** was coupled with 2-chloroacetyl pyrrole (**1-16**) to obtain compound **1-4**. Sodium bicarbonate was used to neutralized the byproduct HCl formed during the reaction. The reaction was carried out in different solvent systems and at different temperatures. A mixture of acetonitrile:DMF (20:1) and 50 °C temperature were found to be the best conditions to give the desired product **1-5** in a better yield (56%). It is also important to keep a higher ratio of amine to alkyl chloride to prevent the formation of dialkylated product. Desired product (**1-4**) and unreacted amine (**1-14**) were separated by column chromatography.

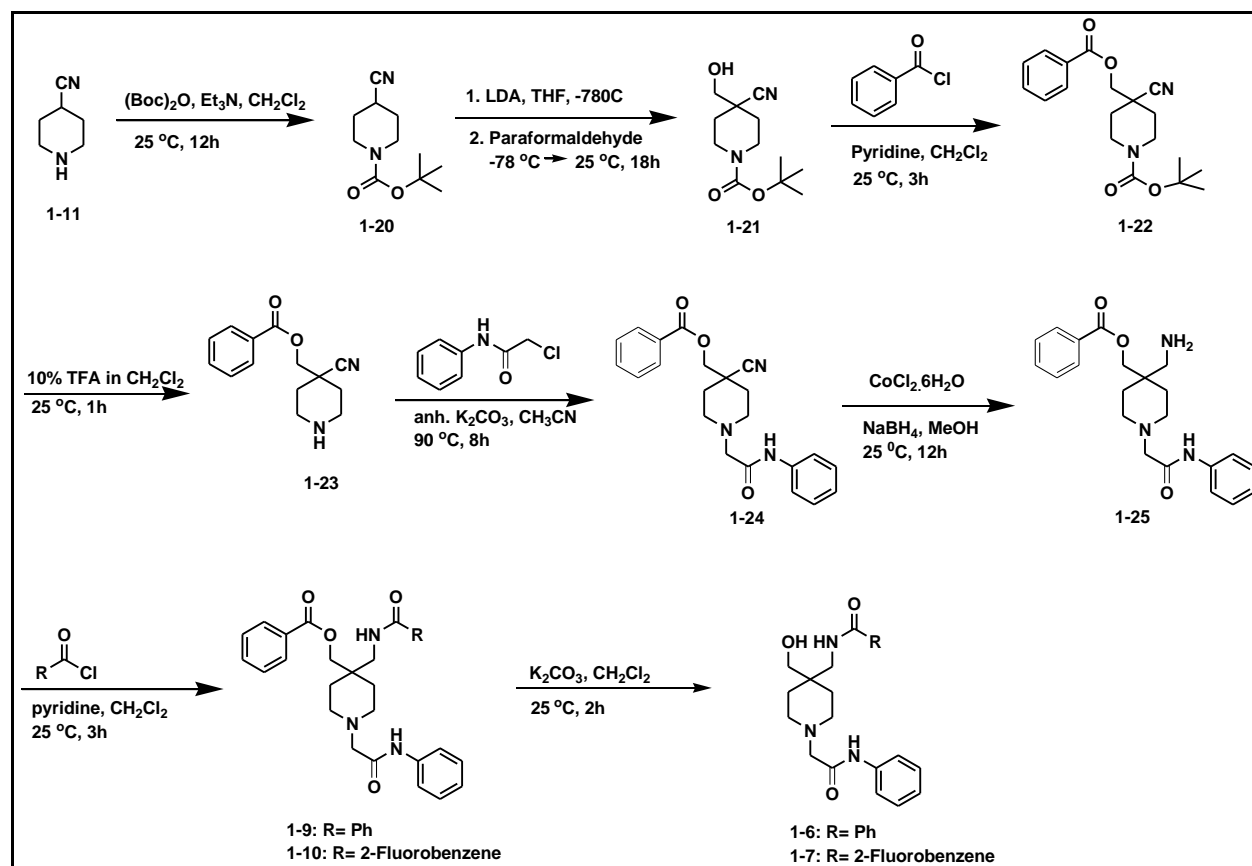
Compound **1-5** was synthesized as depicted in **Scheme 1.3**. Deprotonation of 4-Cyanopiperidine (**1-11**) using 1 equivalent of lithium diisopropylamide followed by the methylation of lithium enolate, followed by quenching with ammonium hydroxide/ammonium chloride yielded the methylated compound **1-17**. This lithium enolate participates in a S_N2 reaction with methyl iodide to form the methylated compound **1-17**. Methylated compound **1-17** was then treated with *N*-phenyl-2-chloroacetamide under basic conditions to give compound **1-18**. *N*-alkylated product **1-18** was then reduced with cobalt(II) chloride hexahydrate/sodium

borohydride to obtain the corresponding amine compound **1-19** followed by benzoylation with under basic condition (pyridine) resulted compound **1-5**.



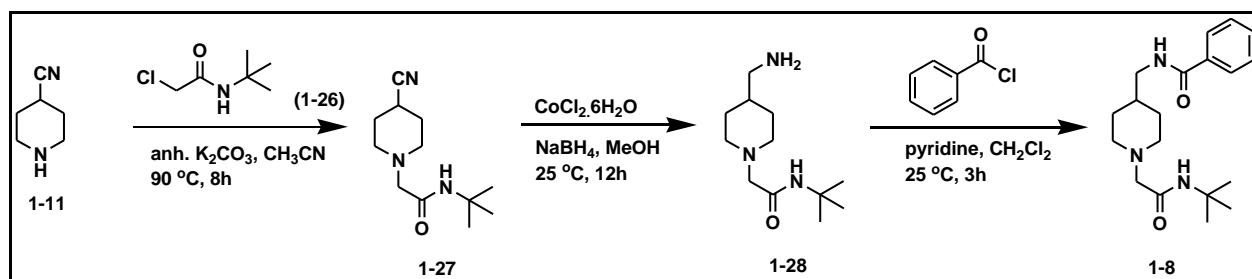
Scheme 1.3 Synthesis of compound **1-5**.

Compounds **1-6**, **1-7** and **1-9**, **1-10** were synthesized according to the procedure outlined in **Scheme 1-4**. The 4-cyanopiperidine was first boc-protected using di-tert-butyl dicarbonate (Boc_2O) and triethyl amine base to give N-boc protected compound **1-20**. Deprotonation of compound **1-20** using an equivalent of lithium diisopropylamide followed by the hydroxymethylation, followed by quenching with ammonium hydroxide/ammonium chloride yielded the hydroxymethylated compound **1-21**. Benzoylation of primary alcohol under basic condition (pyridine) resulted the benzoate ester compound **1-22**. The boc protecting group of **1-22** was removed using 10% TFA in methylene chloride to give the amine intermediate **1-23**, which was subsequently alkylated using N -phenyl-2-chloroacetamide under basic conditions to give compound **1-24**. The cyanide reduction of compound **1-24** was done with cobalt(II) chloride hexahydrate/sodium borohydride to obtain the corresponding amine compound **1-25** followed by the benzoylation with benzoyl chloride and 2-fluorobenzoyl chloride under basic condition (pyridine) resulted compounds **1-9**, and **1-10** respectively. Compounds **1-9**, and **1-10** were treated with potassium carbonate to give debenzoylated products **1-6** and **1-7** respectively.



Scheme 1.4 Synthesis of compounds **1-6**, **1-7** and **1-9**, **1-10**.

Compound **1-8** synthesis was very similar to the synthesis of compound **1-1** except the N-alkylation step of the piperidine ring. First, 4-cyano piperidine was treated with *N*-tert-butyl-2-chloroacetamide under basic conditions to give compound **1-27**. Then the cyanide reduction of compound **1-27** was done with cobalt(II) chloride hexahydrate/sodium borohydride to obtain the corresponding amine compound **1-28** followed by benzylation under basic condition (pyridine) resulted compound **1-8**.



Scheme 1.5 Synthesis of compound **1-8**.

1.3.1.3 Bio-evaluation methods

Bio-evaluation studies were performed by our collaborators Dr. Bende Zou, Dr. Christopher A. Lieu and Dr. Conrado Pascual in Dr. Xinmin (Simon) Xie's laboratory at AfaSci Research Laboratory in Redwood City, California. HEK293 cell expressing Cav3.2 channels and DRG neurons were prepared as described in reference 84.⁸⁵ Patch clamp recordings were performed using a reported procedure.^{85,86} Description of seizure models and Spared nerve injury (SNI) pain models were adapted from reference 84.⁸⁵

1.3.1.3.1 Preparation of HEK293 cell expressing Cav3.2 channels and DRG neurons

Cav3.2 channels were expressed in human embryonic kidney (HEK)-293 cells using a tetracycline inducible expression system (Invitrogen). Mouse dorsal root ganglion (DRG) neurons were prepared from C57/BC6 mice.

1.3.1.3.2 Patch clamp recordings

Whole-cell voltage clamp recordings were performed on mouse DRG neurons within 2 days after acutely dissociation or cultured HEK293 cells expressing T-type channels (encoded by $Ca_v3.1$, $Ca_v3.2$ or $Ca_v3.3$ channels). Whole-cell currents were recorded using a MultiClamp 700B amplifier and analyzed offline with pCLAMP10.4 software (Molecular Devices, LLC, Sunnyvale CA, USA). The current responses were recorded and percent inhibition was calculated. Sigmoidal dose-response curves were generated using XLFit (IDBS, Surrey, UK) or Prism (GraphPad Software, La Jolla, CA, US) to calculate IC_{50} values.

1.3.1.3.4 Seizure models

For the pentylenetetrazole (PTZ)-induced seizure model, male mice (C57BL/6 WT, 8-10 months old, approximately 30 g) were used. Each mouse was pretreated intraperitoneally (I.P.) with either synthesized compound (30 mg/kg), or sodium valproate (150 mg/kg), or vehicle (2% DMSO in 0.5% aqueous hydroxypropyl cellulose (HPC)). Since PTZ-induced seizures are blocked by sodium valproate, it is used as a positive control.¹³ After administration of PTZ, number of deaths of mice in each treatment group within a 20-minute cutoff period were recorded and the percentage of averaged fatality latencies were calculated. The average fatality latencies (in minutes) and the fatality rates of each treatment group (the synthesized compounds' group, sodium valproate group, and the vehicle group (n = 8 mice/group) were used to evaluate the synthesized compounds' ability to either prevent or delay the onset of PTZ- induced seizures and death.

For the maximal electroshock seizure (MES) model, C57BL/6 WT male mice (8-10 months old, approximately 30 g) were used. They were treated intraperitoneally with synthesized compounds (30 mg/kg), sodium valproate (150 mg/kg) or vehicle. A 30 min after injection, MES stimulation was applied through trans auricular (ear-clip) electrodes using a HSE Shock Stimulator Type 221 (Harvard Apparatus, Holliston, MA). Upon completion of the electrical stimulus, the time to onset of seizures was recorded.

1.3.1.3.5 *In vivo* analgesic effects in spared nerve injury (SNI) pain models

Therapeutic effects of the most active compounds were evaluated using a rodent neuropathic pain model called spared nerve injury (SNI) pain model. The nerve injury of the male rats (Sprague-Dawley rats, 275 g - 325 g, Harlan) was induced with tibial and common peroneal nerves ligation, leaving the sural nerve intact. Pre-surgery baselines (100%) of the thermal hyperalgesia and mechanical pain thresholds of the rats' left hind paws were measured using the Hargreaves thermal stimulator and von Frey hair monofilaments respectively.^{87,88} Paw withdrawal thresholds and paw withdrawal latencies in response to thermal and mechanical pain stimulus were measured at 1, 2, 3, 4, 5, 6, 7, and 8 hours after treatment.

1.3.2 Novel PDI inhibitors as anti-influenza agents

1.3.2.1 Molecular design of novel PDI inhibitors

Since no PDI inhibitor for anti-influenza has been reported, we chose previously reported ML359 and modified its structure to synthesize a series of novel 1,4-substituted piperidine molecules using structure-activity relationship (SAR) approach. ML359 is a piperidine based small molecule, which identified as a selective inhibitor of PDI oxidoreductase activity over other thiol isomerases in cells with no cytotoxicity.^{79,80} We designed a series of molecules by changing substituents independently in three regions (A, B, or C) of the 1,4-substituted piperidine core (Figure 1.9). First, upper right part of the molecule (part A) was changed with much smaller nitrile group or hydrogen. Nitrile group was expected to enhance interactions between the synthesized molecule inhibitors and the target protein PDI due to its strong hydrogen bond acceptor property and the smaller size (~8 times smaller than methyl group).⁸⁹ Modification in part B focused on replacement of substituted benzyl moiety with a tertiary butyl ester, a tertiary butyl amide or a benzoic amide. Incorporation of amide and ester groups at α - or β -position of the *N*-alkyl chain was expected to reduce the basicity of the piperidine ring. It is reported that the ethyl ester of ML359 is readily hydrolyzed in murine plasma and the replacement of ester with amide functionality has shown improved murine plasma stability.⁹⁰ Further, part C was replaced with 4-hydroxybenzoyl group to mimic the structure of a known

PDI inhibitor juniferdin. These structural modifications were expected to improve synthesized molecules' potency and selectivity in the PDI inhibition.

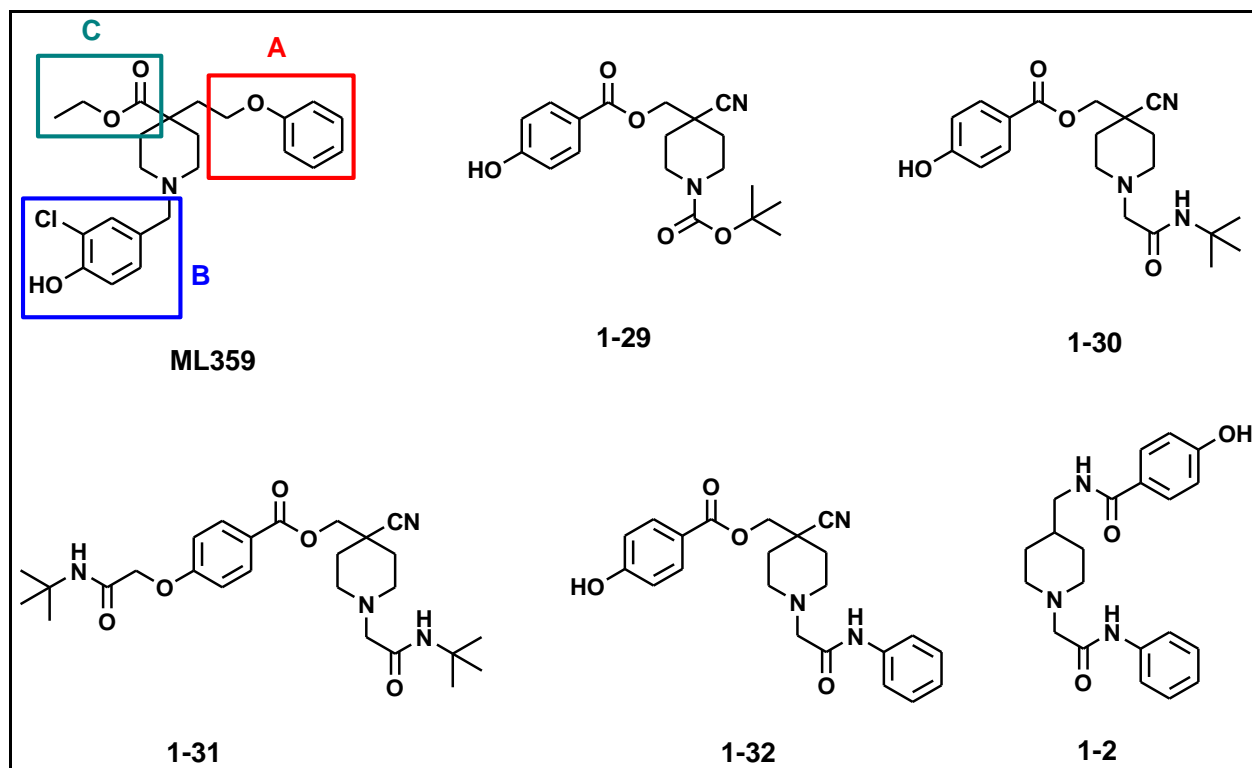


Figure 1.9 Designed 1,4-substituted piperidine compounds as PDI inhibitors.

Table 1.2 Calculated Log P values (lipophilicity) of synthesized piperidine compounds using Molinspiration Predictor.

Compound	Molecular Weight	log P value
1-29	360.41	2.95
1-30	373.45	2.71
1-31	386.61	3.54
1-32	393.44	3.09
1-2	367.45	2.63

All of them, that is compounds **1-29**, **1-30**, **1-31**, **1-32** and **1-2** obeyed “Lipinski’s rule of five”. Therefore, they were expected to have good “drug-like” properties.

In addition to the “Lipinski’s rule of five”, polar surface area (PSA) also influences ligand–target binding interactions, solubility, absorption, distribution, metabolism, elimination and toxicity properties of drug molecules.^{83,91} PSA is defined as the sum of the surface areas of polar atoms in a molecule and it is a simple measure of the hydrogen-bonding capacity of a molecule.⁹² Molecules with a PSA greater than 140 Å² are predicted to have a low capacity for penetrating cell membranes. Calculated PSA values of synthesized piperidine compounds **1-29**, **1-30**, **1-31**, **1-32** and **1-2** using Molinspiration Predictor are shown in figure 1.8. All of them had PSA values less than 140 Å². Therefore, they are expected to have good cell penetration ability.

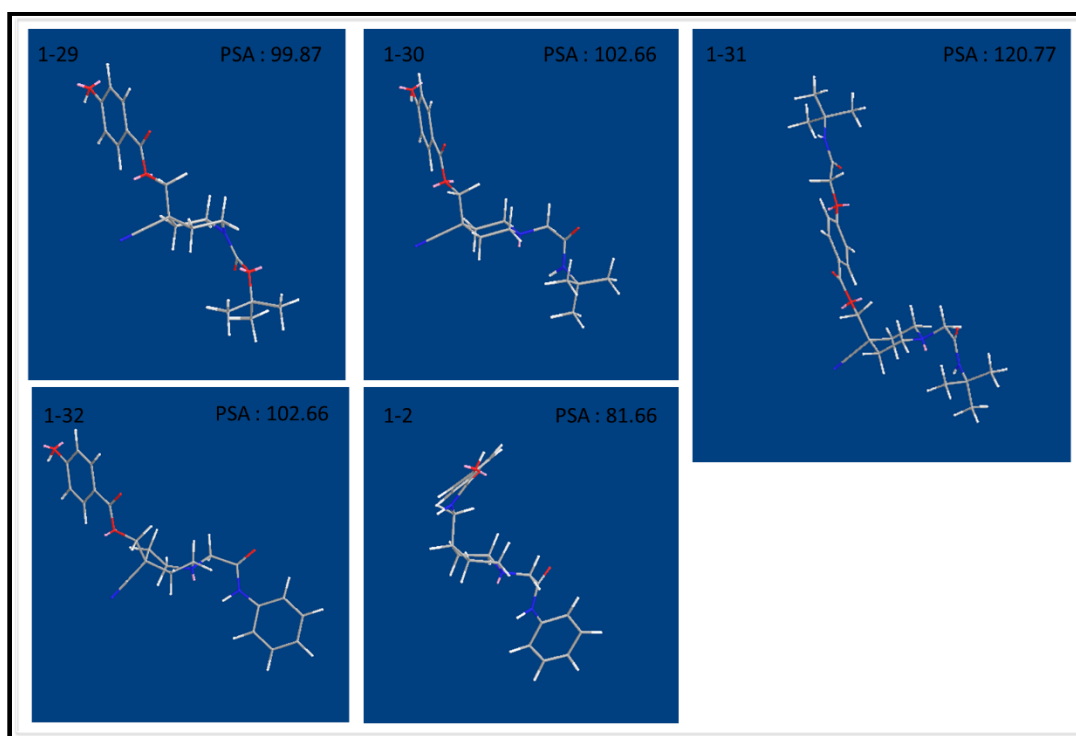
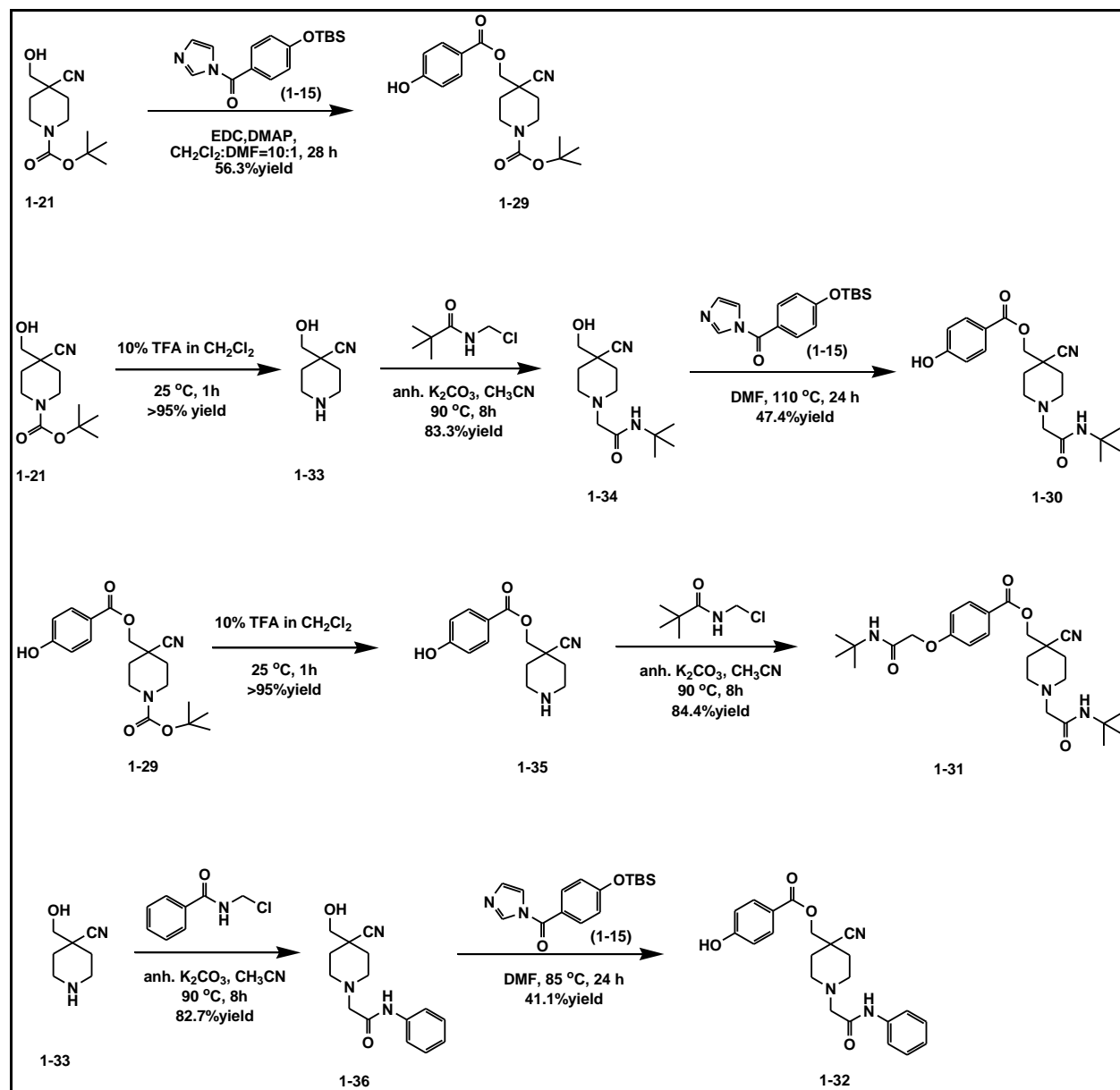


Figure 1.10 Minimum energy conformations of compounds **1-29** to **1-32** and **1-2** with their calculated PSA (polar surface area) values.

1.3.2.2 Synthetic routes



Scheme 1.6 Synthesis of compounds **1-29**, **1-30**, **1-31**, **1-32**.

Compounds **1-29**, **1-30** and **1-31**, **1-32** were synthesized according to the procedure outlined in Scheme 1-6. Synthesis of compound **1-2** was described in section 1.3.1.2. To synthesize compound **1-29**, commercially available 4-cyanopiperidine was first, boc-protected.

Deprotonation of the resulting compound, **1-20** using 1 equivalent of lithium diisopropylamide followed by the hydroxymethylation, followed by quenching with ammonium hydroxide/ammonium chloride yielded the hydroxymethylated compound **1-21**. In a separate reaction vessel, 4-((*tert*-butyldimethylsilyl)oxy)benzoic acid was activated using 1,1'-carbonyldiimidazole (CDI) to obtain compound **1-15**. This activated acid was treated with the alcohol **1-21** in the presence of 1-ethyl-3-(3'-dimethylaminopropyl)-carbodiimide hydrochloride (EDC) and *N,N'*-dimethylaminopyridine (DMAP) to give the coupling product **1-29** in a satisfactory yield. We found that the solubility of the compound **1-15** is crucial for the reaction yield. Therefore, compound **1-15** was dissolved in DMF, and it was cannulated to a mixture of **1-21**, EDC, DMAP in dichloromethane. We dissolved **1-15** in DMF and then diluted the reaction mixture with dichloromethane in 1:10 ratio. In the synthesis of compounds **1-30** and **1-32** first, the boc protecting group of **1-21** was removed using 10% TFA in methylene chloride to give the amine intermediate **1-33**, which was subsequently alkylated using *N*-*tert*-butyl-2-chloroacetamide or *N*-phenyl-2-chloroacetamide under basic conditions to give compound **1-34** and **1-36** respectively. Next, the compound **1-15** was coupled with **1-34** and **1-36** to give compounds **1-30** and **1-32** respectively. In the synthesis of compound **1-31**, boc protecting group of **1-29** was removed using 10% TFA in methylene chloride to give the amine intermediate **1-35**, which was subsequently alkylated at piperidine nitrogen and phenolic oxygen using *N*-*tert*-butyl-2-chloroacetamide under basic conditions to give compound **1-31**.

1.3.2.3 Bio-evaluation methods

Bio-evaluation studies performed by our collaborators Dr. Yunjeong Kim and Dr. Kyeong-Ok Chang in the College of Veterinary Medicine, Kansas State University.

1.3.2.3.2 The screening of compounds **1-29** to **1-32** and **1-2** for PDI inhibition

PDI activities of the compounds were determined by monitoring PDI-catalyzed reduction of insulin in the presence of dithiothreitol (DTT) using a PROTEOSTAT[®] PDI assay kit (Enzo Life Sciences, Inc.). The assay was performed according to the manufacturer's

instructions using different concentrations of each compound (up to 100 μ M). Juniferdin and bacitracin (supplied with the kit) were used as the positive controls. The fluorescence was read using FLx800 (Biotek) microplate reader at excitation of 500 nm and emission of 603 nm.

1.3.2.3.2 The screening of compounds 1-29 to 1-32 and 1-2 for anti-influenza virus activity

Preparation of Madin-Darby canine kidney (MDCK) cells and infection procedure of influenza virus from human (A/PR/8/34 [H1N1], PR8) to MDCK cells have reported previously.⁹³ Influenza virus-infected cells were incubated in the presence of each compound at different concentrations (0.1–20 μ M) with trypsin (1 μ g/ml) in a 96-well plate for up to 4 days. Juniferdin was used as the positive control. After 48 hours of incubation, CellTiter-Glo® reagent was added to each well following the protocol provided by the supplier. The luminescence (RLU) emitted from each well was quantified with a FLx800 (Biotek) microplate reader. EC₅₀, the concentration required to protect 50% of MDCK cells from the cytotoxic effect of influenza virus (A/PR/8/34 [H1N1], PR8), was calculated using the software GraphPad Prism (Graphpad software Inc, San Diego, CA).

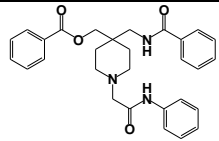
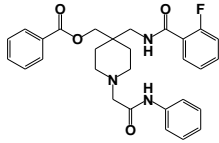
1.4 Results and Discussion

1.4.1 Mouse DRG neurons inhibition (%) of T- type calcium ion channel and inhibition of seizure induced death by the synthesized piperidine compounds

Results for mouse DRG neurons inhibition (%) of T- type calcium ion channel and inhibition of seizure induced death are provided in **Table 1.3**.

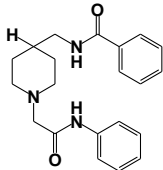
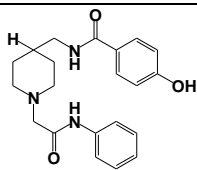
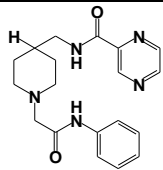
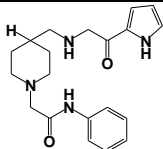
Table 1.3 *In vitro* and *in vivo* bioactivities of synthesized piperidine derivatives. (NT: not tested)

Code name	Chemical structure	Mouse DRG neurons inhibition (%) of ion channel at 1 μ M (unless specified)			Inhibition of seizure induced death (% at 30mg/kg, i.p.)
		T-Ca ²⁺	Na ⁺	K ⁺	
1-1		44 IC ₅₀ = 6.3 μ M	57.8	NT	80
1-2		47.3	NT	NT	0
1-3		40% block: 3 μ M 50% block: 10 μ M 30% block: 10 μ M	NT	NT	NT
1-4		40 Ca _v 3.2 inhibition IC ₅₀ =1 nM	- 4.5%	NT	86 (PTZ)
1-5		83 IC ₅₀ =0.9 μ M	6.5	18.8	0
1-6		100	NT	NT	14.3
1-7		43.6	-4.3	NT	62.5
1-8		40.1 IC ₅₀ =2.4 μ M	2.9	11.7	66.7

1-9		NT	NT	NT	0
1-10		NT	NT	NT	0

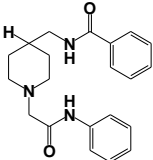
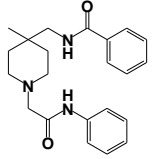
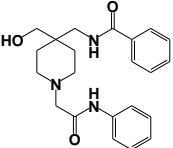
1.4.2 Structure activity relationship of synthesized piperidine compounds

Table 1.4 Comparison of inhibitory activity of compounds **1-1** to **1-4** (changing part A) against T-type calcium channels and seizure induced deaths.

Code name	Chemical structure	Mouse DRG neurons inhibition (%) of ion channel at 1 μ M (unless specified)			Inhibition of seizure induced death (% at 30mg/kg, i.p.)
		T-Ca	Na	K	
1-1		44 IC ₅₀ = 6.3 μ M	57.8	NT	80
1-2		47.3	NT	NT	0
1-3		40% block: 3 μ M 50% block: 10 μ M 30% block: 10 μ M	NT	NT	NT
1-4		40 Ca _v 3.2 inhibition IC ₅₀ =1 nM	- 4.5%	NT	86 (PTZ)

Compounds **1-1** to **1-4** displayed good inhibition against T-type calcium channels, suggesting that N-benzoic amide group is beneficial for the activity. Among them, compound **1-4** showed a very good Ca_v3.2 inhibition with a IC₅₀ value of 1 nM. Investigation of SAR effects by changing part A of the basic structure suggests that, the activity increases as the hydrophobicity of the part A increases. This can be explained by the compounds' lipophilic nature which helps better absorption or permeation. Moreover, drugs' absorption also depends on their ability of ionization in the body. pKa of pyrazine (0.6) is far more less than the pKa of pyrrole (23.0), which suggests that, compound **1-3** is easily get ionized in cells compared to **1-4**. Since ionized structures attract water molecules, they form large complexes which decreases the membrane permeability. This suggests that the compound **1-4** has a better activity than compound **1-3**, could be due to its better absorptivity.

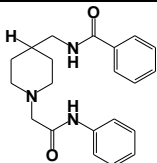
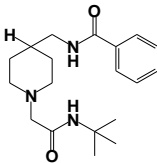
Table 1.5 Comparison of inhibitory activity of compounds **1-1**, **1-5**, and **1-6** (changing part B) against T-type calcium channels and seizure induced deaths.

Code name	Chemical structure	Mouse DRG neurons inhibition (%) of ion channel at 1μM (unless specified)			Inhibition of seizure induced death (% at 30mg/kg, i.p.)
		T-Ca ²⁺	Na ⁺	K ⁺	
1-1		44 IC ₅₀ = 6.3 μM	57.8	NT	80
1-5		83 IC ₅₀ =0.9 μM	6.5	18.8	0
1-6		100	NT	NT	14.3

Structure activity studies related to part B showed that activity tolerates replacement of hydrogen with methyl and hydroxymethyl groups. But in vivo studies of compound **1-5** and **1-6**

showed no or very little activity suggests that hydrogen in part B is beneficial for cell permeability and toxicity.

Table 1.6 Comparison of inhibitory activity of compounds **1-1** and **1-8** (changing part C) against T-type calcium channels and seizure induced deaths.

Code name	Chemical structure	Mouse DRG neurons inhibition (%) of ion channel at 1 μ M (unless specified)			Inhibition of seizure induced death (% at 30mg/kg, i.p.)
		T-Ca ²⁺	Na ⁺	K ⁺	
1-1		44 IC ₅₀ = 6.3 μ M	57.8	NT	80
1-8		40.1 IC ₅₀ = 2.4 μ M	2.9	11.7	66.7

Both compounds **1-1** and **1-8** can inhibit T-type calcium currents and inhibit seizure induced deaths. This suggests that both *N*-benzoic amide and *N*-*tert*-butyl amide possess T-type inhibitory activity. Unfortunately, compound **1-1** showed no selectivity over sodium channels. But, compound **1-8** displayed a significant improvement on selectivity over Na⁺ and K⁺ channels with a better inhibitory activity against T-type calcium channels.

Compounds **1-9** and **1-10** showed no inhibition against seizure induced death. This could be due to their large molecular size, which could result low water solubility and permeability.

Results for *in vivo* analgesic effects of most the active compounds **1-4** and **1-8** in spared nerve injury (SNI) pain models are provided in **Figure 1.11** and **1.12**.

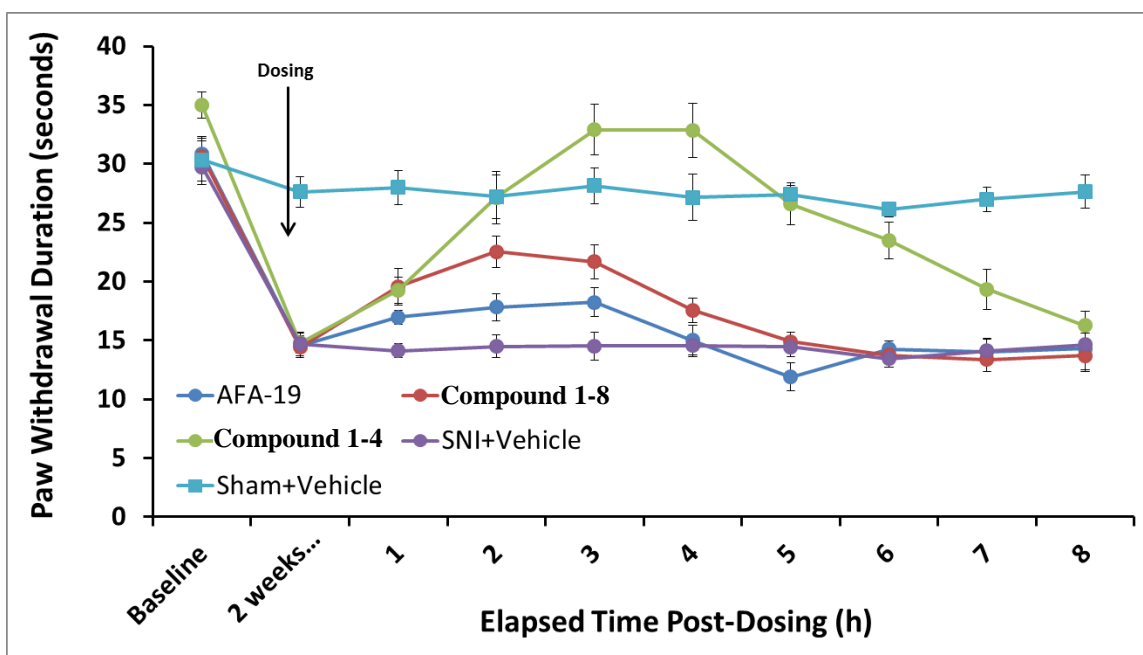


Figure 1.11 Spared Nerve Injury (SNI) rats' left hind paw withdrawal latencies in response to thermal stimulation (Hargreaves test).

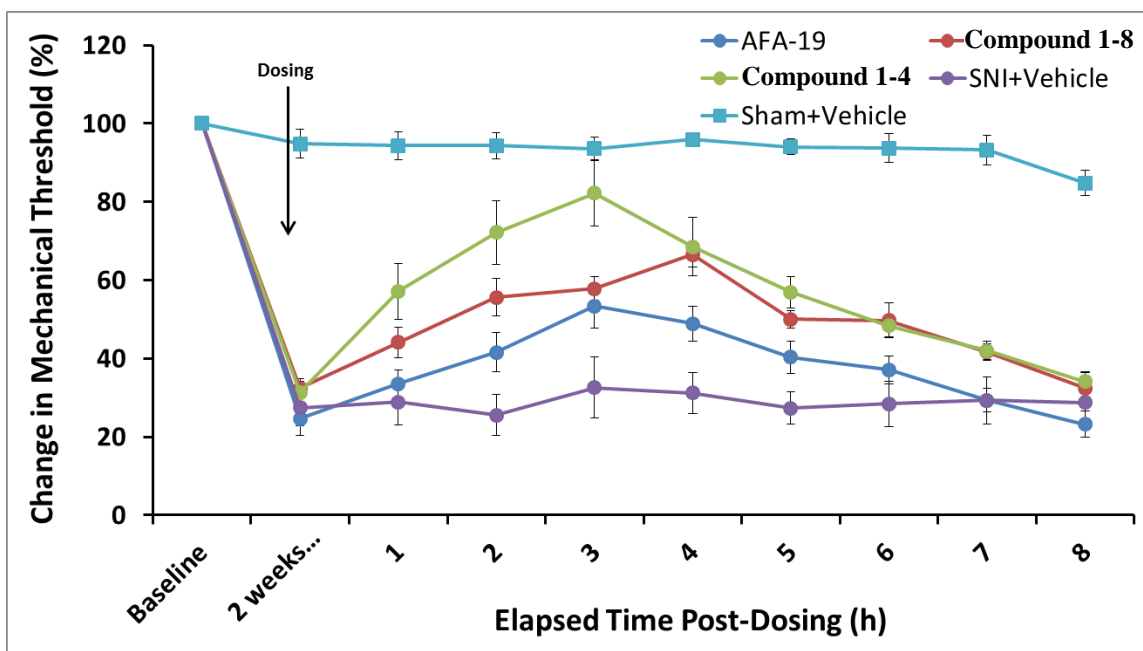


Figure 1.12 Mechanical pain threshold assessment (von Frey monofilament test) of SNI rats' left hind paws.

The tested compounds **1-4** and **1-8** have increased thermal and mechanical thresholds compared to vehicle. The drug actions started around 1 hour post-injection and peaked between 2 and 3 hours, and the drug effects gradually declined to pre-treatment levels over 6 - 7 hours (**Figures 1.11** and **1.12**). These tested compounds produced analgesic effects on both thermal and mechanical pain thresholds, while the SNI-vehicle group remained thermal hyperalgesia and mechanical allodynia conditions. Therefore, compounds **1-4** and **1-8** have the ability to mitigate neuropathic pain induced by Spared Nerve Injury (SNI) in mice.

1.4.3 PDI inhibition and anti-influenza activity of compounds

Table 1.7 PDI inhibition and anti-influenza activity data.

Code name	PDI inhibition	Anti-influenza activity, EC ₅₀ (μ M)
1-29	Yes	2.5
1-30	Yes	18.5
1-31	No	8.3
1-32	Yes	5.6
1-2	No	> 20
Juniferdin	Yes (IC ₅₀ : ~ 1 μ M)	1.5

1.4.4 Structure activity relationship of synthesized piperidine compounds

Compounds **1-29**, **1-30** and **1-32** displayed PDI inhibition while no PDI inhibition was observed for **1-31**, and **1-2**. This suggests that nitrile group at the upper right part of the molecule (part A) is important for the PDI enzyme inhibition. Since nitrile group is a much smaller functional group, it makes the entire molecule a ligand with a smaller size, which helps the ligand to reach the active site and bind easily. Further, the nitrile group enhances interactions between the ligand and the PDI due to its strong hydrogen bond acceptor property. Though **1-31**

has a nitrile group in part A, part B makes **1-31** larger. Compared to other compounds in the series, **1-31** has a larger polar surface area and it is a relatively flat (as indicated in the minimum energy conformation) and hydrophobic molecule. Therefore, active site-ligand interactions will be difficult to locate. In addition, **1-2**, which has an amide derivative at the upper left part showed no inhibitory activity against PDI. Incorporation of tert-butyl amide and tert-butyl ester groups at either α - or β -position of the *N*-alkyl chain retained the PDI inhibitory activity. Therefore, SAR studies suggest that the nitrile group at the part A and ester side chain at the part C of the molecule is important for PDI inhibitory activity.

Compounds **1-29**, **1-30**, **1-31** and **1-32** showed anti-influenza activity with EC₅₀ values less than 20 μ M. Among them, **1-29** showed the best activity (2.5 μ M). Though **1-31** did not inhibit PDI activity, it showed anti-influenza activity of 8.3 μ M. This suggests that, anti-influenza activity of **1-31** is due to an effect except anti-PDI activity. Results indicate that, inhibition of PDI can be used as a potential biological target for the treatment of influenza. This confirms the siRNA knockdown assay results done by Dr. Yunjeong Kim.

Further, **1-2** is neither a PDI inhibitor nor anti-influenza molecule.

1.5 Conclusion

In summary, two different series of 1,4 substituted piperidine derivatives were designed by changing three parts attached to the piperidine ring.

The first series was designed, synthesized and screened for their ability and selectivity towards inhibition of T-type calcium channels and inhibition of seizure induced deaths. Two hit compounds (**1-4** and **1-5**) were found to possess good inhibition on T-type Ca²⁺ currents and inhibition of seizure induced deaths. Compound **1-4** was a good T-type calcium channel inhibitor (Ca_v3.2 inhibition of IC₅₀ = 1 nM), which suppressed 86% of seizure induced death in mice models. Two hit compounds were further tested using in vivo spared nerve injury (SNI) pain

models. Results indicated that compounds **1-4** and **1-8** have good analgesic effects on both thermal and mechanical pain thresholds. This indicate that synthesized T-type calcium channel blockers can be used for the treatment of epilepsy and pain. Further structural optimization of **1-4** could be used to discover more potent and selective T-type calcium channel blockers for the treatment of disorders related to this channel.

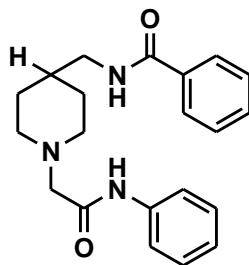
Since the crystal structure of full-length human PDI has not yet been resolved, it is quite a challenge to design PDI specific small molecule inhibitors. We designed and synthesized our second piperidine series and screened them for inhibition of PDI and anti-influenza activities. Among them, **1-29** was found to possess better anti-influenza activity ($EC_{50} = 2.5 \mu M$). Therefore, to develop a more potent anti-influenza drug, **1-29** can be used as a lead compound. Further SAR studies hopefully will lead to identify novel PDI inhibitors for the treatment of influenza.

1.6 Experimental section

1.6.1 General experimental procedures

Nuclear magnetic resonance (NMR) spectra were obtained from a Varian Unity plus 400 MHz Spectrometer in deuterated chloroform ($CDCl_3$), unless otherwise informed. Low-resolution mass spectra were obtained from an API 2000-triple quadrupole ESI-MS/MS mass spectrometer (Applied Biosystems). Chemicals were purchased from Fisher Scientific, VWR international LLC and Chem-Impex International, Inc. Column chromatography was carried out on silica gel (200-400 mesh).

N-((1-(2-Oxo-2-(phenylamino)ethyl)piperidin-4-yl)methyl)benzamide (**1-1**)



1-1

Step A:

A mixture of 4-cyano piperidine (**1-11**) (1 g, 9.1 mmol), *N*-phenyl-2-chloroacetamide (**1-12**) (1.54 g, 9.1 mmol), and potassium carbonate (2.5 g, 18.2 mmol) in acetonitrile (30 mL) was heated to reflux at 90 °C under argon for 8 hours. The resulting mixture was cooled and filtered to remove potassium carbonate. The filtrate was concentrated and column chromatographed on silica gel using a gradient mixture of dichloromethane and methanol (30: 1) as eluent to give 2-(4-cyanopiperidin-1-yl)-*N*-phenylacetamide (**1-13**) (2.2 g, 99.7 % yield) as a white solid. ¹H NMR (400 MHz, CDCl₃) δ ppm 8.92 (br. s., 1H), 7.52 (d, *J* = 7.81 Hz, 2H), 7.29 (t, *J* = 8.01 Hz, 2H), 7.08 (t, *J* = 7.42 Hz, 1H), 3.08 (s, 2H), 2.72 - 2.79 (m, 2H), 2.63 (td, *J* = 3.76, 7.71 Hz, 1H), 2.44 (t, *J* = 8.40 Hz, 2H), 1.84 - 2.00 (m, 4H); ¹³C NMR (100 MHz, CDCl₃) δ ppm 167.83, 137.35, 128.90, 124.19, 121.22, 119.42, 62.09, 51.67, 28.80, 25.36; MS (ESI) *m/z* = 244.5 (M+H)⁺.

Step B:

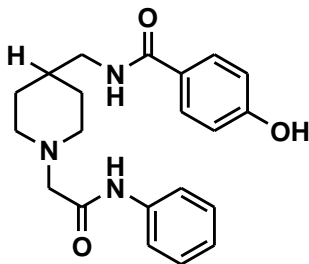
To a cold solution of 2-(4-cyanopiperidin-1-yl)-*N*-phenylacetamide (**1-13**) (0.8 g, 3.29 mmol) and MeOH (25 mL), cobalt (II) chloride hexahydrate (0.39 g, 1.65 mmol) was added followed by the addition of sodium borohydride (0.62 g, 16.45 mmol). After stirring for 15 hours at 25 °C, the reaction solution was diluted with 25 mL of 5% aqueous ammonium hydroxide and extracted three times with dichloromethane. The combined organic layer was washed with brine, dried over anhydrous Na₂SO₄, concentrated column chromatographed on silica gel using a gradient mixture of dichloromethane and methanol (2: 1) as eluent to give 2-(4-

(aminomethyl)piperidin-1-yl)-*N*-phenylacetamide (**1-14**) (0.81 g, 80% yield) as a colorless oil. ¹H NMR (400 MHz, CDCl₃) δ ppm 9.18 (br. s., 1H), 7.56 (d, *J* = 8.20 Hz, 2H), 7.32 (t, *J* = 7.81 Hz, 2H), 7.09 (t, *J* = 7.42 Hz, 1H), 3.09 (s, 2H), 2.92 (d, *J* = 11.33 Hz, 2H), 2.63 (d, *J* = 5.47 Hz, 1H), 2.18 - 2.30 (m, 2H), 1.78 (d, *J* = 10.54 Hz, 2H), 1.21 - 1.37 (m, 4H); ¹³C NMR (100 MHz, CDCl₃) δ ppm 168.92, 137.78, 129.10, 124.20, 119.52, 62.50, 54.24, 48.03, 30.43; MS (ESI) *m/z* = 248.2 (M+H)⁺.

Step C:

To a cold solution of 0.125 g (0.61 mmol) of 2-(4-(aminomethyl)piperidin-1-yl)-*N*-phenylacetamide (**1-14**) in freshly distilled dichloromethane under argon, pyridine 78 μL (0.915 mmol) was added followed by the addition of 70 μL (0.61 mmol) of benzoyl chloride. The reaction was stirred at 0 °C for 30 min. and 25 °C for 3 hours. The reaction solution was diluted with 20 mL of aqueous sodium bicarbonate and extracted three times with dichloromethane. The combined organic layer was washed with brine, dried (anhydrous Na₂SO₄), concentrated, and column chromatographed on silica gel using a mixture of dichloromethane and methanol (10: 1) as eluent to give *N*-((1-(2-oxo-2-(phenylamino)ethyl)piperidin-4-yl)methyl)benzamide (**1-1**) (114 mg, 53%) as a white solid. ¹H NMR (400 MHz, CDCl₃) δ ppm 9.85 (br. s., 1H), 9.59 (br. s., 1H), 8.09 (d, *J* = 7.42 Hz, 2H), 7.79 (d, *J* = 7.42 Hz, 1H), 7.54 - 7.58 (m, 2H), 7.40 - 7.43 (m, 2H), 7.30 (t, *J* = 7.81 Hz, 1H), 7.09 (t, *J* = 7.42 Hz, 1H), 6.65 (t, *J* = 5.86 Hz, 1H), 3.40 (t, *J* = 6.44 Hz, 2H), 3.31 (s, 2H), 3.08 (d, *J* = 11.72 Hz, 2H), 2.34 - 2.45 (m, 2H), 1.82 (d, *J* = 12.50 Hz, 2H), 1.66 - 1.77 (m, 1H), 1.44 - 1.57 (m, 2H); ¹³C NMR (100 MHz, CDCl₃) δ ppm 168.25, 167.62, 137.78, 134.63, 131.80, 129.22, 128.56, 127.19, 124.64, 119.93, 61.97, 53.68, 45.32, 35.49, 29.66; MS (ESI) *m/z* = 352.1 (M+H)⁺.

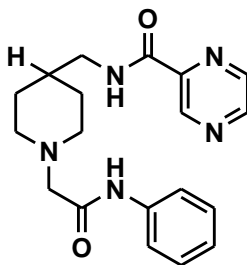
4-Hydroxy-*N*-((1-(2-oxo-2-(phenylamino)ethyl)piperidin-4-yl)methyl)benzamide (**1-2**)



1-2

To a solution of 0.100 g (0.28 mmol) of 2-(4-(aminomethyl)piperidin-1-yl)-*N*-phenylacetamide (**1-14**) in freshly distilled 20:1 mixture of acetonitrile:DMF under argon, (4-(tert-butyldimethylsilyloxy)phenyl)(1*H*-imidazol-1-yl)methanone (**1-15**) 0.86 g (0.28 mmol) was added. The reaction mixture was refluxed at 90 °C for 24 h. The reaction solution was diluted with 20 mL of aqueous sodium bicarbonate and extracted three times with dichloromethane. The combined organic layer was washed with brine, dried (anhydrous Na₂SO₄), concentrated, and column chromatographed on silica gel using a mixture of dichloromethane and methanol (15: 1) as eluent to give 4-hydroxy-*N*-((1-(2-oxo-2-(phenylamino)ethyl)piperidin-4-yl)methyl)benzamide (**1-2**) (52 mg, 51%) as a white solid. ¹H NMR (400 MHz, CDCl₃) δ ppm 9.16 (br. s., 1H), 7.68 (d, *J* = 8.59 Hz, 1H), 7.52 - 7.61 (m, 2H), 7.35 (d, *J* = 7.42 Hz, 2H), 7.07 - 7.18 (m, 2H), 6.87 (d, *J* = 8.59 Hz, 1H), 6.16-6.18 (m, 1H), 3.39 (t, *J* = 6.44 Hz, 1H), 3.04 - 3.15 (m, 2H), 2.93 (d, *J* = 11.72 Hz, 2H), 2.25 (t, *J* = 10.74 Hz, 2H), 1.81 (d, *J* = 10.54 Hz, 2H), 1.66 (d, *J* = 6.25 Hz, 2H), 1.37 - 1.46 (m, 2H); MS (ESI) *m/z* = 368.4 (M+H)⁺.

N-((1-(2-Oxo-2-(phenylamino)ethyl)piperidin-4-yl)methyl)pyrazine-2-carboxamide (**1-3**)

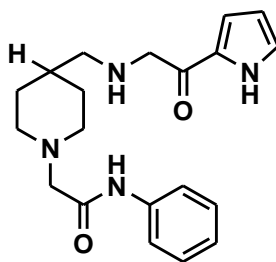


1-3

To a cold solution of 2-(4-(aminomethyl)piperidin-1-yl)-*N*-phenylacetamide (**1-14**) (0.08 g, 0.32 mmol) in freshly distilled dichloromethane under argon, pyridine 40 μL (0.48 mmol) was added followed by the addition of 52 mg (0.36 mmol) of pyrazinoyl chloride. The reaction was stirred at 0 °C for 30 min. and 25 °C for 3 hours. The reaction solution was diluted with 20 mL of aqueous sodium bicarbonate and extracted three times with dichloromethane. The combined organic layer was washed with brine, dried (anhydrous Na₂SO₄), concentrated, and column chromatographed on silica gel using a mixture of dichloromethane and methanol (10: 1) as eluent

to give *N*-((1-(2-oxo-2-(phenylamino)ethyl)piperidin-4-yl)methyl)pyrazine-2-carboxamide (**1-3**) (62 mg, 54%) as a white solid. ^1H NMR (400 MHz, CDCl_3) δ ppm 9.42 (s, 1H), 9.14 (br. s., 1H), 8.77 (d, $J = 2.34$ Hz, 1H), 8.53 (s, 1H), 7.86 - 7.99 (m, 1H), 7.56 (d, $J = 8.20$ Hz, 2H), 7.33 (t, $J = 7.81$ Hz, 2H), 7.11 (t, $J = 7.42$ Hz, 1H), 3.44 (t, $J = 6.64$ Hz, 1H), 3.11 (s, 2H), 2.95 (d, $J = 11.72$ Hz, 2H), 2.26 (t, $J = 10.74$ Hz, 2H), 1.84 (d, $J = 12.11$ Hz, 2H), 1.69 (ddd, $J = 3.91, 7.32, 11.03$ Hz, 2H), 1.39 - 1.49 (m, 2H); ^{13}C NMR (100 MHz, CDCl_3) δ ppm 168.64, 163.27, 147.50, 144.62, 144.45, 142.63, 137.71, 129.17, 124.32, 119.55, 62.45, 54.96, 44.85, 35.93, 30.48; MS (ESI) $m/z = 354.3(\text{M}+\text{H})^+$.

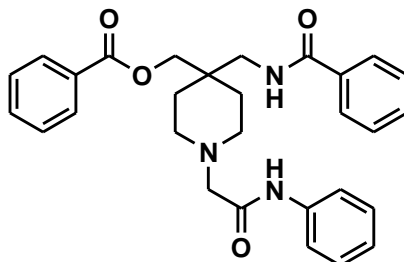
2-(4-((2-Oxo-2-(1H-pyrrol-2-yl)ethylamino)methyl)piperidin-1-yl)-*N*-phenylacetamide (**1-4**)



1-4

A mixture of 2-(4-(aminomethyl)piperidin-1-yl)-*N*-phenylacetamide (**1-14**) (0.10 g, 0.40 mmol), 2-chloroacetyl pyrrole (**1-16**) (0.04 g, 0.28 mmol), and sodium bicarbonate (0.11 g, 0.40 mmol) in a mixture of 20:1 distilled acetonitrile:DMF (5 mL) was heated to heated at 50 °C under argon for 8 hours. The resulting mixture was cooled and filtered to remove potassium carbonate. The filtrate was concentrated and column chromatographed on silica gel using a gradient mixture of dichloromethane and methanol (30:1) as eluent to give 2-(4-((2-oxo-2-(1H-pyrrol-2-yl)ethylamino)methyl)piperidin-1-yl)-*N*-phenylacetamide (**1-4**) (0.056 g, 56 % yield) as a red solid. ^1H NMR (400 MHz, CDCl_3) δ ppm 9.96 (br. S., 1H), 9.19 (br. s., 1H), 7.53 (d, $J = 1.00$ Hz, 2H), 7.33 (t, $J = 1.00$ Hz, 2H), 7.10 (t, $J = 7.42$ Hz, 1H), 7.06 (br. S., 1H), 6.93 (d, $J = 3.51$ Hz, 1H), 6.27 (dd, $J = 1.00$ Hz, 1H), 3.89 (s, 2H), 3.18 (s, 2H), 2.90 (d, $J = 11.33$ Hz, 2H), 2.64 (d, $J = 6.64$ Hz, 2H), 2.38 (s, 1H), 2.23 (t, $J = 10.74$ Hz, 2H), 1.84 (d, $J = 11.72$ Hz, 2H), 1.62 (br. S, 1H), 1.13 - 1.47 (m, 2H); ^{13}C NMR (100 MHz, CDCl_3) δ ppm 188.59, 169.07, 137.85, 130.62, 129.21 (2C), 124.89, 124.31, 119.61 (2C), 116.03, 111.03, 62.59, 55.88, 55.00, 54.31 (2C), 35.98, 31.04 (2C); MS (ESI) $m/z = 355.4(\text{M}+\text{H})^+$, 377.5 ($\text{M}+\text{Na}$) $^+$.

(4-(Benzamidomethyl)-1-(2-oxo-2-(phenylamino)ethyl)piperidin-4-yl)methyl benzoate (**1-9**)



1-9

Step A:

To a solution of 4-cyanopiperidine (**1-11**) (0.5 g, 4.54 mmol) in 25 mL of distilled dichloromethane under argon, distilled triethylamine (1.3 mL, 9.08 mmol) was added. While stirring, the solution was cooled to 0 °C and di-*tert*-butyl dicarbonate (1.19 g, 5.4 mmol) was added in several portions over 15 min (bubbling observed). The resulting mixture was stirred at 25 °C for 12 h, then solvent was evaporated and the residue was purified by column chromatography on silica gel using a mixture of dichloromethane and methanol (30: 1) as an eluent to give *tert*-butyl 4-cyanopiperidine-1-carboxylate (**1-20**), 0.95 g (100% yield) as a colorless thick oil, that solidifies on standing. ¹H NMR (400 MHz, CDCl₃) δ ppm 3.64 (ddd, *J* = 3.91, 7.03, 13.67 Hz, 2H), 3.31 (ddd, *J* = 3.71, 7.81, 13.86 Hz, 2H), 2.73 - 2.83 (m, 1H), 1.82 - 1.92 (m, 2H), 1.72 - 1.82 (m, 2H), 1.44 (s, 9H); ¹³C NMR (100 MHz, CDCl₃) δ ppm 153.57, 120.48, 78.99, 40.77, 27.76, 27.65, 25.45.

Step B:

A solution of *tert*-butyl 4-cyanopiperidine-1-carboxylate (**1-20**) (0.95 g, 4.54 mmol) was dissolved in 25 mL of dry Tetrahydrofuran (THF) and cooled to -78 °C. Lithium diisopropylamide (LDA) (0.23 M in 20 mL, 4.54 mmol) was slowly added to the reaction over 30 min at -78 °C under argon. A pale brown solution was obtained. Stirring continued for 2 h at -78 °C, and a solution of paraformaldehyde (0.16 g, 5.4 mmol) in 25 mL of freshly distilled THF

was added slowly into the reaction solution while keeping the temperature at -78 °C. The reaction mixture was allowed to reach room temperature while stirred for 15 h under argon. The reaction mixture was diluted in 100 mL of water, saturated NaCl (50 mL) was added, and extracted with dichloromethane three times (250 mL each). The combined organic layers were washed with brine (100 mL), dried (Na₂SO₄), concentrated, and column chromatographed on silica gel using a gradient mixture of hexane and ethyl acetate as eluent to give *tert*-butyl 4-cyano-4-(hydroxymethyl)piperidine-1-carboxylate (**1-21**), 0.78 g (72% yield) as a white solid. ¹H NMR (400 MHz, CDCl₃) δ ppm 4.10 - 4.24 (m, 2H), 3.67 (d, *J* = 6.25 Hz, 2H), 2.03 - 2.11 (m, 2H), 1.91 - 2.00 (m, 2H), 1.60 (s, 1H), 1.46 (s, 9H); ¹³C NMR (100 MHz, CDCl₃) δ ppm 154.38, 121.41, 80.05, 67.40, 40.55, 40.03, 30.82, 28.13; MS (ESI) *m/z* = 263.5 (M+Na)⁺.

Step C:

To a solution of *tert*-butyl 4-cyano-4-(hydroxymethyl)piperidine-1-carboxylate (**1-21**) (0.49 g, 2.0 mmol) in dichloromethane (8 mL), pyridine (0.24 mL, 3.03 mmol) was added and the mixture was stirred at 0 °C. Benzoyl chloride (0.25 mL, 2.0 mmol) was added and the reaction mixture was stirred for 8 h at rt. The reaction mixture was partitioned between dichloromethane and water and basified to pH 8 using NaHCO₃. The organic layer was separated, and the aqueous layer was extracted three times with dichloromethane. The combined organic layers were washed with brine (10 mL), dried (Na₂SO₄), filtered, concentrated, and purified by column chromatography on silica gel using a mixture of dichloromethane and methanol (30:1) to obtain 0.21 g (86% yield) of *tert*-butyl 4-((benzoyloxy)methyl)-4-cyanopiperidine-1-carboxylate (**1-22**), as a yellow solid. ¹H NMR (400 MHz, CDCl₃) δ ppm 7.88 - 8.04 (m, 2H), 6.81 - 6.95 (m, 2H), 6.41 (s, 1H), 4.33 (s, 2H), 4.17 (d, *J* = 16.40 Hz, 2H), 3.10 (br. s., 2H), 2.01 (br. s., 2H), 1.53 - 1.61 (m, 2H), 1.47 (s, 9H); ¹³C NMR (100 MHz, CDCl₃) δ ppm 165.61, 160.96, 154.66, 132.33, 121.31, 120.50, 115.60, 80.74, 68.08, 38.78, 31.80, 28.52, 28.50; MS (ESI) *m/z* = 367.0 (M+Na)⁺.

Step D:

A solution of 4-((benzoyloxy)methyl)-4-cyanopiperidine-1-carboxylate (**1-22**) (1.12 mmol) in 2 mL dichloromethane containing 10% trifluoroacetic acid (TFA) was stirred at room temperature for 1 h. The solvent was removed and the remaining solid was kept under high

vacuum to yield 0.27 g (>95% yield) of (4-cyanopiperidin-4-yl)methyl benzoate (**1-23**) as a yellow solid. ¹H NMR (400 MHz, DMSO-*d*₆) δ ppm 8.02 (d, *J* = 7.42 Hz, 2H), 7.71 (t, *J* = 7.42 Hz, 1H), 7.57 (t, *J* = 7.62 Hz, 2H), 4.49 (s, 2H), 3.46-3.48 (m, 2H), 3.02 (t, *J* = 12.11 Hz, 2H), 2.28 (d, *J* = 14.45 Hz, 2H), 1.92 - 2.02 (m, 2H); ¹³C NMR (100 MHz, DMSO-*d*₆) δ ppm 165.14, 134.00, 129.51, 129.04, 128.94, 120.34, 67.24, 40.32, 36.72, 27.75.

Step E:

To a solution of (4-cyanopiperidin-4-yl)methyl benzoate (**1-23**) (0.10 g, 0.41 mmol) in dry CH₃CN, *N*-(chloromethyl)-benzamide (**1-12**) (57 mg, 0.41 mmol) and anhydrous K₂CO₃ (0.17 g, 1.23 mmol) were added and refluxed at 85°C for 12 h. The reaction mixture was filtered and evaporated to yield a yellow oil that was purified by column chromatography on silica gel using a mixture of dichloromethane and methanol (30: 1) as eluent to give (4-cyano-1-(2-oxo-2-(phenylamino)ethyl)piperidin-4-yl)methyl benzoate (**1-24**), 0.15 g (97% yield). ¹H NMR (400 MHz, CDCl₃) δ ppm 8.88 (br. s., 1H), 8.04 - 8.12 (m, 2H), 7.58 - 7.64 (m, 1H), 7.52 - 7.57 (m, 2H), 7.44 - 7.51 (m, 2H), 7.28 - 7.36 (m, 2H), 7.08 - 7.14 (m, 1H), 4.40 (s, 2H), 3.21 (s, 2H), 2.98 (d, *J* = 12.50 Hz, 2H), 2.69 (dt, *J* = 2.34, 12.30 Hz, 2H), 2.13 (d, *J* = 13.28 Hz, 2H), 1.77 - 1.86 (m, 2H); ¹³C NMR (100 MHz, CDCl₃) δ ppm 167.80, 165.85, 137.42, 133.75, 129.85, 129.13, 128.69, 124.49, 120.51, 119.60, 68.34, 61.98, 50.28, 37.71, 32.17; MS (ESI) *m/z* = 378.5 (M+H)⁺.

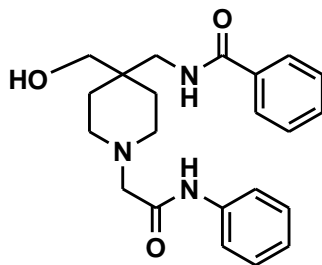
Step F:

To a solution of (4-cyano-1-(2-oxo-2-(phenylamino)ethyl)piperidin-4-yl)methyl benzoate (**1-24**) (0.16 g, 0.42 mmol) in 5 mL of methanol, CoCl₂·6H₂O (51 mg 0.21 mmol) was added and stirred. The reaction mixture was cooled to 0°C and sodium borohydride (86 mg, 2.27 mmol) was added in several portions over 30 min. The resulting solution was stirred for 18 h at 25 °C, diluted with 15 mL of cold saturated NH₄Cl, 15 mL of water and extracted three times with ethyl acetate. The combined organic layers were washed with brine (10 mL), dried (Na₂SO₄), filtered, and concentrated to yield 0.13 g (78% yield) of (4-(aminomethyl)-1-(2-oxo-2-(phenylamino)ethyl)piperidin-4-yl)methyl benzoate (**1-25**), as a white solid. MS (ESI) *m/z* = 382.2 (M+H)⁺.

Step G:

To a solution of (4-(aminomethyl)-1-(2-oxo-2-(phenylamino)ethyl)piperidin-4-yl)methyl benzoate (**1-25**) (50 mg, 0.13 mmol) in dichloromethane (5 mL) was added dry pyridine (19 μ L, 0.24 mmol) and the mixture was stirred at 0 °C. To the reaction solution, benzoyl chloride (19 μ L, 0.16 mmol) was added and the mixture was stirred for 3 h at room temperature. The reaction mixture was partitioned between dichloromethane and water, and basified to pH 8 using NaHCO_3 . The organic layer was separated, and the aqueous layer was extracted three times with dichloromethane. The combined organic layers were washed with brine (10 mL), dried (Na_2SO_4), filtered, concentrated, and purified by column chromatography on silica gel using a mixture of dichloromethane and MeOH (30:1) as eluent to obtain 48 mg (75% yield) of (4-(benzamidomethyl)-1-(2-oxo-2-(phenylamino)ethyl)piperidin-4-yl)methyl benzoate (**1-9**), as a white solid. ^1H NMR (400 MHz, CDCl_3) δ ppm 9.30 (br. s., 1H), 8.68 (br. s., 1H), 8.11 (d, J = 8.20 Hz, 2H), 8.07 (d, J = 8.20 Hz, 2H), 7.87 (d, J = 8.20 Hz, 2H), 7.57 - 7.60 (m, 2H), 7.44 - 7.49 (m, 4H), 7.33 (t, J = 7.62 Hz, 2H), 7.08 - 7.14 (m, 1H), 3.53 (d, J = 5.86 Hz, 2H), 3.26 (s, 2H), 2.84 (dd, J = 4.30, 5.86 Hz, 2H), 2.71 - 2.79 (m, J = 10.54 Hz, 2H), 1.67 - 1.85 (m, 4H); ^{13}C NMR (100 MHz, CDCl_3) δ ppm 168.11, 167.58, 167.39, 137.53, 133.65, 133.23, 131.64, 130.04, 129.77, 128.99, 128.64, 128.35, 126.98, 124.24, 119.56, 68.40, 62.06, 49.46, 42.12, 37.00, 30.58; MS (ESI) m/z = 486.2 ($\text{M}+\text{H}$) $^+$.

N-((4-(Hydroxymethyl)-1-(2-oxo-2-(phenylamino)ethyl)piperidin-4-yl)methyl)benzamide (**1-6**)



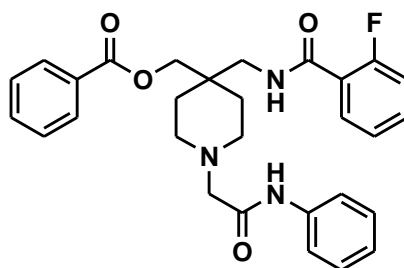
1-6

To a solution of (4-(benzamidomethyl)-1-(2-oxo-2-(phenylamino)ethyl)piperidin-4-yl)methyl benzoate (**1-9**) (45 mg, 0.09 mmol) in methanol, K_2CO_3 (130 mg, 0.93 mmol) was

added and stirred for 2h at 25 °C. The reaction mixture was filtered and purified by column chromatography on silica gel using dichloromethane: methanol (30:1) as eluent to give compound

N-((4-(hydroxymethyl)-1-(2-oxo-2-(phenylamino)ethyl)piperidin-4-yl)methyl)benzamide (**1-6**), 25 mg (71% yield) as a white solid. ¹H NMR (400 MHz, CDCl₃) δ ppm 8.96 (br. s., 1H), 7.76 - 7.85 (m, 1H), 7.51 - 7.62 (m, 3H), 7.42 - 7.50 (m, 2H), 7.34 (t, *J* = 8.01 Hz, 3H), 7.13 (t, *J* = 7.42 Hz, 1H), 3.72 (s, 2H), 3.67 (s, 2H), 3.22 (s, 2H), 2.63 (dt, *J* = 1.95, 12.30 Hz, 2H), 2.34 (t, *J* = 7.42 Hz, 1H), 2.06 (d, *J* = 12.89 Hz, 2H), 1.63 - 1.73 (m, 4H) ; MS (ESI) *m/z* = 382.2 (M+H)⁺.

(4-((2-Fluorobenzamido)methyl)-1-(2-oxo-2-(phenylamino)ethyl)piperidin-4-yl)methyl benzoate
(**1-10**)

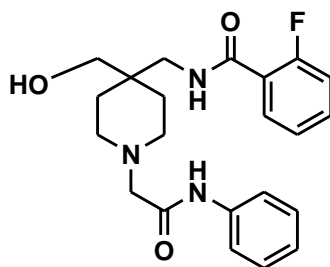


1-10

To a solution of (4-(aminomethyl)-1-(2-oxo-2-(phenylamino)ethyl)piperidin-4-yl)methyl benzoate (**1-25**) (50 mg, 0.13 mmol) in dist. dichloromethane (5 mL) was added dry pyridine (19 μL, 0.17 mmol) and stirred at 0 °C. To the reaction mixture, 2-Fluorobenzoyl chloride (27mg, 0.17 mmol) was added and stirred for 3 h at room temperature. The reaction mixture was partitioned between dichloromethane and water, and basified to pH 8 using NaHCO₃. The organic layer was removed and the aqueous layer was extracted three times with dichloromethane. The combined organic layers were washed with brine (10 mL) and dried (Na₂SO₄), filtered, concentrated and purified by column chromatography on silica gel using a mixture of dichloromethane and methanol (30:1) as eluent to obtained 48 mg (69% yield) of (4-(benzamidomethyl)-1-(2-oxo-2-(phenylamino)ethyl)piperidin-4-yl)methyl benzoate (**1-10**), as a white solid. ¹H NMR (400 MHz, CDCl₃) δ ppm 9.68 (br. s., 1H), 7.97 - 8.04 (m, 2H), 7.83 (d, *J*

= 7.42 Hz, 2H), 7.60 (d, J = 7.81 Hz, 2H), 7.52 (d, J = 6.64 Hz, 2H), 7.41 - 7.47 (m, 2H), 7.29 - 7.36 (m, 2H), 7.12 - 7.17 (m, 2H), 6.10 (br. s., 1H), 4.41 (s, 2H), 3.62 (d, J = 5.86 Hz, 2H), 3.48 (s, 2H), 2.92 - 3.08 (m, 4H), 1.85 (m, 4H); ^{13}C NMR (101 MHz, CDCl_3) δ ppm 167.94, 166.64, 165.24, 163.57, 137.55, 135.15, 134.59, 132.56, 132.34, 131.67, 128.94, 128.61, 126.99, 124.36, 123.95, 119.74, 117.01, 69.20, 61.52, 49.23, 42.27, 36.54, 29.72; MS (ESI) m/z = 504.2 ($\text{M}+\text{H}$) $^+$. 2-Fluoro-*N*-((4-(hydroxymethyl)-1-(2-oxo-2-(phenylamino)ethyl)piperidin-4-yl)methyl)benzamid

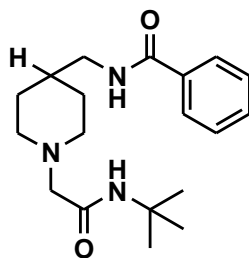
e (**1-7**)



1-7

To a solution of (4-(benzamidomethyl)-1-(2-oxo-2-(phenylamino)ethyl)piperidin-4-yl)methyl benzoate (**1-10**) (30 mg, 0.06 mmol) in methanol, K_2CO_3 (83 mg, 0.6 mmol) was added and stirred for 2h at 25 °C. The reaction mixture was filtered and purified by column chromatography on silica gel using dichloromethane:methanol (30:1) as eluent to give compound *N*-((4-(hydroxymethyl)-1-(2-oxo-2-(phenylamino)ethyl)piperidin-4-yl)methyl)benzamide (**1-7**), 13 mg (55% yield) as a white solid. ^1H NMR (400 MHz, CDCl_3) δ ppm 9.11 (br. s., 1H), 7.78 (d, J = 7.81 Hz, 1H), 7.56 (d, J = 7.81 Hz, 2H), 7.41 - 7.48 (m, 2H), 7.33 (t, J = 7.81 Hz, 2H), 7.08 - 7.22 (m, 1H), 6.78 (d, J = 5.47 Hz, 1H), 3.49 (d, J = 6.25 Hz, 2H), 3.46 (s, 2H), 3.14 (s, 2H), 2.61 (dd, J = 7.03, 11.33 Hz, 4H), 1.60 - 1.68 (m, 4H); ^{13}C NMR (100 MHz, CDCl_3) δ ppm 169.11, 168.47, 137.50, 133.73, 131.93, 129.04, 128.72, 126.96, 124.27, 119.50, 65.83, 62.31, 49.74, 37.00, 30.91; MS (ESI) m/z = 400.0 ($\text{M}+\text{H}$) $^+$.

N-((1-(2-(*tert*-Butylamino)-2-oxoethyl)piperidin-4-yl)methyl)benzamide (**1-8**)



1-8

Step A:

A mixture of 4-cyano piperidine (**1-11**) (1 g, 9.1 mmol), *N*-*tert*-butyl-2- chloroacetamide (**1-26**) (1.35 g, 9.1 mmol), and potassium carbonate (2.5 g, 18.2 mmol) in acetonitrile (30 mL) was heated to reflux under argon for 9 hours. The resulting mixture was cooled and filtered to remove potassium carbonate. The filtrate was concentrated and crystallized from ethyl ether to give *N*-*tert*-butyl-2-(4-cyanopiperidin-1-yl)acetamide (**1-27**) (1.82 g, 90 % yield) as a white solid. ^1H NMR (400 MHz, CDCl_3) δ ppm 2.89 (s, 2H), 2.68 - 2.78 (m, 2H), 2.31 - 2.44 (m, 2H), 1.93 - 2.03 (m, 2H), 1.81 - 1.93 (m, 2H), 1.35 (s, 9H); ^{13}C NMR (100 MHz, CDCl_3) δ ppm 168.88, 121.47, 62.50, 51.82, 50.61, 29.10, 28.85, 25.72; MS (ESI) m/z = 346.3 ($\text{M}+\text{Na}$) $^+$.

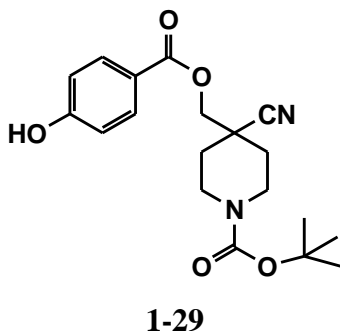
Step B:

To a cold solution of *N*-*tert*-butyl-2-(4-cyanopiperidin-1-yl)acetamide (**1-27**) (0.7 g, 3.1 mmol) and MeOH (20 mL), cobalt (II) chloride hexahydrate (0.37 g, 1.6 mmol) was added followed by the addition of sodium borohydride (0.53 g, 14.1 mmol). After stirring for 15 hours at 25 °C, the reaction solution was diluted with 25 mL of 5% aqueous ammonium hydroxide and extracted three times with dichloromethane. The combined organic layer was washed with brine, dried over anhydrous Na_2SO_4 and concentrated to give 2-(4-(aminomethyl)piperidin-1-yl)-*N*-(*tert*-butyl)acetamide (**1-28**) (0.65 g, 90% yield) as a crude product, which was used in the next step without further purification. ^1H NMR (400 MHz, CDCl_3) δ ppm 7.07 (br. s., 1H), 2.86 (s, 2H), 2.81 (br. s., 1H), 2.61 (d, J = 6.25 Hz, 1H), 2.12 (t, J = 11.13 Hz, 2H), 1.74 (d, J = 11.72 Hz, 2H), 1.35 (s, 9H), 1.17 - 1.25 (m, 2H) ; MS (ESI) m/z = 228.3 ($\text{M}+\text{H}$) $^+$.

Step C:

To a cold solution of 0.20 g (0.88 mmol) of 2-(4-(aminomethyl)piperidin-1-yl)-*N*-(*tert*-butyl)acetamide in freshly distilled dichloromethane under argon, pyridine (1.3 mmol) was added followed by the addition of 0.12 g (0.88 mmol) of benzoyl chloride. The reaction was stirred at 0 °C for 30 min. and 25 °C for 2 hours. The reaction solution was diluted with 20 mL of aqueous sodium bicarbonate and extracted three times with dichloromethane. The combined organic layer was washed with brine, dried (anhydrous Na₂SO₄), concentrated, and column chromatographed on silica gel using a mixture of dichloromethane and methanol (10: 1) as eluent to give *N*-((1-(2-(*tert*-butylamino)-2-oxoethyl)piperidin-4-yl)methyl)benzamide (**1-8**) (0.15 g, 51% yield) as a white solid. ¹H MR (400 MHz, CDCl₃) δ = 7.77 (d, J= 7.4 Hz, 2H), 7.49 (t, 1H), 7.45 (t, 2H), 7.1 (s, 1H), 6.38 (br. s., 1H), 3.37 (t, J= 6.4 Hz, 2H), 2.79 - 2.90 (m, 6H), 2.12 (t, J= 11.3 Hz, 2H), 1.77 (d, J= 12.5 Hz, 2H), 1.55-1.67 (m, 1H), 1.36 (s, 9H). MS (ESI) m/z = 354 (M+Na)⁺.

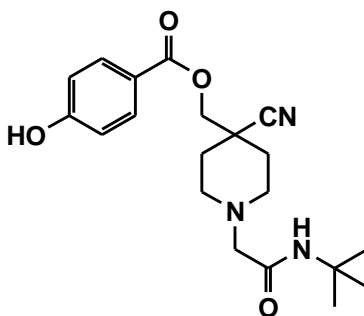
Tert-Butyl 4-cyano-4-((4-hydroxybenzoyloxy)methyl)piperidine-1-carboxylate (**1-29**)



To a solution of *tert*-butyl 4-cyano-4-(hydroxymethyl)piperidine-1-carboxylate (**1-21**) (0.025 g, 0.104 mmol), EDC (0.025 g, 0.208 mmol) and DMAP (0.030 g, 0.156 mmol) in dichloromethane (10 mL), a mixture of (4-(*tert*-butyldimethylsilyloxy)phenyl)(1H-imidazol-1-yl)methanone (**1-15**) 0.038 g (0.125 mmol) in dist. DMF (1 mL) was added. The reaction mixture was stirred under argon at 25 °C for 28 h. The reaction solution was diluted with 50 mL of dichloromethane and neutralized to pH 7 using 10% hydrochloric acid solution. Aqueous layer was extracted three times with dichloromethane. The combined organic layer was washed with brine, dried (anhydrous Na₂SO₄), concentrated, and column chromatographed on silica gel using a mixture of dichloromethane and methanol (30: 1) as eluent to give *tert*-butyl 4-cyano-4-((4-

hydroxybenzoyloxy)methyl)piperidine-1-carboxylate (**1-29**) (0.21 g, 56.3%) as a white solid. ^1H NMR (400 MHz, CDCl_3) δ ppm 7.90 (d, $J = 8.59$ Hz, 2H), 6.86 (d, $J = 8.59$ Hz, 2H), 4.28 (s, 2H), 3.58-3.61 (m, 4H), 1.96 - 2.01 (m, 2H), 1.54 – 1.58 (m, 2H), 1.42 (s, 9H); ^{13}C NMR (100 MHz, CDCl_3) δ ppm 165.89, 162.23, 154.68, 132.29, 121.72, 120.44, 115.72, 80.43, 68.13, 41.09, 28.59, 25.95, 25.82.

(1-(2-(*tert*-Butylamino)-2-oxoethyl)-4-cyanopiperidin-4-yl)methyl 4-hydroxybenzoate (**1-30**)



1-30

Step A:

A solution of *tert*-butyl 4-cyano-4-(hydroxymethyl)piperidine-1-carboxylate (**1-21**) (0.02 g, 0.06 mmol), in 2 mL dichloromethane containing 10% trifluoroacetic acid (TFA) was stirred at room temperature for 1 h. The solvent was removed and the remaining solid was kept under high vacuum to yield 0.014 g (>95% yield) of 4-(hydroxymethyl)piperidine-4-carbonitrile (**1-33**) as a yellow solid.

Step B:

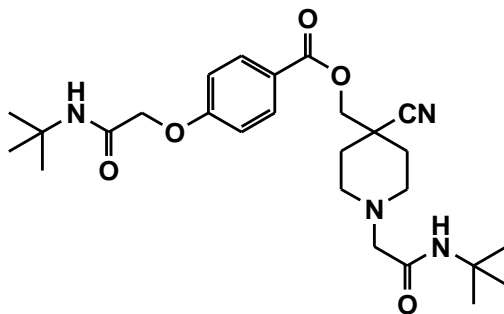
To a solution of 4-(hydroxymethyl)piperidine-4-carbonitrile (**1-33**) (0.07 g, 0.48 mmol), and potassium carbonate (0.13 g, 0.95 mmol) in acetonitrile (10 mL), *N*-*tert*-butyl-2-chloroacetamide (**1-26**) (0.85 g, 0.57 mmol), was heated to reflux under argon for 9 hours. The resulting mixture was cooled and filtered to remove potassium carbonate. The filtrate was concentrated and column chromatographed on silica gel using a mixture of dichloromethane and methanol (30:1) as eluent to give *N*-*tert*-butyl-2-(4-cyano-4-(hydroxymethyl)piperidin-1-

yl)acetamide (**1-34**) (0.10 g, 83.3 % yield) as a white solid. ¹H NMR (400 MHz, CDCl₃) δ ppm 6.91 (br. s., 1H), 3.62 (s, 2H), 2.90 (s, 2H), 2.80 (d, *J* = 12.11 Hz, 2H), 2.41 - 2.49 (m, 2H), 1.95 (d, *J* = 12.11 Hz, 2H), 1.56 (dt, *J* = 3.51, 12.89 Hz, 2H), 1.33 (br. s., 1H), 1.30 (s, 9H); MS (ESI) *m/z* = 254.2 (M+H)⁺, 276.2 (M+Na)⁺.

Step C:

To a solution of 0.09 g (0.38 mmol) of *N-tert*-butyl-2-(4-cyano-4-(hydroxymethyl)piperidin-1-yl)acetamide (**1-34**) in distilled DMF under argon, (4-(*tert*-butyldimethylsilyloxy)phenyl)(1H-imidazol-1-yl)methanone (**1-15**) 0.86 g (0.28 mmol) was added. The reaction mixture was refluxed at 110 °C for 24 h. The reaction solution was diluted with 20 mL of aqueous sodium bicarbonate and extracted three times with dichloromethane. The combined organic layer was washed with brine, dried (anhydrous Na₂SO₄), concentrated, and column chromatographed on silica gel using a mixture of dichloromethane and methanol (30: 1) as eluent to give (1-(2-(*tert*-butylamino)-2-oxoethyl)-4-cyanopiperidin-4-yl)methyl 4-hydroxybenzoate (**1-30**) (11 mg, 47.4%) as a white solid. ¹H NMR (400 MHz, CDCl₃) δ ppm 7.87 - 7.99 (m, 2H), 6.91 (br. s., 1H), 6.83 - 6.89 (d, *J* = 8.59 Hz, 2H), 4.34 (s, 2H), 2.98 (s, 2H), 2.86 (d, *J* = 9.76 Hz, 2H), 2.49 - 2.59 (m, 2H), 2.04 - 2.11 (m, 2H), 1.67 (m, 2H), 1.36 (s, 9H).

(1-(2-(*tert*-Butylamino)-2-oxoethyl)-4-cyanopiperidin-4-yl)methyl-4-(2-(*tert*-butylamino)-2-oxoethoxy)benzoate (**1-31**)



1-31

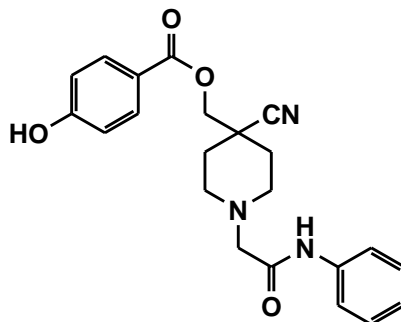
Step A:

A solution of *tert*-butyl 4-cyano-4-((4-hydroxybenzoyloxy)methyl)piperidine-1-carboxylate (**1-29**) (0.076 g, 0.21 mmol), in 2 mL dichloromethane containing 10% trifluoroacetic acid (TFA) was stirred at room temperature for 1 h. The solvent was removed and the remaining solid was kept under high vacuum to yield 0.054 g (>95% yield) of (4-cyanopiperidin-4-yl)methyl 4-hydroxybenzoate (**1-35**) as a yellow solid.

Step B:

To a solution of (4-cyanopiperidin-4-yl)methyl 4-hydroxybenzoate (**1-35**) (0.025 g, 0.096 mmol), and potassium carbonate (0.03 g, 0.23 mmol) in acetonitrile (10 mL), *N-tert*-butyl-2-chloroacetamide (**1-26**) (0.017 g, 0.12 mmol), was heated to reflux under argon for 9 hours. The resulting mixture was cooled and filtered to remove potassium carbonate. The filtrate was concentrated and column chromatographed on silica gel using a mixture of dichloromethane and methanol (30:1) as eluent to give (1-(2-(*tert*-butylamino)-2-oxoethyl)-4-cyanopiperidin-4-yl)methyl-4-(2-(*tert*-butylamino)-2-oxoethoxy)benzoate (**1-31**) (0.019 g, 84.3 % yield) as a white solid. ¹H NMR (400 MHz, CDCl₃) δ ppm 8.05 (d, *J* = 8.98 Hz, 2H), 6.96 (d, *J* = 8.59 Hz, 2H), 6.80 (br. s., 1H), 6.28 (br. s., 1H), 4.42 (s, 2H), 4.35 (s, 2H), 2.97 (s, 2H), 2.84 - 2.91 (m, 2H), 2.55 (t, *J* = 11.33 Hz, 2H), 2.09 (d, *J* = 12.89 Hz, 2H), 1.68 (dt, *J* = 3.71, 12.79 Hz, 2H), 1.39 (s, 9H), 1.34 (s, 9H); ¹³C NMR (100 MHz, CDCl₃) δ ppm 168.8, 166.4, 165.3, 161.3, 132.2, 122.8, 120.7, 114.7, 68.4, 67.6, 62.2, 51.6, 50.7, 50.1, 37.8, 32.2, 28.9, 28.8; MS (ESI) *m/z* = 487.3 (M+H)⁺, 509.3 (M+Na)⁺.

(4-Cyano-1-(2-oxo-2-(phenylamino)ethyl)piperidin-4-yl)methyl 4-hydroxybenzoate (**1-32**)



1-32

Step A:

To a solution of (4-cyanopiperidin-4-yl)methyl 4-hydroxybenzoate (**1-35**) (0.067 g, 0.47 mmol), and potassium carbonate (0.13 g, 0.95 mmol) in acetonitrile (10 mL), *N*-(chloromethyl)benzamide (0.097 g, 0.57 mmol), was heated to reflux under argon for 8 hours. The resulting mixture was cooled and filtered to remove potassium carbonate. The filtrate was concentrated and column chromatographed on silica gel using a mixture of dichloromethane and methanol (30:1) as eluent to give 2-(4-cyano-4-(hydroxymethyl)piperidin-1-yl)-*N*-phenylacetamide (**1-36**) (0.11 g, 82.7 % yield) as a white solid. ¹H NMR (400 MHz, CDCl₃) δ ppm 8.93 (br. s., 1H), 7.50 - 7.59 (m, 2H), 7.34 (t, *J* = 8.01 Hz, 2H), 7.08 - 7.16 (m, 1H), 4.22 (s, 1H), 3.70 (s, 2H), 3.20 (s, 2H), 2.96 (d, *J* = 12.50 Hz, 2H), 2.62 (dt, *J* = 1.95, 12.30 Hz, 2H), 2.05 (d, *J* = 13.28 Hz, 2H), 1.68 (dt, *J* = 3.51, 12.89 Hz, 2H); MS (ESI) *m/z* = 274.3 (M+H)⁺, 296.0 (M+Na)⁺.

Step B:

To a solution of 0.088 g (0.38 mmol) of *N*-*tert*-butyl-2-(4-cyano-4-(hydroxymethyl)piperidin-1-yl)acetamide (**1-34**) in distilled DMF under argon, (4-(*tert*-butyldimethylsilyloxy)phenyl)(1H-imidazol-1-yl)methanone (**1-15**) 0.117 g (0.28 mmol) was added. The reaction mixture was refluxed at 85 °C for 24 h. The reaction solution was diluted with 20 mL of aqueous sodium bicarbonate and extracted three times with dichloromethane. The combined organic layer was washed with brine, dried (anhydrous Na₂SO₄), concentrated, and column chromatographed on silica gel using a mixture of dichloromethane and methanol (30: 1) as eluent to give (4-cyano-1-(2-oxo-2-(phenylamino)ethyl)piperidin-4-yl)methyl 4-hydroxybenzoate (**1-32**) (26 mg, 41.1% calculated based on recovered starting material) as a white solid. ¹H NMR (400 MHz, CDCl₃) δ ppm 7.97 (d, *J* = 8.59 Hz, 2H), 7.54 (d, *J* = 7.42 Hz, 2H), 7.34 (t, *J* = 7.81 Hz, 2H), 7.10 - 7.17 (m, 1H), 6.91 (d, *J* = 8.59 Hz, 2H), 4.37 (s, 2H), 3.23 (s, 2H), 2.95 - 3.02 (m, 2H), 2.68 (t, *J* = 11.33 Hz, 2H), 2.14 (d, *J* = 12.89 Hz, 2H), 1.73 - 1.83 (m, 1H); MS (ESI) *m/z* = 394.5 (M+H)⁺.

1.7 References

- (1) Kaushik, N. K.; Kaushik, N.; Attri, P.; Kumar, N.; Kim, C. H.; Verma, A. K.; Choi, E. H. Biomedical importance of indoles. *Molecules* **2013**, *18*, 6620-6662.
- (2) Chia, Y.-Y.; Liu, K.; Wang, J.-J.; Kuo, M.-C.; Ho, S.-T. Intraoperative high dose fentanyl induces postoperative fentanyl tolerance. *Canadian journal of anesthesia* **1999**, *46*, 872.
- (3) Howland, K. L.; Roland, K. 1-alkylpiperidyl-4-benzhydryl ethers, acid salts thereof and their preparation US 2479843 A.
- (4) Madersbacher, H.; Mürtz, G. Efficacy, tolerability and safety profile of propiverine in the treatment of the overactive bladder (non-neurogenic and neurogenic). *World journal of urology* **2001**, *19*, 324-335.
- (5) Rogers, S. L.; Friedhoff, L. T. The efficacy and safety of donepezil in patients with Alzheimer's disease: results of a US multicentre, randomized, double-blind, placebo-controlled trial. *Dementia and Geriatric Cognitive Disorders* **1996**, *7*, 293-303.
- (6) Schotte, A.; Janssen, P.; Gommeren, W.; Luyten, W.; Van Gompel, P.; Lesage, A.; De Loore, K.; Leysen, J. Risperidone compared with new and reference antipsychotic drugs: in vitro and in vivo receptor binding. *psychopharmacology* **1996**, *124*, 57-73.
- (7) Weis, R.; Kungl, A. J.; Seebacher, W. Synthesis of new analogues of diphenylpyraline. *Tetrahedron* **2003**, *59*, 1403-1411.
- (8) Draper, M. W.; Flowers, D. E.; Neild, J. A.; Muster, W. J.; Zerbe, R. L. Antiestrogenic properties of raloxifene. *Pharmacology* **1995**, *50*, 209-217.
- (9) Baumann, M.; Baxendale, I. R. An overview of the synthetic routes to the best selling drugs containing 6-membered heterocycles. *Beilstein journal of organic chemistry* **2013**, *9*, 2265.
- (10) Watson, P. S.; Jiang, B.; Scott, B. A diastereoselective synthesis of 2, 4-disubstituted piperidines: scaffolds for drug discovery. *Organic letters* **2000**, *2*, 3679-3681.
- (11) Choi, K.-H. The design and discovery of T-type calcium channel inhibitors for the treatment of central nervous system disorders. *Expert opinion on drug discovery* **2013**, *8*, 919-931.
- (12) Cain, S. M.; Hildebrand, M. E.; Snutch, T. P.: T-Type Calcium Channels and Epilepsy. In *Pathologies of Calcium Channels*; Springer, 2014; pp 77-96.
- (13) Powell, K. L.; Cain, S. M.; Snutch, T. P.; O'brien, T. J. Low threshold T-type calcium channels as targets for novel epilepsy treatments. *British journal of clinical pharmacology* **2014**, *77*, 729-739.
- (14) Magrinelli, F.; Zanette, G.; Tamburin, S. Neuropathic pain: diagnosis and treatment. *Practical neurology* **2013**, *13*, 262-307.
- (15) Vranken, J. H. Mechanisms and treatment of neuropathic pain. *Central Nervous System Agents in Medicinal Chemistry (Formerly Current Medicinal Chemistry-Central Nervous System Agents)* **2009**, *9*, 71-78.
- (16) Amarelle, L.; Lecuona, E.; Sznajder, J. I. Anti-influenza treatment: Drugs currently used and under development. *Archivos de Bronconeumología (English Edition)* **2017**, *53*, 19-26.
- (17) Estimated Influenza Illnesses, Medical Visits, Hospitalizations, and Deaths Averted by Vaccination in the United States. <https://www.cdc.gov/flu/about/disease/2015-16.htm> **2016**

- (18) Imai, Y.; Sakuma, T.; Imai, H.; Kuba, K.; Fujiwara, S. Potential cellular targets for anti-influenza drug development. *Cellular Immunology & Immunotherapeutics* **2016**, *1*, 1-12.
- (19) Barrow J.C, D. J. L. Voltage-Gated Calcium Channel Antagonists for the Central Nervous System. *Annual Reports in Medicinal Chemistry* **2010**, *45(C)*, 2-18.
- (20) Cheong, E.; Shin, H.-S. T-type Ca²⁺ channels in normal and abnormal brain functions. *Physiological reviews* **2013**, *93*, 961-992.
- (21) Giordanetto, F.; Knerr, L.; Wållberg, A. T-type calcium channels inhibitors: a patent review. *Expert opinion on therapeutic patents* **2011**, *21*, 85-101.
- (22) Xiang, Z.; Thompson, A. D.; Brogan, J. T.; Schulte, M. L.; Melancon, B. J.; Mi, D.; Lewis, L. M.; Zou, B.; Yang, L.; Morrison, R. The discovery and characterization of ML218: a novel, centrally active T-type calcium channel inhibitor with robust effects in STN neurons and in a rodent model of Parkinson's disease. *ACS chemical neuroscience* **2011**, *2*, 730-742.
- (23) Barrow, J. C. D., Joseph L. Voltage-Gated Calcium Channel Antagonists for the Central Nervous System. *Annual Reports in Medicinal Chemistry* **2010**, *45*, 2-18.
- (24) Iftinca, M. C.; Zamponi, G. W. Regulation of neuronal T-type calcium channels. *Trends in pharmacological sciences* **2009**, *30*, 32-40.
- (25) Kuga, T.; Sadoshima, J.-i.; Tomoike, H.; Kanaide, H.; Akaike, N.; Nakamura, M. Actions of Ca²⁺ antagonists on two types of Ca²⁺ channels in rat aorta smooth muscle cells in primary culture. *Circulation research* **1990**, *67*, 469-480.
- (26) Ono, K.; Iijima, T. Pathophysiological significance of T-type Ca²⁺ channels: properties and functional roles of T-type Ca²⁺ channels in cardiac pacemaking. *Journal of pharmacological sciences* **2005**, *99*, 197-204.
- (27) Chen, Y.; Parker, W. D.; Wang, K. The role of T-type calcium channel genes in absence seizures. *Frontiers in neurology* **2014**, *5*, 45.
- (28) Tringham, E.; Powell, K. L.; Cain, S. M.; Kuplast, K.; Mezeyova, J.; Weerapura, M.; Eduljee, C.; Jiang, X.; Smith, P.; Morrison, J.-L. T-type calcium channel blockers that attenuate thalamic burst firing and suppress absence seizures. *Science translational medicine* **2012**, *4*, 121ra119.
- (29) Cain, S. M.; Snutch, T. P. T-type calcium channels in burst-firing, network synchrony, and epilepsy. *Biochimica et Biophysica Acta (BBA)-Biomembranes* **2013**, *1828*, 1572-1578.
- (30) Jagodic, M. M.; Pathirathna, S.; Nelson, M. T.; Mancuso, S.; Joksovic, P. M.; Rosenberg, E. R.; Bayliss, D. A.; Jevtovic-Todorovic, V.; Todorovic, S. M. Cell-specific alterations of T-type calcium current in painful diabetic neuropathy enhance excitability of sensory neurons. *Journal of Neuroscience* **2007**, *27*, 3305-3316.
- (31) Choi, S.; Na, H.; Kim, J.; Lee, J.; Lee, S.; Kim, D.; Park, J.; Chen, C. C.; Campbell, K.; Shin, H. S. Attenuated pain responses in mice lacking CaV3. 2 T-type channels. *Genes, Brain and Behavior* **2007**, *6*, 425-431.
- (32) Chen, W.-K.; Liu, I. Y.; Chang, Y.-T.; Chen, Y.-C.; Chen, C.-C.; Yen, C.-T.; Shin, H.-S.; Chen, C.-C. Cav3. 2 T-type Ca²⁺ channel-dependent activation of ERK in paraventricular thalamus modulates acid-induced chronic muscle pain. *Journal of Neuroscience* **2010**, *30*, 10360-10368.
- (33) Tanaka, H.; Shigenobu, K. Efonidipine Hydrochloride: A Dual Blocker of L-and T-Type Ca²⁺ Channels. *Cardiovascular Therapeutics* **2002**, *20*, 81-92.

- (34) Santi, C. M.; Cayabyab, F. S.; Sutton, K. G.; McRory, J. E.; Mezeyova, J.; Hamming, K. S.; Parker, D.; Stea, A.; Snutch, T. P. Differential inhibition of T-type calcium channels by neuroleptics. *Journal of Neuroscience* **2002**, *22*, 396-403.
- (35) Suzuki, S.; Kawakami, K.; Nishimura, S.; Watanabe, Y.; Yagi, K.; Scino, M.; Miyamoto, K. Zonisamide blocks T-type calcium channel in cultured neurons of rat cerebral cortex. *Epilepsy research* **1992**, *12*, 21-27.
- (36) Leppik, I. E. Zonisamide: chemistry, mechanism of action, and pharmacokinetics. *Seizure* **2004**, *13*, S5-S9.
- (37) Kito, M.; Maehara, M.; Watanabe, K. Mechanisms of T-type calcium channel blockade by zonisamide. *Seizure* **1996**, *5*, 115-119.
- (38) Dogrul, A.; Gardell, L. R.; Ossipov, M. H.; Tulunay, F. C.; Lai, J.; Porreca, F. Reversal of experimental neuropathic pain by T-type calcium channel blockers. *Pain* **2003**, *105*, 159-168.
- (39) Jacus, M. O.; Uebele, V. N.; Renger, J. J.; Todorovic, S. M. Presynaptic Cav3. 2 channels regulate excitatory neurotransmission in nociceptive dorsal horn neurons. *Journal of Neuroscience* **2012**, *32*, 9374-9382.
- (40) Modrow, S.; Falke, D.; Truyen, U.; Schätzl, H.: Viruses with Single-Stranded, Segmented, Negative-Sense RNA Genomes. In *Molecular Virology*; Springer, 2013; pp 437-520.
- (41) Bouvier, N. M.; Palese, P. The biology of influenza viruses. *Vaccine* **2008**, *26*, D49-D53.
- (42) Paules, C.; Subbarao, K. Influenza. *The Lancet* **2017**, *390*, 697-708.
- (43) Samji, T. Influenza A: understanding the viral life cycle. *The Yale journal of biology and medicine* **2009**, *82*, 153.
- (44) Taubenberger, J. K.; Morens, D. M. The pathology of influenza virus infections. *Annu. Rev. pathmechdis. Mech. Dis.* **2008**, *3*, 499-522.
- (45) Webster, R. G.; Bean, W. J.; Gorman, O. T.; Chambers, T. M.; Kawaoka, Y. Evolution and ecology of influenza A viruses. *Microbiological reviews* **1992**, *56*, 152-179.
- (46) Youzbashi, E.; Marschall, M.; Chaloupka, I.; Meier-Ewert, H. Distribution of influenza C virus infection in dogs and pigs in Bavaria. *Tierärztliche Praxis* **1996**, *24*, 337-342.
- (47) Osterhaus, A.; Rimmelzwaan, G.; Martina, B.; Bestebroer, T.; Fouchier, R. Influenza B virus in seals. *Science* **2000**, *288*, 1051-1053.
- (48) Gasparini, R.; Amicizia, D.; Lai, P. L.; Bragazzi, N. L.; Panatto, D. Compounds with anti-influenza activity: present and future of strategies for the optimal treatment and management of influenza. Part I: influenza life-cycle and currently available drugs. *Journal of preventive medicine and hygiene* **2014**, *55*, 69.
- (49) Das, K.; Aramini, J. M.; Ma, L.-C.; Krug, R. M.; Arnold, E. Structures of influenza A proteins and insights into antiviral drug targets. *Nature structural & molecular biology* **2010**, *17*, 530-538.
- (50) He, H.: Vaccines and Antiviral Agents. In *Current Issues in Molecular Virology-Viral Genetics and Biotechnological Applications*; InTech, 2013; pp 239-250.
- (51) De Clercq, E. Antiviral agents active against influenza A viruses. *Nature reviews. Drug discovery* **2006**, *5*, 1015-1025.
- (52) Stolf, B. S.; Smyrnias, I.; Lopes, L. R.; Vendramin, A.; Goto, H.; Laurindo, F. R.; Shah, A. M.; Santos, C. X. Protein disulfide isomerase and host-pathogen interaction. *The Scientific World Journal* **2011**, *11*, 1749-1761.

- (53) Gallina, A.; Hanley, T. M.; Mandel, R.; Trahey, M.; Broder, C. C.; Viglianti, G. A.; Ryser, H. J.-P. Inhibitors of protein-disulfide isomerase prevent cleavage of disulfide bonds in receptor-bound glycoprotein 120 and prevent HIV-1 entry. *Journal of Biological Chemistry* **2002**, 277, 50579-50588.
- (54) Cooper, G. M.; Hausman, R. E.: The Endoplasmic Reticulum. In *The Cell: A Molecular Approach*; 4th ed.; Sinauer Associates Sunderland, 2000; Vol. 85; pp 386-406.
- (55) Segal, M. S.; Bye, J. M.; Sambrook, J. F.; Gething, M. Disulfide bond formation during the folding of influenza virus hemagglutinin. *The Journal of cell biology* **1992**, 118, 227-244.
- (56) Braakman, I.; Hebert, D. N. Protein folding in the endoplasmic reticulum. *Cold Spring Harbor perspectives in biology* **2013**, 5, a013201.
- (57) Hebert, D. N.; Molinari, M. In and Out of the ER: Protein Folding, Quality Control, Degradation, and Related Human Diseases. *Physiological Reviews* **2007**, 87, 1377-1408.
- (58) Puig, A.; Gilbert, H. F. Protein disulfide isomerase exhibits chaperone and anti-chaperone activity in the oxidative refolding of lysozyme. *Journal of Biological Chemistry* **1994**, 269, 7764-7771.
- (59) Khan, H. A.; Mutus, B. Protein disulfide isomerase a multifunctional protein with multiple physiological roles. *Frontiers in chemistry* **2014**, 2, 70.
- (60) Marcus, N.; Shaffer, D.; Farrar, P.; Green, M. Tissue distribution of three members of the murine protein disulfide isomerase (PDI) family. *Biochimica et Biophysica Acta (BBA)-Gene Structure and Expression* **1996**, 1309, 253-260.
- (61) Appenzeller-Herzog, C.; Ellgaard, L. The human PDI family: versatility packed into a single fold. *Biochimica et Biophysica Acta (BBA)-Molecular Cell Research* **2008**, 1783, 535-548.
- (62) Tian, G.; Xiang, S.; Noiva, R.; Lennarz, W. J.; Schindelin, H. The crystal structure of yeast protein disulfide isomerase suggests cooperativity between its active sites. *Cell* **2006**, 124, 61-73.
- (63) Noiva, R. Protein disulfide isomerase: the multifunctional redox chaperone of the endoplasmic reticulum. *Seminars in cell & developmental biology* **1999**, 10, 481-493.
- (64) Primm, T. P.; Gilbert, H. F. Hormone binding by protein disulfide isomerase, a high capacity hormone reservoir of the endoplasmic reticulum. *Journal of Biological Chemistry* **2001**, 276, 281-286.
- (65) Cai, H.; Wang, C.-C.; Tsou, C.-L. Chaperone-like activity of protein disulfide isomerase in the refolding of a protein with no disulfide bonds. *Journal of Biological Chemistry* **1994**, 269, 24550-24552.
- (66) Quan, H.; Fan, G.; Wang, C.-c. Independence of the chaperone activity of protein disulfide isomerase from its thioredoxin-like active site. *Journal of Biological Chemistry* **1995**, 270, 17078-17080.
- (67) Dai, Y.; Wang, C.-c. A mutant truncated protein disulfide isomerase with no chaperone activity. *Journal of Biological Chemistry* **1997**, 272, 27572-27576.
- (68) Koivunen, P.; Pirneskoski, A.; Karvonen, P.; Ljung, J.; Helaakoski, T.; Notbohm, H.; Kivirikko, K. I. The acidic C-terminal domain of protein disulfide isomerase is not critical for the enzyme subunit function or for the chaperone or disulfide isomerase activities of the polypeptide. *The EMBO journal* **1999**, 18, 65-74.

- (69) Horibe, T.; Nagai, H.; Sakakibara, K.; Hagiwara, Y.; Kikuchi, M. Ribostamycin inhibits the chaperone activity of protein disulfide isomerase. *Biochemical and biophysical research communications* **2001**, *289*, 967-972.
- (70) Zai, A.; Rudd, M. A.; Scribner, A. W.; Loscalzo, J. Cell-surface protein disulfide isomerase catalyzes transnitrosation and regulates intracellular transfer of nitric oxide. *Journal of Clinical Investigation* **1999**, *103*, 393-399.
- (71) Tsibris, J. C.; Hunt, L.; Ballejo, G.; Barker, W.; Toney, L.; Spellacy, W. Selective inhibition of protein disulfide isomerase by estrogens. *Journal of Biological Chemistry* **1989**, *264*, 13967-13970.
- (72) Karala, A. R.; Ruddock, L. W. Bacitracin is not a specific inhibitor of protein disulfide isomerase. *The FEBS journal* **2010**, *277*, 2454-2462.
- (73) Mizunaga, T.; Katakura, Y.; Miura, T.; Maruyama, Y. Purification and characterization of yeast protein disulfide isomerase. *The Journal of Biochemistry* **1990**, *108*, 846-851.
- (74) Wang, E.-J.; Snyder, R. D.; Fielden, M. R.; Smith, R. J.; Gu, Y.-Z. Validation of putative genomic biomarkers of nephrotoxicity in rats. *Toxicology* **2008**, *246*, 91-100.
- (75) Godin, B.; Touitou, E. Mechanism of bacitracin permeation enhancement through the skin and cellular membranes from an ethosomal carrier. *Journal of controlled Release* **2004**, *94*, 365-379.
- (76) Dickerhof, N.; Kleffmann, T.; Jack, R.; McCormick, S. Bacitracin inhibits the reductive activity of protein disulfide isomerase by disulfide bond formation with free cysteines in the substrate-binding domain. *The FEBS journal* **2011**, *278*, 2034-2043.
- (77) Jasuja, R.; Passam, F. H.; Kennedy, D. R.; Kim, S. H.; van Hessem, L.; Lin, L.; Bowley, S. R.; Joshi, S. S.; Dilks, J. R.; Furie, B. Protein disulfide isomerase inhibitors constitute a new class of antithrombotic agents. *The Journal of clinical investigation* **2012**, *122*, 2104-2113.
- (78) Khan, M. M.; Simizu, S.; Lai, N. S.; Kawatani, M.; Shimizu, T.; Osada, H. Discovery of a small molecule PDI inhibitor that inhibits reduction of HIV-1 envelope glycoprotein gp120. *ACS chemical biology* **2011**, *6*, 245-251.
- (79) Kennedy, D. R.; Nag, P. P.; Galinski, C. N.; Bowley, S.; Bekendam, R. H.; Dilks, J. R.; Scalise, A. A.; van Hessem, L.; Pu, J.; Pilyugina, T.; Dandapani, S. Development Of Second Generation Thiol Isomerase Inhibitors To Prevent Thrombus Formation. *Blood* **2013**, *122*, 926.
- (80) Bendapudi, P. K.; Bekendam, R. H.; Lin, L.; Huang, M.; Furie, B.; Flaumenhaft, R. ML359, a Small Molecule Inhibitor of Protein Disulfide Isomerase That Prevents Thrombus Formation and Inhibits Oxidoreductase but Not Transnitrosylase Activity. *Blood* **2014**, *124*, 2880.
- (81) Yang, Z.-Q.; Barrow, J. C.; Shipe, W. D.; Schlegel, K.-A. S.; Shu, Y.; Yang, F. V.; Lindsley, C. W.; Rittle, K. E.; Bock, M. G.; Hartman, G. D. Discovery of 1, 4-substituted piperidines as potent and selective inhibitors of T-type calcium channels. *Journal of medicinal chemistry* **2008**, *51*, 6471-6477.
- (82) Rutkowska, E.; Pajak, K.; Jóźwiak, K. Lipophilicity--methods of determination and its role in medicinal chemistry. *Acta poloniae pharmaceutica* **2013**, *70*, 3-18.
- (83) Van De Waterbeemd, H.; Gifford, E. ADMET in silico modelling: towards prediction paradise? *Nature reviews. Drug discovery* **2003**, *2*, 192.

- (84) Dunetz, J. R.; Magano, J.; Weisenburger, G. A. Large-scale applications of amide coupling reagents for the synthesis of pharmaceuticals. *Organic Process Research & Development* **2016**, *20*, 140-177.
- (85) Xie, X.; Kayser, F.: Ion channel inhibitory compounds, pharmaceutical formulations and uses. Google Patents, 2017.
- (86) Lu, J.; Aguilar, A.; Zou, B.; Bao, W.; Koldas, S.; Shi, A.; Desper, J.; Wangemann, P.; Xie, X. S.; Hua, D. H. Chemical synthesis of tetracyclic terpenes and evaluation of antagonistic activity on endothelin-A receptors and voltage-gated calcium channels. *Bioorganic & medicinal chemistry* **2015**, *23*, 5985-5998.
- (87) Hargreaves, K.; Dubner, R.; Brown, F.; Flores, C.; Joris, J. A new and sensitive method for measuring thermal nociception in cutaneous hyperalgesia. *Pain* **1988**, *32*, 77-88.
- (88) Chaplan, S. R.; Bach, F.; Pogrel, J.; Chung, J.; Yaksh, T. Quantitative assessment of tactile allodynia in the rat paw. *Journal of neuroscience methods* **1994**, *53*, 55-63.
- (89) Fleming, F. F.; Yao, L.; Ravikumar, P.; Funk, L.; Shook, B. C. Nitrile-containing pharmaceuticals: efficacious roles of the nitrile pharmacophore. *Journal of medicinal chemistry* **2010**, *53*, 7902-7917.
- (90) Khodier, C.; VerPlank, L.; Nag, P. P.; Pu, J.; Wurst, J.; Pilyugina, T.; Dockendorff, C.; Galinski, C. N.; Scalise, A. A.; Passam, F. Identification of ML359 as a small molecule inhibitor of protein disulfide isomerase. *Probe Reports from the NIH Molecular Libraries Program* **2010**.
- (91) Artursson, P.; Neuhoﬀ, S.; Tavelin, S.; Matsson, P.: Passive permeability and active transport models for the prediction of oral absorption. In *Comprehensive Medicinal Chemistry II*, 2007; pp 259–278.
- (92) Fernandes, J.; Gattass, C. R. Topological polar surface area defines substrate transport by multidrug resistance associated protein 1 (MRP1/ABCC1). *Journal of medicinal chemistry* **2009**, *52*, 1214-1218.
- (93) Kim, Y.; Narayanan, S.; Chang, K.-O. Inhibition of influenza virus replication by plant-derived isoquercetin. *Antiviral research* **2010**, *88*, 227-235.

Chapter 2 - Design, synthesis and bio-evaluation of novel peptide-based calcitonin gene-related peptide receptor antagonists for the treatment of inflammatory pain

2.1 Introduction

Pain can be described as an unpleasant sensational experience which warns individuals about harmful environmental stimuli or about harmful physiological changes. According to the International Association for the Study of Pain, pain is defined as “an unpleasant sensory and emotional experience associated with actual or potential tissue damage, or described in terms of such damage”. Although pain is not fatal, it causes a significant social and economic burden on the person as well as to the society. Therefore, various therapeutic methods are available to treat pain such as non-opioid analgesics (such as nonsteroidal anti-inflammatory drugs (NSAIDs), e.g. aspirin), opioid analgesics (e.g. morphine), antidepressants (e.g. amitriptyline), anticonvulsants (e.g. gabapentin and pregabalin).¹ Despite a wide number of treatment options available, management of pain still remains a problem due to their less effectivity and safety issues.

2.2 Background

Based on the pathophysiological mechanism, pain is mainly divided into two types as nociceptive pain and neuropathic pain.² Nociceptive pain is a warning signal of tissue damage, which is caused by an accidental injury, inflammation or surgery etc.² Neuropathic pain, however, is caused by a damage to the peripheral or the central nervous system.² Nociceptive pain can be divided further into two types as somatic and visceral pain based on the location of activated nociceptors (nociceptive receptors).³ Somatic pain is caused by the activation of nociceptors in the skin, or deep tissues such as bone, muscle or connective tissue.³ Visceral pain, however, is caused by the activation of nociceptors located in the internal organs of the body.³

In nociceptive pain, tissue damage can be caused by stimuli such as a strong mechanical pressure, extreme heat, extreme cold, chemical damage, etc and the primary sensors for such stimuli in the body are called peripheral nociceptive neurons.³⁻⁵ Peripheral nociceptive neurons are first order neurons and are located in the trigeminal and dorsal root ganglia (DRG).⁶ They give rise to myelinated (A δ) and unmyelinated axons (C-fibers).⁶ Nociceptive neurons release a broad range of neurotransmitters such as glutamate, substance P, calcitonin gene-related peptide (CGRP), somatostatin which are important in the pain signaling pathway.⁴ Studies performed in several animal models also support the idea that CGRP has a key role in the pain pathology.^{7,8} Further, studies have shown that blocking the function of calcitonin gene related peptide (CGRP) by the use of CGRP receptor antagonists can reduce pain.⁹⁻¹¹ Therefore, the use of CGRP receptor antagonists has been identified as an attractive approach for the treatment of pain.

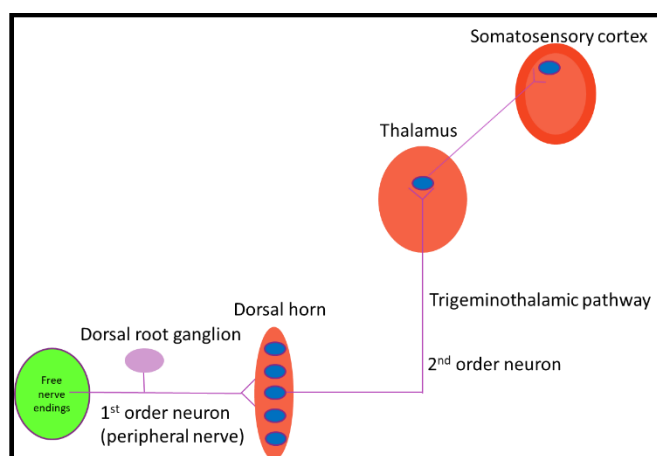


Figure 2.1 Schematic diagram of trigeminothalamic pain signaling pathway.¹²

2.2.1 Calcitonin gene-related peptide (CGRP)

Inflammatory mediator, calcitonin gene-related peptide (CGRP) is a 37-amino acid neuropeptide.¹³⁻¹⁵ It belongs to the calcitonin family which also includes calcitonin, adrenomedullin, amylin, and intermedin (adrenomedullin-2).¹³⁻¹⁵ Calcitonin and calcitonin gene related peptide (CGRP) are both encoded by CT/CGRP gene, which is located at chromosome 11 in humans.¹⁶ Tissue specific alternative splicing of RNA leads to two different mRNAs called CT and CGRP transcripts.^{15,17} CT mRNA predominates in the thyroid to encode hormone CT

while CGRP-specific mRNA predominates in the hypothalamus.^{15,17} CGRP is mainly expressed in the A δ and C sensory fibers, trigeminal and dorsal root ganglia (DRG), and the central nervous system.¹⁸ CGRP commonly co-exists with other neurotransmitters.^{13,17} In perivascular sensory nerves CGRP co-exist with neurotransmitters such as substance P and in motor neurons, CGRP co-exist with neurotransmitters such as acetylcholine.¹⁹

There are two isoform types of CGRP, called as α -CGRP and β -CGRP.^{13,17} α -CGRP is encoded by the CALC I gene in neuronal tissues while β -CGRP is encoded by a CALC II gene in specific neuronal sites such as medullary thyroid in humans.^{13,17} It is found that rat α -CGRP differs from rat β -CGRP by one amino acid while human α -CGRP differs from human β -CGRP by three amino acids.^{13,17} In fact, the biological activities of these two isoforms are proved to be very similar.^{13,15,17} Although, these two isoforms are found to be co-localized in most neurons, immunohistological studies have shown that α -CGRP is predominantly expressed in sensory neurons while β -CGRP is expressed preferentially in motor neurons.^{13,15,17,20}

Human α - CGRP	ACDTATCVTH RLAGLLSRSG GVVKNFVPT NVGSKAF
Human β - CGRP	ACNTATCVTH RLAGLLSRSG GMVKS NFVPT NVGSKAF

Figure 2.2 Amino acid sequences of human α - CGRP and β - CGRP.¹⁷

CGRP peptide forms a Cys-Cys disulfide bonded loop structure between residues two and seven in the N-terminus, which is found to be essential for the receptor activation.²¹ Residue 8 to 18 then forms an α - helix, which is found to be important in the receptor binding.^{17,21} Another key structural feature in CGRP is the C-terminal amide group.²¹

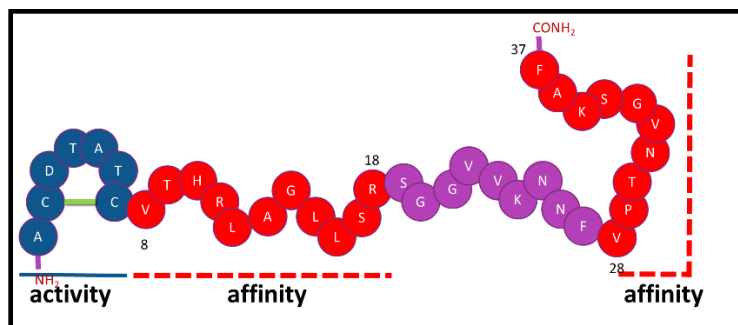


Figure 2.3 Proposed functional regions of the primary structure of human α CGRP (CGRP₁₋₃₇).

A wide distribution of CGRP has implicated its wide range of biologically important functions. CGRP has found to play important roles in cardiovascular, digestive, and sensory functions.¹⁸ CGRP is one of the most potent vasodilators known and involved in reducing blood pressure.¹⁷ In the cardiovascular system, CGRP increases heart rate.¹⁷ In addition, CGRP is involved in the thermoregulation, regulation of calcium metabolism and insulin secretion, and reduction of gastric acid secretion in the body.²² In the central nervous system, CGRP modulates the sensory and motor systems, thereby regulate pain perception.¹⁷ It is reported that in the peripheral nervous system, CGRP modulate acetylcholine receptor function at the neuromuscular junction as well as induces degranulation of dural mast cells and thereby releasing pro-inflammatory agents that mediate sensitization of trigeminal nociceptors.^{15,17} It has been found that the CGRP gene is upregulated by factors such as nerve growth factor (NGF) and tissue inflammation, and CGRP is released from nerves in response to several stimuli, such as capsaicin and low pH, proteinase-activated receptor (PAR activation), and mediators (eg, kinins and prostaglandins).²³ Clinical studies have shown that CGRP is involved in the development of neurogenic inflammation and the level CGRP is upregulated in inflammatory pain, neuropathic pain and migraine pain conditions.^{15,18,23}

2.2.2 The calcitonin gene related peptide receptor

CGRP receptor is a heterodimeric complex consisting of a seven-transmembrane domain protein called calcitonin receptor-like receptor (CLR) and a receptor activity-modifying protein (RAMP1).²⁴ CGRP receptor requires another accessory protein called receptor component protein (RCP) for its downstream signaling pathways.²⁵⁻²⁷ These receptor components are expressed in peripheral and central nervous systems as well as in the trigeminovascular, cardiovascular, gastrointestinal, respiratory, musculoskeletal and endocrine systems.^{13,15,28}

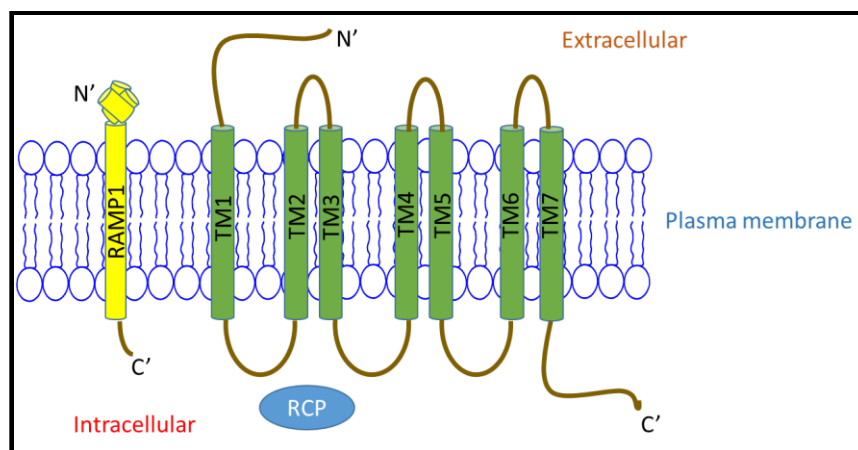


Figure 2.4 Representative cartoon structure of CGRP receptor.²⁹

Calcitonin-like receptor (CLR) is a member of secretin family (family B) of G-protein coupled receptors (GPCRs).²⁴ Hence it is homologous to the receptors for calcitonin (CTR), glucagon, secretin, vasoactive intestinal peptide (VIP), parathyroid hormone (PTH), corticotropin-releasing factor (CRF), pituitary adenylate cyclase-activating peptide (PACAP) and growth hormone releasing hormone.²⁴ It has been suggested that the N-terminus of CLR is determining the specificity of CLR for CGRP binding and CGRP mediated signaling, while the transmembrane and short C-terminus have been suggested to be important in RAMP interactions.^{15,20,24} Based on mutagenesis studies, it is suggested that these CLR extracellular N-terminal residues are crucial for forming the functional CGRP receptor.³⁰

Receptor Activity Modifying Protein 1 (RAMP1) is a single transmembrane protein with a large extracellular N-terminus and a short intracellular C-terminus.^{20,24,31} Crystal structure of RAMP1 domain shows three alpha helices (α R1- α R3), aligned roughly perpendicular to the helix α C1 of CLR.^{32,33} There are 91 amino acid residues in the extracellular N-terminal region of RAMP1, including the first RAMP1 helix, α R1, which is formed by residues starting from E29 to V51.³²⁻³⁴ It is followed by a short loop consisting of residues E53 to L55 (loop-1), which connects α -helices 1 and 2.³²⁻³⁴ Helix α R2 is formed by residues from W59 to L80, and it is anti-parallel to the other two helices.³²⁻³⁴ According to the crystal structure of RAMP1, residues R67, D71, W74 and E78 are important in ligand binding.³¹ They are located at the α R2 helix.³¹ Another important residue W84 is located on a loop (loop-2) between the α R2 and α R3 helices

with its side chain oriented in the same direction as W74 to form a hydrophobic pocket.³¹ The final helix, α R3 is formed by residues from A87 to Y100.³⁴ The crystal structure of RAMP1 have further revealed that extracellular N-terminal region has three disulfide between C27–C82, C40–C72 and C57–C104 which are important to stabilize RAMP1's three helix topology.^{33,34} In addition, RAMP1's transmembrane domain has 22 residues which has been suggested to be important in RAMP-receptor interactions.^{31,35} Intracellular C- terminus of RAMP1 consists of residues 105–117 (PISGRAVRDPPGS) which acts as an endoplasmic reticulum retention signal.^{32,33} Removal of this tail is found to result in CLR- independent transport of RAMP1 to the cell surface.^{32,33}

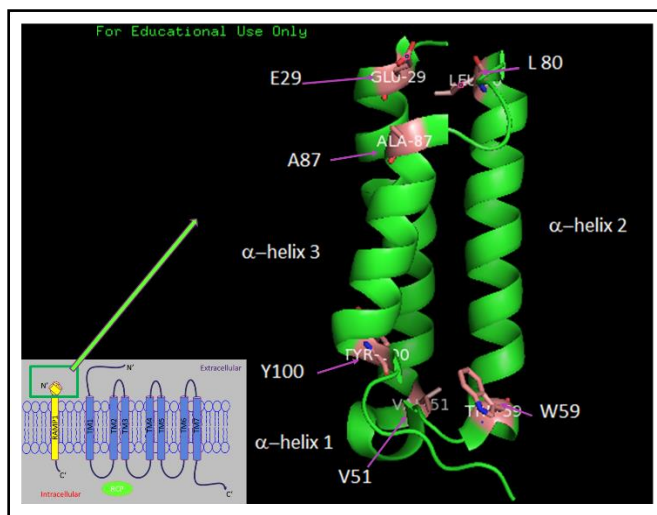


Figure 2.5 The expanded portion shows the crystal structure of the human RAMP1 N-terminus (RAMP1_{127–107}). PDB code: 2YX8³²

The third component related to CGRP receptor, called receptor component protein (RCP), is an intracellular peripheral membrane protein, which is expressed in CGRP responsive tissues.^{20,26} It is reported that, RCP has several conserved sites for phosphorylation, suggesting that RCP function may be regulated by phosphorylation *in vivo*.³¹ Data obtained from cell lines that express antisense RCP RNA, have shown that the RCP protein expression correlates with the CGRP mediated signal transduction.^{20,26,31} It is also suggested that RCP is not to be a chaperone but it behaves more like a coupling protein to CGRP receptor for signal transduction.³¹ Further, co-immunoprecipitation studies suggest that RCP directly interacts with

CLR via ionic interactions.^{20,26,31} However, the nature of the coupling mediated by RCP is still unclear.

2.2.3 The role of CGRP and CGRP receptors in the induction and maintenance of pain

When a tissue injury occurs, a complex immune response called “inflammation” occurs in the damaged tissue area to remove the corresponding harmful stimulus and avoid further damage.^{4,5} As an inflammatory response, a broad range of inflammatory mediators such as glutamate, bradykinin, prostaglandins, histamine, nerve growth factor (NGF), substance P (SP), calcitonin gene-related peptide (CGRP), nitric oxide (NO), cytokines, etc. is released by different cell types in response to tissue injury.^{4,5} These inflammatory mediators are believed to excite the peripheral terminals of nociceptive neurons, thereby generate action potentials, or facilitate the firing of the nociceptors, thereby resulting peripheral sensitization.⁴⁻⁶ Studies have shown that electrical stimulation of a peripheral nerve generates action potentials which helps generating dorsal root reflex (DRR) in adjacent peripheral nerve fibers.^{36,37} This dorsal root reflex is assumed to propagate the neurogenic inflammatory response from the site of injury.^{36,37}

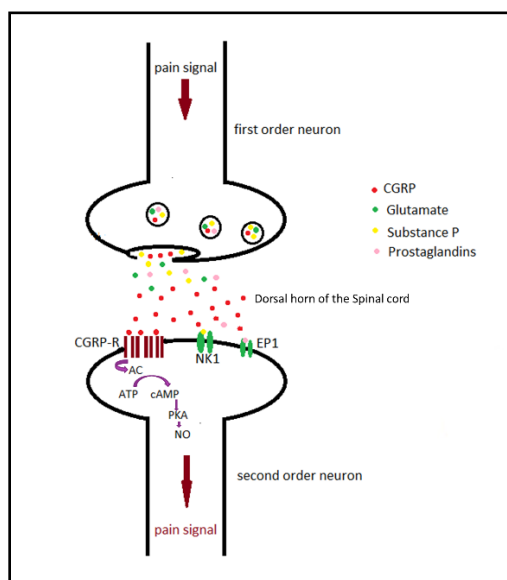


Figure 2.6 Role of CGRP in the central sensitization.

Further, studies suggest that dorsal root reflex cause releases of CGRP from peripheral terminals of A δ and C fibers, which is assumed to contribute to the peripheral sensitization.^{38,39} In the spinal dorsal horn, CGRP increases sensitivity of second-order neurons to the sensory impulses from first order neurons thereby increases excitability of second order neurons.⁸ This enhanced response in the pain transmission of neurons in the central nervous system (from dorsal horn of the spinal cord to the somatosensory area of the cortex) is known as central sensitization and it lowers pain threshold (hyperalgesia) and causing inflammatory pain (allodynia).⁸

2.2.4 Pain inhibition by CGRP antagonists

Studies have shown that blocking the effects of CGRP, either with the small molecule CGRP antagonists (such as BIBN4096BS) or peptide based CGRP antagonists (such as CGRP₈₋₃₇), reduced inflammatory pain in animal models.⁴⁰⁻⁴² Yu et al. have demonstrated that intrathecal administration of CGRP₈₋₃₇ induces antinociceptive effects and increases pain thresholds in rats with inflammation.⁴³ Hirsch et al have demonstrated that the intravenous administration of the small-molecule CGRP antagonist BIBN4096BS reversed mechanical hypersensitivity in rats which was induced by complete Freund's adjuvant (CFA) treatment.⁴² Further, LY2951742 which is a high affinity, neutralizing antibody to CGRP have shown inhibitory effects in CGRP-mediated induction of cAMP in SK-N-MC cells *in vitro* and capsaicin-induced dermal blood flow in the rat.¹³

2.2.5 Reported peptide based CGRP receptor antagonists

The first CGRP receptor antagonist has been developed by the N-terminal truncation of the first seven amino acids of the natural CGRP peptide.⁴⁴ This CGRP(8-37) fragment, which has a of H₂N-V-T-H-R-L-A-G-L-L-S-R-S-G-G-V-V-K-N-N-F-V-P-T-N-V-G-S-K-A-F-CONH₂ blocks the CGRP binding to the CGRP receptor in a competitive manner.^{45,46} Even though CGRP(8-37) has shown a IC₅₀ of 4.87 nM and a binding affinity (K_i) of 3.2 nM, its' *in vivo* development was not successful due to the short half-life (t_{1/2}). Further, CGRP(8-37) was found to be a weak antagonist to adrenomedullin receptors AM1 and AM2 as well.⁴⁷ Another N-

terminal truncated fragment CGRP(27-37) was shown to be a selective, competitive and reversible CGRP receptor antagonist, but with less potency (IC_{50} of 3 μ M).⁴⁸ However, the affinity of CGRP(27-37) has been optimized with substitutions at residue positions 29, 31, 34, and 35.^{22,47} NMR spectroscopy of [Asp31, Pro34, Phe35]-human CGRP(27-37) analog has shown a γ -turn centered at Pro34 and a C-terminal helical turn in the bioactive conformation.⁴⁹ It is suggested that these turns help the structure to orient critical residues (T30,V32 and F37) appropriately in the receptor binding.⁴⁹

Receptor binding studies showed K_i of 14 nM for [Asp31, Pro34, Phe35]-human CGRP(27-37) while 19 nM for [Asn31, Pro34, Phe35]-human CGRP(27-37).²² However, [Asp31,Pro34,Phe35]-human CGRP(27-37) has shown a very short half-life. It is suggested that Asp is more susceptible to be degraded by proteases.²² Another study has shown that [Aib29,Asp31,Pro34,Phe35]CGRP(27-37) has a K_i of 0.002 ± 0.001 nM.⁵⁰ This highest affinity is explained by its hydrophobic nature at residue 29 which stabilizes the secondary structure of the peptide.⁵⁰ Despite improvements in receptor potency, these CGRP peptide antagonists suffer from poor metabolic stability.

2.3 Molecular design, synthetic routes and bio-evaluation methods

2.3.1 Molecular design

The aim of this research was to design and synthesis high affinity CGRP antagonists possibly with an increased plasma stability. Since the literature evidences showed that CGRP(27-37) fragment has CGRP receptor antagonist activity, we chose this undecane peptide for further modifications. We synthesized a series of five different peptides. In order to improve binding affinity, we replaced Ser34 with Pro and Lys35 with Phe as [P34, F35]CGRP(27-37) fragment was shown to have a better binding affinity, K_i of 19 nM. Second analogue [I28, P34, F35]CGRP(27-37) was designed by replacing Val28 with Ile to maintain the hydrophobic nature of the peptide. Third peptide, [P34, F35]CGRP(26-37) was designed to identify the importance of Asn26 in the receptor binding. Forth peptide, [W27, P34, F35]CGRP(27-37) was designed by

replacing Phe with Trp to maintain hydrophobicity. Peptide 5 was a 13 amino acid peptide, [D25,P34, F35]CGRP(25-37). Replacement of Asn25 with Asp was expected to have favorable hydrogen bonding interactions and to have a high affinity to the receptor.

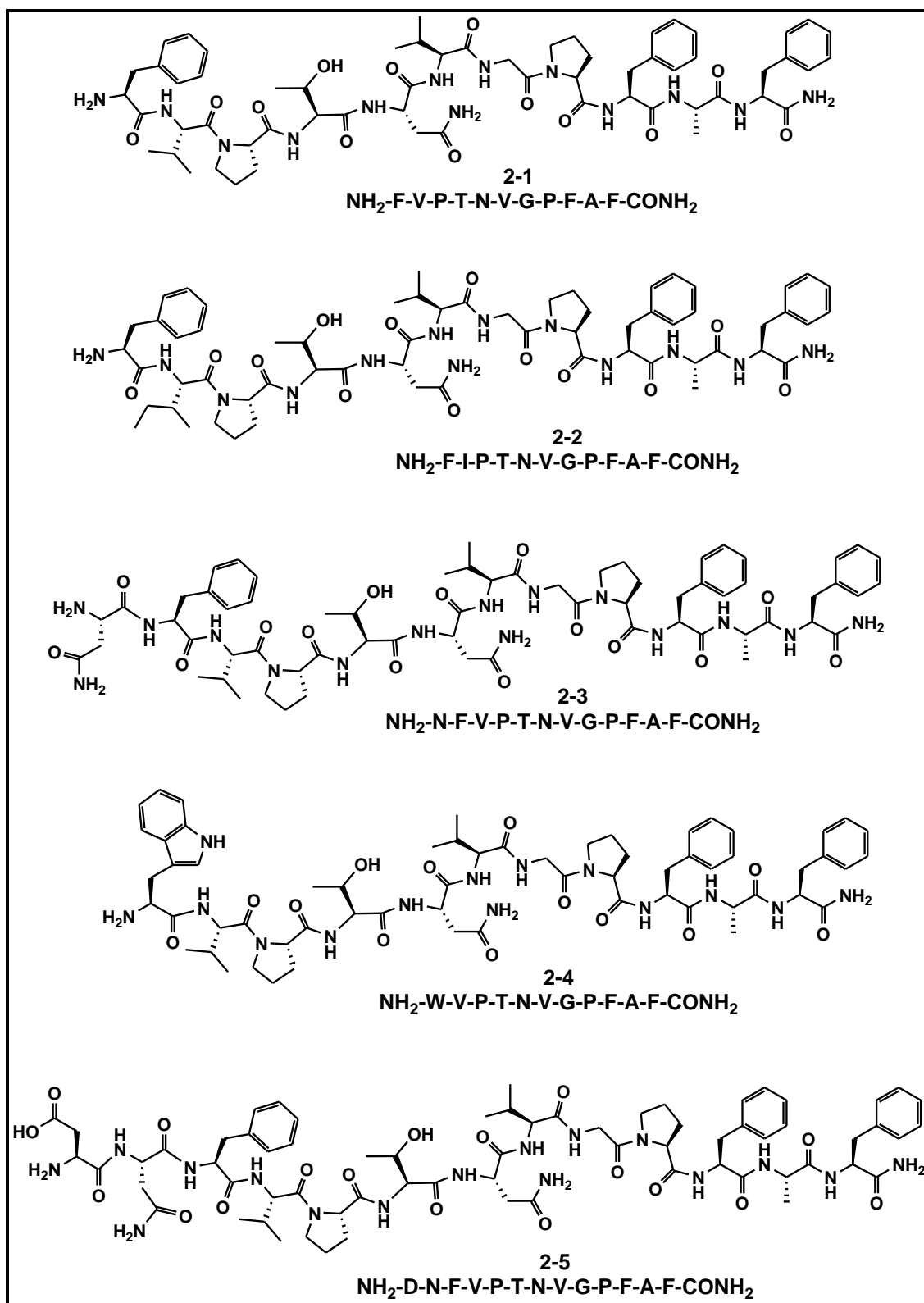
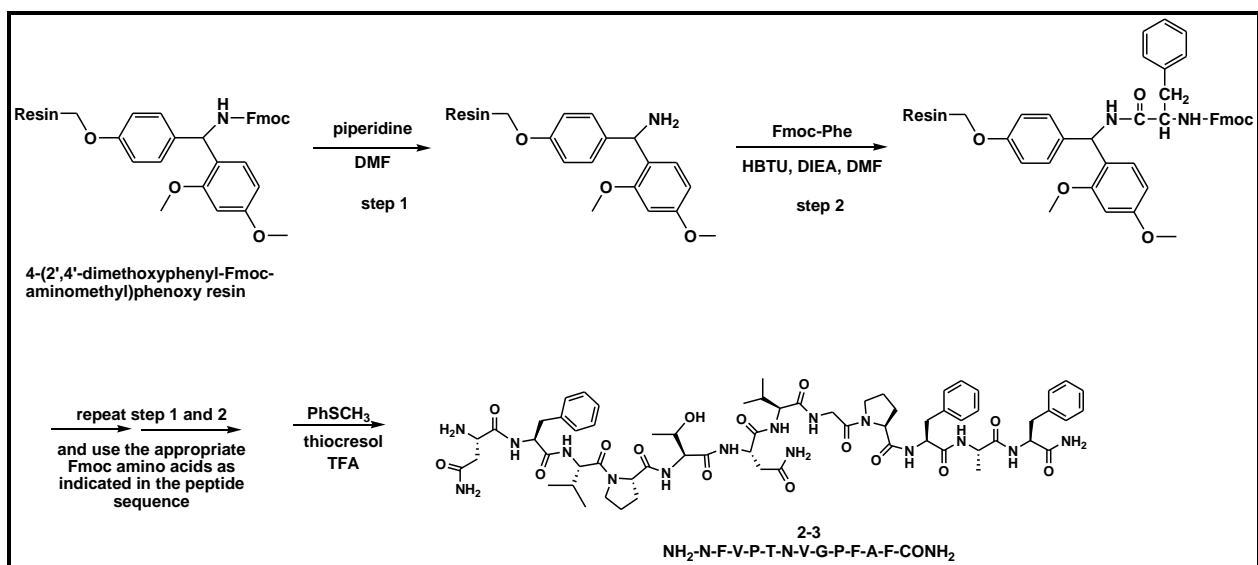


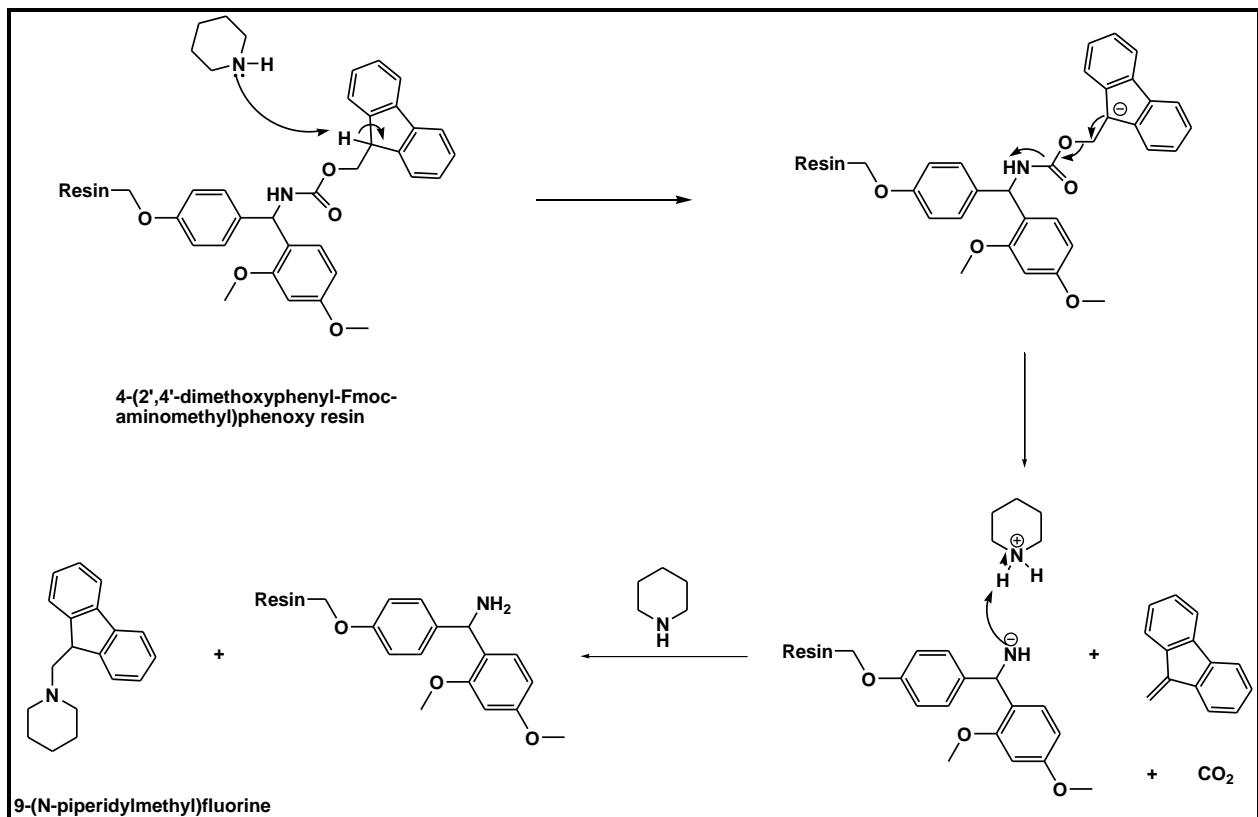
Figure 2.7 Synthesized CGRP receptor antagonists, 2-1 to 2-5.

2.3.2 Peptide synthesis

The linear CGRP peptide antagonist analogues were prepared by automated solid-phase peptide synthesis (SPPS) using a Rink amide resin. The Rink amide resin was chosen because it provides C-terminus peptides capping with amino function. First step of the peptide synthesis was the removal of 9-Fluorenylmethyl carbamate (Fmoc) protecting group by a nucleophilic base, piperidine (20% in DMF) via a base induced beta elimination. Removal of the Fmoc protecting group was monitored by the formation of by-product, 9-(N-piperidylmethyl)fluorene using mass spectrometry. The resulting free amine was coupled with the first amino acid. Peptide coupling on the resin was carried out using the corresponding Fmoc protected amino acid, a coupling reagent HATU (1-[bis(dimethylamino)methylene]-1H-1,2,3-triazolo[4,5-b]pyridinium 3-oxid hexafluorophosphate), and a base diisopropylethylamine (DIEA). DMF was used as the solvent. Completion of the peptide bond formation was monitored by a ninhydrin test. The resulting protected peptide resins were deprotected and cleaved from the resin using trifluoroacetic acid/thioanisole/thiocresol (90:5:5 v/v). The crude peptides were purified by reverse-phase high-performance liquid chromatography (HPLC) using a C18 column with water/acetonitrile gradient containing 0.1% trifluoroacetic acid. The identity of the peptides was confirmed by a high-resolution mass spectrometry (HRMS) recorded on a Waters G2-XS QToF mass spectrometer.



Scheme 2.1 A representative synthesis of CGRP receptor antagonist, **2-3**.



Scheme 2.2 Mechanism of deprotection of Fmoc-protected Rink amide resin.

2.3.3 Bio-evaluation

Bio-evaluation studies were performed in our collaborator Dr. Xinmin (Simon) Xie's laboratory at AfaSci Research Laboratory in Redwood City, California.

2.3.3.1 Binding assay

Binding assays on human CGRP1 membrane were performed according to a reported procedure.⁵¹ Experiments were performed in duplicate or triplicate, repeated twice and data are presented as mean \pm SD. Nonspecific binding was determined by using 1 μ M of rat CGRP peptide. IC₅₀ values and hillslope values were determined by using the program Graphpad/PRISM. Inhibition constant K_i for each peptide was calculated using a reported formula.⁵² K_i represents the concentration of competing ligand in a competition assay which would occupy 50% of the receptors (1 μ M) if no ligand were present.⁵¹

2.3.3.2 Effects of peptide 2-3 and 2-4 on rats' facial pain

CGRP peptides' effectivity against pain sensation was tested using A δ fiber and C fiber pain testing. A δ fiber and C fiber nerves are responsible for transmitting pain signals to the sensory cortex of brain.⁵³ Since A δ fibers are myelinated, they transmit pain signals faster than unmyelinated C fibers.⁵³ An electrocutaneous stimulation was used to induce inflammation in rats' left cheeks.

For the facial thermal pain threshold assessment, WT Sprague-Dawley male rats (~ 220 g - 240 g) were used. Prior to electrocutaneous facial stimulation, rats were habituated individually in a tip-less decapicone for 15 minutes and baseline thermal pain thresholds measured on the rats' depilated left cheeks via A δ fiber and C fiber pain testing. Thermal Thresholds were assessed using Yeomans' thermal testing lamp and the lamp was set 7 cm above depilated left cheek of rat.⁵⁴ Voltage of the regulator was set to 90V and 45V for A-delta fiber pain testing and for C fiber pain testing respectively. A cutoff of 6 seconds and 20 seconds was set for A-delta fiber and C fiber testing respectively. Then an electrocutaneous facial stimulation (0.4mA intensity, 10ms

duration, 1s inter-pulse interval) was applied to each rat to induce inflammation. After 24 hours, thermal pain thresholds of each rat were reassessed. Then, each rat was treated with synthesized peptides (1 μ M, n=6 rats/group) or vehicle (0.9% NaCl; n=2 rats) intranasally (I.N.). Thermal thresholds in response to thermal pain stimulus were measured once every 0.5 hr for the first 3 hours post- dosing, and 4, 5, and 6 hr post-dosing.

2.4 Results and Discussion

2.4.1 Binding affinity results of CGRP peptide fragments and peptide 2-3 on human CGRP receptor membranes

Results for binding affinities of CGRP peptide fragments and peptide 2-3 on human CGRP receptor membranes are provided in **Table 2.1** below.

Table 2.1 Binding affinity of peptides on hCGRP receptor.

Compound	Hillslope	K _i (nM)
CGRP27-37	1.62±0.25	697.4±51.0
CGRP8-37	1.21±0.20	59.8±0.4
rat CGRP	0.80±0.07	8.9±1.0
2-3	1.20±0.02	33.3±0.4

2.4.2 Synthesized CGRP peptide effects on rats' facial pain

2.4.2.1 A δ thermal pain test

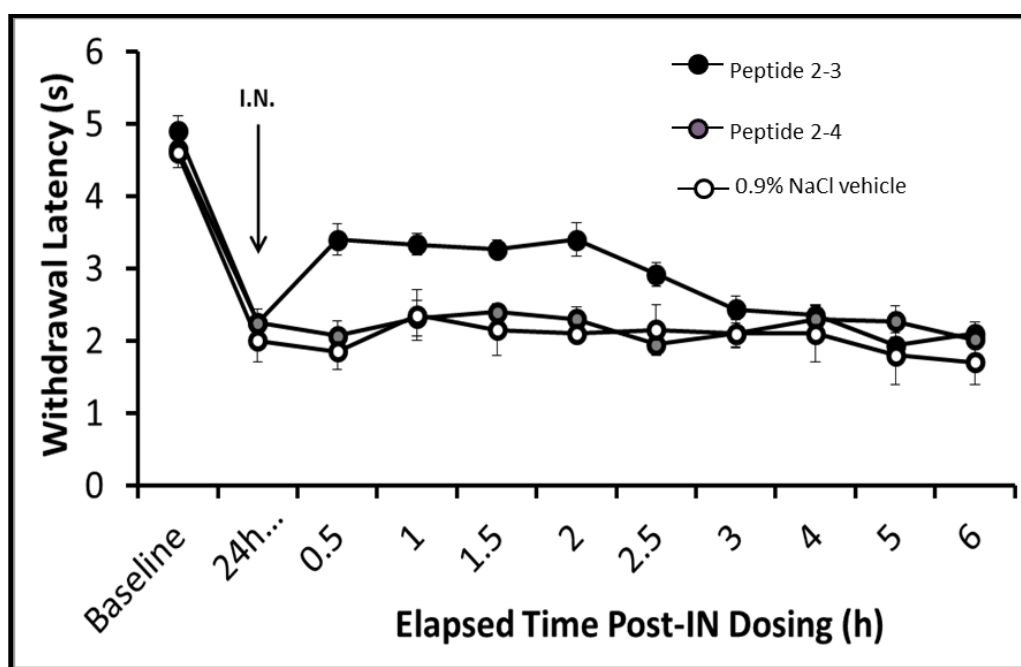


Figure 2.8 A δ thermal pain threshold assessment of rats' depilated left cheeks.

Prior to electrocutaneous facial stimulation, rats showed baseline thermal pain threshold value of 4.9 ± 0.05 s in the A δ fiber pain testing. A 24 hour after electrocutaneous facial stimulation, rats showed reduced pain thresholds of 2.3 ± 0.2 s, confirming the hyperalgesia. After 0.5 h of treatment of CGRP peptide 2-3, rats exhibited increased thermal pain threshold value of 3.4 ± 0.05 s and maintained that value up to 2 h. After 3 h post I.N. treatment, the analgesic effect started to gradually decrease. The treatments with CGRP peptide 2-4 and the blank vehicle showed no significant change in the thermal pain threshold value, hence showed no analgesic effects in the A δ fiber pain testing.

2.4.2.2 C-fiber thermal pain test

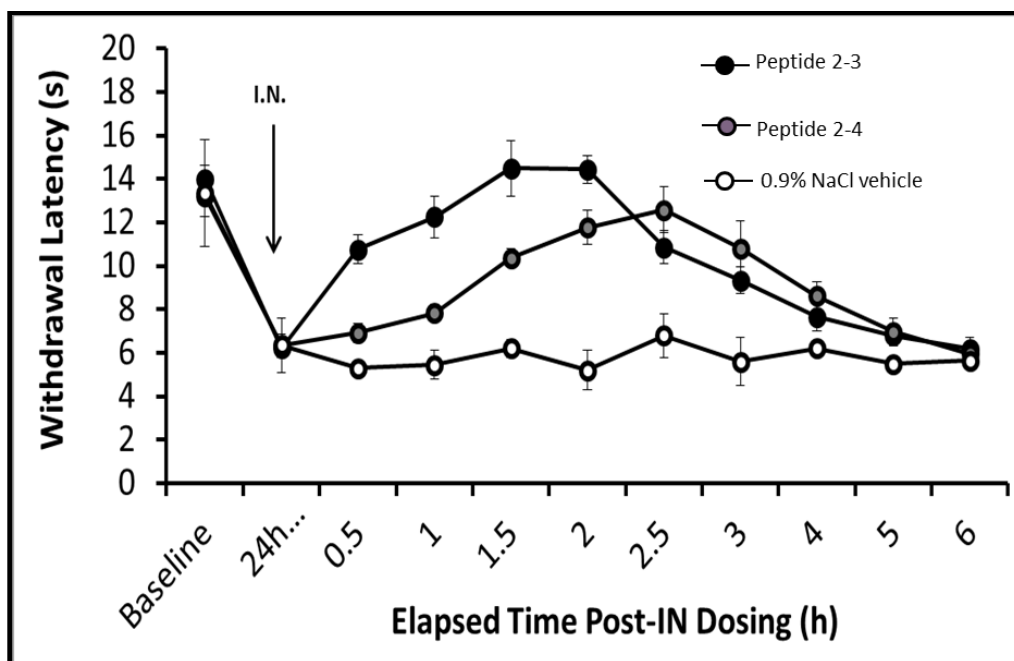


Figure 2.9 C-fiber thermal pain threshold assessment of rats' depilated left cheeks.

In the C-fiber thermal pain test, rats showed baseline thermal pain threshold (average) value of 13.5 ± 0.10 s. A 24 hour after electrocutaneous facial stimulation, rats showed reduced pain thresholds of 6.0 ± 1.0 s, confirming the occurrence of hyperalgesia. After 0.5 h of treatment of CGRP peptide **2-3**, rats exhibited increased thermal pain threshold value of 10.5 ± 0.5 s. Analgesic effect of CGRP peptide 2-3 was gradually increased with time up to 2 h. After 3 h post I.N. treatment, the analgesic effect started to gradually decrease. The treatments with CGRP peptide **2-4** also showed increasing analgesic effects up to 2.5 h. The blank vehicle showed no significant change in the thermal pain threshold value, confirming vehicle has no effect on C-fiber pain test. Since C- fibers transmit pain signals to brain slowly, withdrawal latencies in the C-fiber pain test were longer than in the $A\delta$ fiber pain testing.

2.5 Conclusion

Even though there are various therapeutics available to treat inflammatory pain, still there is no effective therapeutic option available for the management of inflammatory pain. We describe herein a series of peptide based CGRP receptor antagonists for the treatment of inflammatory pain. Peptides **2-1** to **2-5** were designed, synthesized and screened for their ability to bind to the CGRP receptor and their ability in increasing A δ and c-fiber thermal pain thresholds. Among them, peptide **2-3** showed a higher affinity towards the CGRP receptor than previously reported antagonists CGRP8-37 and CGRP27-37. Further, treatment of peptide **2-3** exhibited analgesic effect up to 2 h in both A δ and c-fiber pain tests. In future, peptide **2-3** will further be evaluated for its specificity towards CGRP receptor over other homologous receptors and toxicity in animal models. Further, if the native structure of peptide **2-3** could be identified by conformational analysis, it will provide more details about the structure-activity relationship. Moreover, peptide **2-3** can be used for further structure optimization to achieve better inhibitory effects.

2.6 Experimental section

2.6.1 General experimental procedures

Nuclear magnetic resonance (NMR) spectra were obtained from a Varian Unity plus 400 MHz Spectrometer in deuterated chloroform (CDCl₃), unless otherwise informed. High resolution mass spectra (HRMS) were obtained from a Waters G2-XS QToF mass spectrometer. Chemicals were purchased from Fisher Scientific, VWR international LLC and Chem-Impex International, Inc. Purification of peptides were carried out on a Varian Prostar 210 HPLC with a UV-Vis detector (254 nm). A C18 reverse phase preparative column from Phenomenex-Jupiter (250 x 10 mm, 10 micron) was used for the analysis.

Peptide 2-1, NH₂-Phe-Val-Pro-Thr-Asn-Val-Gly-Pro-Phe-Ala-Phe-CONH₂.

To 1.0 g (0.52 mmol) of the Fmoc protected resin, a solution of 20% piperidine in DMF (20 mL) was added and subjected to microwave irradiation (50 W, 5 min, 75 °C). The reaction mixture was filtered and washed with DMF (10 ml each, 5 times). To couple the next amino acid phenylalanine, a solution of Fmoc-Phe-OH (1.56 mmol, 3 equiv.) and HBTU (1.40 mmol, 2.7 equiv.) in dry DMF (13 mL) containing 4.2 % diisopropylethyl amine was added to the deprotected resin. The mixture was subjected to microwave irradiation (25 W, 8 min, 75 °C) with stirring. The reaction mixture was filtered and washed with DMF (10 mL each, 5 times). Similarly, deprotecting and coupling steps were repeated until the desired sequence was obtained. Then the standard procedure for cleavage of the peptide from resin was followed. The above resin was washed with dichloromethane (20 mL) and mixed with 15 mL of a cleavage cocktail solution consists of 90% trifluoroacetic acid (TFA), 5% thioanisole, and 5% thiocresol. The mixture was irradiated under a microwave reactor (20 W, 38 °C) for 18 min. The reaction mixture was filtered into a 100 mL flask and diluted with 100 mL of cold diethyl ether to precipitate out the desired peptide. The solid peptide was collected by centrifugation (2500 rpm) and washed three times with cold diethyl ether to give a white solid (254 mg; 41% yield). It was injected and separated on a HPLC using a preparative column (Phenomenex-Jupiter C18) and eluting with 40% methanol/water to 100 % methanol/water over 40 min with a 10 ml/min flow rate. The fractions containing the desired product were combined and lyophilized to yield NH₂-Phe-Val-Pro-Thr-Asn-Val-Gly-Pro-Phe-Ala-Phe-CONH₂ as a white solid (13 mg; 4% yield).

Peptide 2-2, (NH₂-F-I-P-T-N-V-G-P-F-A-F-CONH₂), 2-3, (NH₂-N-F-V-P-T-N-V-G-P-F-A-F-CONH₂), 2-4, (NH₂-W-V-P-T-N-V-G-P-F-A-F-CONH₂), 2-5, (NH₂-D-N-F-V-P-T-N-V-G-P-F-A-F-CONH₂)

Peptides **2-2**, **2-3**, **2-4** and **2-5** were synthesized using a synthetic method similar to the description aforementioned. From 0.7 g (0.364 mmol) of the 4-(2',4'-dimethoxyphenyl-fmoc-aminomethyl)-phenoxy resin, 36 mg (8% yield) of NH₂-F-I-P-T-N-V-G-P-F-A-F-CONH₂ was obtained as a white solid.

From 1.35 g (0.7 mmol) of the 4-(2',4'-dimethoxyphenyl-fmoc-aminomethyl)-phenoxy resin, 46 mg (10% yield) of NH₂-N-F-V-P-T-N-V-G-P-F-A-F-CONH₂ was obtained as a white solid. HRMS (QTof) m/z = 1308.7018 (M+H)⁺, 1330.6888 (M+Na)⁺.

From 0.7 g (0.364 mmol) of the 4-(2',4'-dimethoxyphenyl-fmoc-aminomethyl)-phenoxy resin, 13 mg (3% yield) of NH₂-W-V-P-T-N-V-G-P-F-A-F-CONH₂ was obtained as a white solid. HRMS (QTof) m/z = 1233.6879 (M+H)⁺, 1255.6694 (M+Na)⁺.

From 1.0 g (0.52 mmol) of the 4-(2',4'-dimethoxyphenyl-fmoc-aminomethyl)-phenoxy resin, 16 mg (2.2% yield) of NH₂-D-N-F-V-P-T-N-V-G-P-F-A-F-CONH₂ was obtained as a white solid.

2.7 References

- (1) Park, H. J.; Moon, D. E. Pharmacologic management of chronic pain. *The Korean journal of pain* **2010**, 23, 99-108.
- (2) Nicholson, B. Differential diagnosis: nociceptive and neuropathic pain. *The American journal of managed care* **2006**, 12, S256-262.
- (3) Organization, W. H.: Classification of pain in children. In *WHO guidelines on the pharmacological treatment of persisting pain in children with medical illnesses* World Health Organization, 2012.
- (4) Dubin, A. E.; Patapoutian, A. Nociceptors: the sensors of the pain pathway. *The Journal of clinical investigation* **2010**, 120, 3760.
- (5) Linley, J. E.; Rose, K.; Ooi, L.; Gamper, N. Understanding inflammatory pain: ion channels contributing to acute and chronic nociception. *Pflügers Archiv-European Journal of Physiology* **2010**, 459, 657-669.
- (6) Stein, C.; Clark, J. D.; Oh, U.; Vasko, M. R.; Wilcox, G. L.; Overland, A. C.; Vanderah, T. W.; Spencer, R. H. Peripheral mechanisms of pain and analgesia. *Brain research reviews* **2009**, 60, 90-113.
- (7) Nakamura-Craig, M.; Gill, B. K. Effect of neurokinin A, substance P and calcitonin gene related peptide in peripheral hyperalgesia in the rat paw. *Neuroscience letters* **1991**, 124, 49-51.
- (8) Iyengar, S.; Ossipov, M. H.; Johnson, K. W. The role of calcitonin gene-related peptide in peripheral and central pain mechanisms including migraine. *Pain* **2017**, 158, 543.
- (9) Sun, R.-Q.; Lawand, N. B.; Willis, W. D. The role of calcitonin gene-related peptide (CGRP) in the generation and maintenance of mechanical allodynia and hyperalgesia in rats after intradermal injection of capsaicin. *Pain* **2003**, 104, 201-208.
- (10) Kawamura, M.; Kuraishi, Y.; Minami, M.; Satoh, M. Antinociceptive effect of intrathecally administered antiserum against calcitonin gene-related peptide on thermal and

mechanical noxious stimuli in experimental hyperalgesic rats. *Brain research* **1989**, 497, 199-203.

(11) Yu, Y.; Lundeberg, T.; Yu, L.-C. Role of calcitonin gene-related peptide and its antagonist on the evoked discharge frequency of wide dynamic range neurons in the dorsal horn of the spinal cord in rats. *Regulatory peptides* **2002**, 103, 23-27.

(12) Simons, L. E.; Elman, I.; Borsook, D. Psychological processing in chronic pain: a neural systems approach. *Neuroscience & Biobehavioral Reviews* **2014**, 39, 61-78.

(13) Benarroch, E. E. CGRP sensory neuropeptide with multiple neurologic implications. *Neurology* **2011**, 77, 281-287.

(14) Benemei, S.; Nicoletti, P.; Capone, J. G.; Geppetti, P. CGRP receptors in the control of pain and inflammation. *Current opinion in pharmacology* **2009**, 9, 9-14.

(15) Villalón, C. M.; Olesen, J. The role of CGRP in the pathophysiology of migraine and efficacy of CGRP receptor antagonists as acute antimigraine drugs. *Pharmacology & therapeutics* **2009**, 124, 309-323.

(16) Steenbergh, P.; Höppener, J.; Zandberg, J.; Lips, C.; Jansz, H. A second human calcitonin/CGRP gene. *FEBS letters* **1985**, 183, 408-412.

(17) Ma, H. Calcitonin gene-related peptide (CGRP). *Nat Sci* **2004**, 2, 41-47.

(18) Eftekhari, S.; Edvinsson, L. Possible sites of action of the new calcitonin gene-related peptide receptor antagonists. *Therapeutic advances in neurological disorders* **2010**, 3, 369-378.

(19) Changeux, J. Compartmentalized transcription of acetylcholine receptor genes during motor endplate epigenesis. *The New biologist* **1991**, 3, 413-429.

(20) Russo, A.; Dickerson, I. CGRP: A multifunctional neuropeptide. In *Handbook of neurochemistry and molecular neurobiology*; Springer, 2006; pp 391-426.

(21) Russell, F.; King, R.; Smillie, S.-J.; Kodji, X.; Brain, S. Calcitonin gene-related peptide: physiology and pathophysiology. *Physiological reviews* **2014**, 94, 1099-1142.

(22) Rist, B.; Lacroix, J. S.; Entzeroth, M.; Doods, H. N.; Beck-Sickinger, A. G. CGRP 27–37 analogues with high affinity to the CGRP 1 receptor show antagonistic properties in a rat blood flow assay. *Regulatory peptides* **1999**, 79, 153-158.

(23) Gherardini, G.; Curinga, G.; Colella, G.; Freda, N.; Rauso, R. Calcitonin gene-related peptide and thermal injury: review of literature. *Eplasty* **2009**, 9.

(24) Ittner, L. M.; Koller, D.; Muff, R.; Fischer, J. A.; Born, W. The N-terminal extracellular domain 23– 60 of the calcitonin receptor-like receptor in chimeras with the parathyroid hormone receptor mediates association with receptor activity-modifying protein 1. *Biochemistry* **2005**, 44, 5749-5754.

(25) Rosenblatt, M. I.; Dahl, G. P.; Dickerson, I. M. Characterization and localization of the rabbit ocular calcitonin gene-related peptide (CGRP)-receptor component protein (RCP). *Investigative ophthalmology & visual science* **2000**, 41, 1159-1167.

(26) Prado, M.; Evans-Bain, B.; Dickerson, I. Receptor component protein (RCP): a member of a multi-protein complex required for G-protein-coupled signal transduction. Portland Press Limited, 2002.

(27) Evans, B. N.; Rosenblatt, M. I.; Mnayer, L. O.; Oliver, K. R.; Dickerson, I. M. CGRP-RCP, a novel protein required for signal transduction at calcitonin gene-related peptide and adrenomedullin receptors. *Journal of Biological Chemistry* **2000**, 275, 31438-31443.

(28) Edvinsson, L.; Ho, T. W. CGRP receptor antagonism and migraine. *Neurotherapeutics* **2010**, 7, 164-175.

- (29) Walker, C. S.; Conner, A. C.; Poyner, D. R.; Hay, D. L. Regulation of signal transduction by calcitonin gene-related peptide receptors. *Trends in pharmacological sciences* **2010**, *31*, 476-483.
- (30) Koth, C. M.; Abdul-Manan, N.; Lepre, C. A.; Connolly, P. J.; Yoo, S.; Mohanty, A. K.; Lippke, J. A.; Zwahlen, J.; Coll, J. T.; Doran, J. D. Refolding and characterization of a soluble ectodomain complex of the calcitonin gene-related peptide receptor. *Biochemistry* **2010**, *49*, 1862-1872.
- (31) Moore, E. L.; Salvatore, C. A. Targeting a family B GPCR/RAMP receptor complex: CGRP receptor antagonists and migraine. *British journal of pharmacology* **2012**, *166*, 66-78.
- (32) Kusano, S.; Kukimoto-Niino, M.; Akasaka, R.; Toyama, M.; Terada, T.; Shirouzu, M.; Shindo, T.; Yokoyama, S. Crystal structure of the human receptor activity-modifying protein 1 extracellular domain. *Protein Science* **2008**, *17*, 1907-1914.
- (33) ter Haar, E.; Koth, C. M.; Abdul-Manan, N.; Swenson, L.; Coll, J. T.; Lippke, J. A.; Lepre, C. A.; Garcia-Guzman, M.; Moore, J. M. Crystal structure of the ectodomain complex of the CGRP receptor, a class-B GPCR, reveals the site of drug antagonism. *Structure* **2010**, *18*, 1083-1093.
- (34) Qi, T.; Hay, D. L. Structure–function relationships of the N-terminus of receptor activity-modifying proteins. *British journal of pharmacology* **2010**, *159*, 1059-1068.
- (35) Barwell, J.; Miller, P. S.; Donnelly, D.; Poyner, D. R. Mapping interaction sites within the N-terminus of the calcitonin gene-related peptide receptor; the role of residues 23–60 of the calcitonin receptor-like receptor. *Peptides* **2010**, *31*, 170-176.
- (36) Sluka, K.; Willis, W.; Westlund, K. In *Tilte* 1995; Elsevier.
- (37) Willis Jr, W. Dorsal root potentials and dorsal root reflexes: a double-edged sword. *Experimental Brain Research* **1999**, *124*, 395-421.
- (38) Li, D.; Ren, Y.; Xu, X.; Zou, X.; Fang, L.; Lin, Q. Sensitization of primary afferent nociceptors induced by intradermal capsaicin involves the peripheral release of calcitonin gene-related Peptide driven by dorsal root reflexes. *The Journal of Pain* **2008**, *9*, 1155-1168.
- (39) Lin, Q.; Zou, X.; Willis, W. D. A δ and C primary afferents convey dorsal root reflexes after intradermal injection of capsaicin in rats. *Journal of Neurophysiology* **2000**, *84*, 2695-2698.
- (40) Yu, L.-C.; Hou, J.-F.; Fu, F.-H.; Zhang, Y.-X. Roles of calcitonin gene-related peptide and its receptors in pain-related behavioral responses in the central nervous system. *Neuroscience & Biobehavioral Reviews* **2009**, *33*, 1185-1191.
- (41) Benschop, R.; Collins, E.; Darling, R.; Allan, B.; Leung, D.; Conner, E.; Nelson, J.; Gaynor, B.; Xu, J.; Wang, X.-F. Development of a novel antibody to calcitonin gene-related peptide for the treatment of osteoarthritis-related pain. *Osteoarthritis and cartilage* **2014**, *22*, 578-585.
- (42) Hirsch, S.; Corradini, L.; Just, S.; Arndt, K.; Doods, H. The CGRP receptor antagonist BIBN4096BS peripherally alleviates inflammatory pain in rats. *PAIN®* **2013**, *154*, 700-707.
- (43) Yu, L. C.; Hansson, P.; Brodda-Jansen, G.; Theodorsson, E.; Lundeberg, T. Intrathecal CGRP8–37-induced bilateral increase in hindpaw withdrawal latency in rats with unilateral inflammation. *British journal of pharmacology* **1996**, *117*, 43-50.

- (44) Chiba, T.; Yamaguchi, A.; Yamatani, T.; Nakamura, A.; Morishita, T.; Inui, T.; Fukase, M.; Noda, T.; Fujita, T. Calcitonin gene-related peptide receptor antagonist human CGRP-(8-37). *American Journal of Physiology-Endocrinology And Metabolism* **1989**, *256*, E331-E335.
- (45) Donoso, M. V.; Fournier, A.; St-Pierre, S.; Huidobro-Toro, J. P. Pharmacological characterization of CGRP1 receptor subtype in the vascular system of the rat: studies with hCGRP fragments and analogs. *Peptides* **1990**, *11*, 885-889.
- (46) Maggi, C. A.; Chiba, T.; Giuliani, S. Human α -calcitonin gene-related peptide-(8-37) as an antagonist of exogenous and endogenous calcitonin gene-related peptide. *European journal of pharmacology* **1991**, *192*, 85-88.
- (47) Miranda, L. P.; Holder, J. R.; Shi, L.; Bennett, B.; Aral, J.; Gegg, C. V.; Wright, M.; Walker, K.; Doellgast, G.; Rogers, R. Identification of potent, selective, and metabolically stable peptide antagonists to the calcitonin gene-related peptide (CGRP) receptor. *Journal of medicinal chemistry* **2008**, *51*, 7889-7897.
- (48) Maton, P.; Pradhan, T.; Zhou, Z.-C.; Gardner, J.; Jensen, R. Activities of calcitonin gene-related peptide (CGRP) and related peptides at the CGRP receptor. *Peptides* **1990**, *11*, 485-489.
- (49) Carpenter, K. A.; Schmidt, R.; von Mentzer, B.; Haglund, U.; Roberts, E.; Walpole, C. Turn structures in CGRP C-terminal analogues promote stable arrangements of key residue side chains. *Biochemistry* **2001**, *40*, 8317-8325.
- (50) Lang, M.; De Pol, S.; Baldauf, C.; Hofmann, H.-J.; Reiser, O.; Beck-Sickinger, A. G. Identification of the key residue of calcitonin gene related peptide (CGRP) 27- 37 to obtain antagonists with picomolar affinity at the CGRP receptor. *Journal of medicinal chemistry* **2006**, *49*, 616-624.
- (51) Xie, X.; Pascual, C.; Lieu, C.; Oh, S.; Wang, J.; Zou, B.; Xie, J.; Li, Z.; Xie, J.; Yeomans, D. C. Analgesic Microneedle Patch for Neuropathic Pain Therapy. *ACS nano* **2016**, *11*, 395-406.
- (52) Yung-Chi, C.; Prusoff, W. H. Relationship between the inhibition constant (K_i) and the concentration of inhibitor which causes 50 per cent inhibition (I_{50}) of an enzymatic reaction. *Biochemical pharmacology* **1973**, *22*, 3099-3108.
- (53) Moore, P. A., Hersh, Eliot V.,: Principals of pain management in dentistry. In *The ADA practical guide to substance use disorders and safe prescribing* O'Neil, M., Ed.; John Wiley & Sons, 2015.
- (54) Banik, R. K.; Kabadi, R. A. A modified Hargreaves' method for assessing threshold temperatures for heat nociception. *Journal of neuroscience methods* **2013**, *219*, 41-51.

Chapter 3 - Synthesis of substituted 6-(dimethylamino)-2-phenylisoindolin-1-ones for the inhibition of luciferase

3.1 Introduction

Drugs that enter biological systems tend to act directly or indirectly on either receptor proteins, transporter proteins, ion channels or enzymes to exert their pharmacological effects. Therefore, identification of the molecular targets to which the drug binds, is important for improving the potency, selectivity, physiochemical properties of a drug molecule as well as to understand its toxicological effects.^{1,2}

A class of proteins called luciferase enzymes has been identified as an excellent candidate (protein target) for the drug-protein binding studies due to its high sensitivity to drugs such as anaesthetics.² Light emitting luciferase has been commonly used as a reporter in cells expressing a luciferase gene or its enzymatic activity under the control of a promoter of interest to assess its transcriptional activity.^{3,4} However, the direct inhibition of luciferase in cells, is independent from promoter-specific transcriptional activity.⁵ Since luciferase based assays utilize luciferase enzyme (Luc), luciferin substrate and cellular energy source ATP, firefly luciferase is also used as a sensor of the ATP content in cells as a measure of cell viability, and in biochemical assays to measure ATP-dependent enzyme reactions such as kinases.^{6,7}

Though, a number of luciferase inhibitors with carboxylic acid moiety have been reported, it is suggested that carboxylic acid moiety of the compounds may also be associated with side reactions in cells, such as formation of acyl-glucuronide conjugates and acyl-CoA thioesters.⁸ Therefore, to investigate true inhibitory activities and to understand possible toxicological effects, study of firefly luciferase inhibitory mechanisms is highly relevant.

3.1.1 Firefly luciferase enzyme

Firefly luciferase enzyme is an oxidative enzyme which belongs to oxidoreductases family of enzymes.⁹ Crystal structure of firefly luciferase has shown two distinct domains, a large N-terminal domain (residues 1–436) and a small C-terminal domain (residues 440–550,), separated by a wide cleft.¹⁰ It is suggested that, seven residues (Gly200, Lys206, Glu344, Asp422, Arg437, Gly446 and Glu455) play a crucial role in the binding of ATP and in adenylate formation.¹⁰ Hence, the active site of luciferase is proposed to locate on the surface of both domains facing each other across a large cleft.¹⁰ Further, it is believed that upon substrate binding, the two domains move together to form the active center.¹⁰ Site-directed mutation studies has shown that Lys529 is crucial for effective substrate orientation and for transition state stabilization which lead to efficient adenylate formation.¹¹

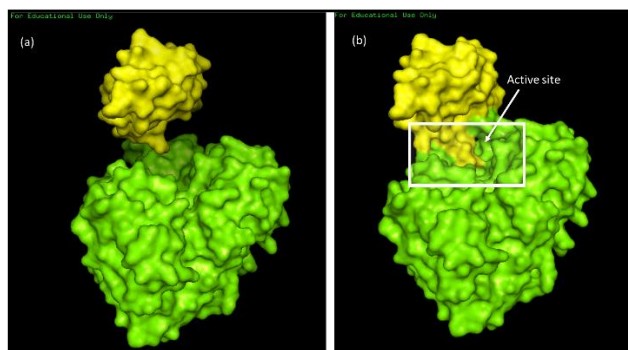


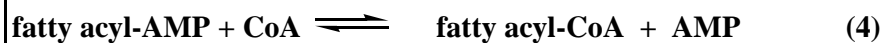
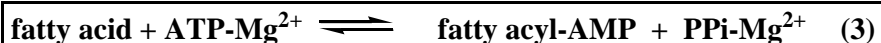
Figure 3.1 Surface view of (a) firefly luciferase (Protein Data Bank accession number 1LCI) without its substrate¹⁰ (b) firefly luciferase in complex with bromoform (Protein Data Bank accession number 1ba3).¹²

Natural substrate of luciferase enzyme is the D-isomer of firefly luciferin (D-LH₂) which is chemically defined as (*S*)-2-(6'-hydroxy-2'-benzothiazolyl)-2-thiazoline-4-carboxylic acid.⁹ The bioluminescent chemical reaction catalyzed by luciferase is a two-step process.^{7,9}



In the first step of the bioluminescent reaction, D-luciferyl-adenylate (D-LH₂-AMP) intermediate is formed by the reaction of D-luciferin (D-LH₂) and ATP in the presence of Mg²⁺.^{7,9} Oxidation of luciferyl-adenylate (D-LH₂-AMP) intermediate with molecular oxygen in the following step produces AMP, oxyluciferin and light.^{7,9}

Besides the light emitting reactions, firefly luciferase catalyzes fatty acyl-CoA synthesis as well.¹³ First, long-chain fatty acids are adenylated in the presence of ATP and Mg²⁺, and the subsequent step is the thioesterification with CoA.^{13,14} The catalytic reaction of acyl-CoA synthetase is as follows¹⁴:



It is reported that the primary structure of firefly luciferase has a high sequence similarity to a long-chain acyl-CoA synthetase.¹⁵

3.1.2 Inhibitors of firefly luciferase

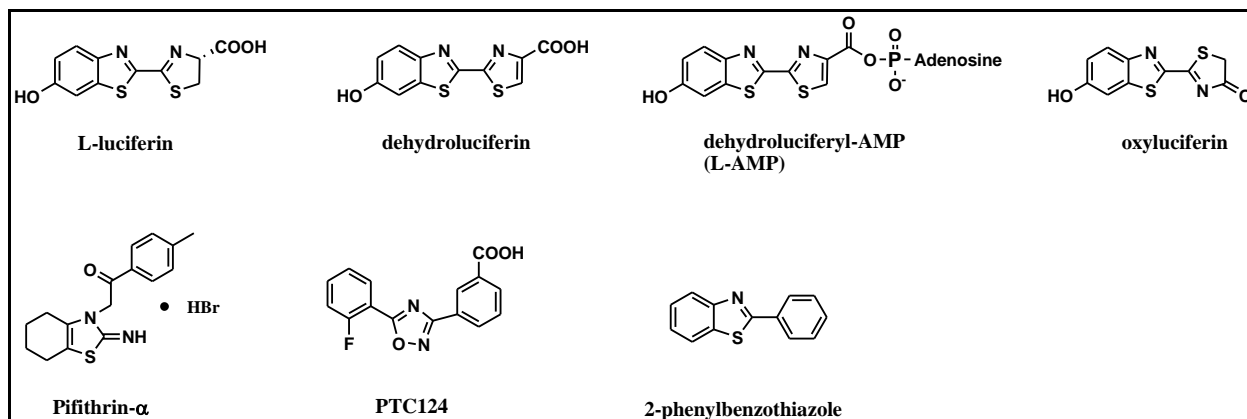
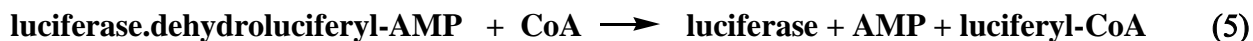
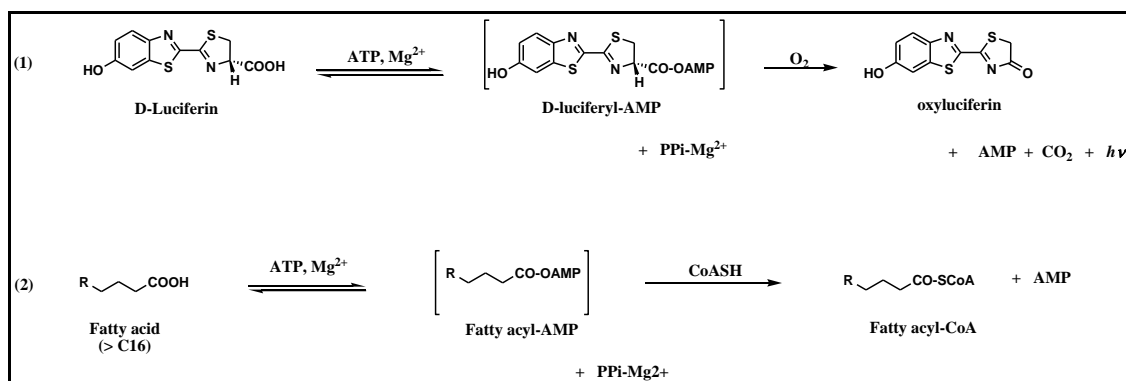


Figure 3.2 Reported firefly luciferase inhibitors.

FLuc inhibitors can be divided as compounds inhibit FLuc activity and compounds increase FLuc activity. Common inhibitors that inhibit FLuc activity are found to be substrate related compounds, intermediates or products of the luciferase catalyzed reaction and fatty acids.⁹ Substrate related compounds such as L-luciferin, dehydroluciferin, intermediates such as dehydroluciferyl-adenylate (L-AMP), and products such as pyrophosphate (PPi) and oxyluciferin were found to inhibit bioluminescent light emission in a competitive or noncompetitive manner.¹⁶⁻²⁰ However, coenzyme A (CoA) was found to prevent this inhibition by reacting with dehydroluciferyl-adenylate (L-AMP).²¹ CoA reaction with L-AMP results free luciferase and luciferyl-CoA (L-CoA) which is found to be a weaker inhibitor in the bioluminescence reaction.^{21,22}



Long chain fatty acids (C12-C20) have also been reported as competitive inhibitors of firefly luciferase against luciferin in micromolar concentration level.^{14,22} It is suggested that luciferase catalyzes the adenylation of fatty acids via carboxylic acid moiety in a mechanism similar to the adenylation step of the bioluminescence reaction of luciferase.²³



Scheme 3.1 Luciferase catalyzed reactions (1) in the presence of D-luciferin D-LH₂ (2) in the presence of long chain fatty acids.¹³

In addition, a small molecule inhibitor of p53 transcriptional activity, Pifithrin- α has also been found to suppress light production/emission activity of firefly luciferase without inhibiting firefly luciferase protein expression activity *in vivo* and *in vitro*.²⁴

In cells, Luc has only a short half-life (~3 h) due to its sensitivity to proteolysis.²⁵ However, when some luciferase inhibitor compounds are added in cell based assays, an increased Luc activity has been observed.²⁵ This increased activity is found to be resulted from a lower rate of degradation of the enzyme due to the formation of stable Luc enzyme-inhibitor (E·I) complexes in cells.²⁵ It has been reported that a 3,5-diaryl-oxadiazole molecule, PTC124-AMP bound to firefly luciferase increases luciferase protein stability through a ligand-induced conformational change.²⁶ Another study has found that 2-phenylbenzothiazole protects Luc from trypsin digestion, resulting increased Luc activity.²⁵

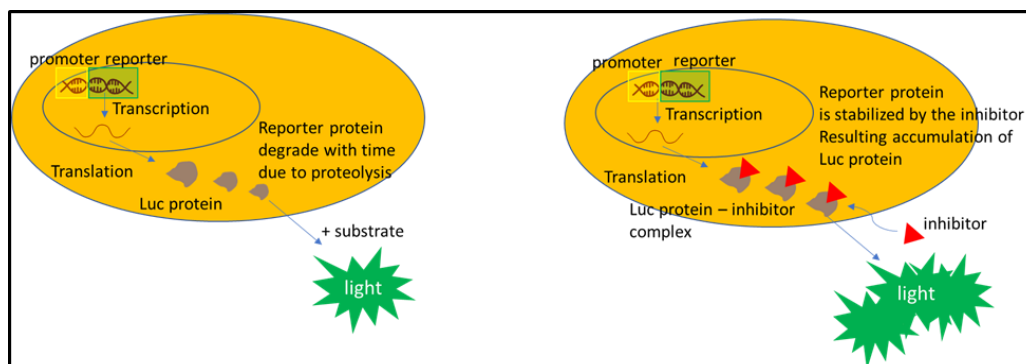


Figure 3.3 An illustration of how firefly luciferase activity is increased by PTC124 inhibitor.

3.1.3 Potential toxicological effects of carboxylic acid moiety

A number of drugs have been withdrawn from the market due to their adverse side effects. Therefore, toxicity is one of the important criteria for a drug to be approved. It is suggested the covalent interaction of electrophilic metabolites of drugs with nucleophiles in macromolecules such as proteins or DNA can cause toxicity.²⁷ Particularly, biotransformation reactions of carboxylic acid such as glucuronidation, CoA conjugation and amino acid conjugation are suggested to cause toxicity.^{28,29} It is reported that carboxylic acids can undergo glucuronidation to give 1-*O*- β -glucuronide in the presence of uridine 5'-diphosphoglucuronosyltransferase (UDP-glucuronosyltransferase, UGT) enzyme and uridine 5'-diphosphoglucuronic acid co-factor and followed by isomerization reactions to give 2-*O*- β -glucuronide, 3-*O*- β -glucuronide and 4-*O*- β -glucuronide. These acyl glucuronides are suggested to contribute to drug toxicity by conjugation with proteins via a trans-acylation or a glycation mechanism.²⁸ ,

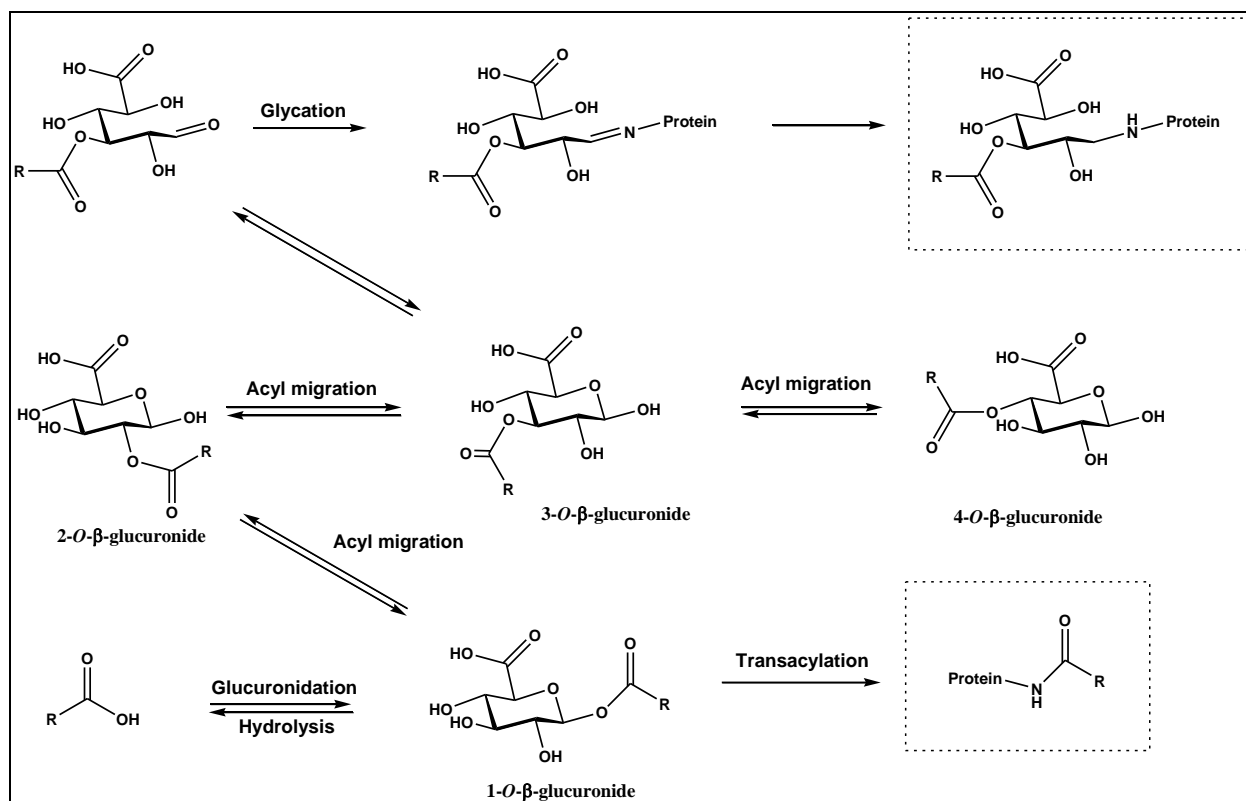


Figure 3.4 Glucuronidation and protein conjugation of carboxylic acid containing drugs.²⁸

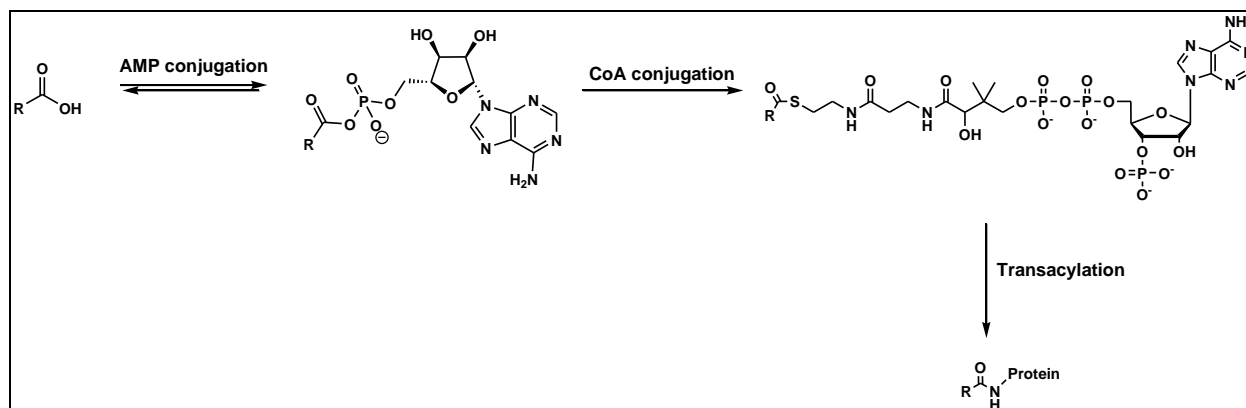


Figure 3.5 CoA conjugation and protein conjugation of carboxylic acid containing drugs.²⁸

Carboxylic acid-containing drugs can also be conjugated with coenzyme A (CoA) to form acyl coenzyme A conjugates.²⁸ It is reported that acyl CoA molecules can be conjugated

with amino acids such as glycine and taurine.³⁰ It is assumed that these conjugates can inhibit enzymes involved in β -oxidation and mitochondrial respiratory chain reactions.³⁰

3.2 Molecular design and synthetic routes

3.2.1 Molecular design of substituted 6-(dimethylamino)-2-phenylisoindolin-1-ones

Nakagomi and coworkers have reported an aromatic carboxylic acid, F-53 which inhibits the enzymatic activity of firefly luciferase by covalently binding to a regulatory lysine residue (Lys529) via an amide bond formation.³¹ Based on experimental results, they proposed that the carboxylic acid of F-53 is first activated to its CoA-thioester derivative by luciferase via its acyl-CoA synthetase activity.³¹ This F-53-CoA derivative is found to selectively inactivate luciferase via acylation of Lys-529 by an unknown cellular acetyltransferase.³¹ With knowledge of above mentioned results, our research efforts focused on synthesizing two analogous probes of F-53 possessing ortho 3-azidopropyl substituent on the phenyl ring with (**3-1**) and without (**3-2**) butyric acid group (**Figure 3.6**). We hypothesized that compound **3-1** acts on luciferase by competing for the binding site of the luciferin substrate which is involved in the light emission. Therefore, these two probe molecules will be used to study the mechanism of luciferase inhibition further for understanding effects of carboxylic acid-containing drugs.

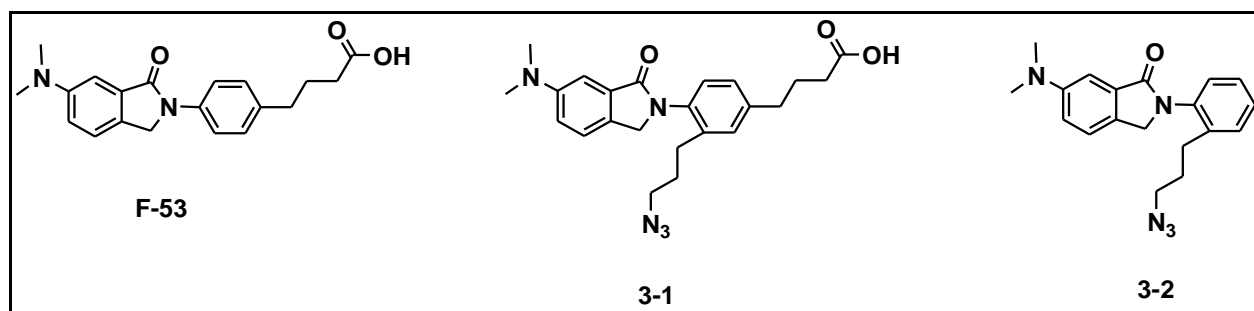


Figure 3.6 Chemical structures of compounds **F-53**, **3-1** and **3-2**.

To predict the binding interactions between the probe molecule **3-1** and the active site of the firefly luciferase, a computational docking experiment was carried out. Computational docking experiments allow prediction of ligand conformations and orientations in the active with their binding affinities.³² We used AutoDock Vina computational docking program as the docking method. Protein data bank (pdb) file of firefly luciferase co-crystalized with PTC124-AMP adduct, 3IES was used for docking studies. Compounds were drawn in Chem3D and energy minimization of the structures was carried out prior to docking. Docking results were visualized using PyMOL software.

To validate our computational docking results, first, we carried out a docking experiment for PTC124-AMP adduct with 3IES. Docking results are shown in **Figure 3.7**. Since the minimum energy binding conformation (out of nine minimum energy conformations) obtained for PTC124-AMP complexed with the protein structure (3IES) from molecular docking experiment was agreed with the crystal structure conformation, we assumed AutoDock Vina docking is able to mimic the real binding interactions between ligand and the protein.

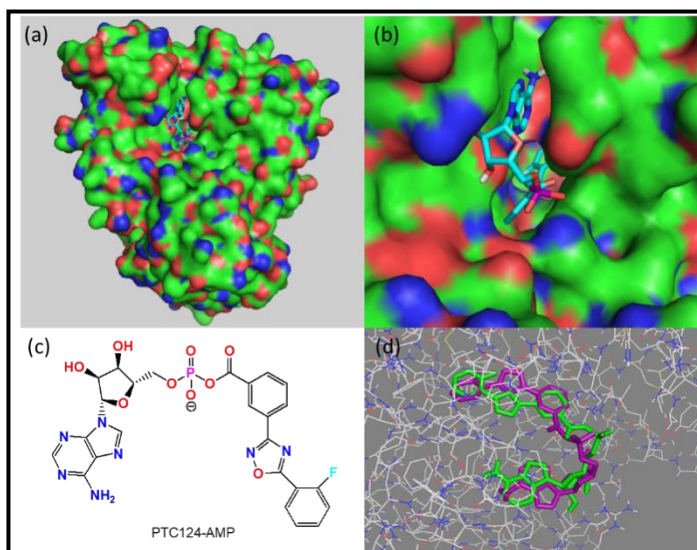


Figure 3.7(a) surface view of conformation #1 of PTC124-AMP complexed with firefly luciferase 3IES structure. (b) zoomed surface view of conformation #1 of PTC124-AMP bound to the active site of firefly luciferase 3IES structure. (c) Chemical structure of PTC124-AMP. (d) overlay of the docking conformation of PTC124-AMP (in purple) and the crystal structure of PTC124-AMP at the active site of firefly luciferase 3IES structure.

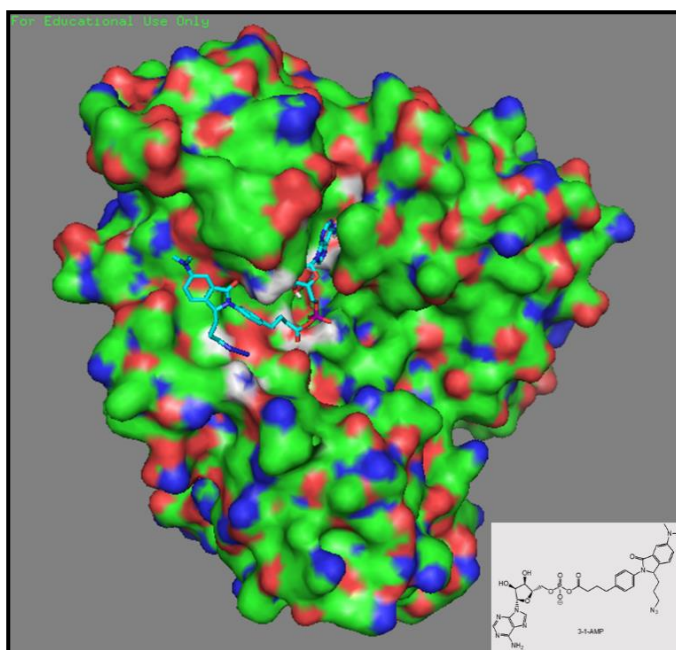


Figure 3.8 Surface view of docking conformation #1 of compound 3-1-AMP complexed with Firefly luciferase (protein pdb code: 3IES).

The lowest binding energy conformation (#1) obtained for **3-1-AMP** from docking results was assumed to stimulate the real binding mode of 3-1 with firefly luciferase enzyme. Surface view of conformation #1 of **3-1-AMP** complexed with firefly luciferase 3IES structure are shown in **Figure 3.9**.

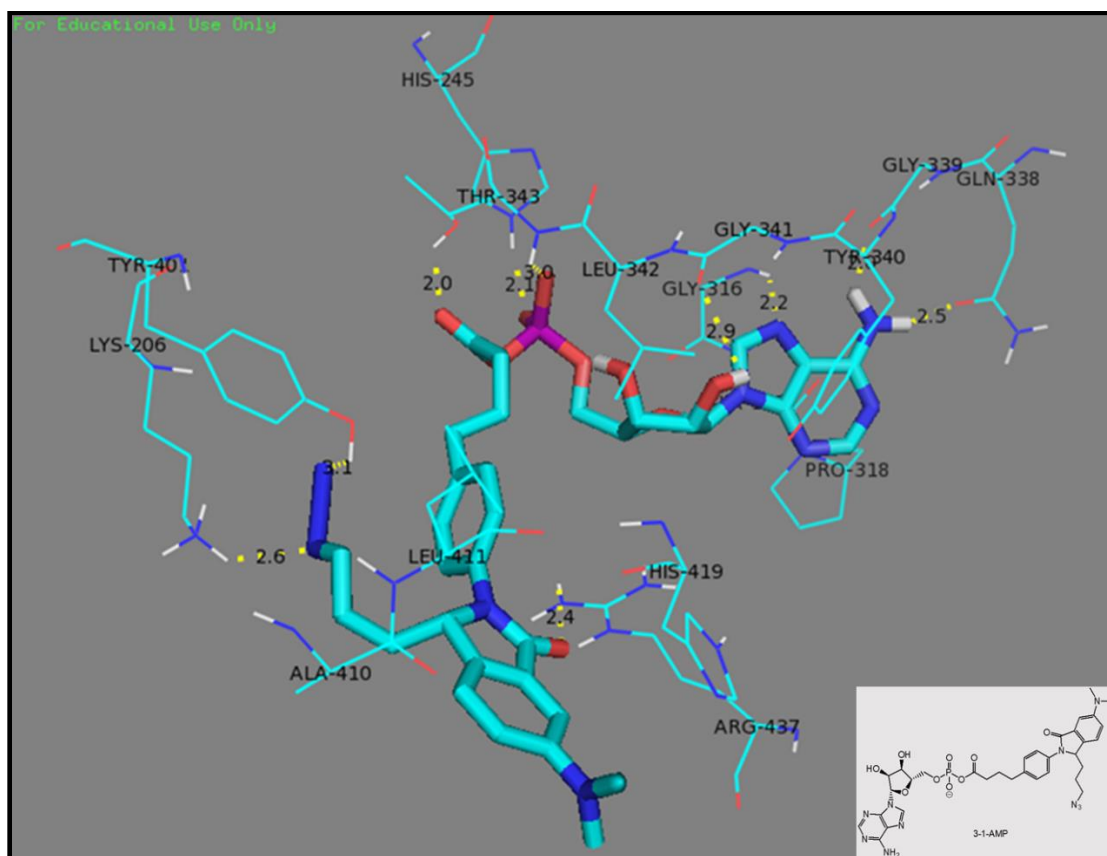


Figure 3.9 Close-up structure of docking conformation #1 of compound **3-1-AMP** with firefly luciferase (protein pdb code: 3IES) showing hydrogen bond and hydrophobic interactions between **3-1-AMP** and the protein. Bonding distances are given in Å.

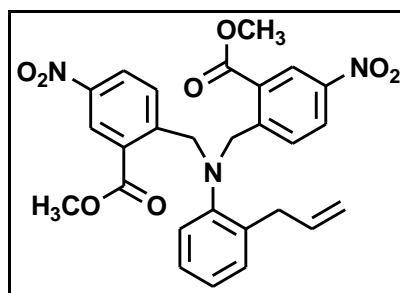
Docking results show several hydrogen bonding interactions. The NH_2 hydrogens of adenine amine of compound **3-1-AMP** form strong hydrogen bonds with the backbone carbonyl of Gln338 and Gly339 of the protein. Also, one of the hydroxyl hydrogen of the ribose sugar form a hydrogen bond with backbone carbonyl group of Gly341. In addition, oxygen atoms of

the phosphate form hydrogen bond with the side chain OH of Thr343 and His245. Further, nitrogen atoms of azide form hydrogen bonds with side chain NH of Lys206 and side chain OH of Tyr401. Carbonyl group of the γ -lactam ring of **3-1-AMP** also forms a hydrogen bond with side chain NH of Arg437. Besides hydrogen bonding, **3-1-AMP** can have hydrophobic interactions as well. The phenyl group of adenine moiety forms hydrophobic interactions with Pro318 and Tyr340. In addition, butyric carbon chain forms hydrophobic interactions with Leu411 and Leu342. Further, Ala410 and His419 are also able to form hydrophobic interactions with the **3-1-AMP** molecule. Since compound **3-1-AMP** has several ligand-protein interactions, we assume compound **3-1** will have strong binding with the firefly luciferase protein at its active site.

3.2.2 Synthetic routes

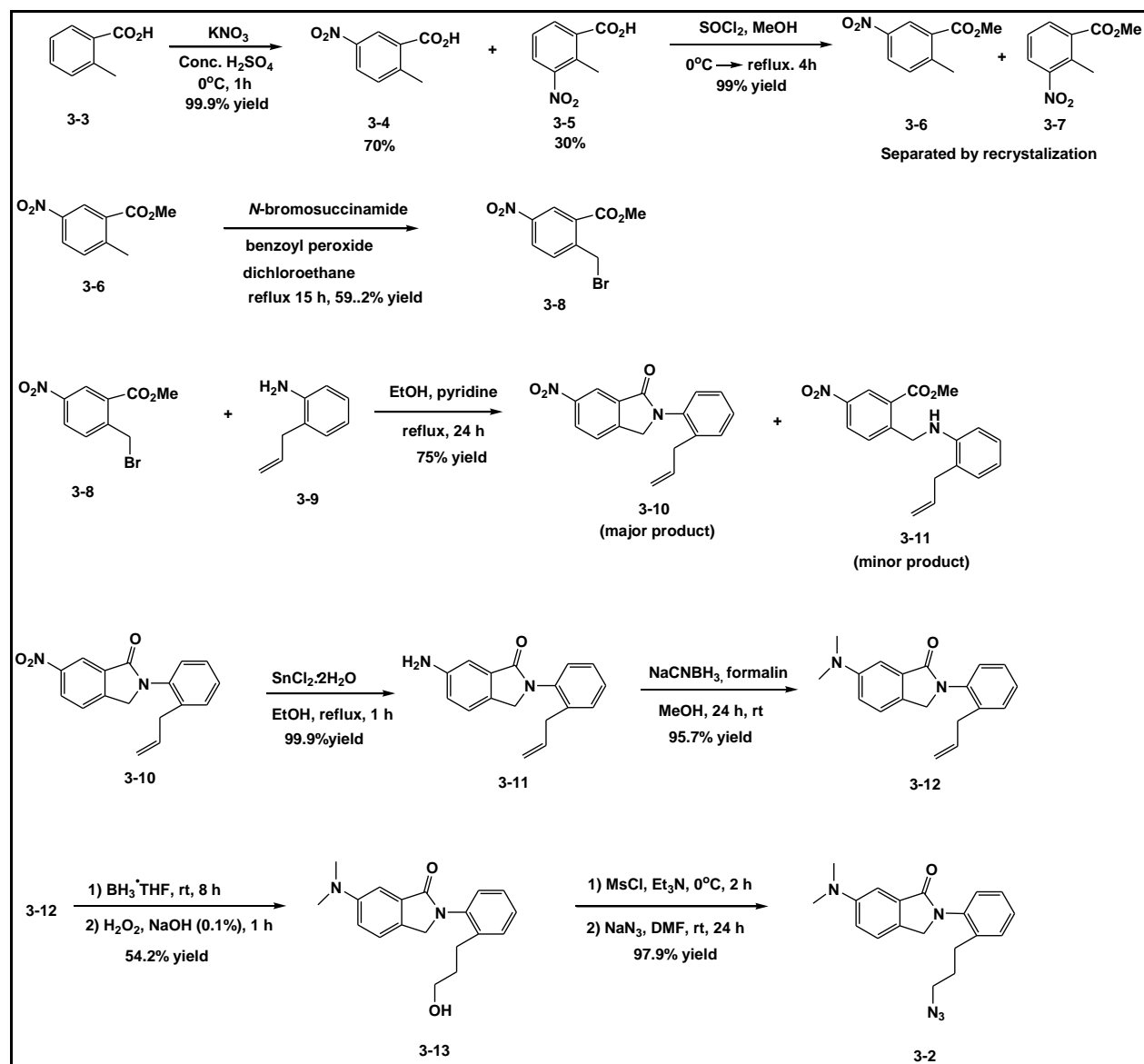
The synthetic route of compound **3-2** is shown in Scheme 3.2. In brief, O-toluic acid, **3-3** in conc. sulfuric acid was treated with a solution of potassium nitrate in conc. sulfuric acid following a reported procedure.³³ In this reaction, potassium nitrate reacts with sulfuric acid to form nitric acid and potassium bisulfate. Sulfuric acid being a stronger acid than nitric acid facilitates generation of NO^{2+} in situ. Importantly, to avoid the formation of di-nitrated product, potassium nitrate in conc. sulfuric acid should be added dropwise to keep the nitronium ion concentration low and the reaction should be carried out at 0 °C to slow down the reaction. During workup, since mixing concentrated sulfuric acid with water gives off much heat, reaction mixture should be added to ice rather than water. The resulting product was a mixture of 2-methyl-5-nitrobenzoic acid, **3-4** (70%) and 2-methyl-3-nitrobenzoic acid, **3-5** (30%). Since, 2-methyl-5-nitrobenzoic acid, **3-4** 2-methyl-3-nitrobenzoic acid, **3-5** are very polar and they both have very similar R_f values, separation using column chromatography was not successful. Therefore, the mixture of **2** and **3** was directly treated with thionyl chloride in methanol.³⁴ Reaction mixture was refluxed to give a mixture of corresponding methyl esters **3-6** and **3-7** in a quantitative yield. In this reaction, methanol reacts with thionyl chloride to provide anhydrous HCl in situ, which leads to acid catalyzed esterification. Resultant compound, **3-6** was able to separate from compound **3-7** using hexane via recrystallization. Benzylic bromination of

compound **3-6** using N-bromosuccinimide and a radical initiator, benzoyl peroxide afforded compound **3-8**.³³ In a separate reaction, 2-allylaniline (**3-9**) was obtained using commercially available *N*-allyl aniline via a thermal induced aromatic amino-Claisen rearrangement and 1 equivalent of boron trifluoride diethyl ether complex ($\text{BF}_3 \cdot \text{OEt}_2$) as a catalyst.³⁵ This reaction was done in a sealed tube at a temperature of 140 °C for 6 h to get the product in 65%. Higher temperatures to 140 °C were resulted cyclized product, 2-Methyl-1*H*-indole which was difficult to separate from 2-allylaniline. Next, the coupling of 2-bromomethyl-5-nitrobenzoic acid methyl ester, **3-8** with 2-allylaniline, **3-9** in EtOH at reflux temperature for 24 h resulted its condensation product, **3-10**.³¹ Low temperature and less reaction times resulted uncyclized product **3-11**. Slight excess of 2-allylaniline was used in this coupling reaction to avoid the formation of the di-substituted product, **3-11B**.



3-11B

The aryl nitro group of compound **3-10** was selectively reduced to obtain the corresponding aryl amine **3-11**, in a quantitative yield and in a short reaction time using stannous chloride.³⁶ Reductive methylation of aryl amino group of compound **3-11** was achieved using formaldehyde and sodium cyanoborohydride to obtain *N,N*-dimethyl product **3-12**. Hydroboration of compound **3-12** followed by oxidation with alkaline hydrogen peroxide yielded the anti-Markovnikov product **3-13**, (compound with the hydroxyl group is attached to the less-substituted carbon). The hydroxymethyl group of compound **3-13** was mesylated using methanesulfonyl chloride/ Et_3N and followed by the azidation with sodium azide to give compound **3-2** in a quantitative yield. In order to make the water-soluble powder of compound **3-2**, it was treated with 1 equivalent of 1N HCl to obtain the HCl salt of molecule **3-2**.



Scheme 3.2 Synthesis of molecule **3-2**.

3.4 Future work

In the future, probe molecules **3-1** and **3-2** will be used for identifying the firefly luciferase inhibition and other possible target protein(s) in cells with the use of click chemistry. Probe molecule **3-1** consists of three elements, which are important in the activity-based protein profiling studies. Those key elements are: a reactive carboxylic group that can covalently reacts

with a residue in the active site of the target enzyme, a spacer for selectivity, and an azide group that can undergo Cu(I)-catalyzed 3 + 2 dipolar cycloaddition with an alkyne bearing a fluorescent detection tag.³⁷⁻³⁹ Probe molecule **3-2**, which does not have a butyric acid group will be used as the negative control.

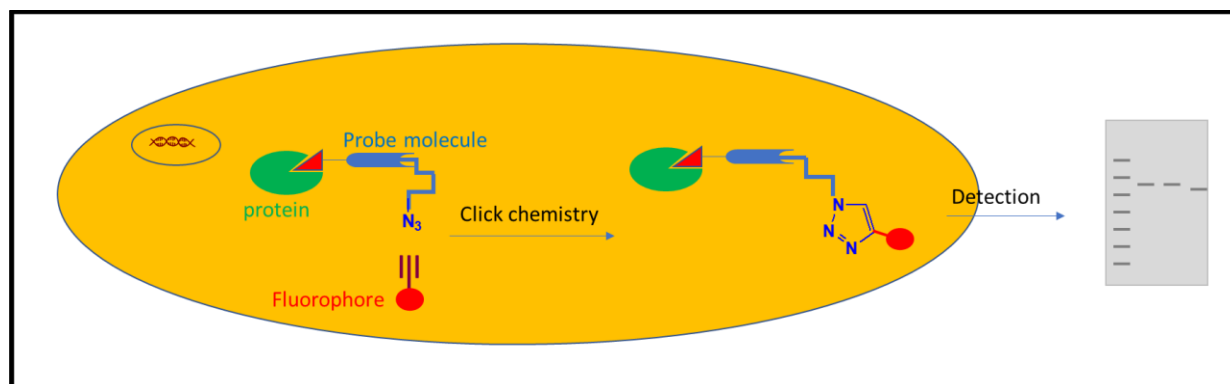
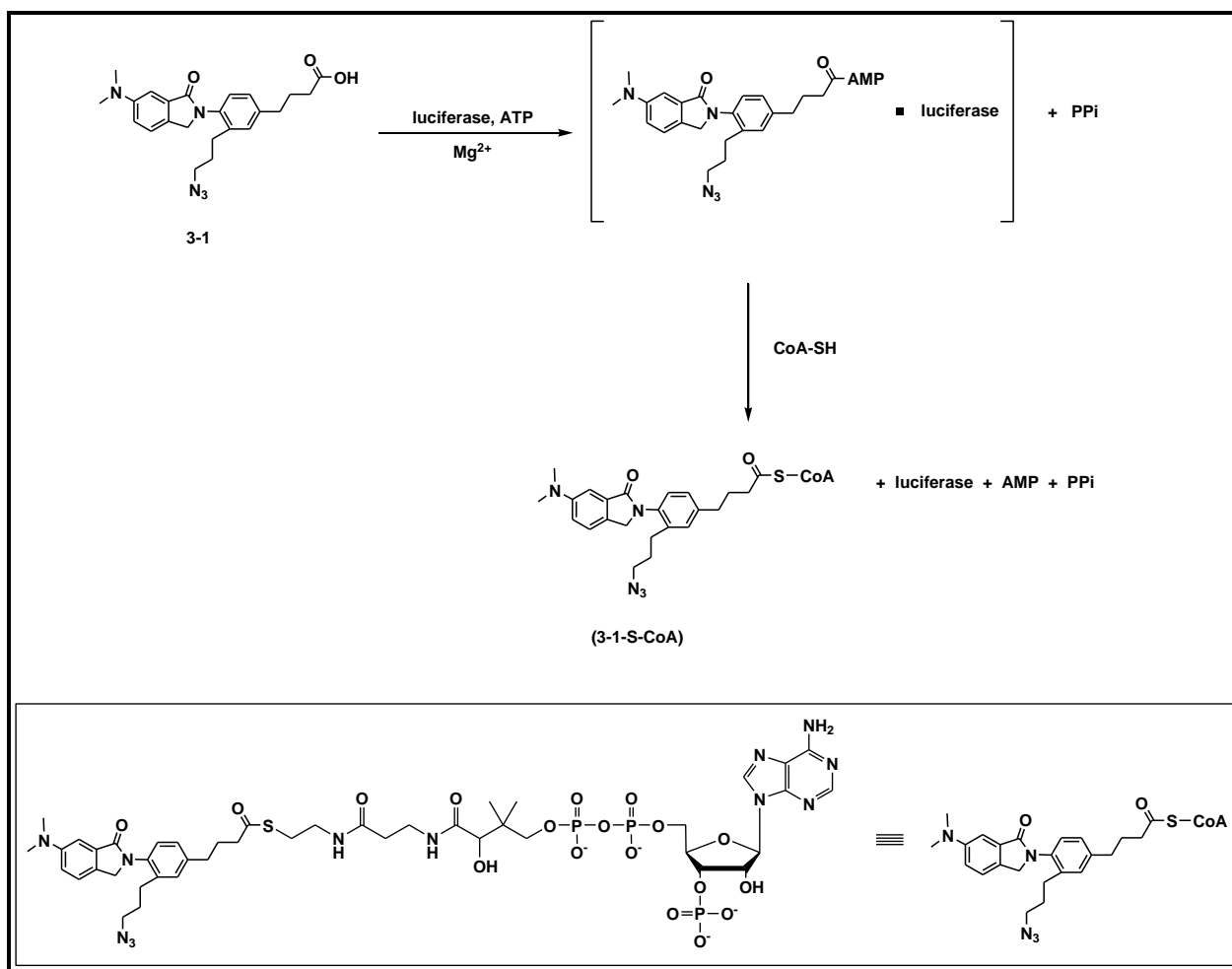


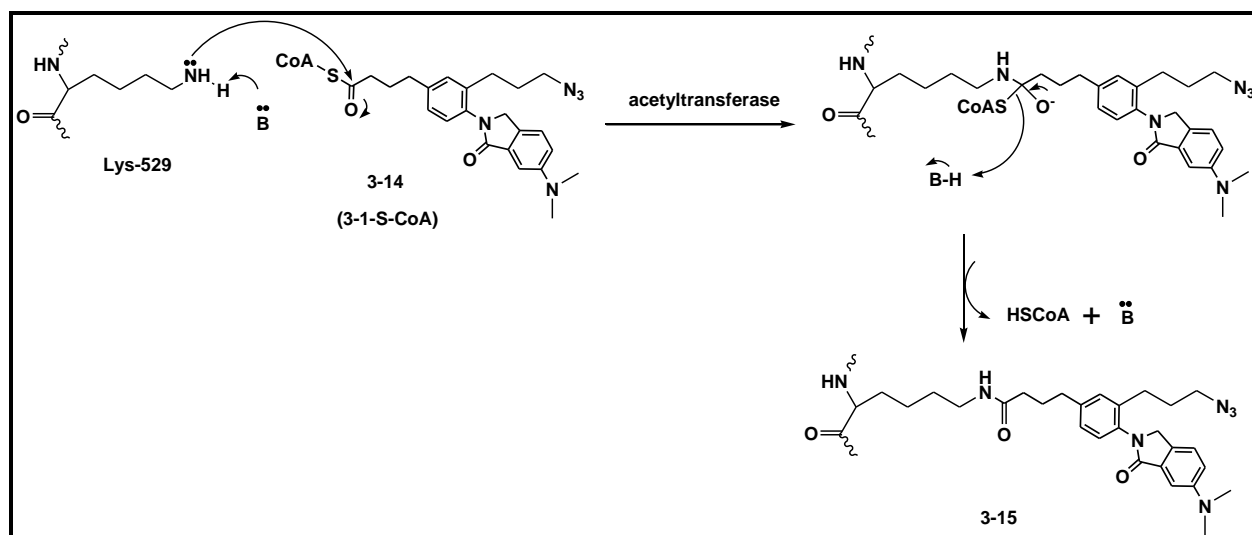
Figure 3.10 Schematic representation of activity-based protein profiling using click chemistry.

Based on previous F-53 experimental results, we propose that the carboxylic acid of **3-1** is first activated to its CoA-thioester derivative by luciferase via its acyl-CoA synthetase activity. A schematic representation for proposed **3-1-S-CoA** synthesis by firefly luciferase is shown in the **Scheme 3.3**.



Scheme 3.3 Schematic representation for 3-1-S-CoA synthesis by firefly luciferase.

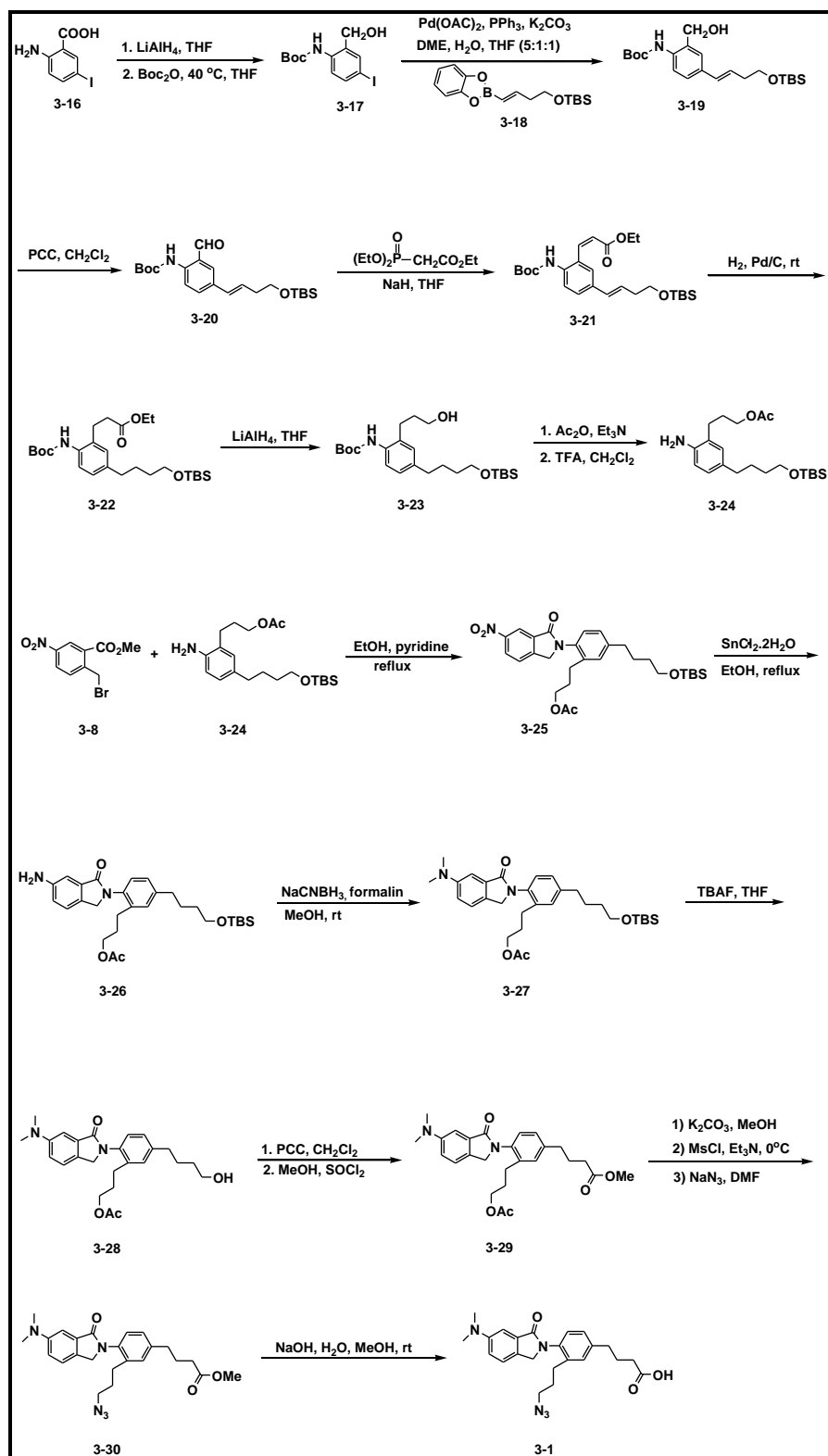
This **3-1-CoA** derivative is proposed to inactivate luciferase via acylation of Lys-529 by an unknown cellular acetyltransferase. Proposed mechanism for the reaction of **3-1-CoA** with firefly luciferase is shown in **Scheme 3.4**.



Scheme 3.4 Proposed mechanism for the reaction of 3-1-CoA with firefly luciferase.

The synthesis of compound **3-1** will be done by Mr. Bo Hao in Prof. Duy Hua's laboratory. The proposed synthetic route of compound **3-1** is shown in **Scheme 3.5**. In brief, the starting material 2-amino-5-iodobenzoic acid (**3-16**), will be treated with lithium aluminum hydride (LiAlH_4) to reduce the carboxylic acid to the alcohol. The free amino group of the resulting compound will be protected using boc anhydride to obtain compound **3-17**. Palladium-catalyzed cross-coupling of alkenyl boronic acid **3-18** with aryl iodide **3-17** will afford compound **3-19**. Alkenyl boronic acid **3-18** can be prepared from 3-butyne-1-ol by silylation, followed by treatment of the protected alkyne (tert-butyldimethyl(3-butyneoxy)silane) with catecholborane. Primary alcohol of the compound **3-19** will then be selectively oxidized to its aldehyde compound **3-20** using pyridinium chlorochromate (PCC) in dichloromethane. The resulting aldehyde **3-20** will be treated with triethyl phosphonoacetate in the presence of NaH base to obtain the Wittig-Horner reaction product **3-21**. The two double bonds of the resulting ethyl ester compound **3-21** will then be reduced using 10% palladium on carbon and H_2 gas. The resulting compound **3-22** can then be reduced to its corresponding alcohol compound **3-23** using LiAlH_4 . Then the resultant alcohol will be protected using acetic anhydride in the presence of triethyl amine base. Then, the boc protected amine will be deprotected using 10% trifluoroacetic acid in dichloromethane to obtain compound **3-24**. Coupling of 2-bromomethyl-5-nitrobenzoic acid methyl ester, **3-8** with compound **3-24** in EtOH at reflux temperature is anticipated to give

its condensation product, **3-25**. The aryl nitro group of compound **3-25** will then be selectively reduced to obtain the corresponding aryl amine **3-26** using a reflux reaction with dehydrated stannous chloride. Reductive methylation of aryl amino group of compound **3-26** using formaldehyde and sodium cyanoborohydride will give the N, N-dimethyl product **3-27**. Then, the *O-tert*-butyldimethylsilyl (OTBS) protecting group will be removed using tetrabutylammonium fluoride solution (TBAF) in THF. Resulting compound, **3-28** will be oxidized to its corresponding acid using PCC and the acid will then be converted to its methyl ester using methanol in acidic condition. Then the acetate protecting group of the resulting compound, **3-29** will be removed by potassium carbonate base in methanol. The resulting hydroxymethyl group of compound **3-29** will be mesylated using methanesulfonyl chloride/Et₃N and followed by the azidation with sodium azide will give compound **3-30**. The methyl ester of the compound **3-30** will then be deprotected using an alkaline medium will give the final product **3-1**.



Scheme 3.5 Proposed synthesis of compound **3-1**.

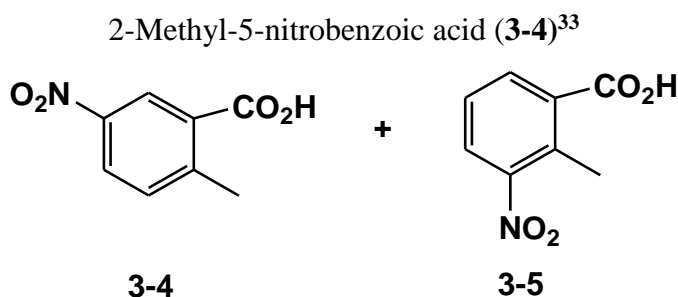
3.5 Conclusion

Probe molecules **3-1** and **3-2** were designed and **3-2** was synthesized. Synthesis of **3-1** is in progress. A plausible synthetic plan for **3-1** is proposed. Compound **3-1** is expected to interact with the active site of firefly luciferase. Compound **3-2** which does not have a reactive carboxylic group, will be used as a negative control in the study. Azido functional group of **3-1** and **3-2** will be coupled with an alkyne bearing a detection tag. Therefore, these two molecules will be used to study firefly luciferase inhibition mechanism and to identify other proteins associated with the **3-1** (carboxylic acid containing active molecule) metabolism.

3.6 Experimental section

3.6.1 General experimental procedures

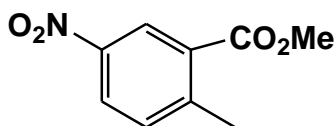
Nuclear magnetic resonance (NMR) spectra were recorded on a Varian Unity plus 400 MHz for ^1H and ^{13}C in deuterated chloroform (CDCl_3), unless otherwise indicated. Low-resolution mass spectra were taken from an API 2000-triple quadrupole ESI-MS/MS mass spectrometer (from Applied Biosystems). Infrared spectra were taken from a ThermoScientific Nicolet 380 FT-IR instrument. Chemicals were purchased from Fisher Scientific Co., Aldrich Chemical Co., Chem-Impex International and VWR.



To a solution of O-toluic acid, **3.3** (15 g, 110.17 mmol) in conc. sulfuric acid (90 mL), a solution of potassium nitrate (15 g, 143.22 mmol) in conc. sulfuric acid (90 mL) was added dropwise over 1 h at 0 °C. After, the reaction mixture was added to a 100 g of ice chips and

stirred vigorously until all ice melted. The resulting precipitate was re-dissolved in ether. Ether layer was washed with water and dried with anhydrous sodium sulfate. The solvent was evaporated under reduced pressure to obtain 19.86 g (99.5% yield) of a mixture of 2-methyl-5-nitrobenzoic acid, **3-4** (70%) and 2-methyl-3-nitrobenzoic acid, **3-5** (30%) as a white solid.

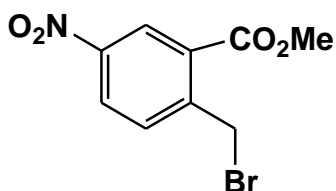
2-Methyl-5-nitrobenzoic acid methyl ester (**3-6**)



3-6

To a mixture of 2-methyl-5-nitrobenzoic acid, **3-4** (70%) and 2-methyl-3-nitrobenzoic acid, **3-5** (30%) (6.88 g, 38.01 mmol) in methanol (80 mL), thionyl chloride (5.52 mL, 76.02 mmol) was added dropwise at 0 °C and it was allowed to stir for 4 h at reflux temperature. The reaction was concentrated under reduced pressure, then re-dissolved in ethyl acetate (100 mL). A solution of sat. sodium bicarbonate (50 mL) was added to adjust the pH to 8. The product was extracted from the aqueous layer using ethyl acetate twice. Combined organic layer was washed with sat. sodium chloride (50 mL) and dried over anhydrous sodium sulfate. The solvent was evaporated under reduced pressure and recrystallized with hexane to obtain 4.78 g (99% yield) of 2-methyl-5-nitrobenzoic acid methyl ester, **3-6** as a white solid. ^1H NMR (400 MHz, CDCl_3) δ ppm 8.78 (d, $J = 2.73$ Hz, 1H), 8.25 (dd, $J = 2.54, 8.40$ Hz, 1H), 7.44 (d, $J = 8.20$ Hz, 1H), 3.96 (s, 3H), 2.73 (s, 3H); ^{13}C NMR (100 MHz, CDCl_3) δ ppm 165.75, 147.80, 145.90, 132.69, 130.40, 126.04, 125.62, 52.34, 21.77; MS (ESI) $m/z = 196.2$ ($\text{M}+\text{H}$) $^+$.

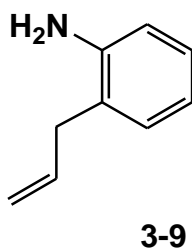
Methyl 2-(bromomethyl)-5-nitrobenzoate (**3-8**)



3-8

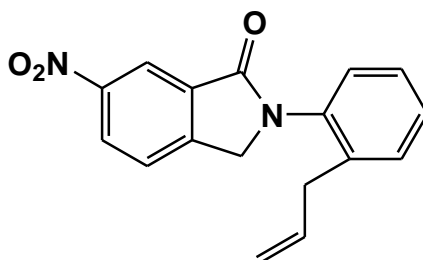
A mixture of 2-methyl-5-nitrobenzoic acid methyl ester, **3-6** (2 g, 10.6 mmol) and *N*-bromosuccinimide (2.07 g, 11.7 mmol) in dichloroethane (80 mL), in the presence of a catalytic amount of benzoyl peroxide (51 mg) was refluxed for 15 h. The reaction mixture was neutralized with sat. sodium bicarbonate and extracted with dichloromethane. The organic layer was dried over anhydrous sodium sulfate. The solvent was evaporated under reduced pressure and the residue was purified by column chromatography (hexanes: ethyl acetate = 9:1) to obtain 1.66 g (59.2% yield) of methyl 2-(bromomethyl)-5-nitrobenzoate, **3-8** as a white solid. ^1H NMR (400 MHz, CDCl_3) δ 8.82 (d, J = 1.95 Hz, 1H), 8.34 (dd, J = 2.54, 8.40 Hz, 1H), 7.69 (d, J = 8.59 Hz, 1H), 5.01 (s, 2H), 4.02 (s, 3H); ^{13}C NMR (100 MHz, CDCl_3) δ ppm 165.05, 147.44, 146.12, 133.02, 130.31, 126.96, 126.45, 53.08, 29.31.

2-Allylaniline (**3-9**)³⁵



To a solution of *N*-allyl aniline (2.5 g, 18.7 mmol) in *o*-xylene (10 mL), $\text{BF}_3 \cdot \text{Et}_2\text{O}$ (2.4 mL, 18.7 mmol) was added. The reaction mixture was stirred for 8 h at 140 °C in a sealed tube. After cooled to room temperature, the reaction was quenched by the addition of 10% NaOH. The reaction mixture was extracted with ethyl acetate. Combined organic layer was washed with sat. sodium chloride (50 mL) and dried over anhydrous sodium sulfate. The solvent was evaporated under reduced pressure and the residue was purified by column chromatography (hexanes: ethyl acetate = 20:1) to obtain 1.62 g (64.8% yield) of 2-allylaniline, **3-9** as a colorless oil. ^1H NMR (400 MHz, CDCl_3) δ 6.98 - 7.14 (m, 2H), 6.76 (t, J = 7.42 Hz, 1H), 6.63 - 6.73 (m, 1H), 5.96 (dq, J = 5.66, 10.87 Hz, 1H), 5.05 - 5.19 (m, 2H), 3.66 (br. s., 2H), 3.32 (d, J = 6.25 Hz, 2H); ^{13}C NMR (100 MHz, CDCl_3) δ ppm 144.64, 135.70, 129.75, 127.18, 123.58, 118.34, 115.71, 115.43, 36.03.

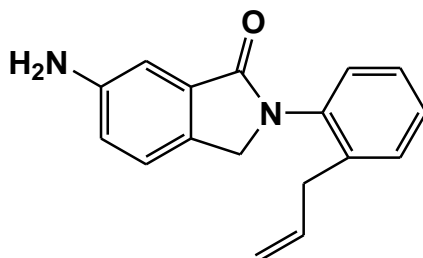
2-(2-Allylphenyl)-6-nitroisindolin-1-one (**3-10**)



3-10

To a solution of 2-bromomethyl-5-nitrobenzoic acid methyl ester, **3-8** (0.7 g, 2.54 mmol) and 2-allylaniline, **3-9** (0.337 g, 2.54 mmol) in absolute ethanol (25 mL), dry pyridine (0.27 mL, 3.30 mmol) was added under argon. The reaction mixture was refluxed at 80 °C for 24 h. After cooled to room temperature, the reaction was neutralized with sat. sodium bicarbonate. The reaction mixture was extracted with ethyl acetate. Combined organic layer was washed with sat. sodium chloride (50 mL) and dried over anhydrous sodium sulfate. The solvent was evaporated under reduced pressure and the residue was purified by column chromatography (hexanes: ethyl acetate = 1:1) to obtain 0.56 g (75% yield) of 2-(2-allylphenyl)-6-nitroisindolin-1-one, **3-10** as a yellow solid. ¹H NMR (400 MHz, CDCl₃) δ 8.80 (s, 1H), 8.49 (dd, *J* = 2.15, 8.40 Hz, 1H), 7.68 (d, *J* = 8.59 Hz, 1H), 7.32 - 7.42 (m, 3H), 7.27 (s, 1H), 5.88 (tdd, *J* = 6.44, 10.15, 16.79 Hz, 1H), 4.87 - 4.98 (m, 2H), 4.82 (s, 2H), 3.40 (d, *J* = 6.25 Hz, 2H); ¹³C NMR (100 MHz, CDCl₃) δ ppm 165.43, 148.34, 147.43, 138.05, 136.10, 135.94, 133.74, 130.6, 128.72, 127.60, 127.48, 126.47, 124.18, 119.33, 116.09, 53.43, 36.17; MS (ESI) *m/z* = 295.1 (M+H)⁺, 317.1 (M+Na)⁺.

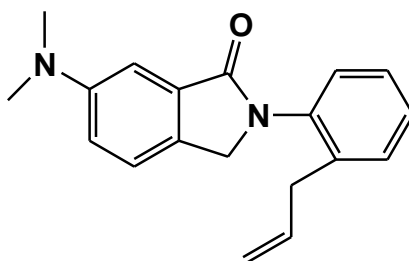
2-(2-Allylphenyl)-6-aminoisindolin-1-one (**3-11**)



3-11

A mixture of **3-10** (0.520 g, 1.77 mmol) and $\text{SnCl}_2 \cdot 2\text{H}_2\text{O}$ (2.0 g, 8.86 mmol) in 30 mL of absolute ethanol was heated at 70 °C under argon. After 1h, the solution was allowed to cool to room temperature and diluted with ethyl acetate. The reaction was neutralized with sat. sodium bicarbonate. The reaction mixture was extracted with ethyl acetate. Combined organic layer was washed with sat. sodium chloride (50 mL) and dried over anhydrous sodium sulfate. The solvent was evaporated under reduced pressure to obtain 0.467 g (99.9% yield) of 2-(2-allylphenyl)-6-aminoisoindolin-1-one, **3-11** as a light yellow solid. ^1H NMR (400 MHz, CDCl_3) δ ppm 7.34 (dt, $J = 2.34, 4.30$ Hz, 2H), 7.29 (td, $J = 3.27, 6.35$ Hz, 1H), 7.25 (s, 1H), 7.23 (s, 1H), 7.20 (d, $J = 1.95$ Hz, 1H), 6.90 (dd, $J = 2.15, 8.01$ Hz, 1H), 5.89 (tdd, $J = 6.64, 10.15, 16.79$ Hz, 1H), 4.88 - 5.02 (m, 2H), 4.60 (s, 2H), 3.90 (br. s., 2H), 3.38 (d, $J = 6.64$ Hz, 2H); ^{13}C NMR (100 MHz, CDCl_3) δ ppm 168.20, 147.07, 138.56, 137.22, 136.61, 133.63, 131.49, 130.63, 128.39, 128.01, 127.45, 123.45, 119.19, 116.23, 109.43, 53.41, 36.28; MS (ESI) $m/z = 265.4$ ($\text{M}+\text{H}$) $^+$, 287.0 ($\text{M}+\text{Na}$) $^+$.

2-(2-Allylphenyl)-6-(dimethylamino)isoindolin-1-one (**3-12**)

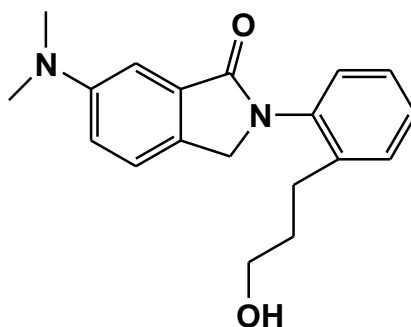


3-12

To a solution of **3-11** (0.77 g, 2.92 mmol) in MeOH, formalin (37% W/W, 4.75 g, 58.4 mmol) and sodium cyanoborohydride (1.1 g, 17.5 mmol) were added, and the mixture was stirred for 24 h at room temperature. Then, the mixture was neutralized with sat. sodium bicarbonate and extracted with ethyl acetate. Combined organic layer was washed with sat. sodium chloride (50 mL) and dried over anhydrous sodium sulfate. The solvent was evaporated under reduced pressure and the residue was purified by column chromatography (hexanes: ethyl acetate = 1:1) to obtain 0.816 g (95.7% yield) of 2-(2-allylphenyl)-6-(dimethylamino)isoindolin-1-one, **3-12** as a white solid. ^1H NMR (400 MHz, CDCl_3) δ 7.27 - 7.39 (m, 4H), 7.24 (d, $J = 2.34$ Hz, 1H), 6.98 (dd, $J = 2.54, 8.40$ Hz, 1H), 5.90 (dd, $J = 10.15, 16.79$ Hz, 1H), 4.85 - 5.03

(m, 2H), 4.53 - 4.67 (m, 2H), 3.29 - 3.43 (m, 2H), 3.08 (br. s., 1H), 2.91 - 3.06 (m, 5H); ^{13}C NMR (100 MHz, CDCl_3) δ ppm 168.79, 151.17, 138.64, 137.35, 136.65, 133.35, 130.66, 129.36, 128.40, 128.06, 127.48, 123.16, 116.71, 116.28, 106.94, 53.36, 41.04, 36.29; MS (ESI) m/z = 293.3 ($\text{M}+\text{H}$) $^+$, 315.5 ($\text{M}+\text{Na}$) $^+$.

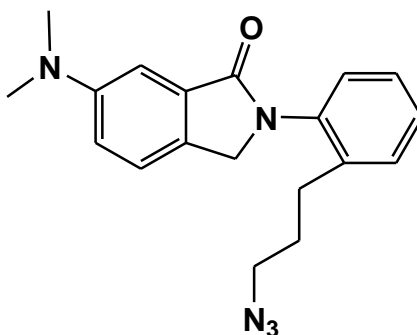
6-(Dimethylamino)-2-(2-(3-hydroxypropyl)phenyl)isoindolin-1-one (**3-13**)



3-13

A solution of borane (1M THF solution, 1.97 mL, 1.97 mmol) was added to a solution of **3-12** (0.720 g, 1.30 mmol) in dry THF under argon. The reaction mixture was stirred at room temperature for 8h. Then the reaction mixture was treated with a basic solution of hydrogen peroxide (30% V/V H_2O_2 , 2.51 mL, 0.025 mmol, 1N NaOH, 5.9 mL, 5.9 mmol) at 0°C. The reaction was stirred at 0°C for 1 h. Then the reaction mixture was extracted with ethyl acetate. Combined organic layer was washed with sat. sodium chloride (50 mL) and dried over anhydrous sodium sulfate. The solvent was evaporated under reduced pressure to obtain 0.414 g (54.2% yield) of 6-(dimethylamino)-2-(2-(3-hydroxypropyl)phenyl)isoindolin-1-one, **3-13** as a yellow solid. ^1H NMR (400 MHz, CDCl_3) δ 7.26 - 7.42 (m, 4H), 7.19 - 7.25 (m, 2H), 6.98 (dd, J = 2.54, 8.40 Hz, 1H), 4.63 (s, 2H), 3.58 (q, J = 5.86 Hz, 2H), 3.03 (s, 6H), 2.68 (t, J = 7.42 Hz, 2H), 2.21 (t, J = 6.05 Hz, 1H), 1.84 - 1.99 (m, 2H); ^{13}C NMR (100 MHz, CDCl_3) δ ppm 169.40, 151.17, 140.22, 137.28, 133.19, 129.84, 129.30, 128.51, 128.21, 127.08, 123.18, 116.79, 106.92, 61.56, 53.71, 40.99, 32.71, 26.81; MS (ESI) m/z = 333.2 ($\text{M}+\text{Na}$) $^+$.

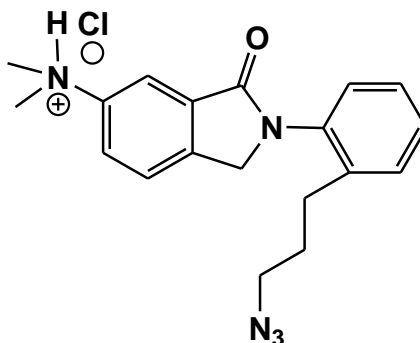
2-(2-(3-Azidopropyl)phenyl)-6-(dimethylamino)isoindolin-1-one (**3-2**)



3-2

To a mixture of **3-13** (0.2 g, 0.64 mmol) and dry triethylamine (126 μ L, 0.90 mmol) in 10 mL of dry dichloromethane, methane sulfonyl chloride was added dropwise at 0°C. The reaction mixture was stirred for 2 h at 0°C. After, the reaction mixture was extracted with dichloromethane. The organic layer was washed with sat. sodium chloride (50 mL) and dried over anhydrous sodium sulfate. The solvent was evaporated under reduced pressure to obtain 0.250 g (100% yield) of methane sulfonate product as a yellow oil. Then, to the solution of methane sulfonate (0.250 g, 0.64 mmol) in dry DMF, NaN₃ (166 mg, 2.56 mmol) was added. The reaction mixture was stirred at room temperature for 24 h. After, the reaction mixture was extracted with dichloromethane, and the organic layer was washed with sat. sodium bicarbonate (50 mL) then, dried over anhydrous sodium sulfate. The solvent was evaporated under reduced pressure and the residue was purified by column chromatography (dichloromethane: methanol = 70:1) to obtain 0.210 g (97.9% yield) of 2-(2-(3-azidopropyl)phenyl)-6-(dimethylamino)isoindolin-1-one, **3-2** as a yellow oil. ¹H NMR (400 MHz, CDCl₃) δ 7.33 - 7.37 (m, 2H), 7.28 - 7.33 (m, 2H), 7.24 (dd, J = 2.15, 5.66 Hz, 2H), 6.99 (dd, J = 1.95, 8.20 Hz, 1H), 4.63 (s, 2H), 3.25 (t, J = 6.83 Hz, 2H), 3.04 (s, 4H), 2.63 - 2.71 (m, 3H), 1.89 (td, J = 7.18, 14.94 Hz, 3H); ¹³C NMR (101 MHz, CDCl₃) δ ppm 168.98, 151.16, 139.49, 137.37, 133.18, 130.04, 129.21, 128.47, 128.25, 127.45 (s) 123.22 (s) 116.73 (s) 106.87 (s) 53.45 (s) 51.02 (s) 40.97 (s) 29.25 (s) 28.56 (s); MS (ESI) m/z = 335.8 (M+H)⁺, 357.9 (M+Na)⁺.

2-(2-(3-Azidopropyl)phenyl)-N,N-dimethyl-3-oxoisindolin-5-aminium chloride



Molecule **3-2** was re-dissolved in acetonitrile and treated with 1 equivalent of 1N HCl. Then it was diluted with de-ionized water and lyophilized to obtain 0.232 g (100% yield) of 2-(2-(3-azidopropyl)phenyl)-N,N-dimethyl-3-oxoisindolin-5-aminium chloride as a yellow solid. ^1H NMR (400 MHz, CDCl_3) δ 8.38 (d, $J = 7.81$ Hz, 1H), 8.11 (s, 1H), 7.67 (d, $J = 8.20$ Hz, 1H), 7.30 - 7.41 (m, 3H), 7.22 (d, $J = 7.81$ Hz, 1H), 4.79 (s, 2H), 3.24 (t, $J = 6.44$ Hz, 2H), 3.20 (s, 6H), 2.60 - 2.66 (m, 2H), 1.82 - 1.91 (m, 2H); ^{13}C NMR (101 MHz, CDCl_3) δ ppm 166.68, 144.28, 142.38, 139.47, 136.25, 134.66, 130.40, 129.34, 128.16, 127.87, 125.92, 125.44, 115.52, 53.80, 50.94, 46.64, 29.47, 28.56; MS (ESI) $m/z = 335.8$ ($\text{M}+\text{H}$) $^+$, 357.8 ($\text{M}+\text{Na}$) $^+$.

3.7 References

- (1) Franks, N. P.; Lieb, W. Do general anaesthetics act by competitive binding to specific receptors? *Nature* **1984**, *310*, 599-601.
- (2) Franks, N.; Lieb, W. Molecular mechanisms of general anaesthesia. *Nature* **1982**, *300*, 487-493.
- (3) Thorne, N.; Shen, M.; Lea, W. A.; Simeonov, A.; Lovell, S.; Auld, D. S.; Inglese, J. Firefly luciferase in chemical biology: a compendium of inhibitors, mechanistic evaluation of chemotypes, and suggested use as a reporter. *Chemistry & biology* **2012**, *19*, 1060-1072.
- (4) Fan, F.; Wood, K. V. Bioluminescent assays for high-throughput screening. *Assay and drug development technologies* **2007**, *5*, 127-136.
- (5) Braeuning, A. Firefly luciferase inhibition: a widely neglected problem. *Archives of toxicology* **2015**, *89*, 141-142.
- (6) Kricka, L. J.; Thorpe, G. H. Chemiluminescent and bioluminescent methods in analytical chemistry. A review. *Analyst* **1983**, *108*, 1274-1296.

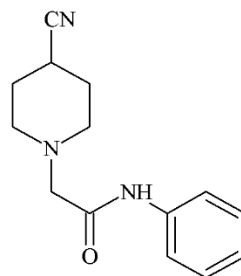
- (7) Auld, D. S.; Southall, N. T.; Jadhav, A.; Johnson, R. L.; Diller, D. J.; Simeonov, A.; Austin, C. P.; Inglese, J. Characterization of chemical libraries for luciferase inhibitory activity. *Journal of medicinal chemistry* **2008**, *51*, 2372-2386.
- (8) Skonberg, C.; Olsen, J.; Madsen, K. G.; Hansen, S. H.; Grillo, M. P. Metabolic activation of carboxylic acids. *Expert opinion on drug metabolism & toxicology* **2008**, *4*, 425-438.
- (9) Leitão, J. M.; da Silva, J. C. E. Firefly luciferase inhibition. *Journal of Photochemistry and Photobiology B: Biology* **2010**, *101*, 1-8.
- (10) Conti, E.; Franks, N. P.; Brick, P. Crystal structure of firefly luciferase throws light on a superfamily of adenylate-forming enzymes. *Structure* **1996**, *4*, 287-298.
- (11) Branchini, B. R.; Murtiashaw, M. H.; Magyar, R. A.; Anderson, S. M. The role of lysine 529, a conserved residue of the acyl-adenylate-forming enzyme superfamily, in firefly luciferase. *Biochemistry* **2000**, *39*, 5433-5440.
- (12) Franks, N.; Jenkins, A.; Conti, E.; Lieb, W.; Brick, P. Structural basis for the inhibition of firefly luciferase by a general anesthetic. *Biophysical journal* **1998**, *75*, 2205-2211.
- (13) Oba, Y.; Ojika, M.; Inouye, S. Firefly luciferase is a bifunctional enzyme: ATP-dependent monooxygenase and a long chain fatty acyl-CoA synthetase. *FEBS letters* **2003**, *540*, 251-254.
- (14) Inouye, S. Firefly luciferase: an adenylate-forming enzyme for multicatalytic functions. *Cellular and molecular life sciences* **2010**, *67*, 387-404.
- (15) Suzuki, H.; Kawarabayasi, Y.; Kondo, J.; Abe, T.; Nishikawa, K.; Kimura, S.; Hashimoto, T.; Yamamoto, T. Structure and regulation of rat long-chain acyl-CoA synthetase. *Journal of Biological Chemistry* **1990**, *265*, 8681-8685.
- (16) Airth, R.; Rhodes, W.; McElroy, W. The function of coenzyme A in luminescence. *Biochimica et biophysica acta* **1958**, *27*, 519-532.
- (17) McElroy, W.; Hastings, J.; Coulombre, J.; Sonnenfeld, V. The mechanism of action of pyrophosphate in firefly luminescence. *Archives of biochemistry and biophysics* **1953**, *46*, 399-416.
- (18) Nakamura, M.; Maki, S.; Amano, Y.; Ohkita, Y.; Niwa, K.; Hirano, T.; Ohmiya, Y.; Niwa, H. Firefly luciferase exhibits bimodal action depending on the luciferin chirality. *Biochemical and biophysical research communications* **2005**, *331*, 471-475.
- (19) Lemasters, J. J.; Hackenbrock, C. R. Kinetics of product inhibition during firefly luciferase luminescence. *Biochemistry* **1977**, *16*, 445-447.
- (20) da Silva, L. P.; da Silva, J. C. E. Kinetics of inhibition of firefly luciferase by dehydroluciferin-coenzyme A, dehydroluciferin and L-luciferin. *Photochemical & Photobiological Sciences* **2011**, *10*, 1039-1045.
- (21) Fontes, R.; Dukhovich, A.; Sillero, A.; Sillero, M. A. G. Synthesis of dehydroluciferin by firefly luciferase: effect of dehydroluciferin, coenzyme A and nucleoside triphosphates on the luminescent reaction. *Biochemical and biophysical research communications* **1997**, *237*, 445-450.
- (22) Matsuki, H.; Suzuki, A.; Kamaya, H.; Ueda, I. Specific and non-specific binding of long-chain fatty acids to firefly luciferase: cutoff at octanoate. *Biochimica et Biophysica Acta (BBA)-General Subjects* **1999**, *1426*, 143-150.
- (23) Marques, S. M.; Esteves da Silva, J. C. Firefly bioluminescence: a mechanistic approach of luciferase catalyzed reactions. *IUBMB life* **2009**, *61*, 6-17.

- (24) Rocha, S.; Campbell, K. J.; Roche, K. C.; Perkins, N. D. The p53-inhibitor pifithrin- α inhibits firefly luciferase activity in vivo and in vitro. *BMC molecular biology* **2003**, *4*, 9.
- (25) Thompson, J. F.; Hayes, L. S.; Lloyd, D. B. Modulation of firefly luciferase stability and impact on studies of gene regulation. *Gene* **1991**, *103*, 171-177.
- (26) Auld, D. S.; Lovell, S.; Thorne, N.; Lea, W. A.; Maloney, D. J.; Shen, M.; Rai, G.; Battaile, K. P.; Thomas, C. J.; Simeonov, A. Molecular basis for the high-affinity binding and stabilization of firefly luciferase by PTC124. *Proceedings of the National Academy of Sciences* **2010**, *107*, 4878-4883.
- (27) Uetrecht, J. Prediction of a new drug's potential to cause idiosyncratic reactions. *Current opinion in drug discovery & development* **2001**, *4*, 55-59.
- (28) Lassila, T.; Hokkanen, J.; Aatsinki, S.-M.; Mattila, S.; Turpeinen, M.; Tolonen, A. Toxicity of carboxylic acid-containing drugs: The role of acyl migration and CoA conjugation investigated. *Chemical research in toxicology* **2015**, *28*, 2292-2303.
- (29) Smith, D. A.: *Metabolism, pharmacokinetics, and toxicity of functional groups: impact of the building blocks of medicinal chemistry in ADMET*; Royal Society of Chemistry, 2010.
- (30) Darnell, M.; Weidolf, L. Metabolism of xenobiotic carboxylic acids: focus on coenzyme A conjugation, reactivity, and interference with lipid metabolism. *Chemical research in toxicology* **2013**, *26*, 1139-1155.
- (31) Nakagomi, M.; Fujimaki, N.; Ito, A.; Toda, T.; Fukasawa, H.; Shudo, K.; Tomita, R. A Novel Aromatic Carboxylic Acid Inactivates Luciferase by Acylation of an Enzymatically Active Regulatory Lysine Residue. *PloS one* **2013**, *8*, e75445.
- (32) Meng, X.-Y.; Zhang, H.-X.; Mezei, M.; Cui, M. Molecular docking: a powerful approach for structure-based drug discovery. *Current computer-aided drug design* **2011**, *7*, 146-157.
- (33) Gobbi, S.; Cavalli, A.; Negri, M.; Schewe, K. E.; Belluti, F.; Piazzzi, L.; Hartmann, R. W.; Recanatini, M.; Bisi, A. Imidazolylmethylbenzophenones as highly potent aromatase inhibitors. *Journal of medicinal chemistry* **2007**, *50*, 3420-3422.
- (34) Ghosh, A. K.; Takayama, J.; Aubin, Y.; Ratia, K.; Chaudhuri, R.; Baez, Y.; Sleeman, K.; Coughlin, M.; Nichols, D. B.; Mulhearn, D. C. Structure-Based Design, Synthesis, and Biological Evaluation of a Series of Novel and Reversible Inhibitors for the Severe Acute Respiratory Syndrome– Coronavirus Papain-Like Protease. *Journal of medicinal chemistry* **2009**, *52*, 5228-5240.
- (35) Yamamoto, H.; Ho, E.; Namba, K.; Imagawa, H.; Nishizawa, M. Hg (OTf) 2–BINAPHANE-Catalyzed Enantioselective Anilino Sulfonamide Allyl Alcohol Cyclization. *Chemistry-A European Journal* **2010**, *16*, 11271-11274.
- (36) Bellamy, F. D.; Ou, K. Selective reduction of aromatic nitro compounds with stannous chloride in non acidic and non aqueous medium. *Tetrahedron Letters* **1984**, *25*, 839-842.
- (37) Speers, A. E.; Cravatt, B. F. Profiling enzyme activities in vivo using click chemistry methods. *Chemistry & biology* **2004**, *11*, 535-546.
- (38) Kolb, H. C.; Sharpless, K. B. The growing impact of click chemistry on drug discovery. *Drug discovery today* **2003**, *8*, 1128-1137.
- (39) Li, L.; Zhang, Z. Development and applications of the copper-catalyzed azide-alkyne cycloaddition (CuAAC) as a bioorthogonal reaction. *Molecules* **2016**, *21*, 1393.

Appendix A - Supplemental data

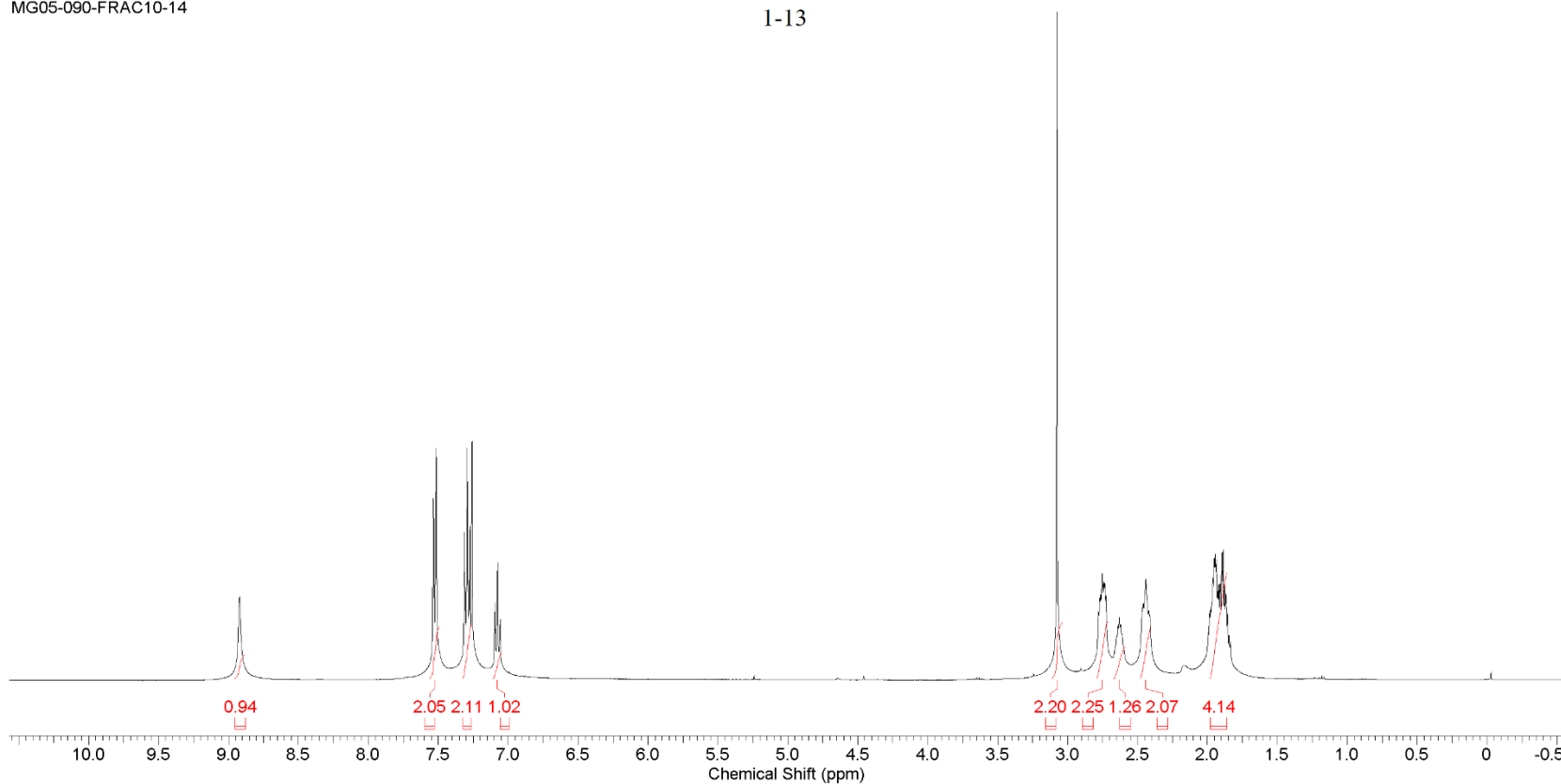
This report was created by ACD/NMR Processor Academic Edition. For more information go to www.acdlabs.com/nmrproc/

Formula	C ₁₄ H ₁₇ N ₃ O	FW	243.3043
---------	--	----	----------



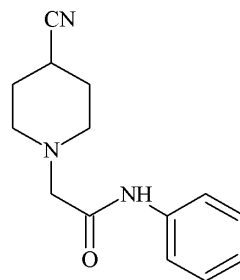
MG05-090-FRAC10-14

1-13



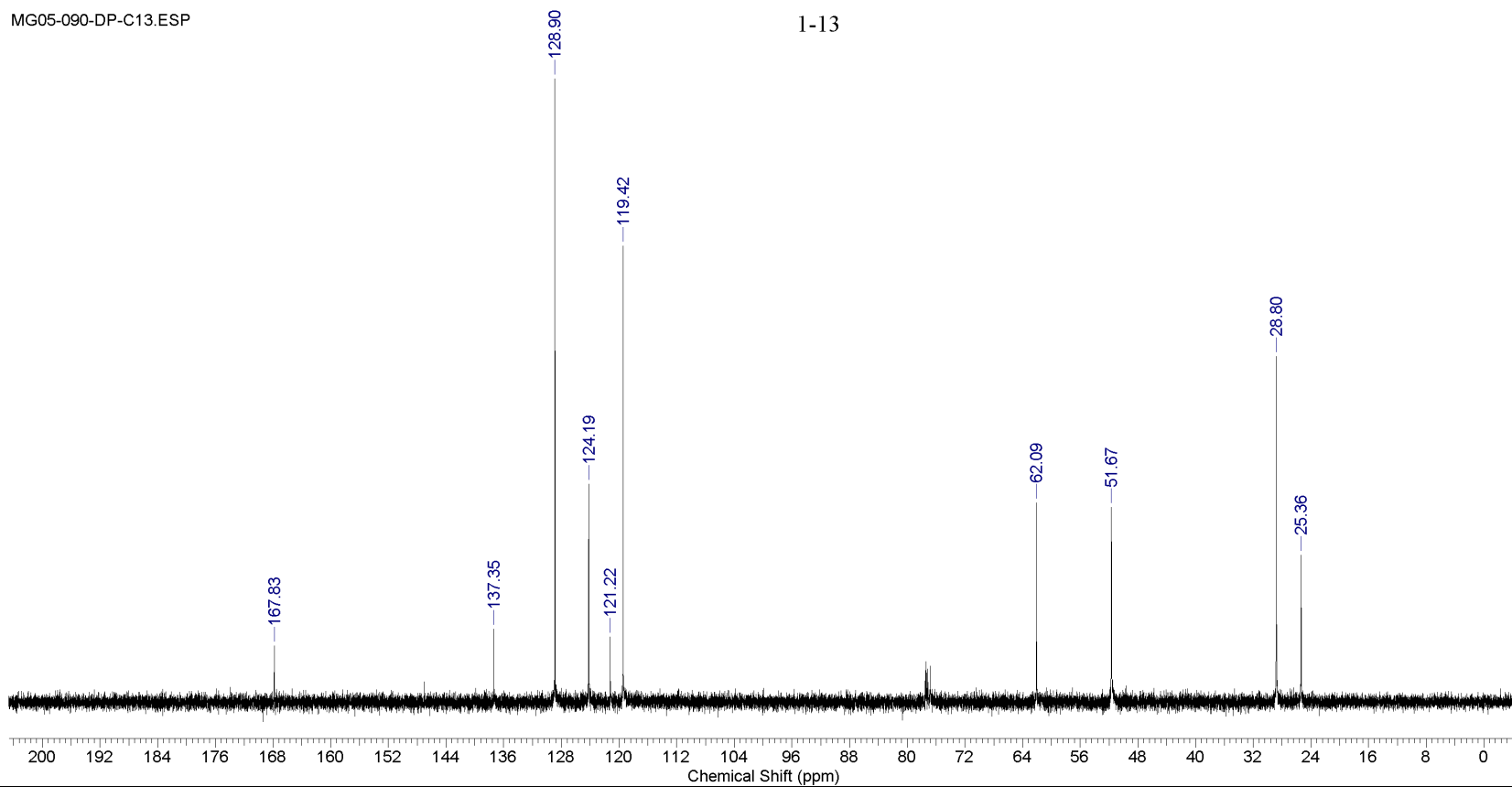
This report was created by ACD/NMR Processor Academic Edition. For more information go to www.acdlabs.com/nmrproc/

Formula	C ₁₄ H ₁₇ N ₃ O	FW	243.3043
---------	--	----	----------



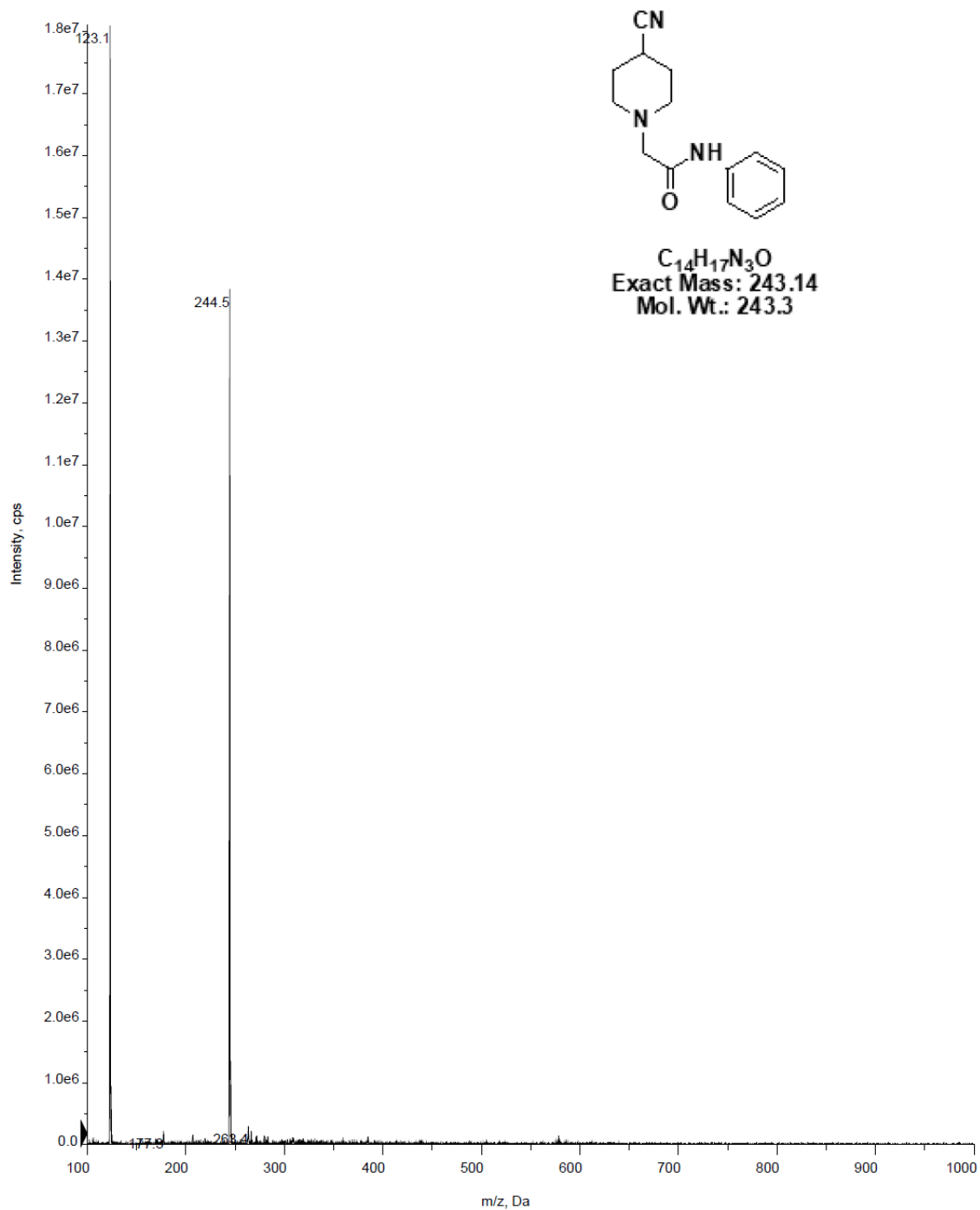
1-13

MG05-090-DP-C13.ESP



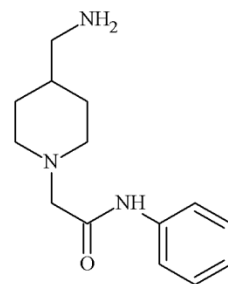
■ +Q1: 34 MCA scans from Sample 1 (TuneSampleID) of MT20140605180920.wiff (Turbo Spray)

Max. 1.8e7 cps.



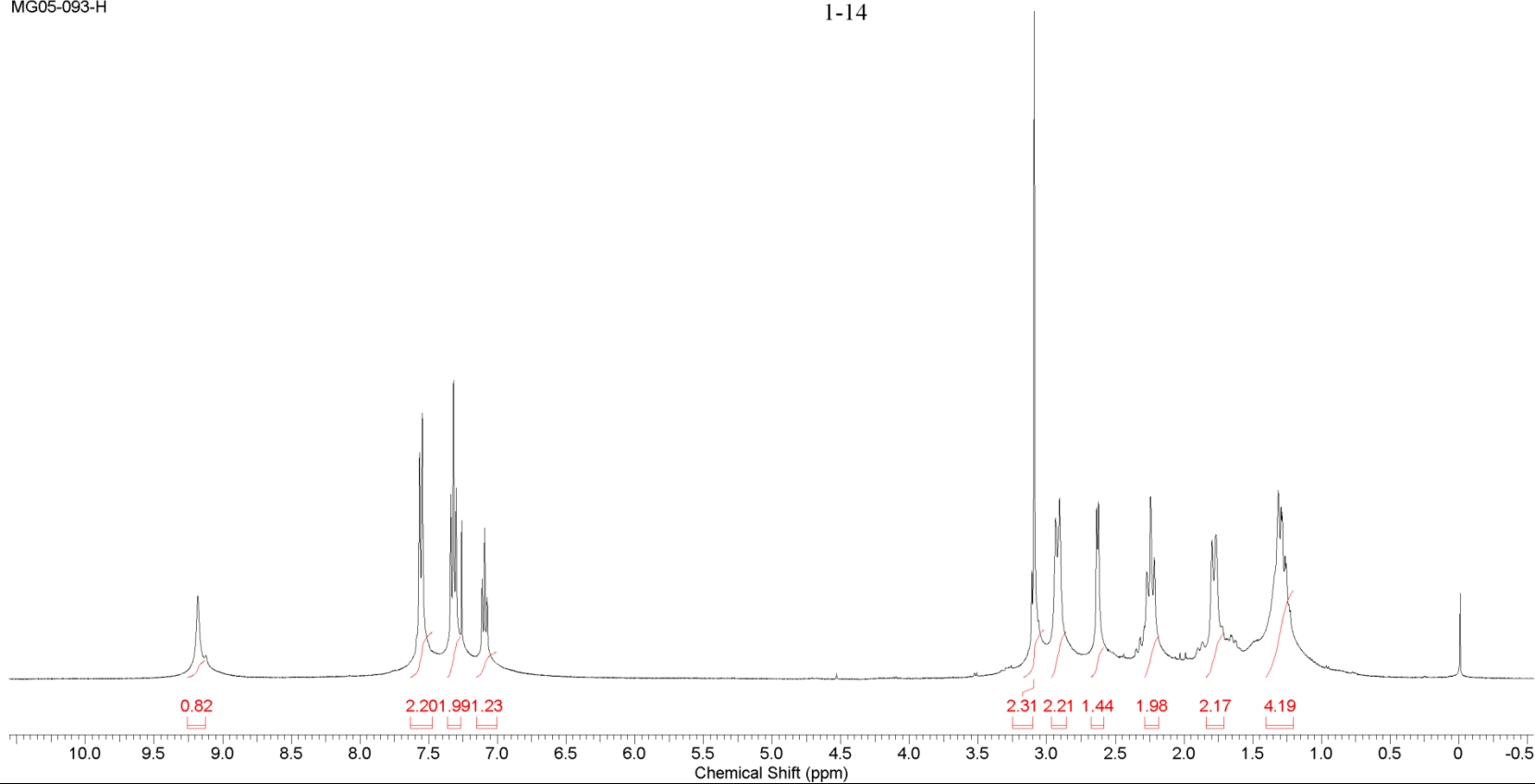
This report was created by ACD/NMR Processor Academic Edition. For more information go to www.acdlabs.com/nmrproc/

Formula	C ₁₄ H ₂₁ N ₃ O	FW	247.3360
---------	--	----	----------

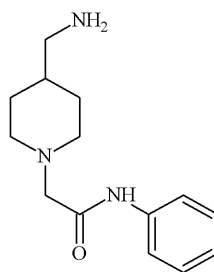


MG05-093-H

1-14

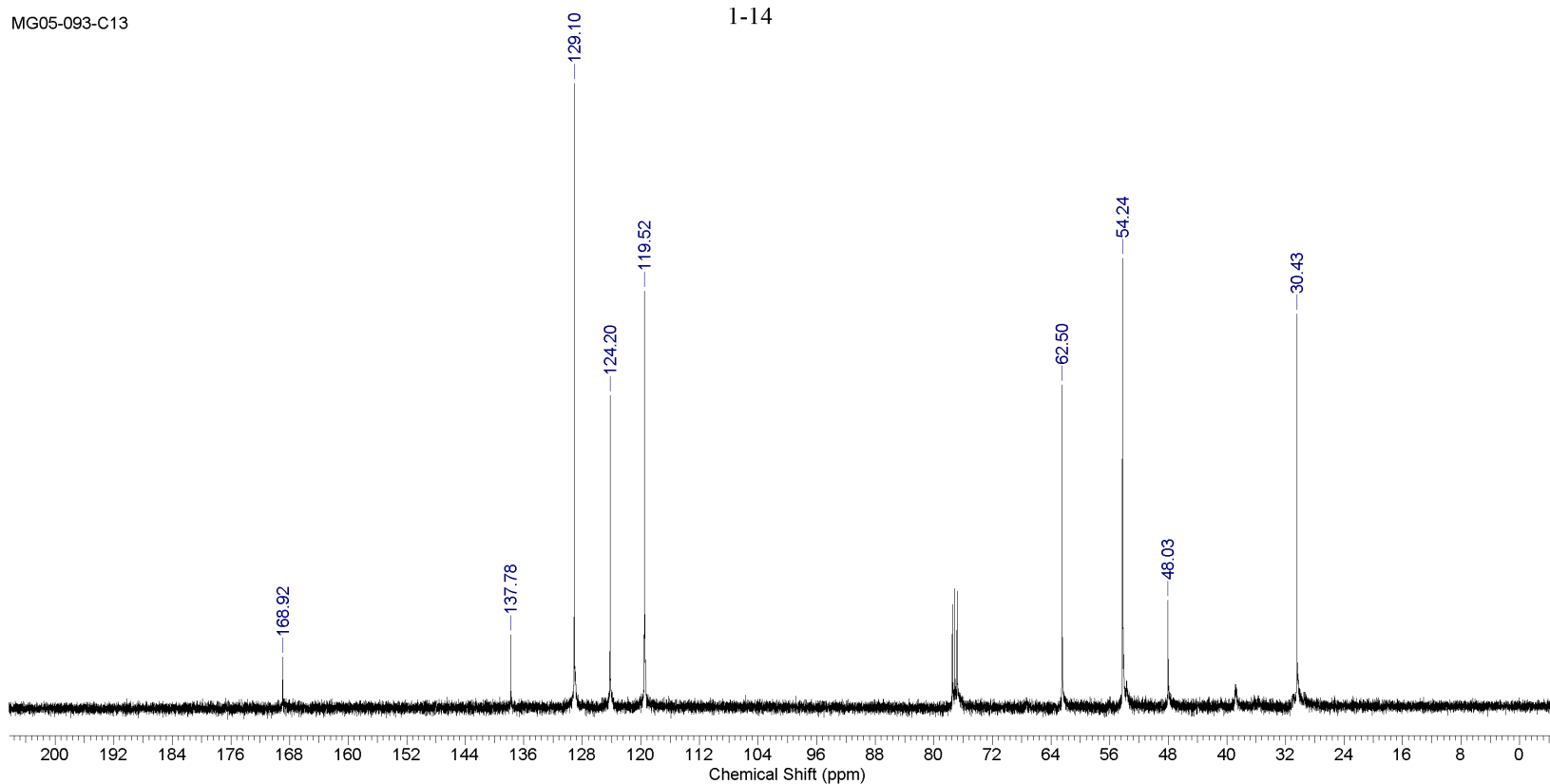


Formula C₁₄H₂₁N₃O FW 247.3360



1-14

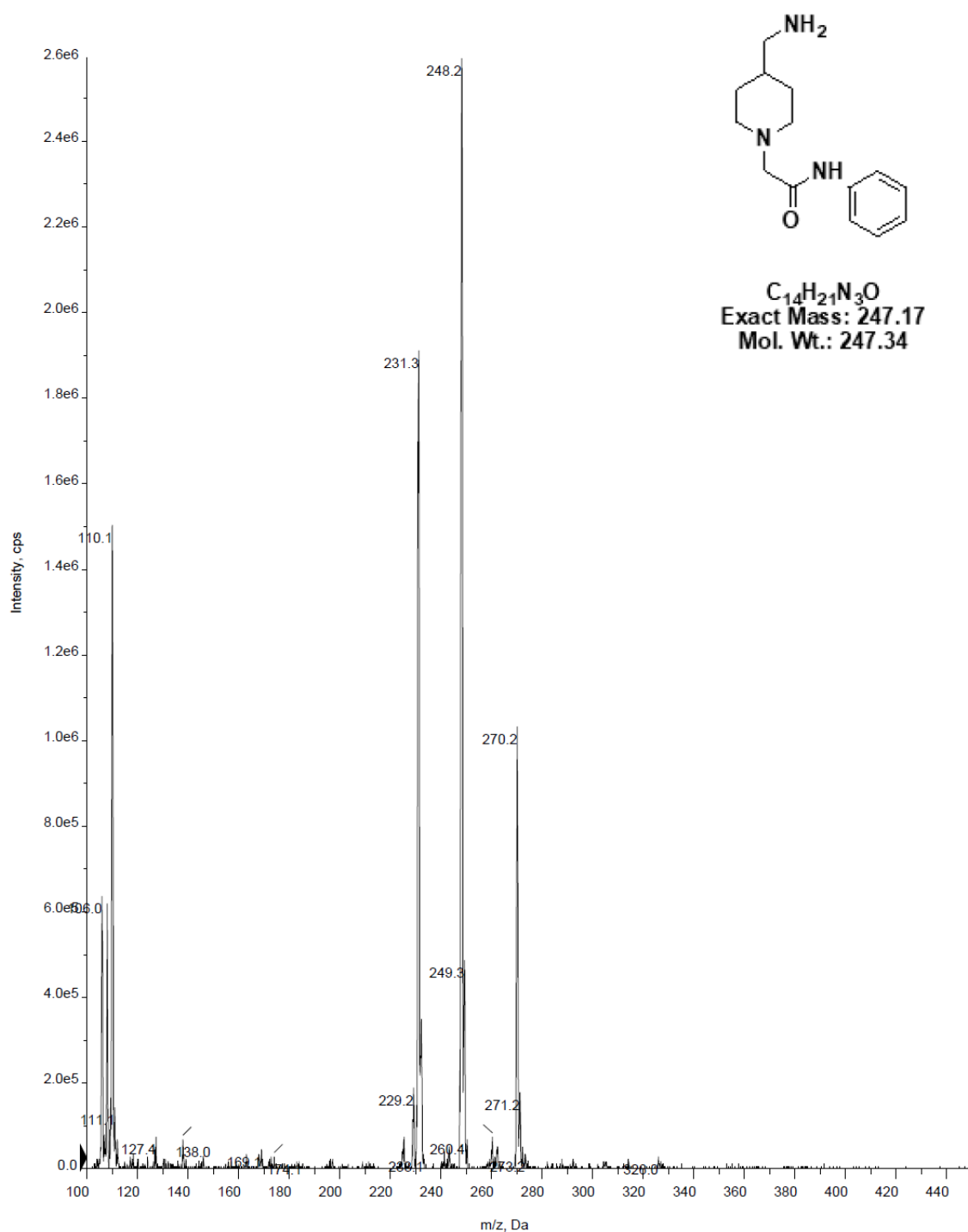
MG05-093-C13



J:\NOTEBOOK5\MG05-093-C13

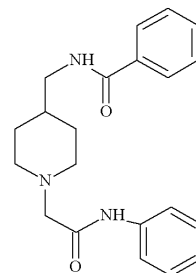
■ +Q1: 5 MCA scans from Sample 1 (TuneSampleID) of MT20140114185714.wiff (Turbo Spray)

Max. 2.6e6 cps.



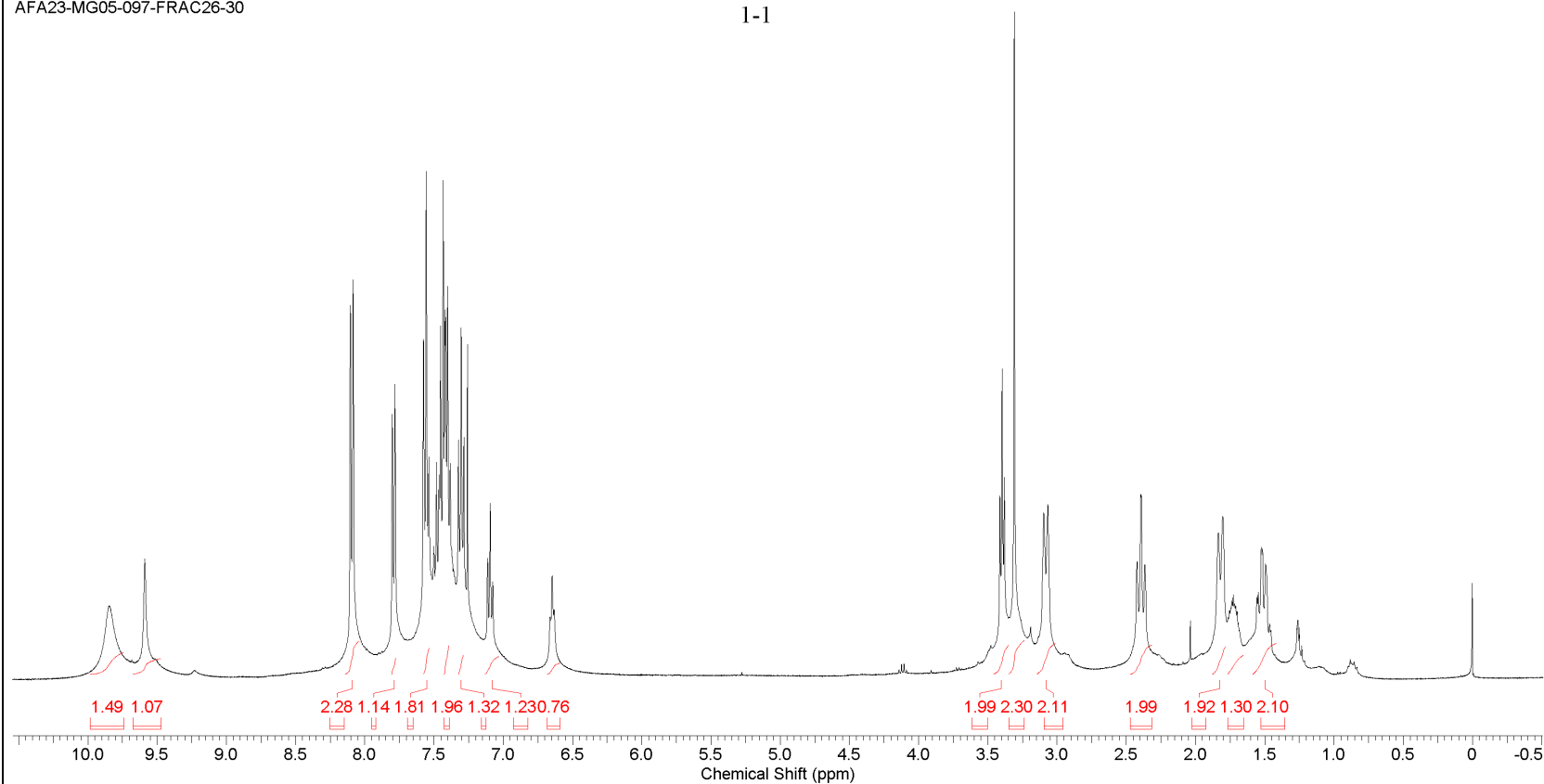
This report was created by ACD/NMR Processor Academic Edition. For more information go to www.acdlabs.com/nmrproc/

Formula $C_{21}H_{25}N_3O_2$ FW 351.4421



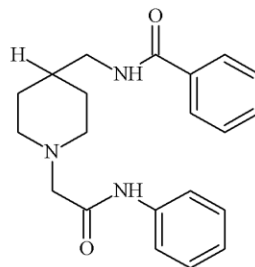
AFA23-MG05-097-FRAC26-30

1-1



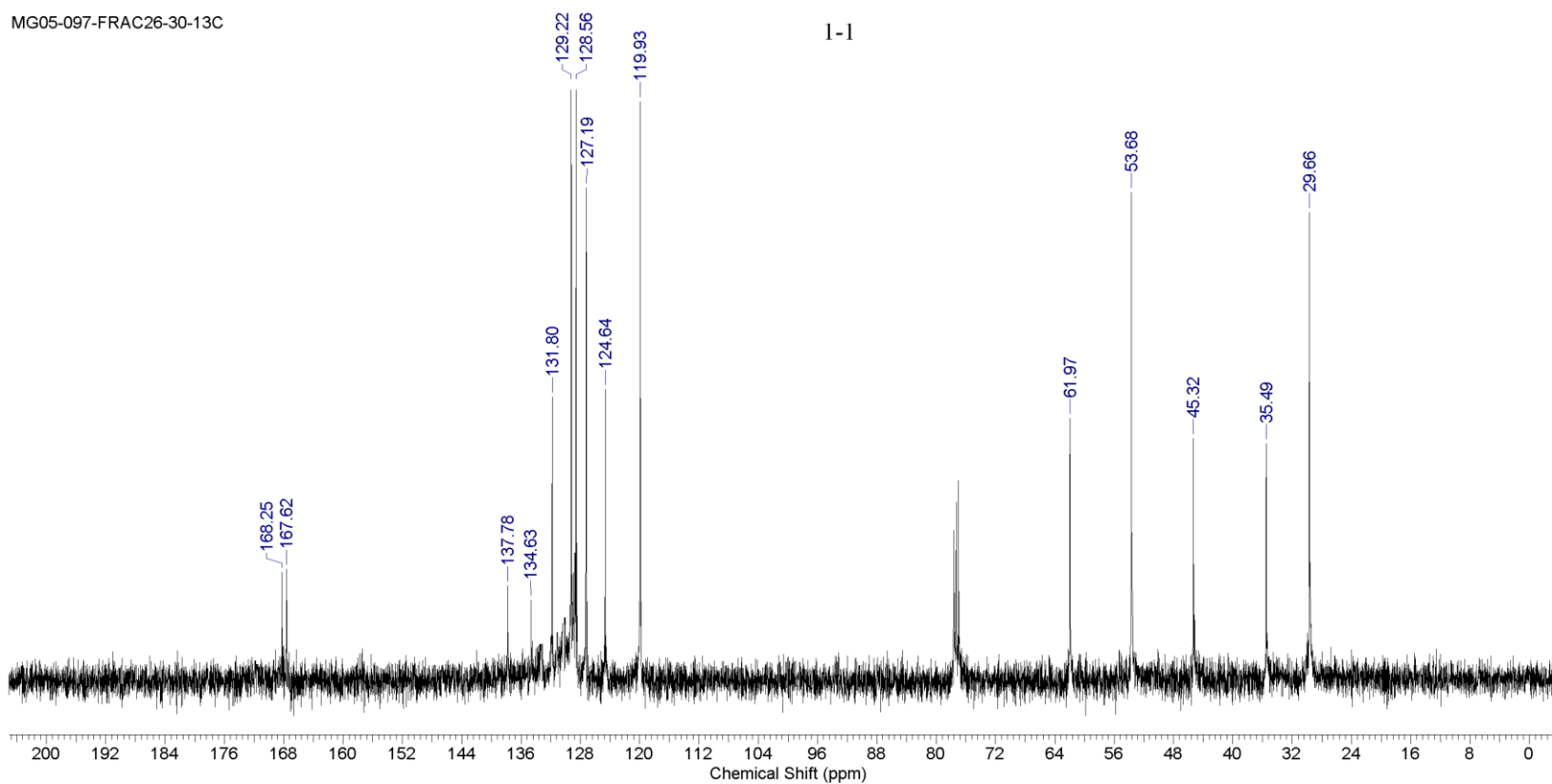
This report was created by ACD/NMR Processor Academic Edition. For more information go to www.acdlabs.com/nmrproc/

Formula $C_{21}H_{26}N_2O_2$ FW 351.4421



1-1

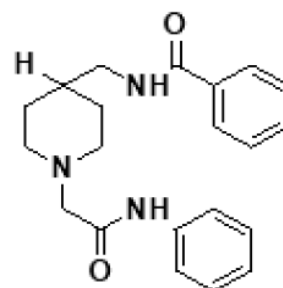
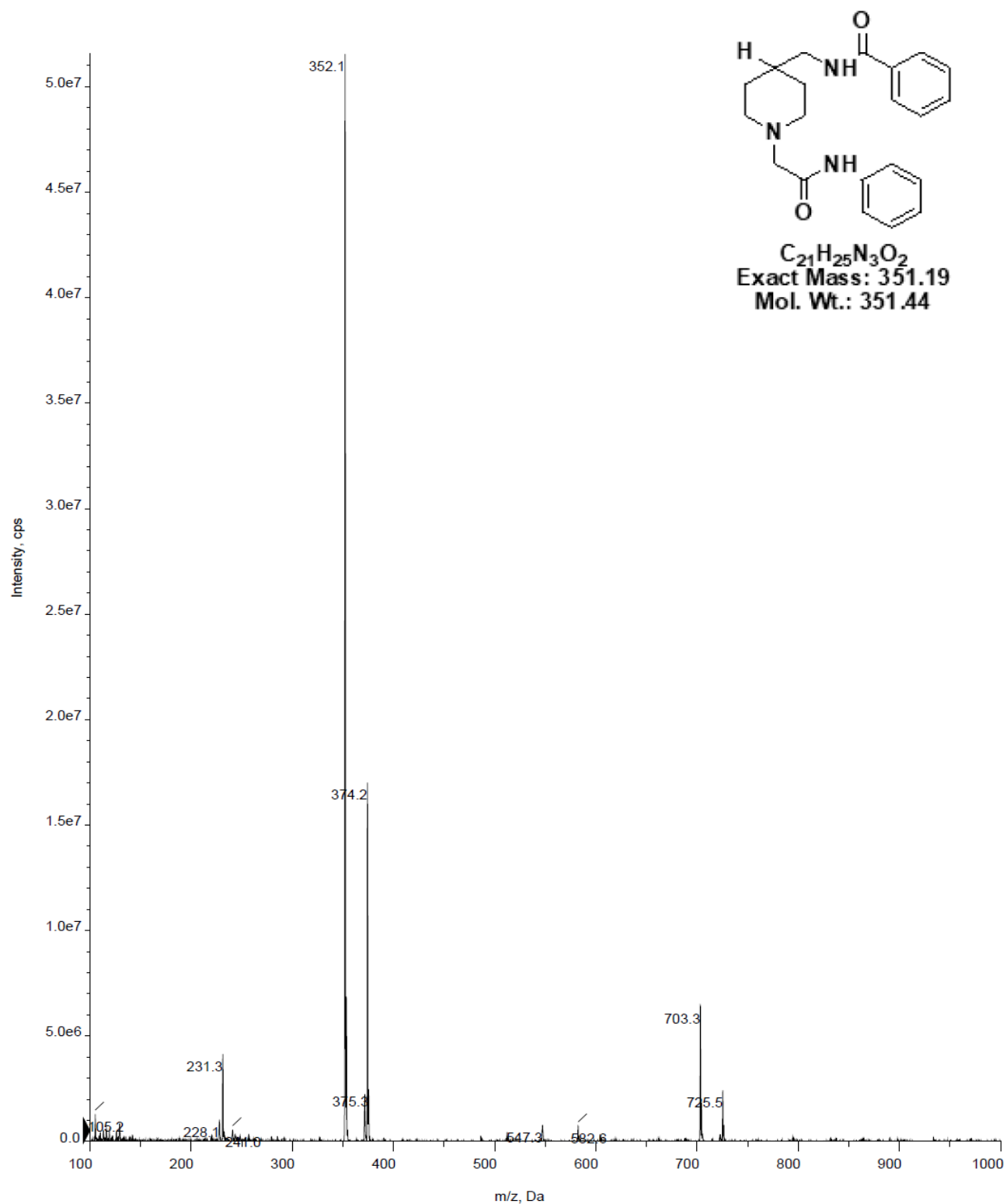
MG05-097-FRAC26-30-13C



J:\NOTEBOOK5\MG05-097-FRAC26-30-13C

+Q1: 13 MCA scans from Sample 1 (TuneSampleID) of MT20140606182211.wiff (Turbo Spray)

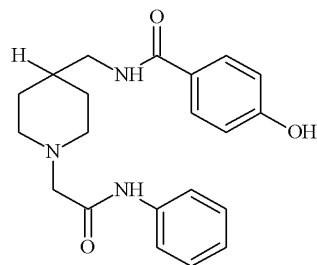
Max. 5.2e7 cps.



$C_{21}H_{25}N_3O_2$
Exact Mass: 351.19
Mol. Wt.: 351.44

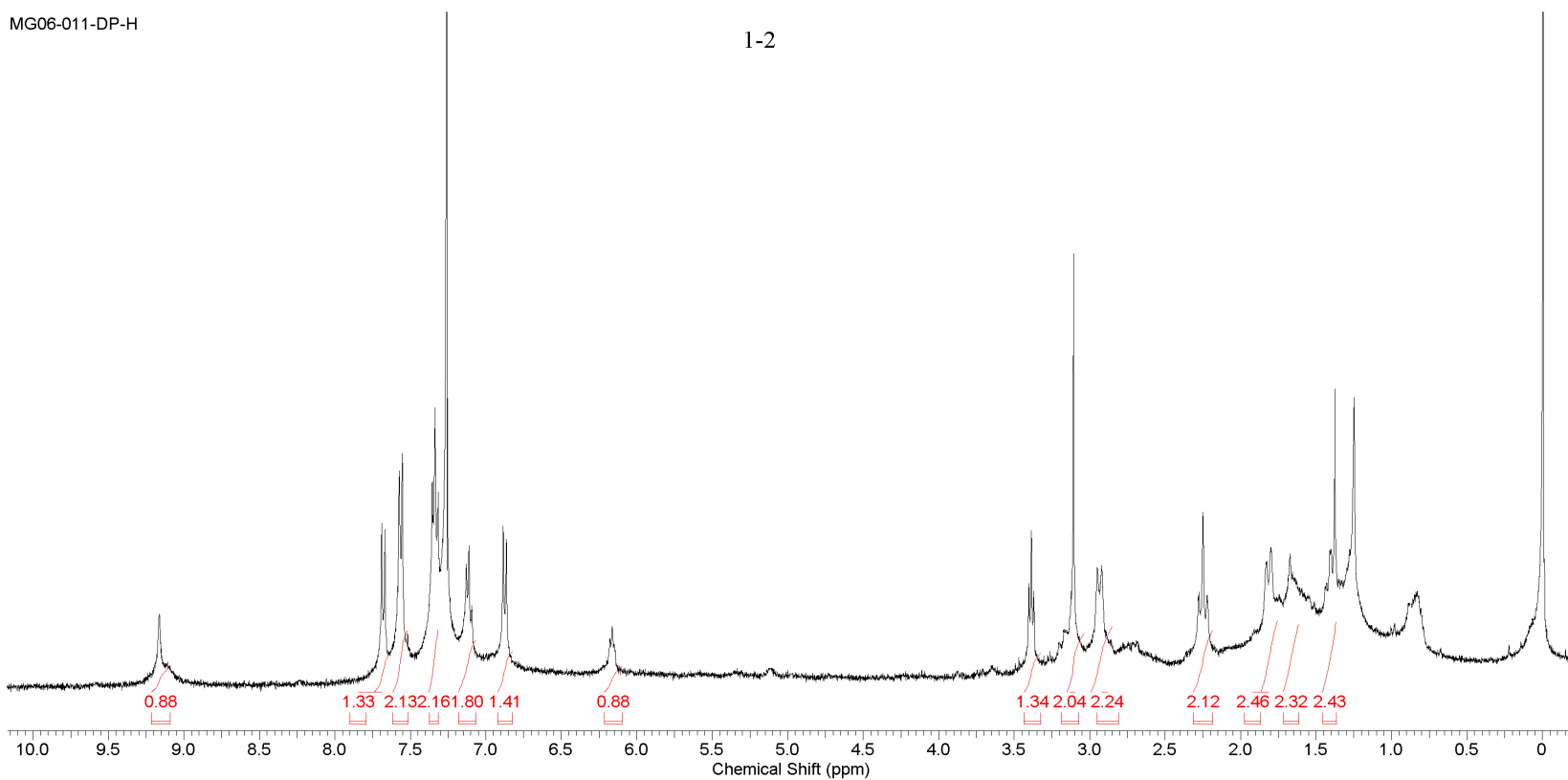
This report was created by ACD/NMR Processor Academic Edition. For more information go to www.acdlabs.com/nmrproc/

Formula C₂₁H₂₅N₃O₃ **FW** 367.4415



1-2

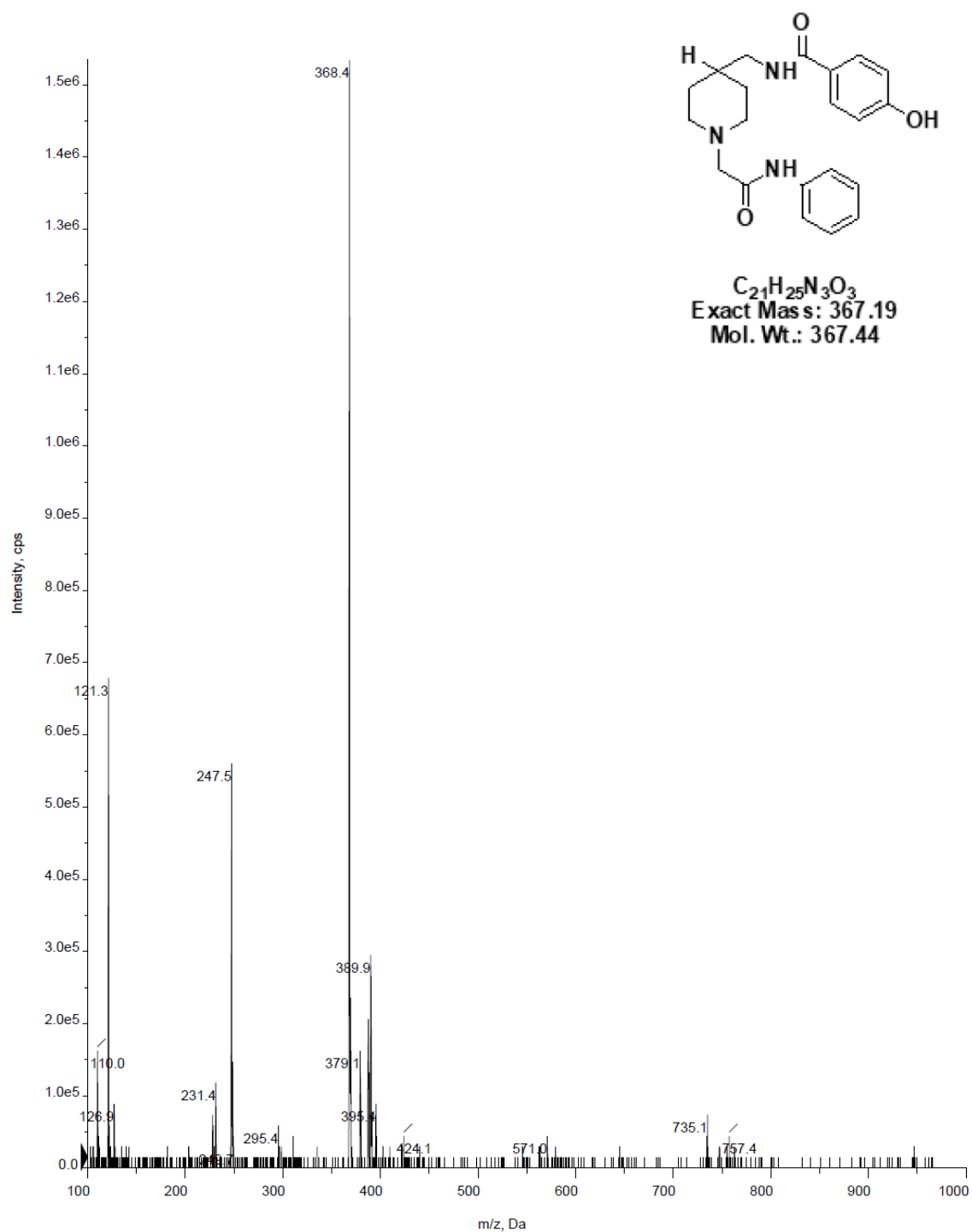
MG06-011-DP-H



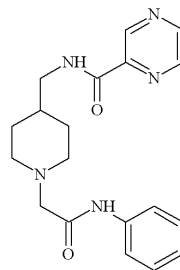
JAT-TYPE CALCIUM CHANNEL\NMR\1-2\MG06-011-DP-H.ESP

■ +Q1: 8 MCA scans from Sample 1 (TuneSampleID) of MT20140708214256.wiff (Turbo Spray)

Max. 1.5e6 cps.

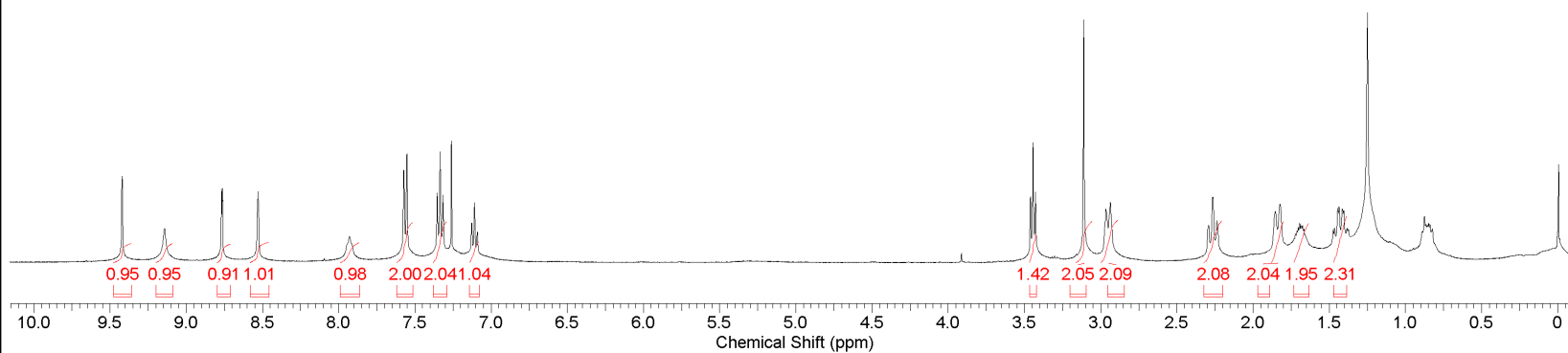


Formula C₁₉H₂₃N₅O₂ **FW** 353.4182



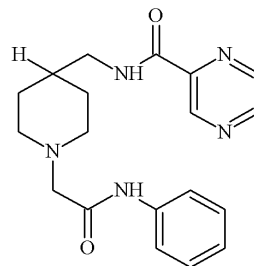
MG07-023-DP-H

1-3



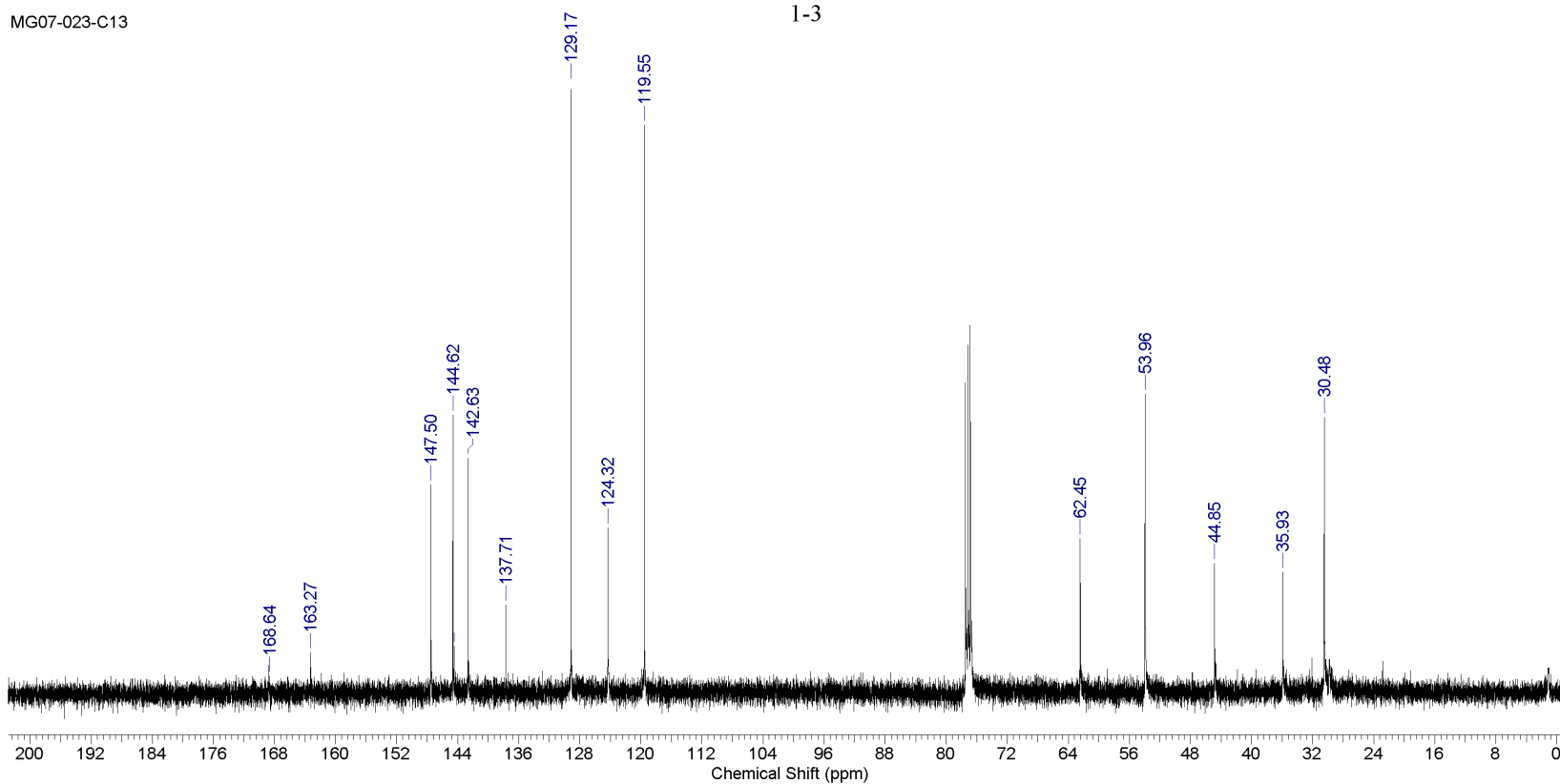
J:\NOTEBOOK7\MG07-023-DP-H

Formula C₁₉H₂₃N₅O₂ FW 353.4182



1-3

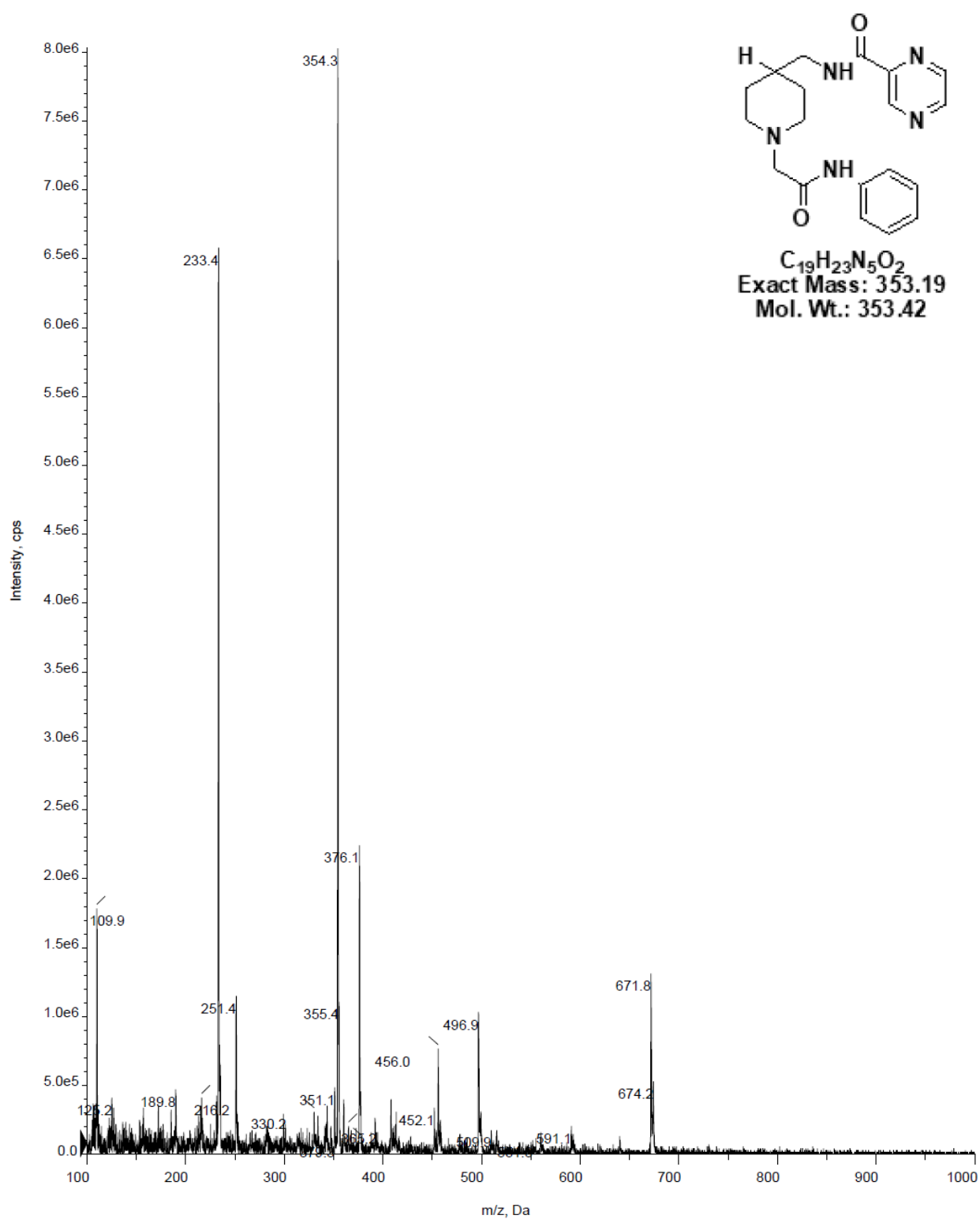
MG07-023-C13



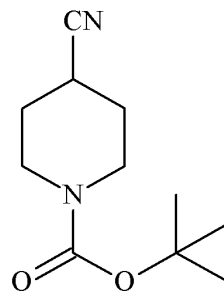
J:\NOTEBOOK7\MG07-023-C13

■ +Q1: 5 MCA scans from Sample 1 (TuneSampleID) of MT20150313102738.wiff (Turbo Spray)

Max. 8.0e6 cps.

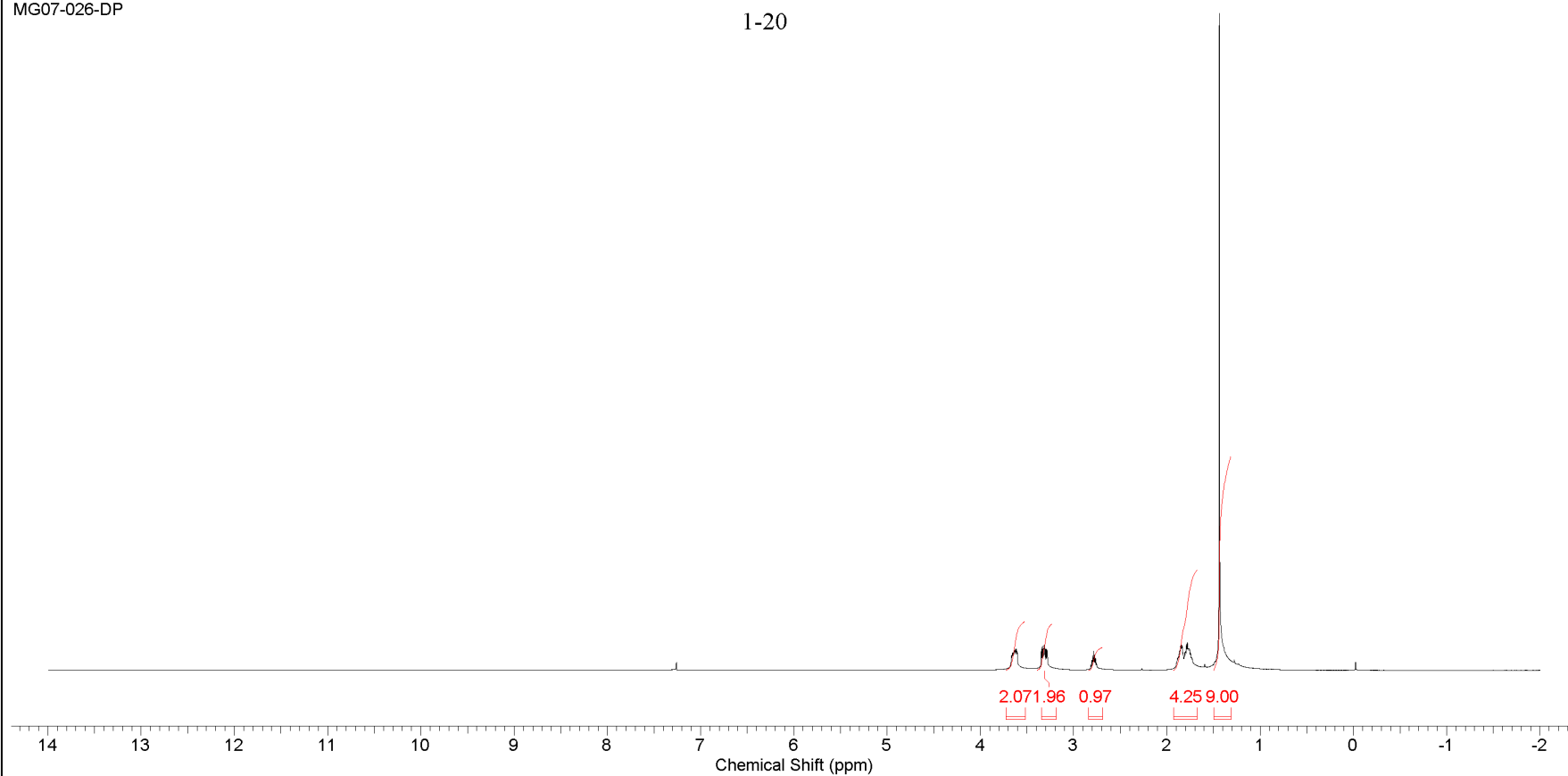


Formula	C ₁₁ H ₁₈ N ₂ O ₂	FW	210.2728
----------------	---	-----------	----------

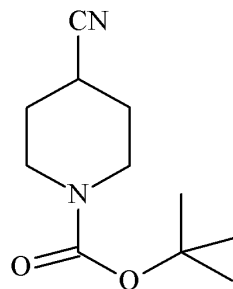


1-20

MG07-026-DP

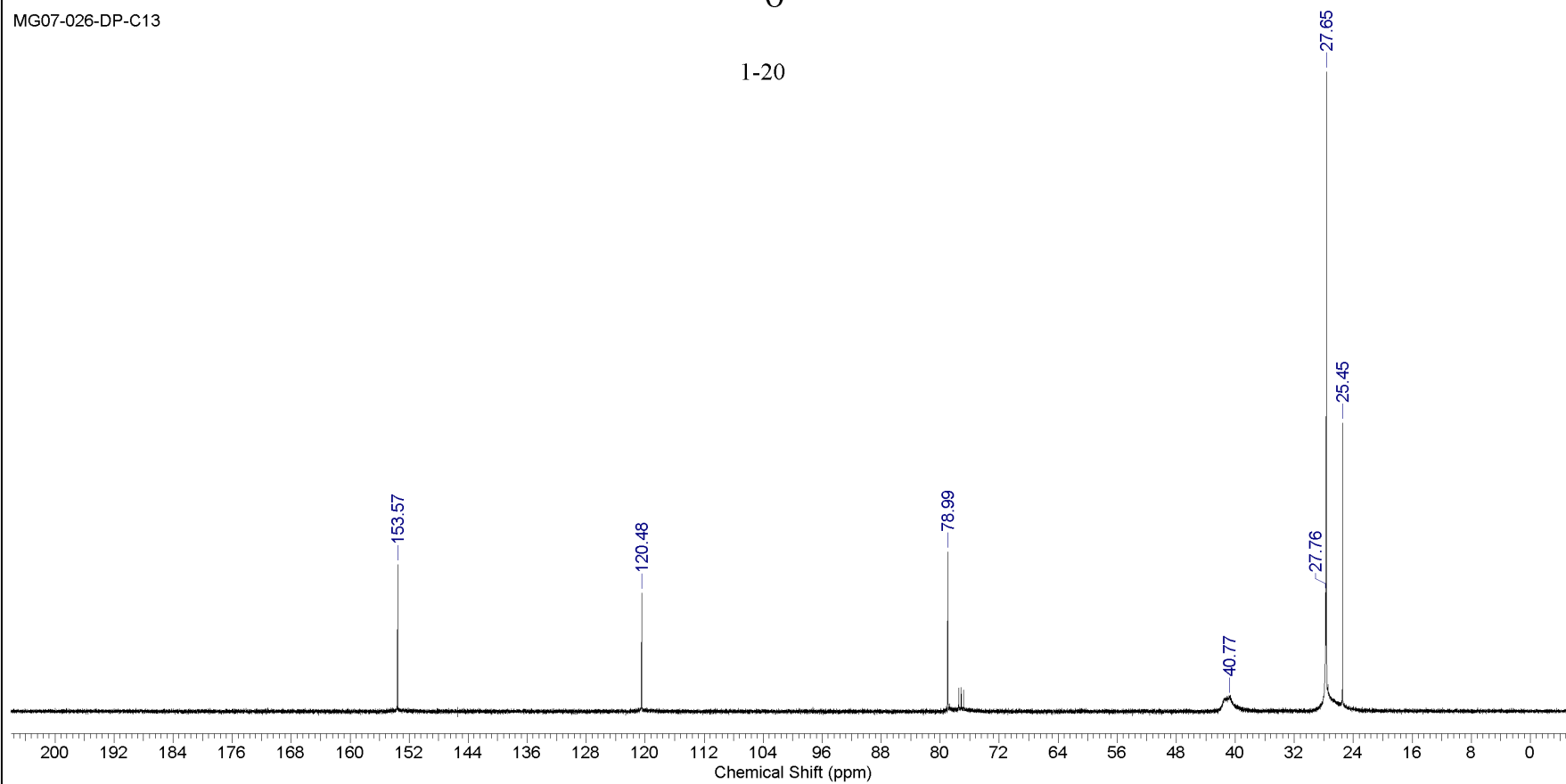


Formula	C ₁₁ H ₁₈ N ₂ O ₂	FW	210.2728
----------------	---	-----------	----------



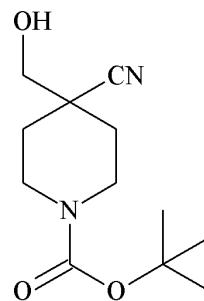
1-20

MG07-026-DP-C13



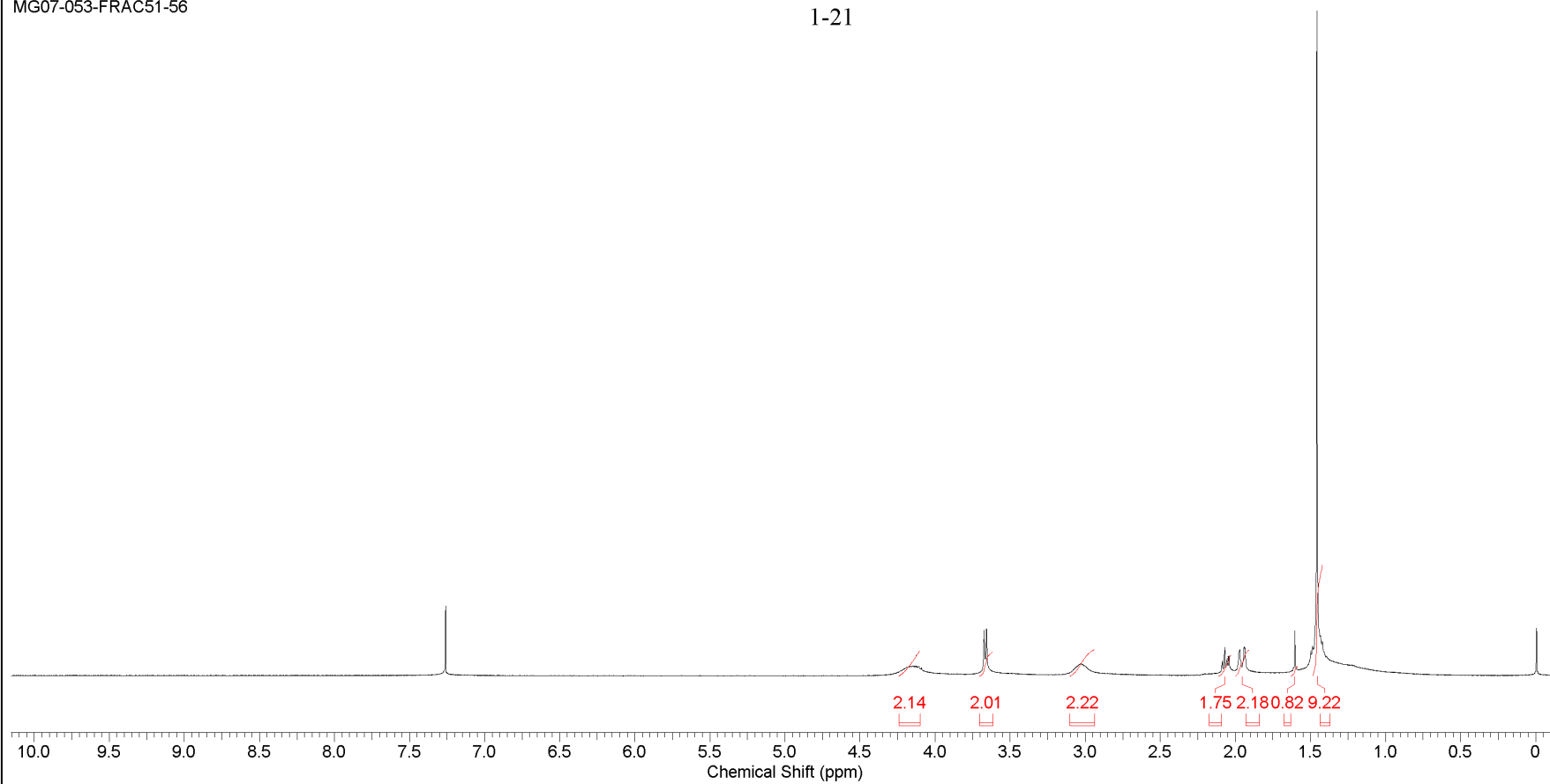
J:\NOTEBOOK7\MG07-026-DP-C13

Formula C ₁₂ H ₂₀ N ₂ O ₃	FW 240.2988
--	--------------------



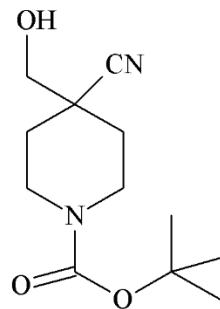
1-21

MG07-053-FRAC51-56



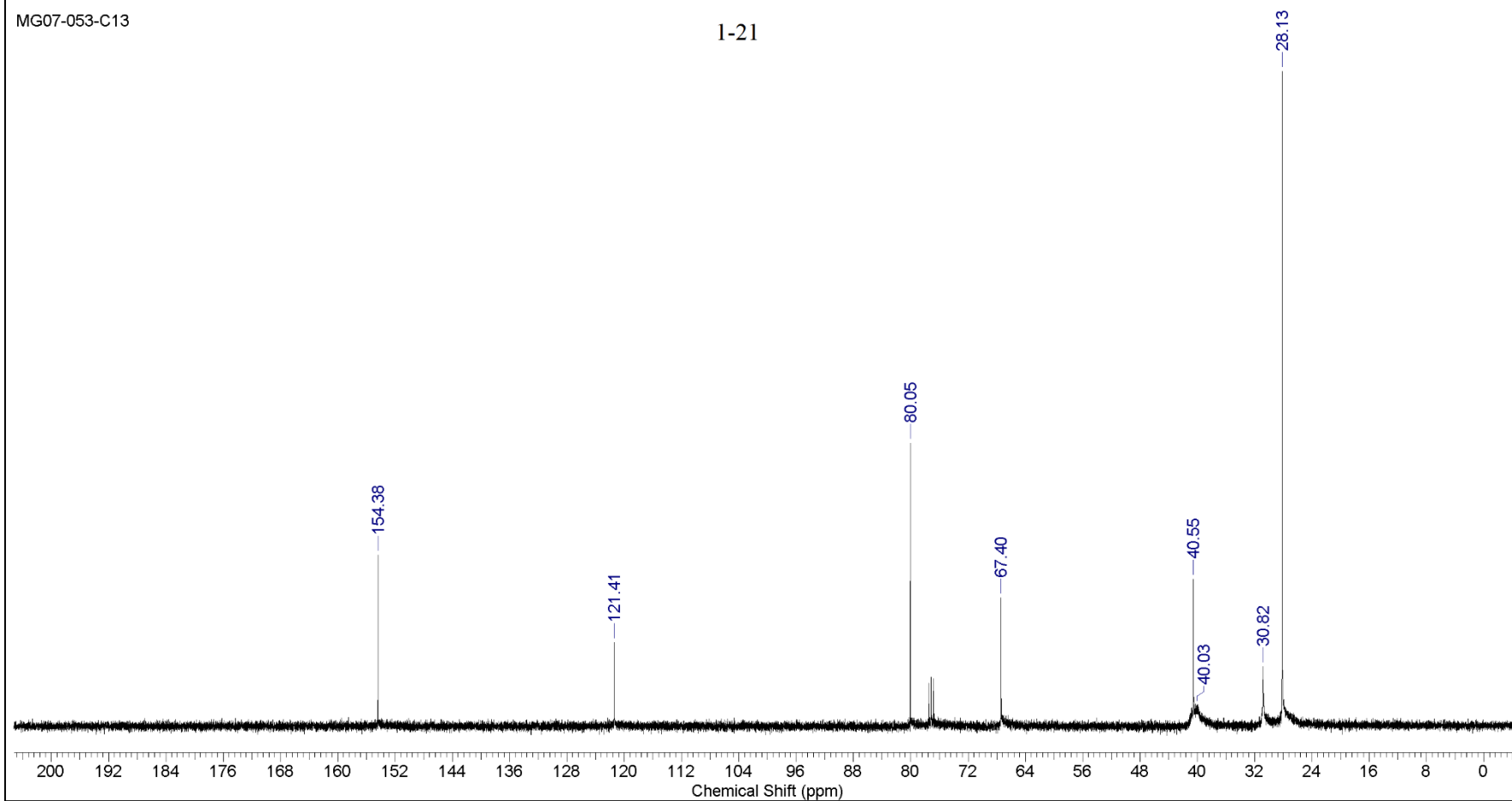
This report was created by ACD/NMR Processor Academic Edition. For more information go to www.acdlabs.com/nmrproc/

Formula	C ₁₂ H ₂₀ N ₂ O ₃
FW	240.2988



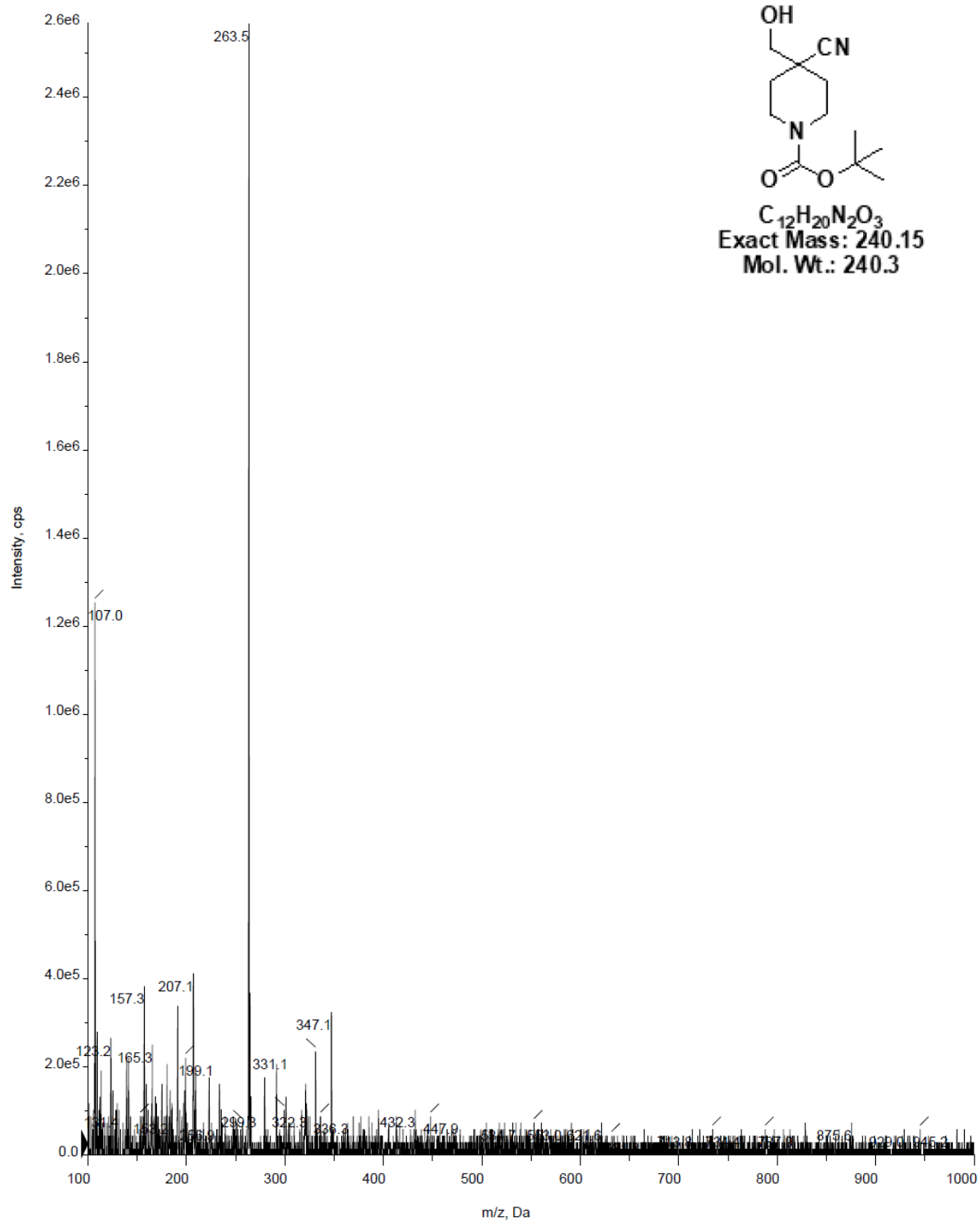
1-21

MG07-053-C13

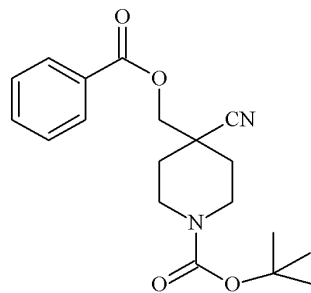


■ +Q1: 21 MCA scans from Sample 1 (TuneSampleID) of MT20140723181728.wiff (Turbo Spray)

Max. 2.6e6 cps.

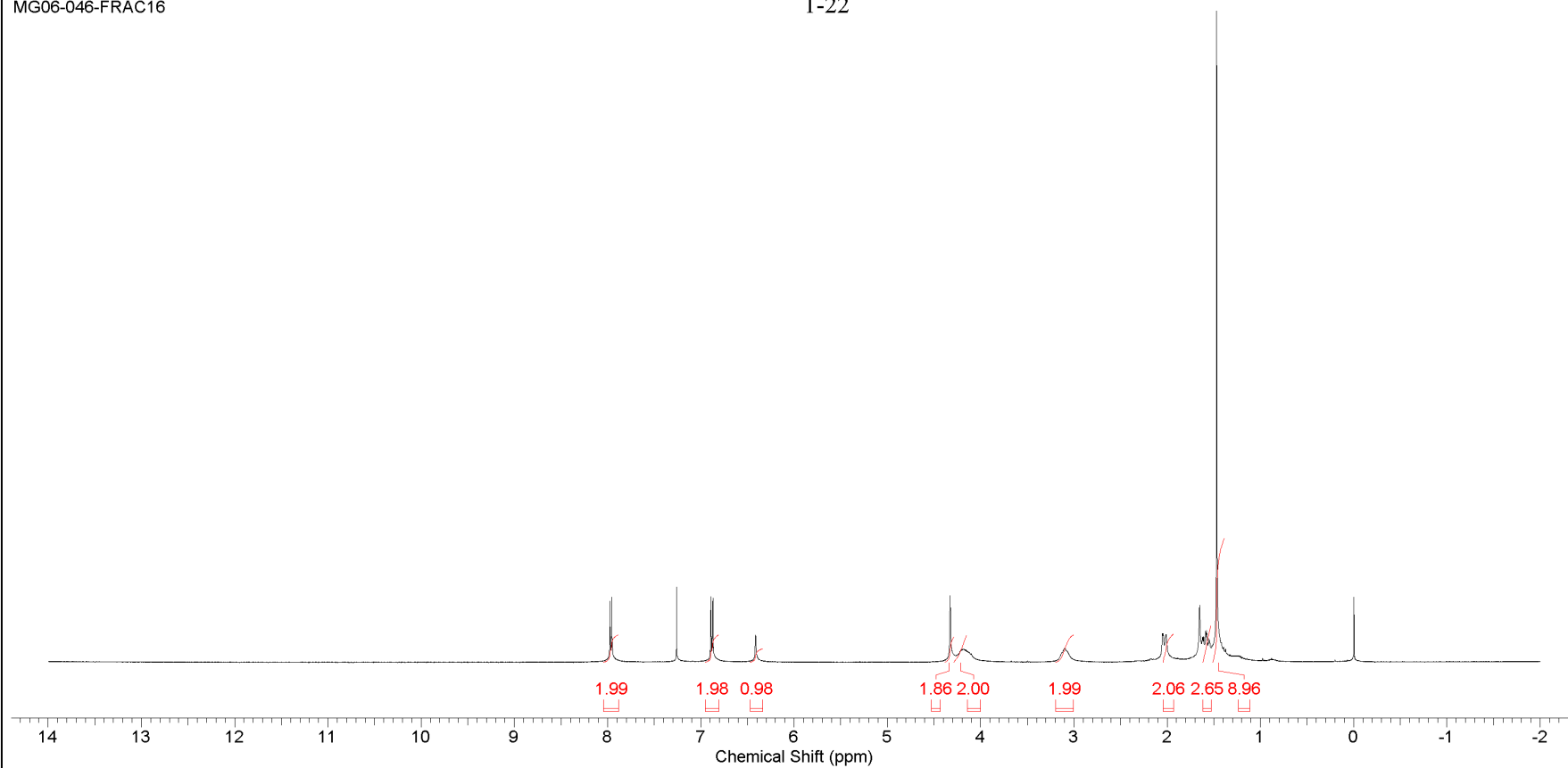


Formula C ₁₉ H ₂₄ N ₂ O ₄	FW 344.4049
--	--------------------



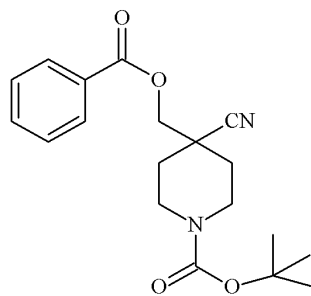
1-22

MG06-046-FRAC16



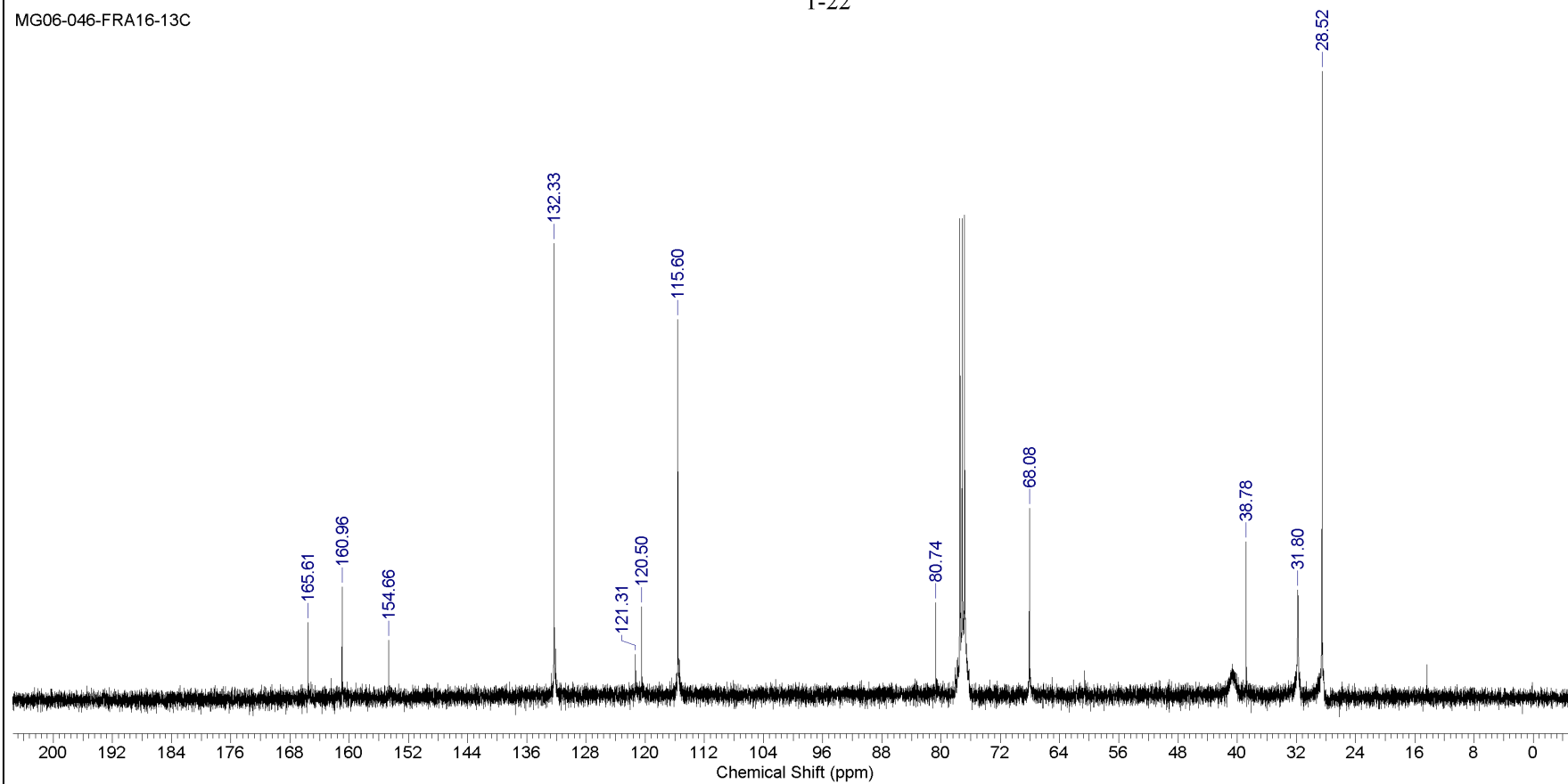
This report was created by ACD/NMR Processor Academic Edition. For more information go to www.acdlabs.com/nmrproc/

Formula	C ₁₉ H ₂₄ N ₂ O ₄	FW	344.4049
----------------	---	-----------	----------



1-22

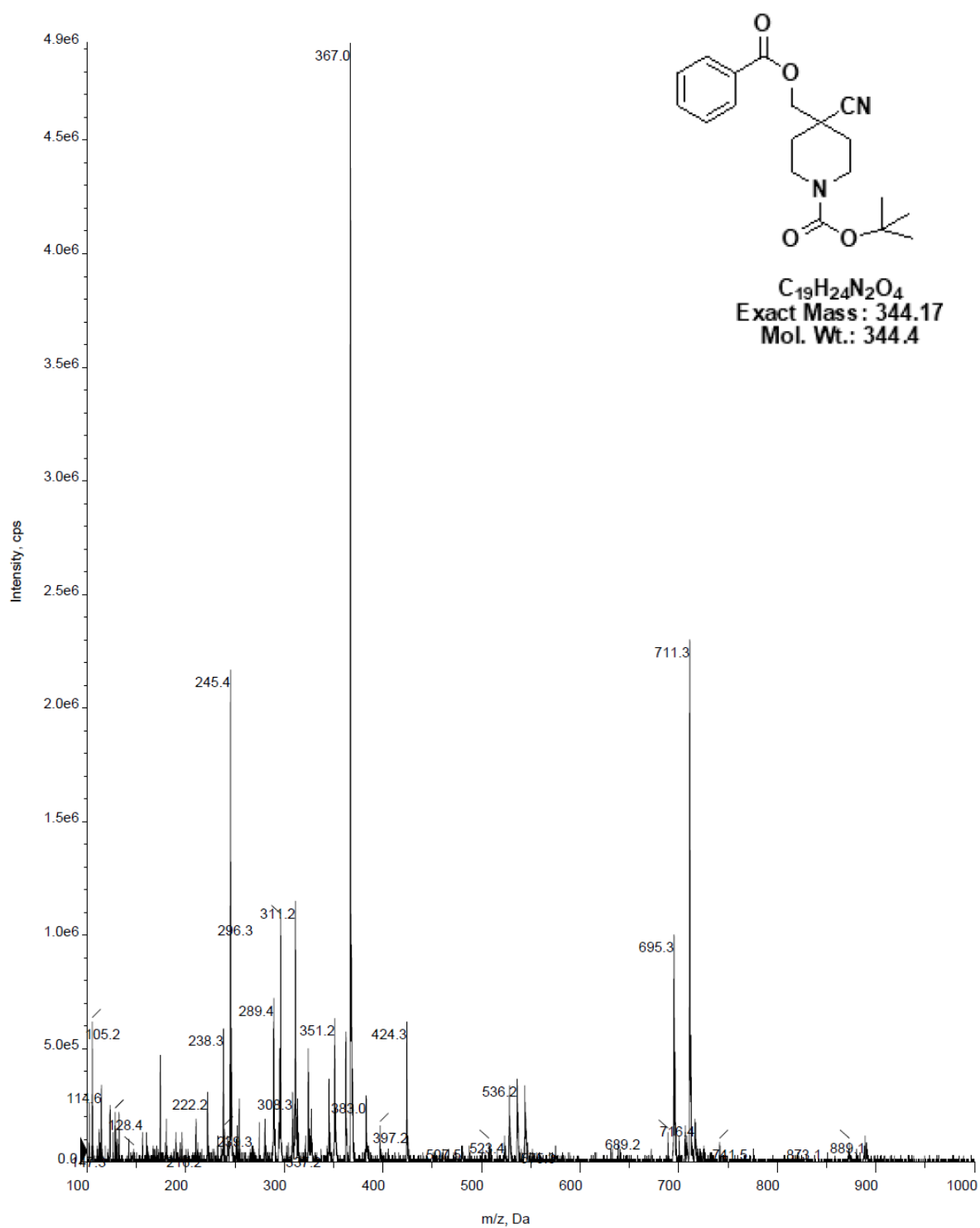
MG06-046-FRA16-13C



J:\NOTEBOOK6\MG06-046-FRA16-13C

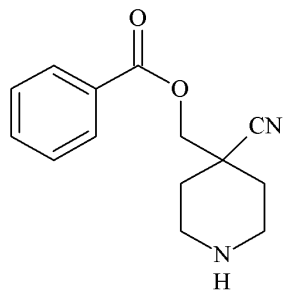
■ +Q1: 15 MCA scans from Sample 1 (TuneSampleID) of MT20140418122515.wiff (Turbo Spray)

Max. 4.9e6 cps.



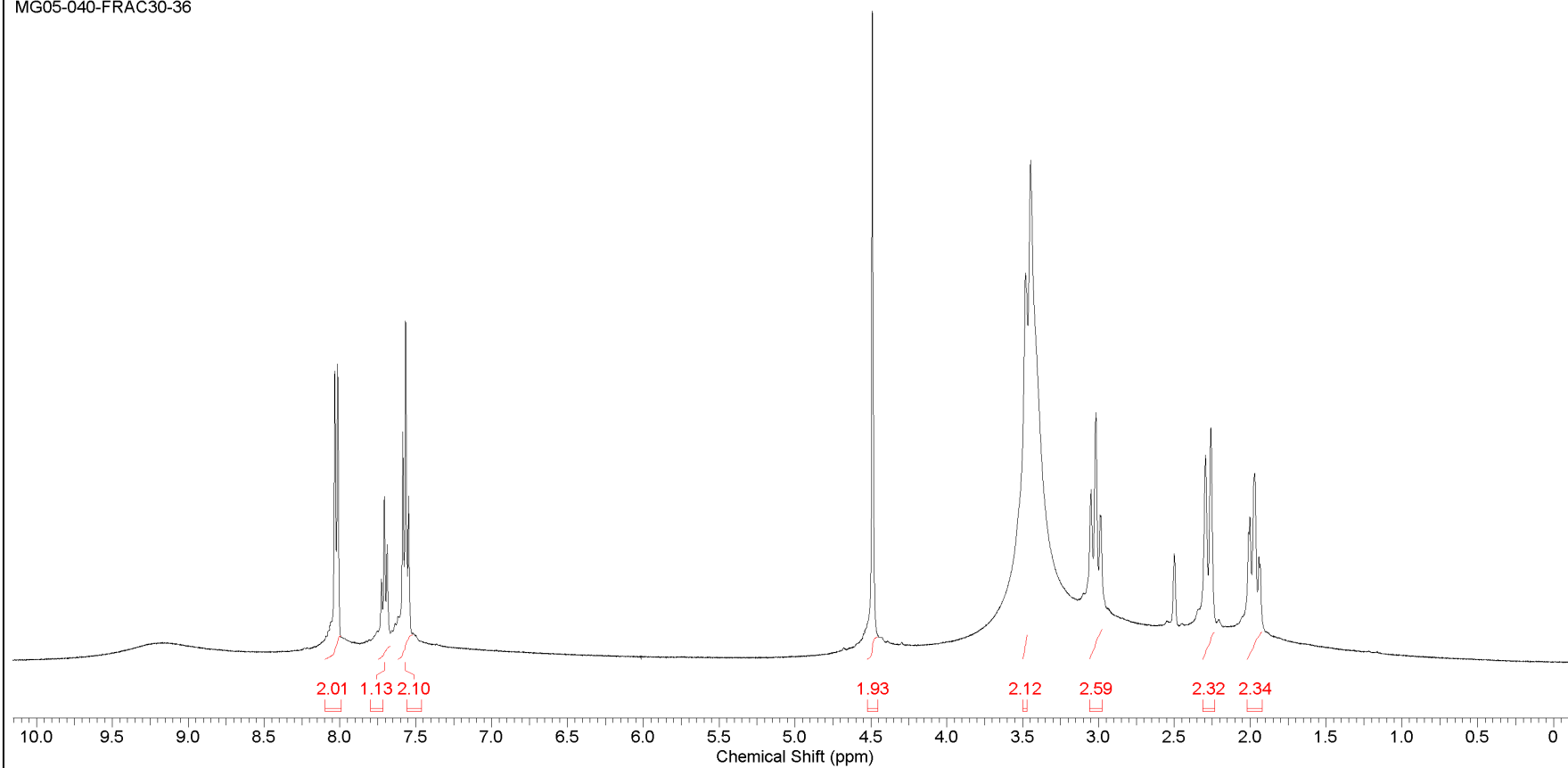
This report was created by ACD/NMR Processor Academic Edition. For more information go to www.acdlabs.com/nmrproc/

Formula C ₁₄ H ₁₆ N ₂ O ₂	FW 244.2890
--	--------------------



1-23

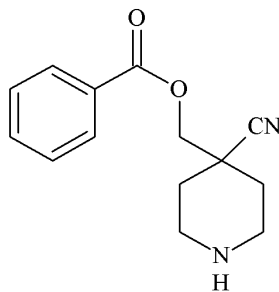
MG05-040-FRAC30-36



J:\NOTEBOOK5\MG05-040-FRAC30-36

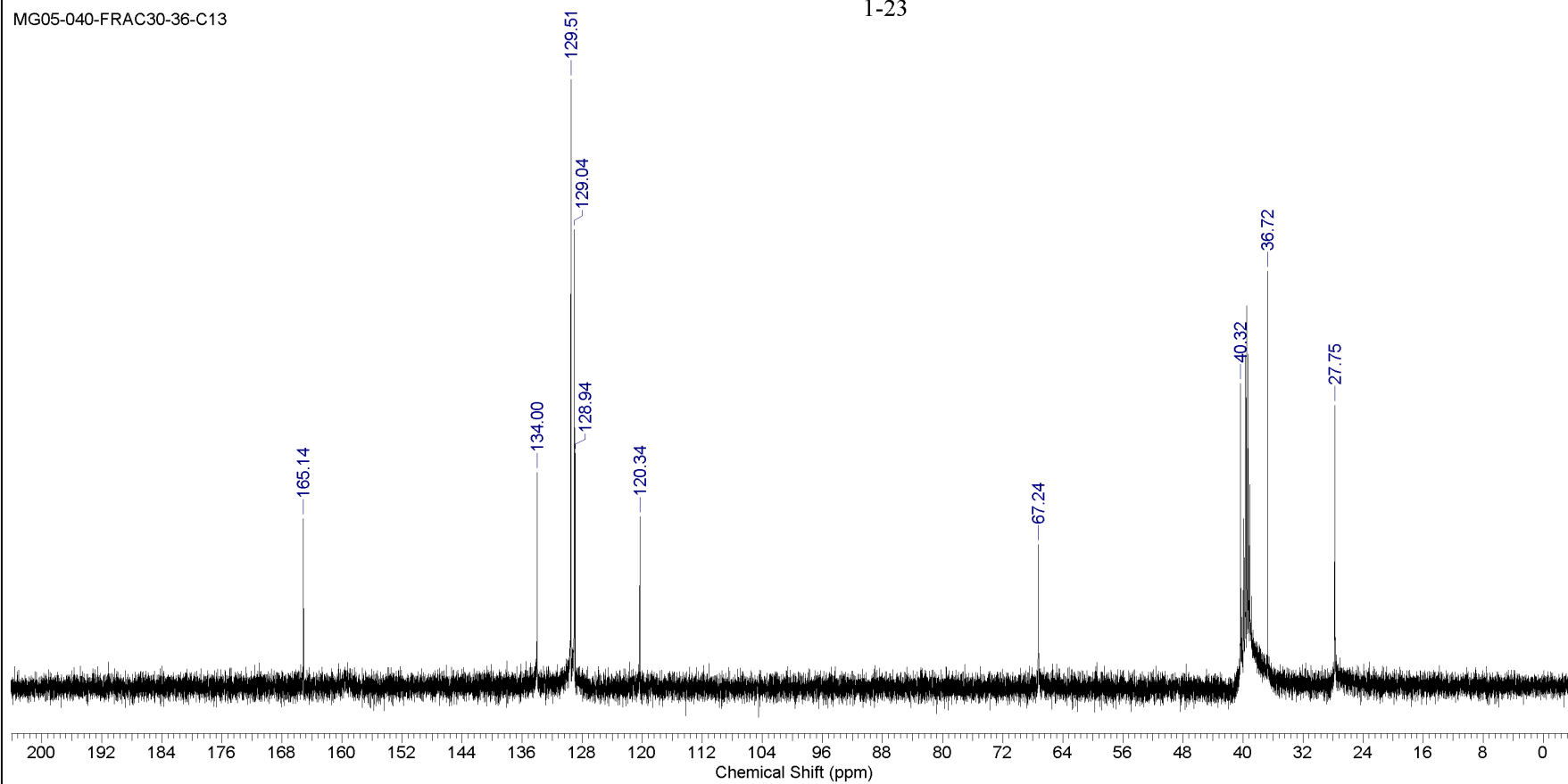
This report was created by ACD/NMR Processor Academic Edition. For more information go to www.acdlabs.com/nmrproc/

Formula C ₁₄ H ₁₆ N ₂ O ₂	FW 244.2890
--	--------------------



1-23

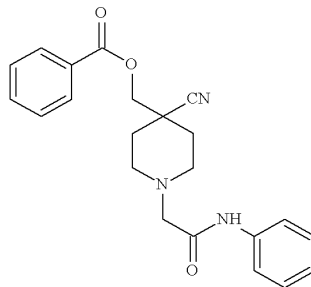
MG05-040-FRAC30-36-C13



J:\NOTEBOOK5\MG05-040-FRAC30-36-C13

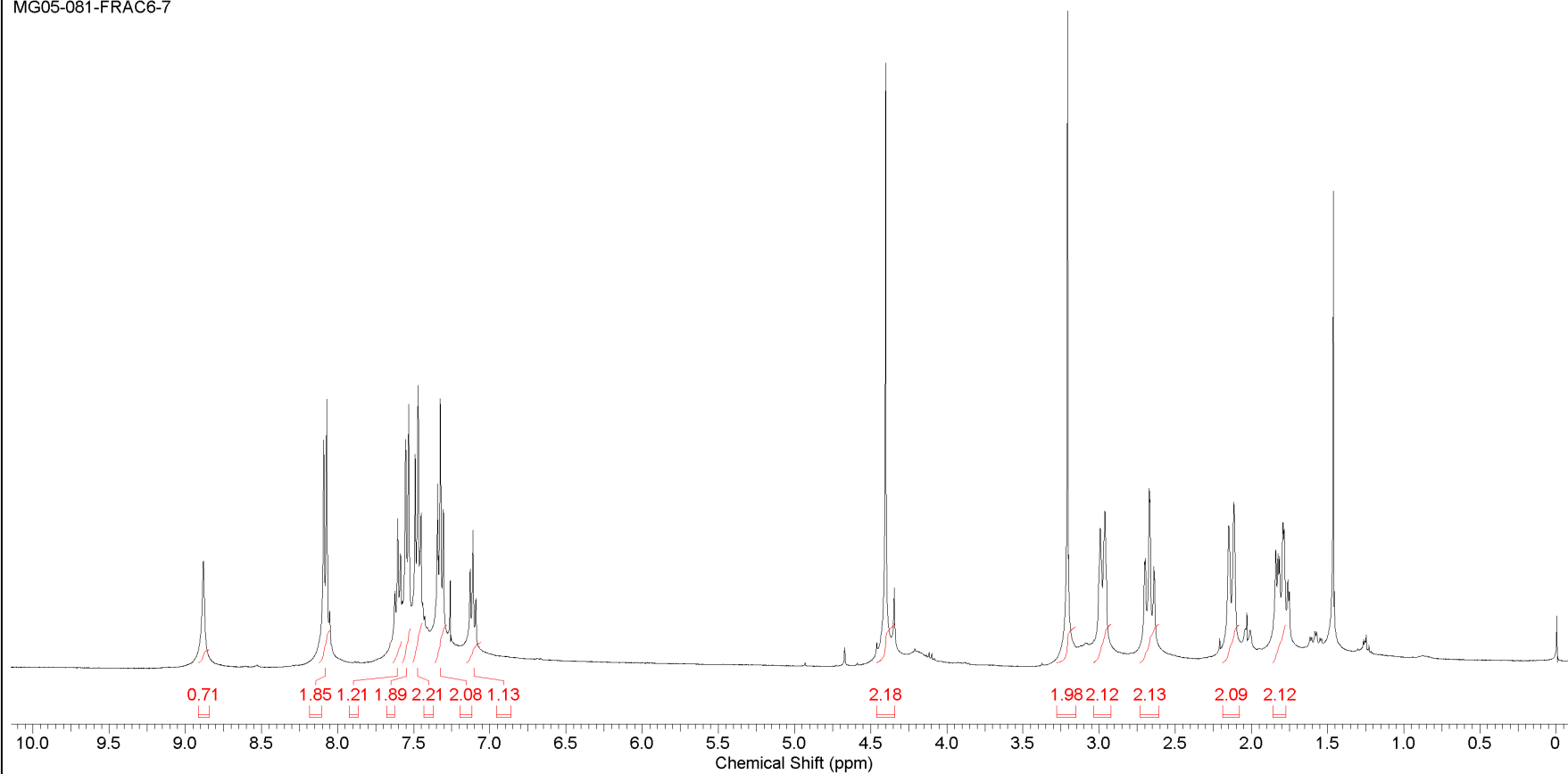
This report was created by ACD/NMR Processor Academic Edition. For more information go to www.acdlabs.com/nmrproc/

Formula C₂₂H₂₃N₃O₃ FW 377.4363



1-24

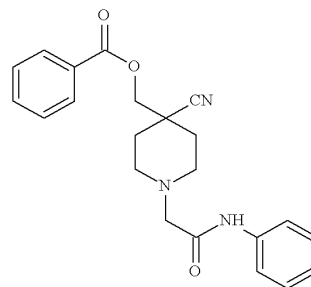
MG05-081-FRAC6-7



J:\T-TYPE CALCIUM CHANNEL\NMR\1-24\MG05-081-FRAC6-7

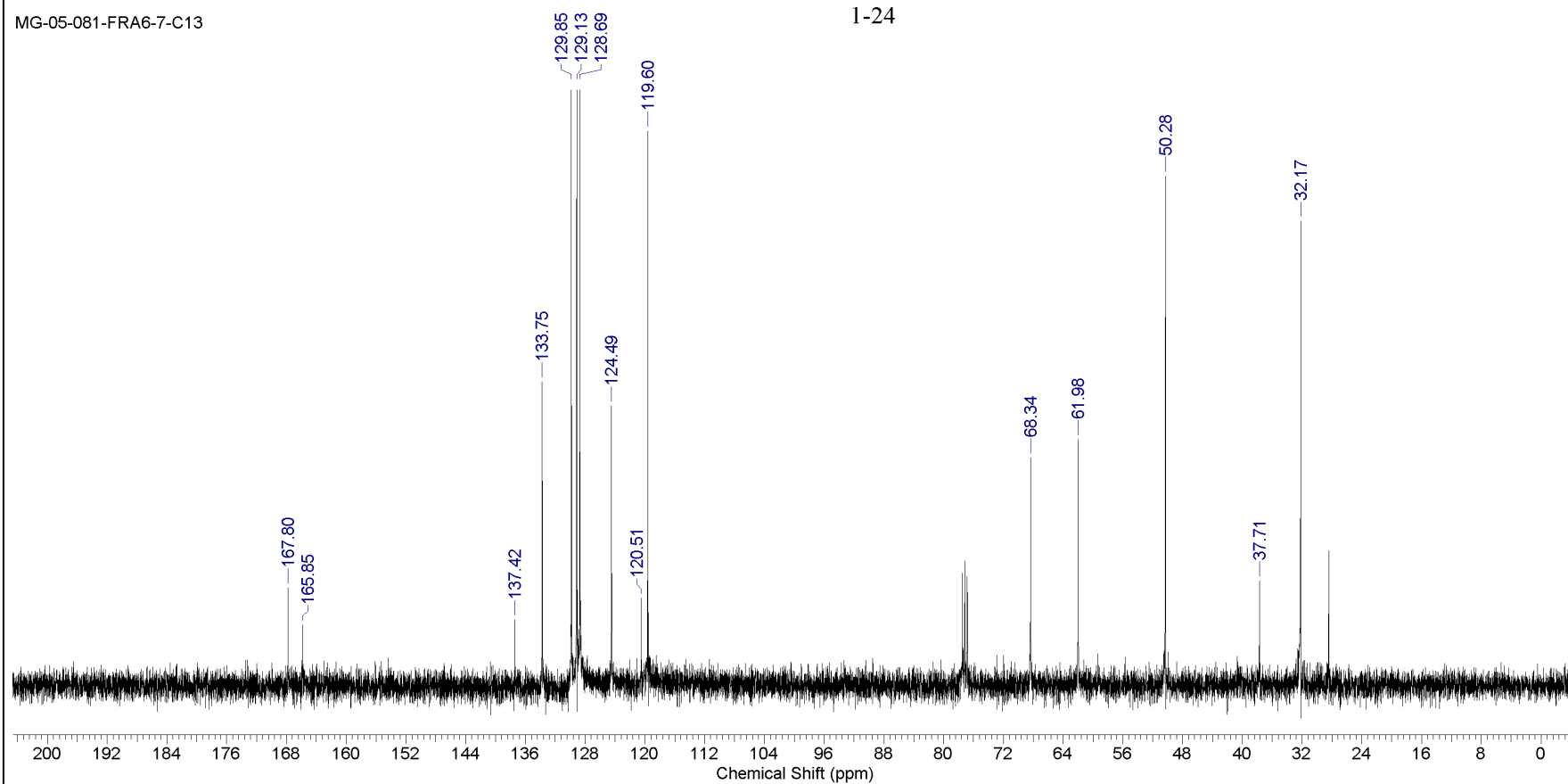
This report was created by ACD/NMR Processor Academic Edition. For more information go to www.acdlabs.com/nmrproc/

Formula	C ₂₂ H ₂₃ N ₃ O ₃	FW	377.4363
----------------	---	-----------	----------



1-24

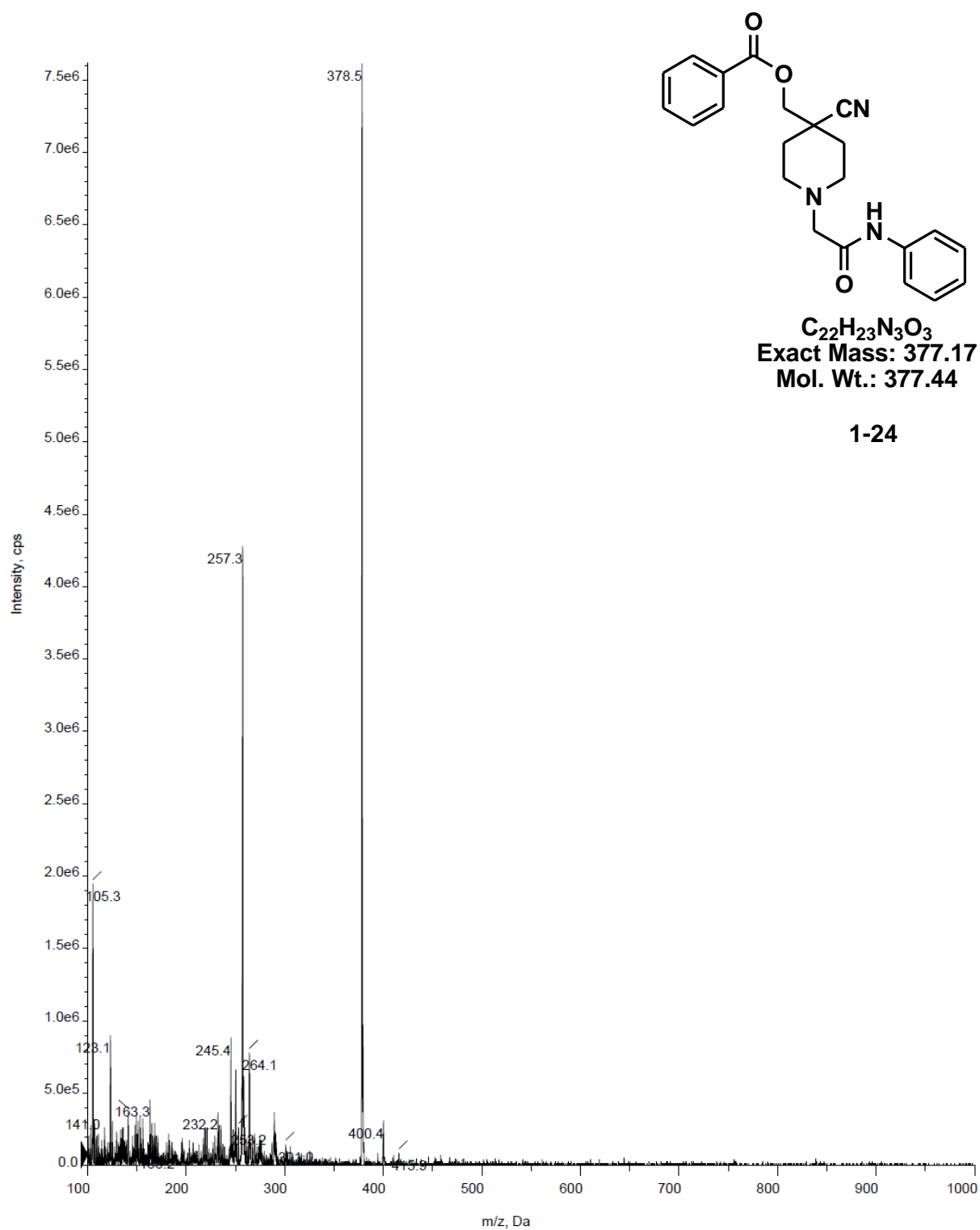
MG-05-081-FRA6-7-C13



J:\T-TYPE CALCIUM CHANNEL\NMR\1-24\MG-05-081-FRA6-7-C13.ESP

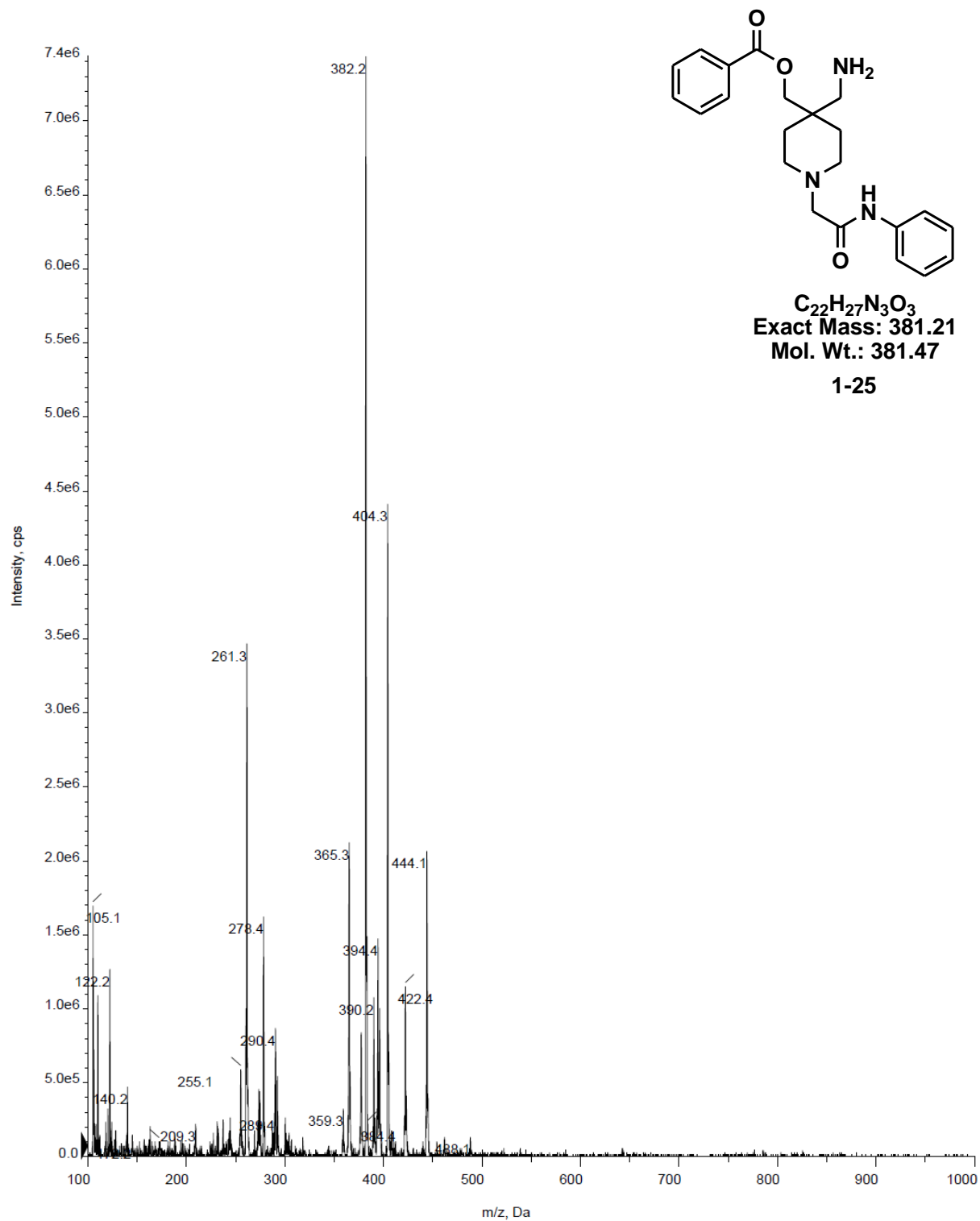
■ +Q1: 13 MCA scans from Sample 1 (TuneSampleID) of MT20140530114917.wiff (Turbo Spray)

Max. 7.6e6 cps.



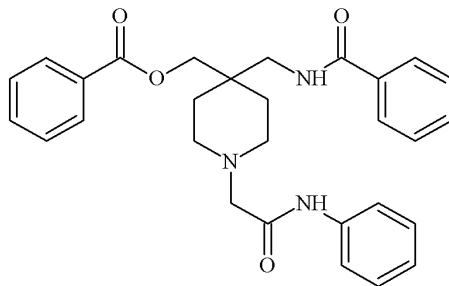
+Q1: 16 MCA scans from Sample 1 (TuneSampleID) of MT20140426113325.wiff (Turbo Spray)

Max. 7.4e6 cps.



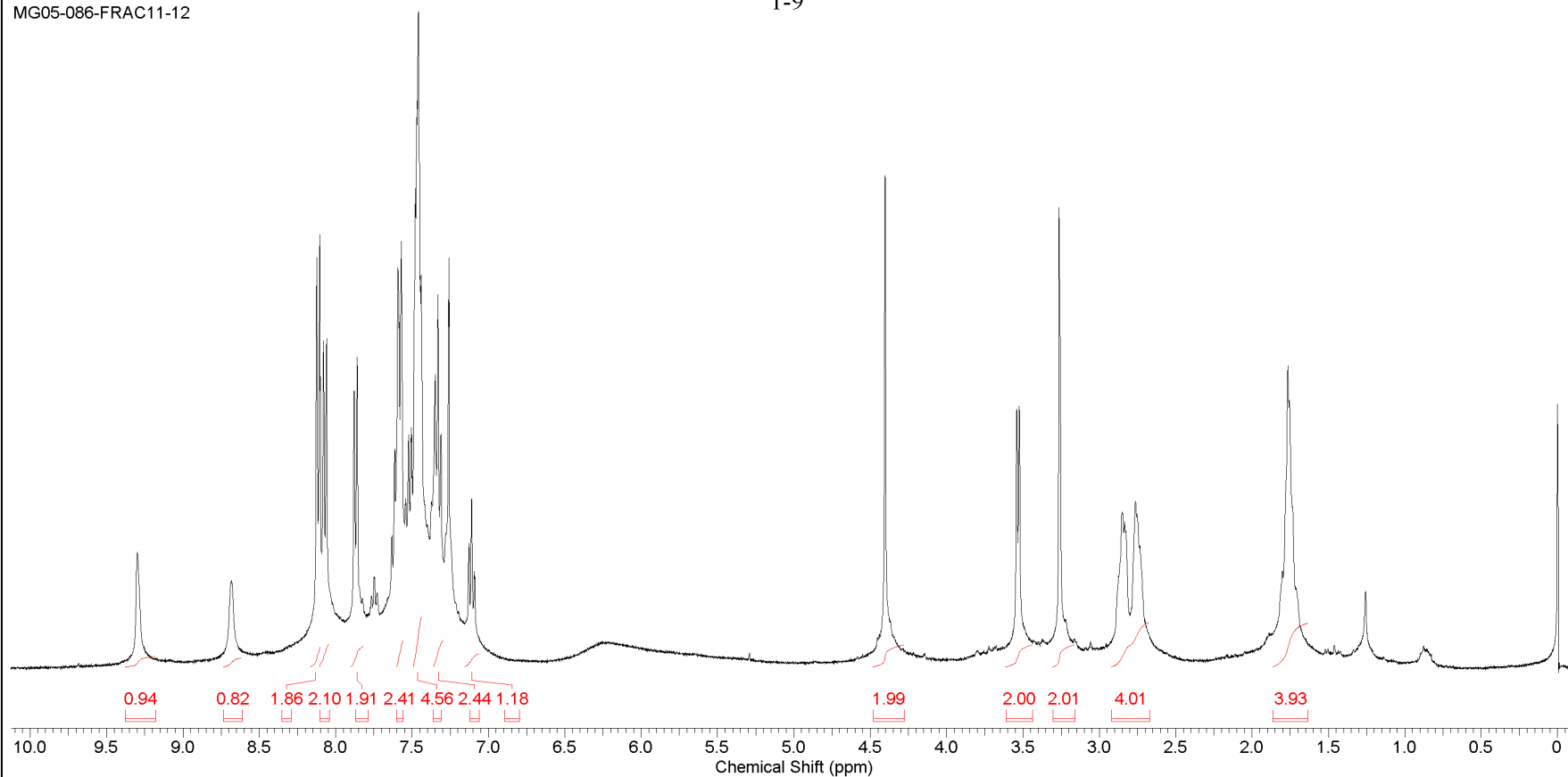
This report was created by ACD/NMR Processor Academic Edition. For more information go to www.acdlabs.com/nmrproc/

Formula C₂₉H₃₁N₃O₄ FW 485.5741



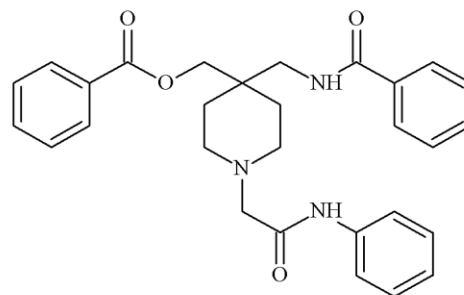
1-9

MG05-086-FRAC11-12



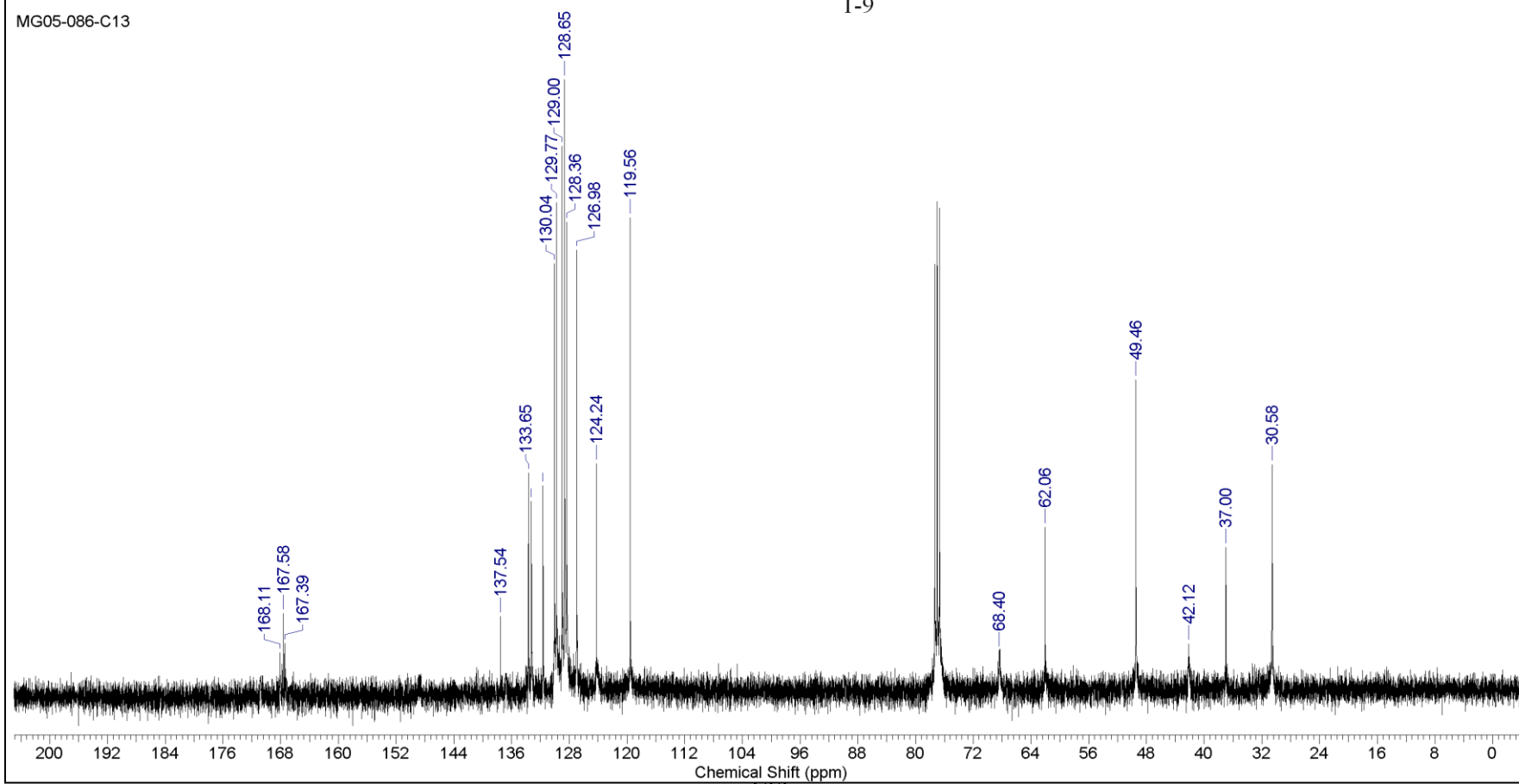
J:\T-TYPE CALCIUM CHANNEL\NMR\1-9\MG05-086-FRAC11-12

Formula $C_{29}H_{31}N_3O_4$ FW 485.5741



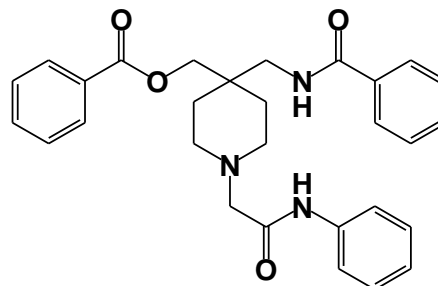
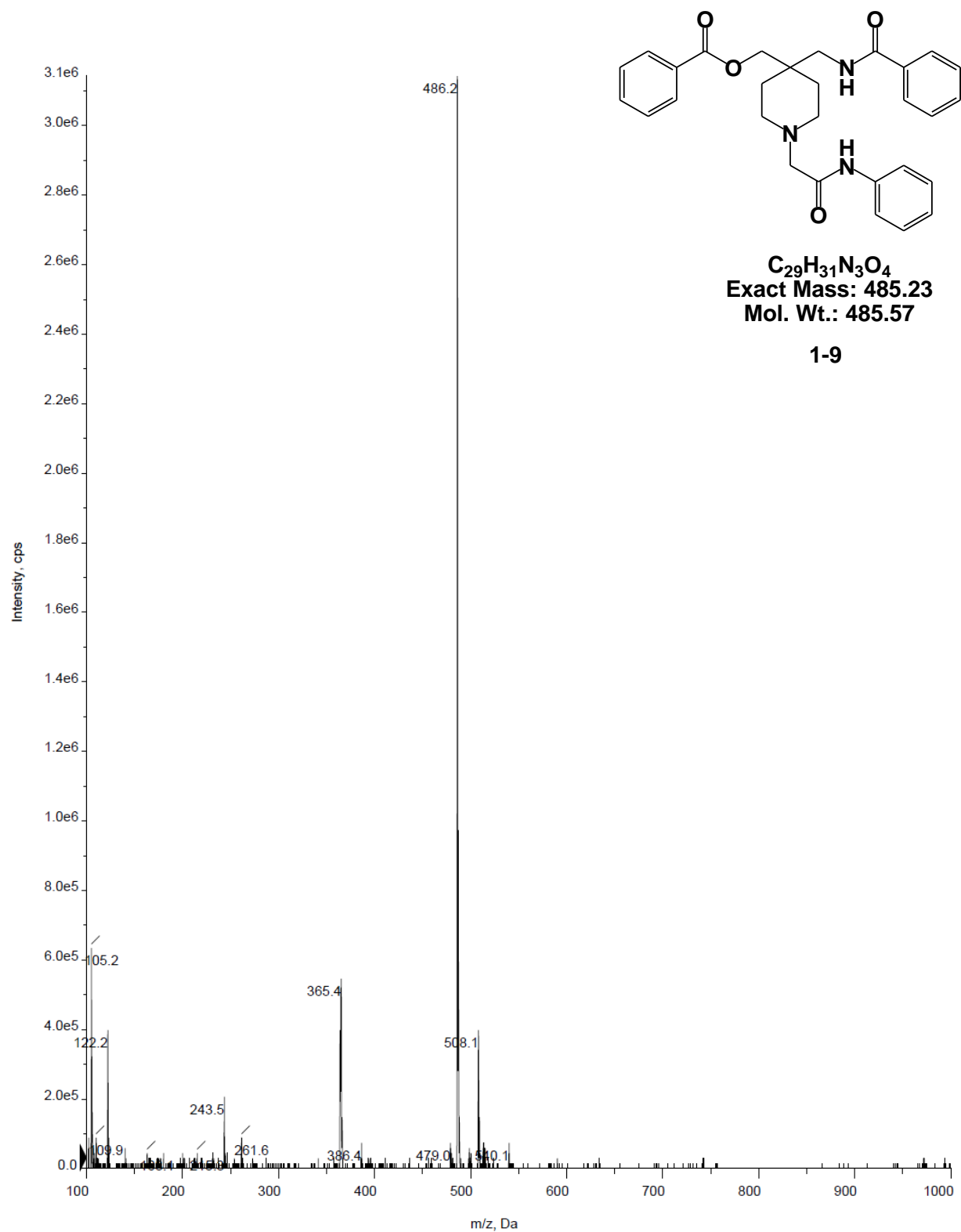
1-9

MG05-086-C13



■ +Q1: 13 MCA scans from Sample 1 (TuneSampleID) of MT20140326170058.wiff (Turbo Spray)

Max. 3.1e6 cps.

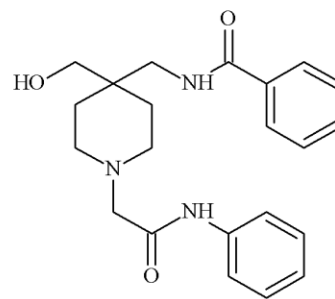


C₂₉H₃₁N₃O₄
Exact Mass: 485.23
Mol. Wt.: 485.57

1-9

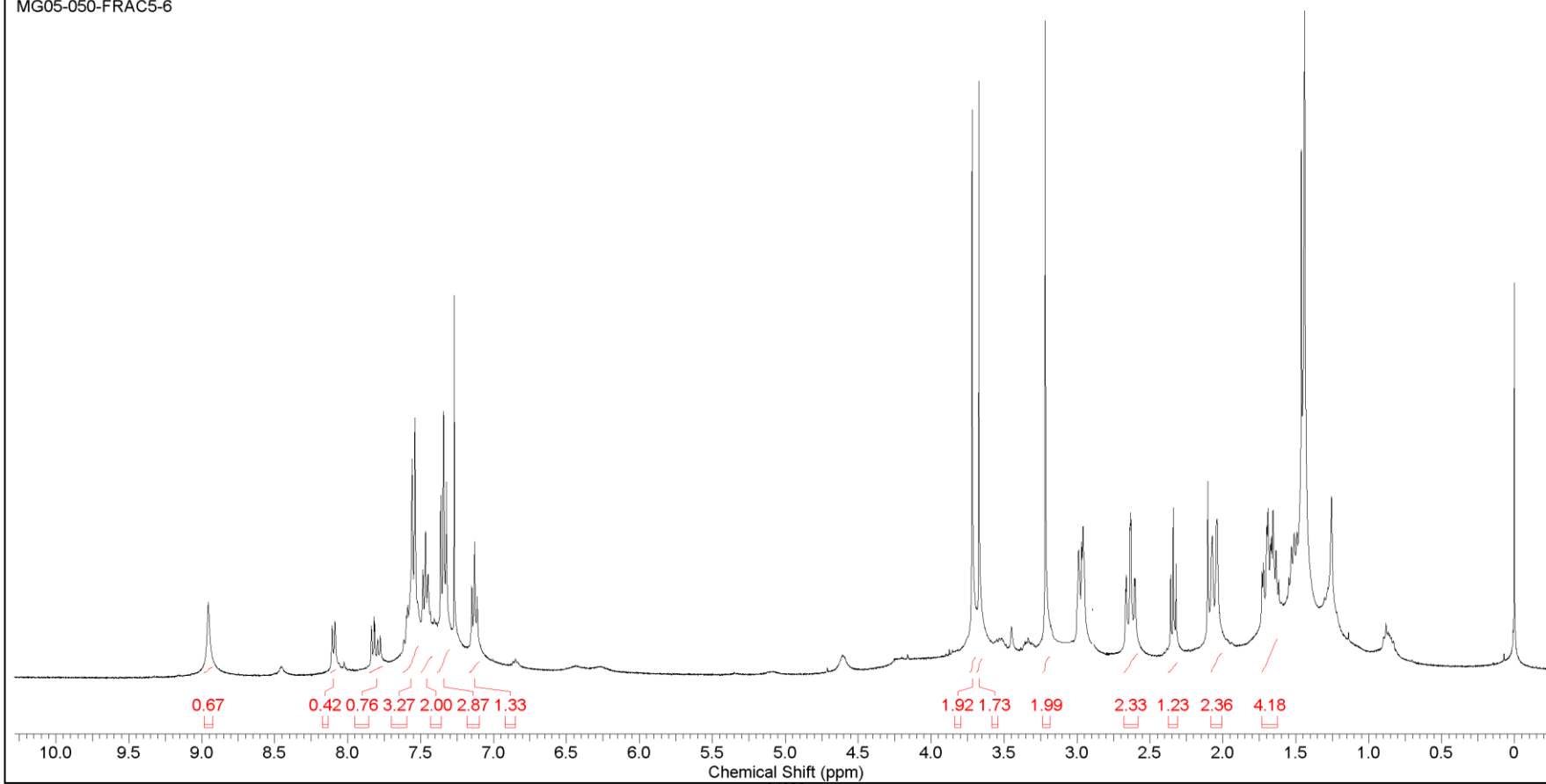
This report was created by ACD/NMR Processor Academic Edition. For more information go to www.acdlabs.com/nmrproc/

Formula $C_{22}H_{27}N_3O_3$ FW 381.4681



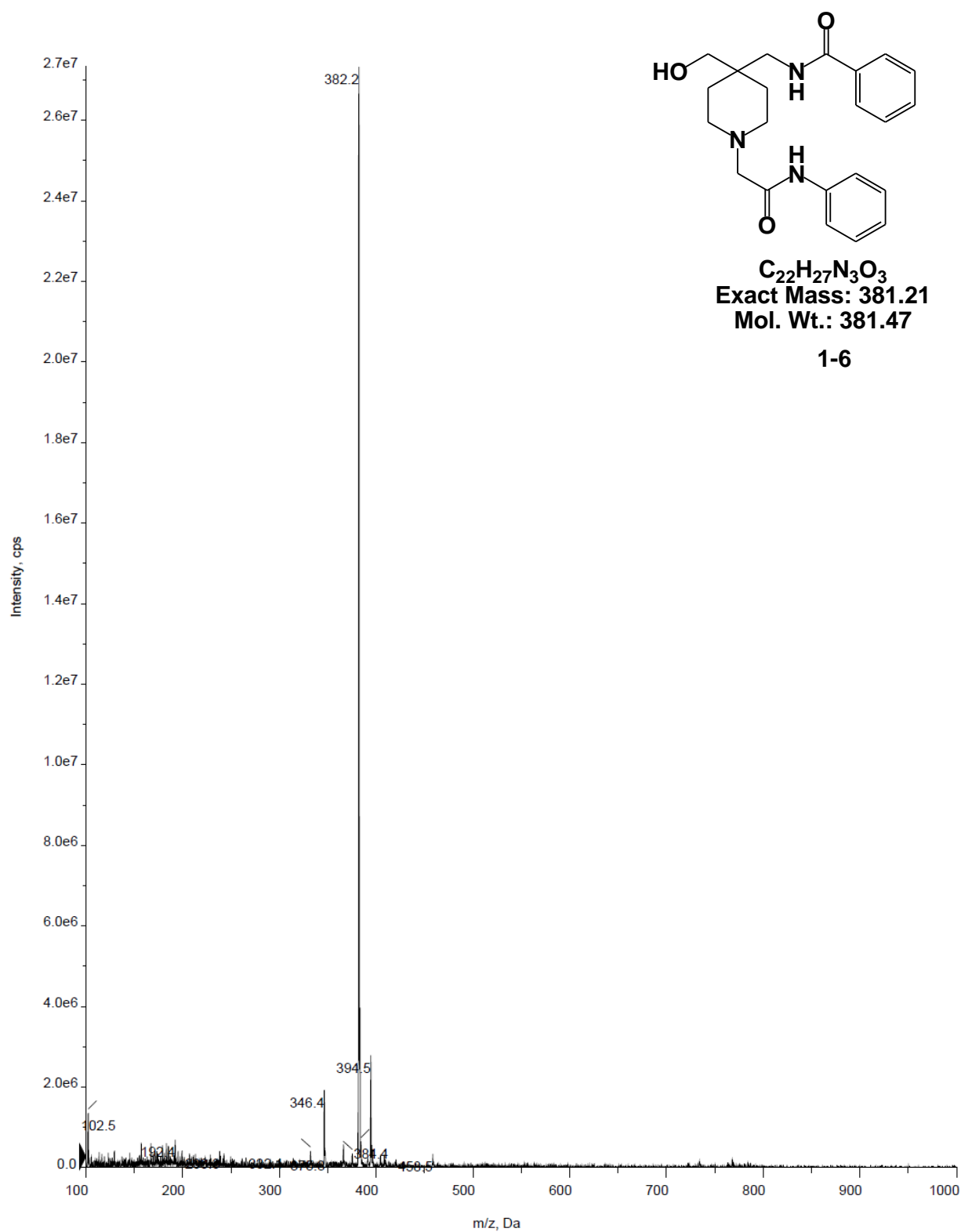
1-6

MG05-050-FRAC5-6



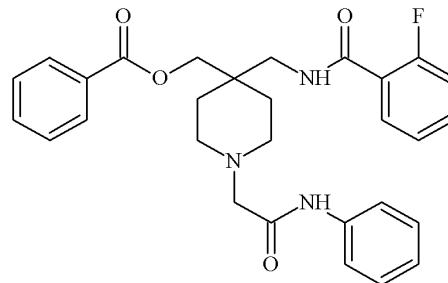
+Q1: 9 MCA scans from Sample 1 (TuneSampleID) of MT20140327205324.wiff (Turbo Spray)

Max. 2.7e7 cps.



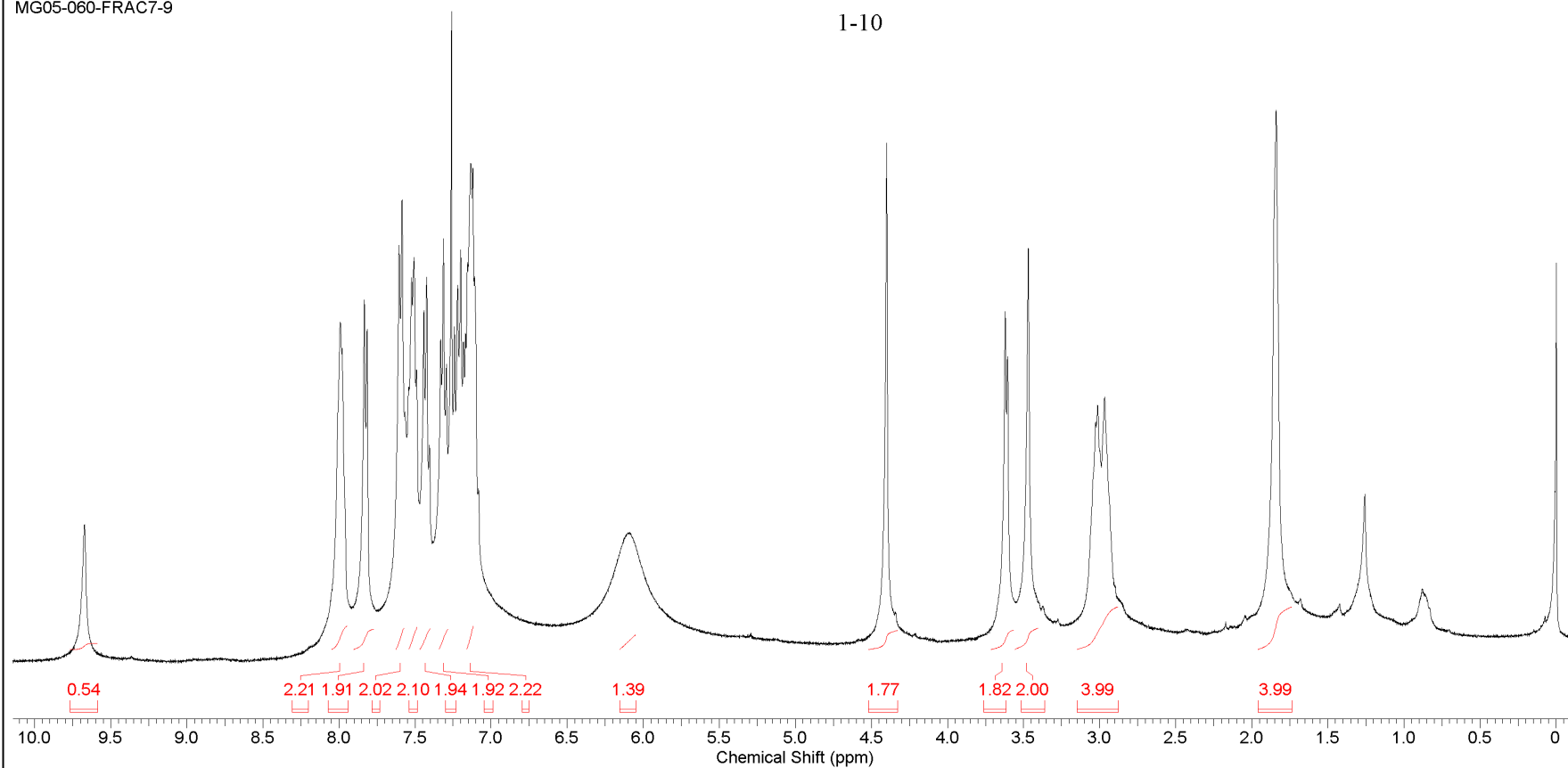
This report was created by ACD/NMR Processor Academic Edition. For more information go to www.acdlabs.com/nmrproc/

Formula $C_{29}H_{30}FN_3O_4$ FW 503.5646



MG05-060-FRAC7-9

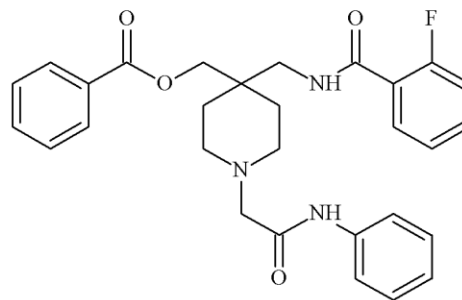
1-10



J:\NOTEBOOK5\MG05-060-FRAC7-9

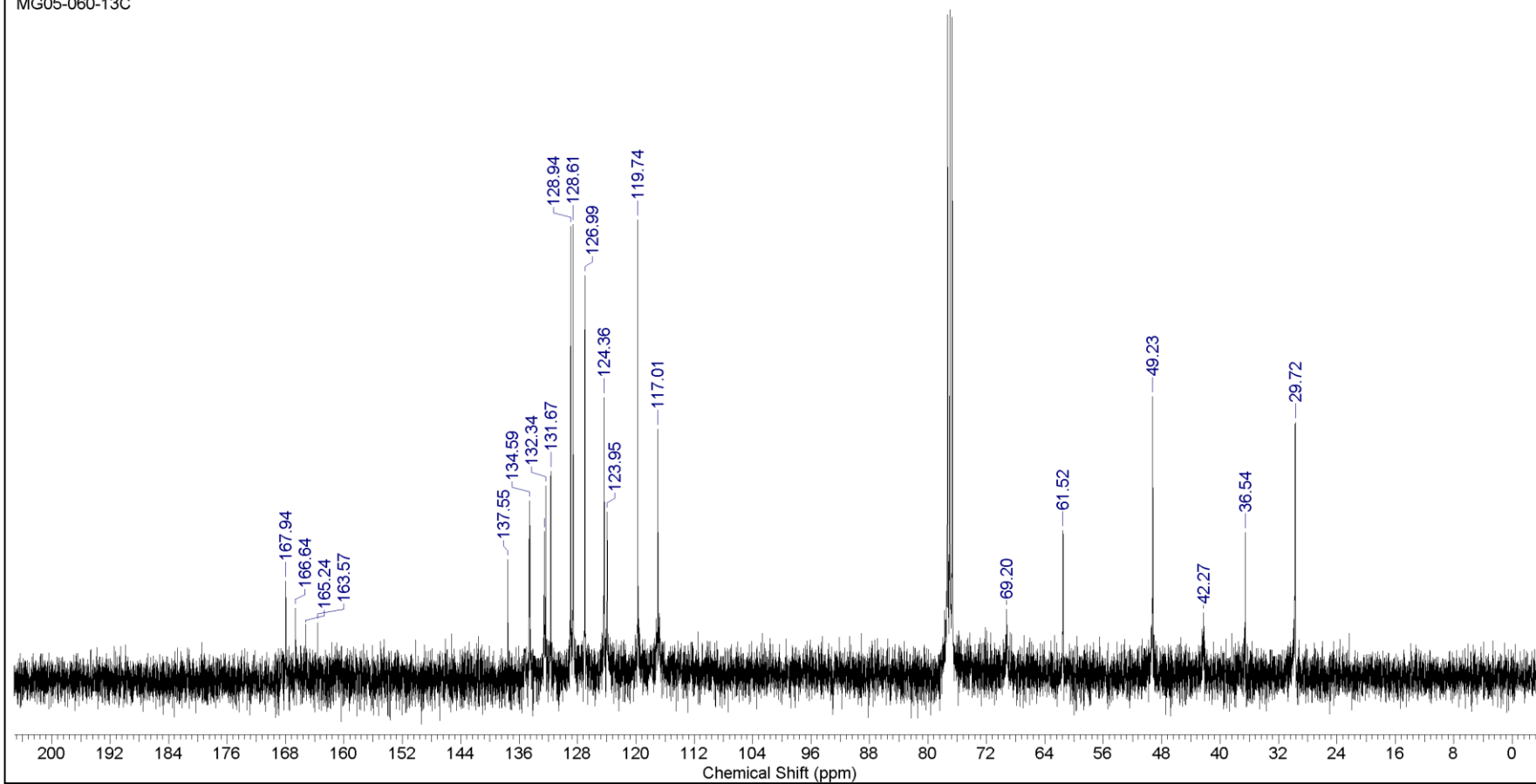
This report was created by ACD/NMR Processor Academic Edition. For more information go to www.acdlabs.com/nmrproc/

Formula $C_{29}H_{30}FN_3O_4$ FW 503.5646



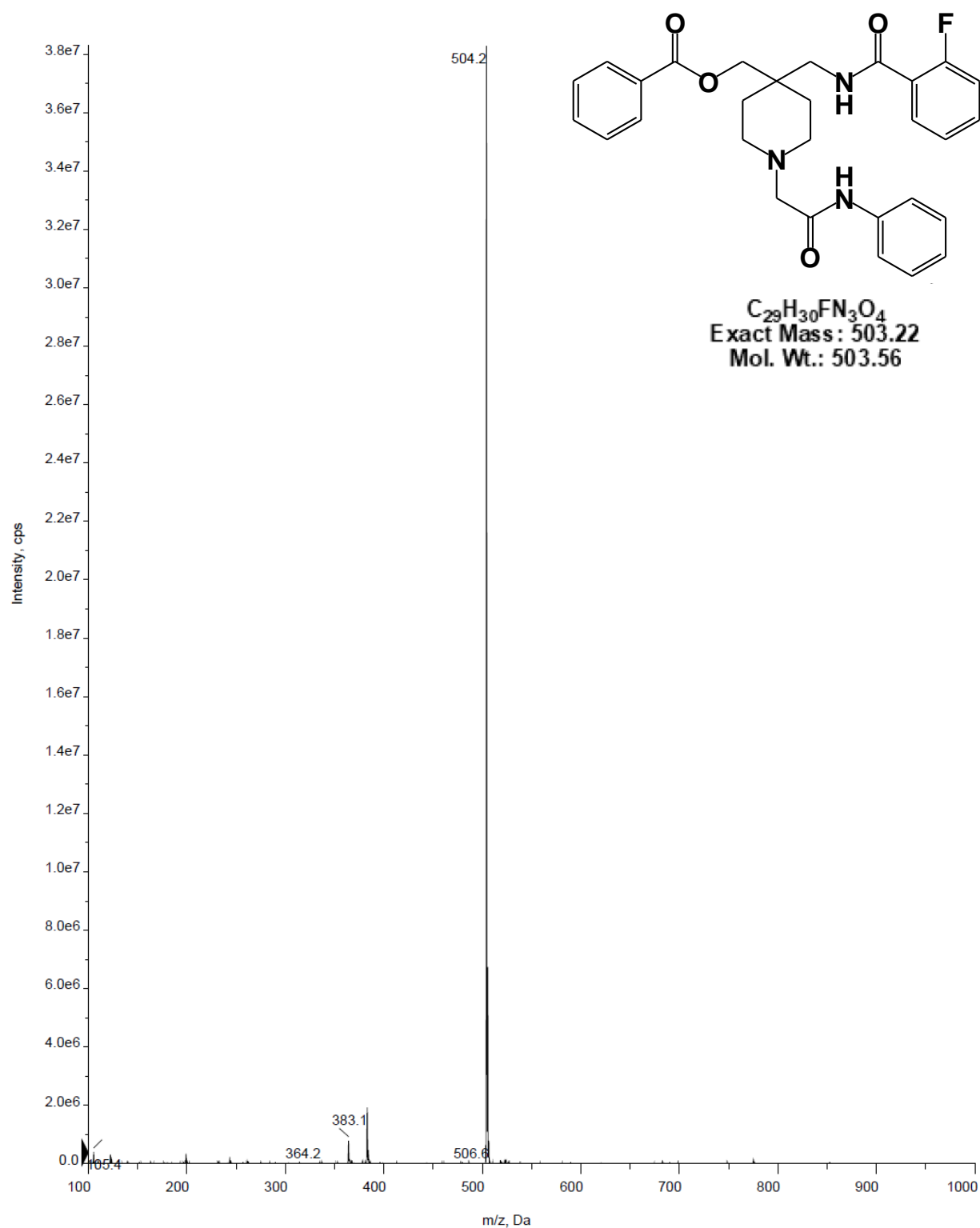
1-10

MG05-060-13C



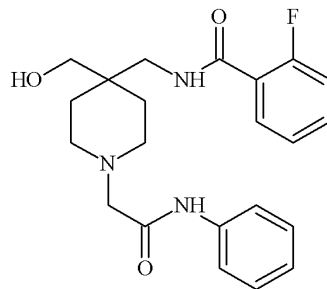
■ +Q1: 7 MCA scans from Sample 1 (TuneSampleID) of MT20140526112851.wiff (Turbo Spray)

Max. 3.8e7 cps.



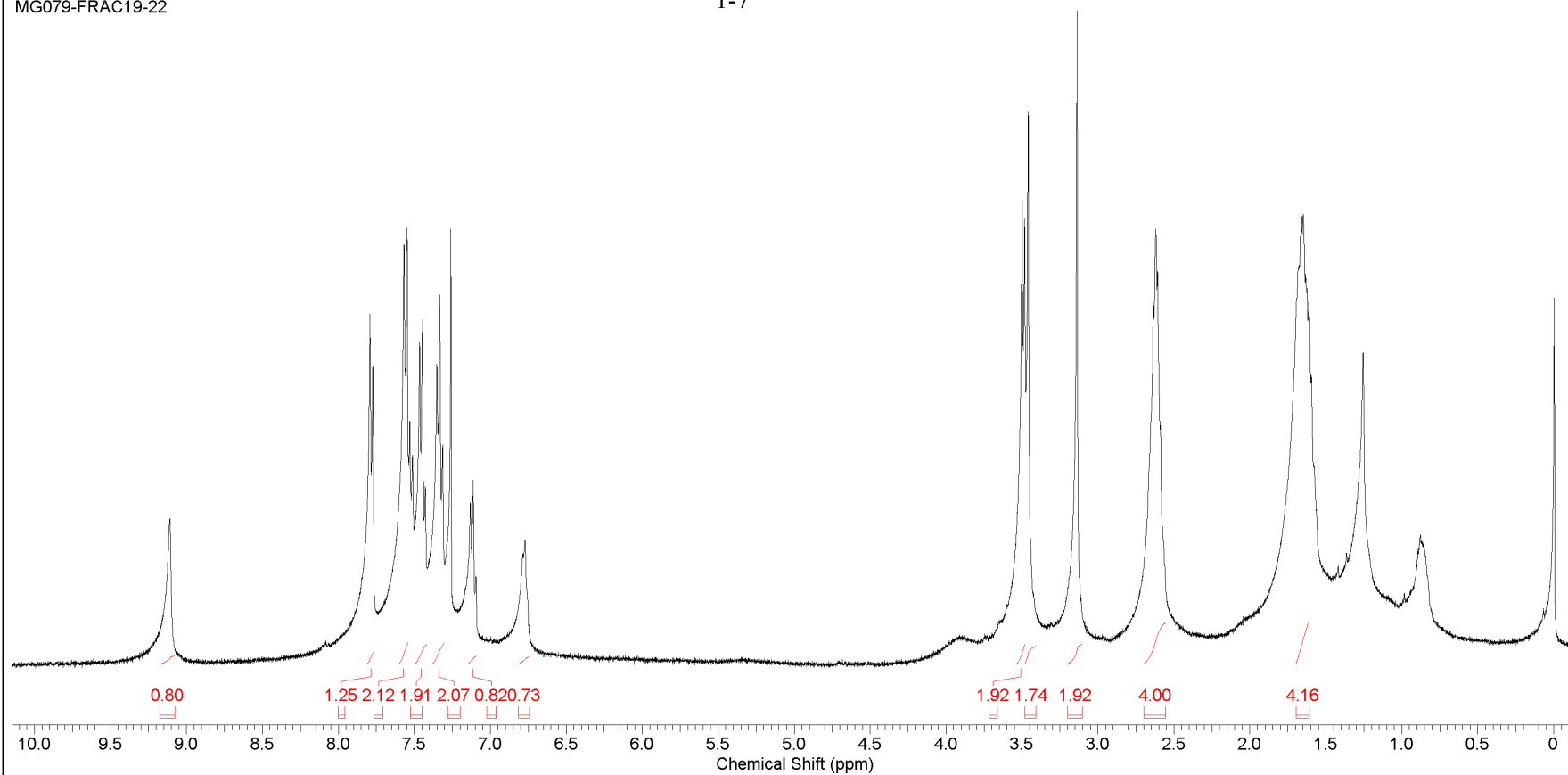
This report was created by ACD/NMR Processor Academic Edition. For more information go to www.acdlabs.com/nmrproc/

Formula $C_{22}H_{26}FN_3O_3$ FW 399.4585



1-7

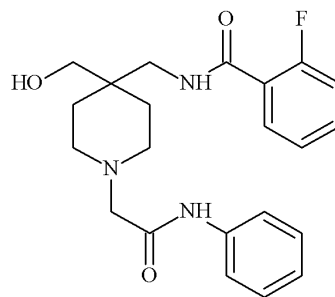
MG079-FRAC19-22



J:\T-TYPE CALCIUM CHANNEL\NMR\1-7\MG079-FRAC19-22

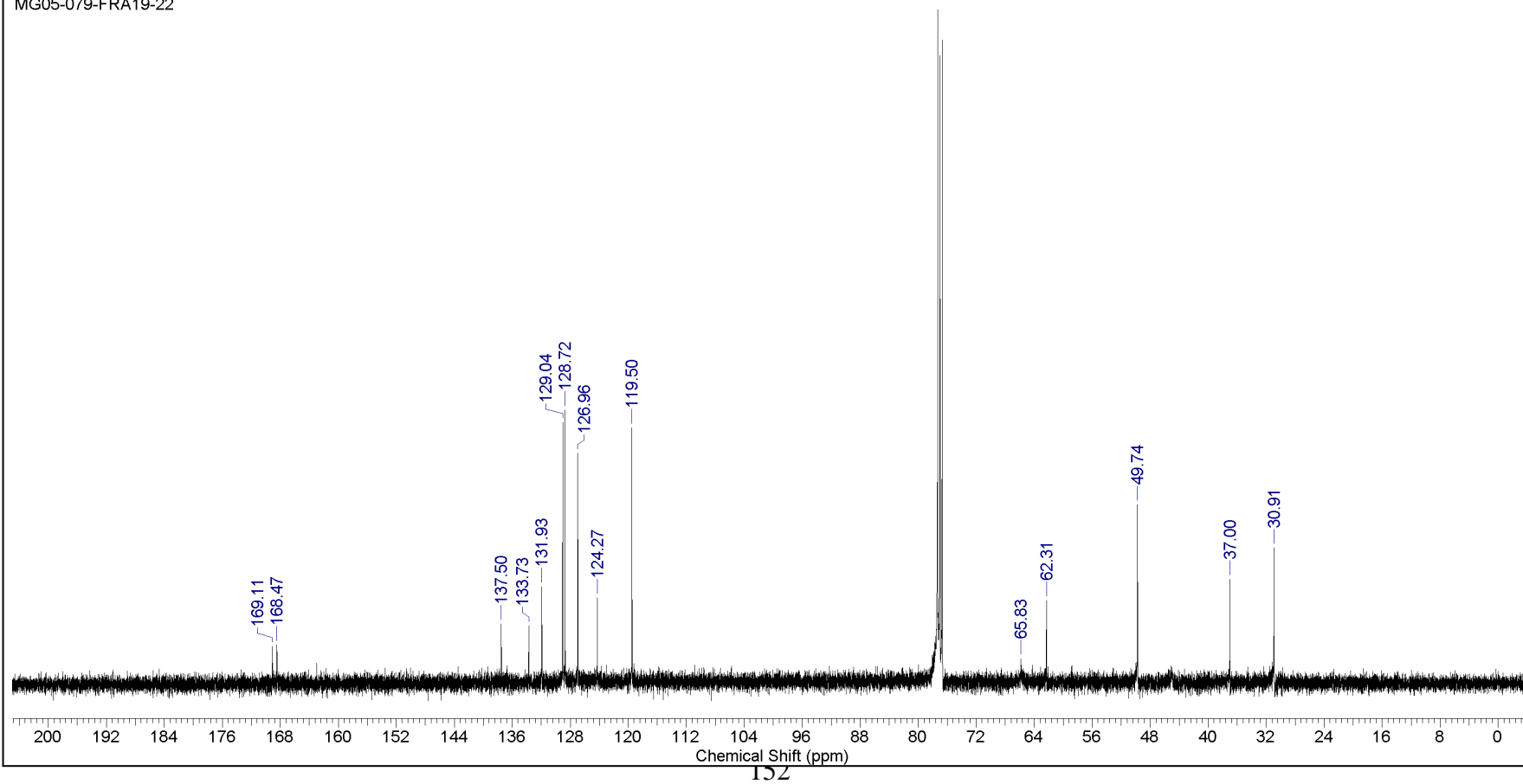
This report was created by ACD/NMR Processor Academic Edition. For more information go to www.acdlabs.com/nmrproc/

Formula $C_{22}H_{26}FN_3O_3$ FW 399.4585



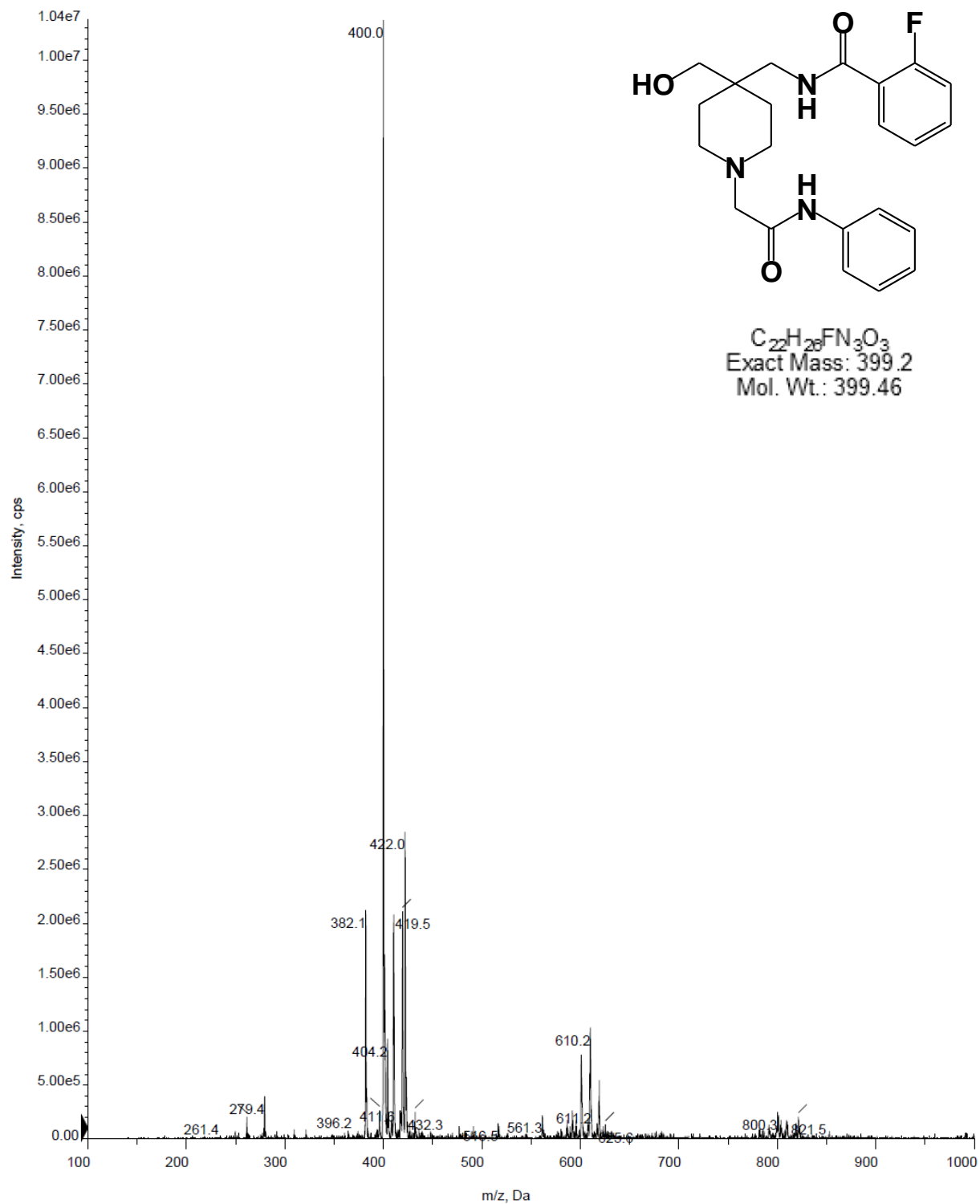
1-7

MG05-079-FRA19-22

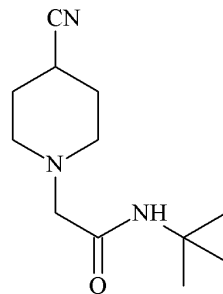


■ +Q1: 39 MCA scans from Sample 1 (TuneSampleID) of MT20140527122209.wiff (Turbo Spray)

Max. 1.0e7 cps.

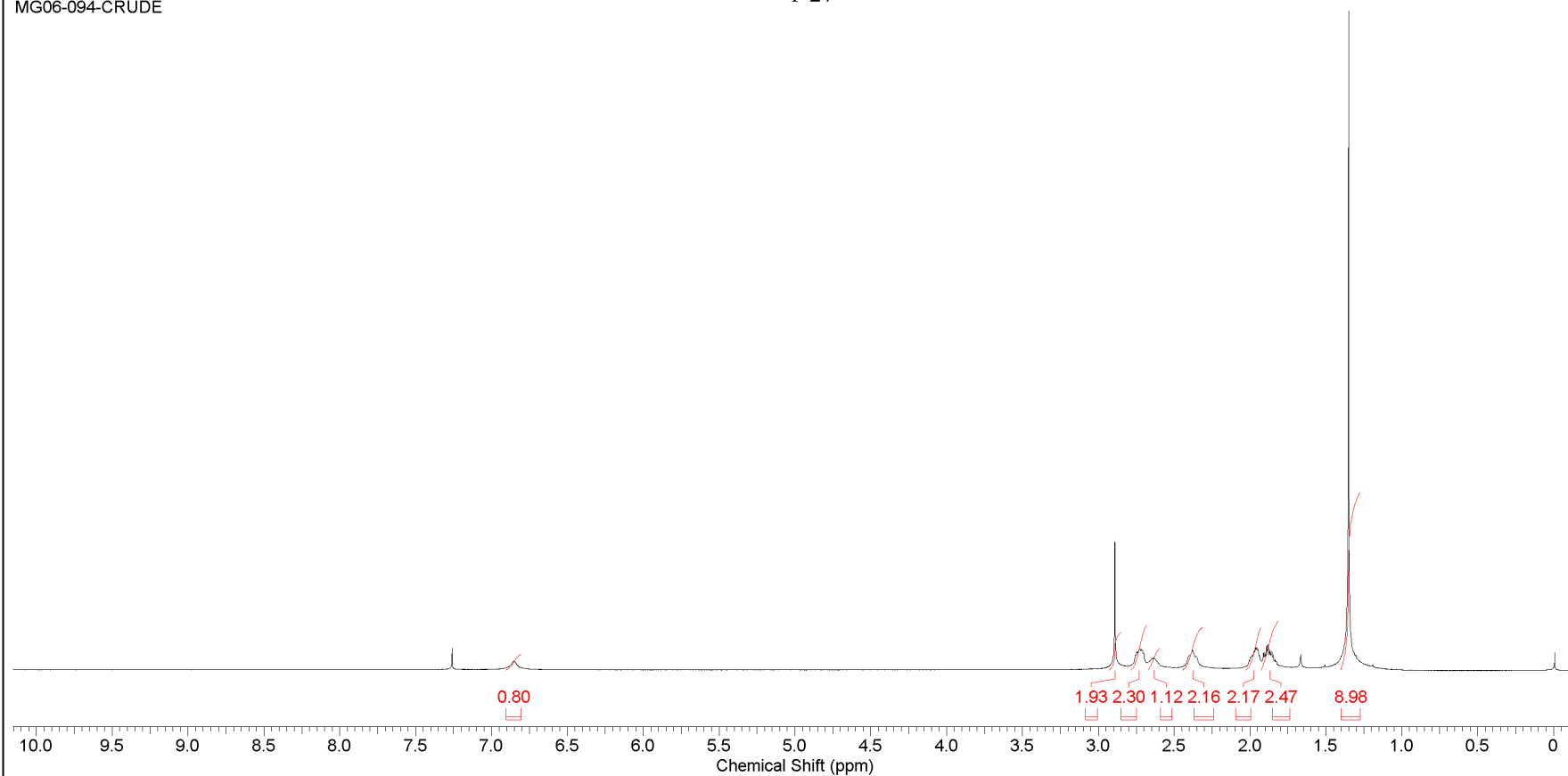


Formula	C ₁₂ H ₂₁ N ₃ O	FW	223.3146
----------------	--	-----------	----------



1-27

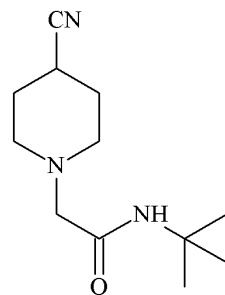
MG06-094-CRUDE



J:\NOTEBOOK6\MG06-094-CRUDE

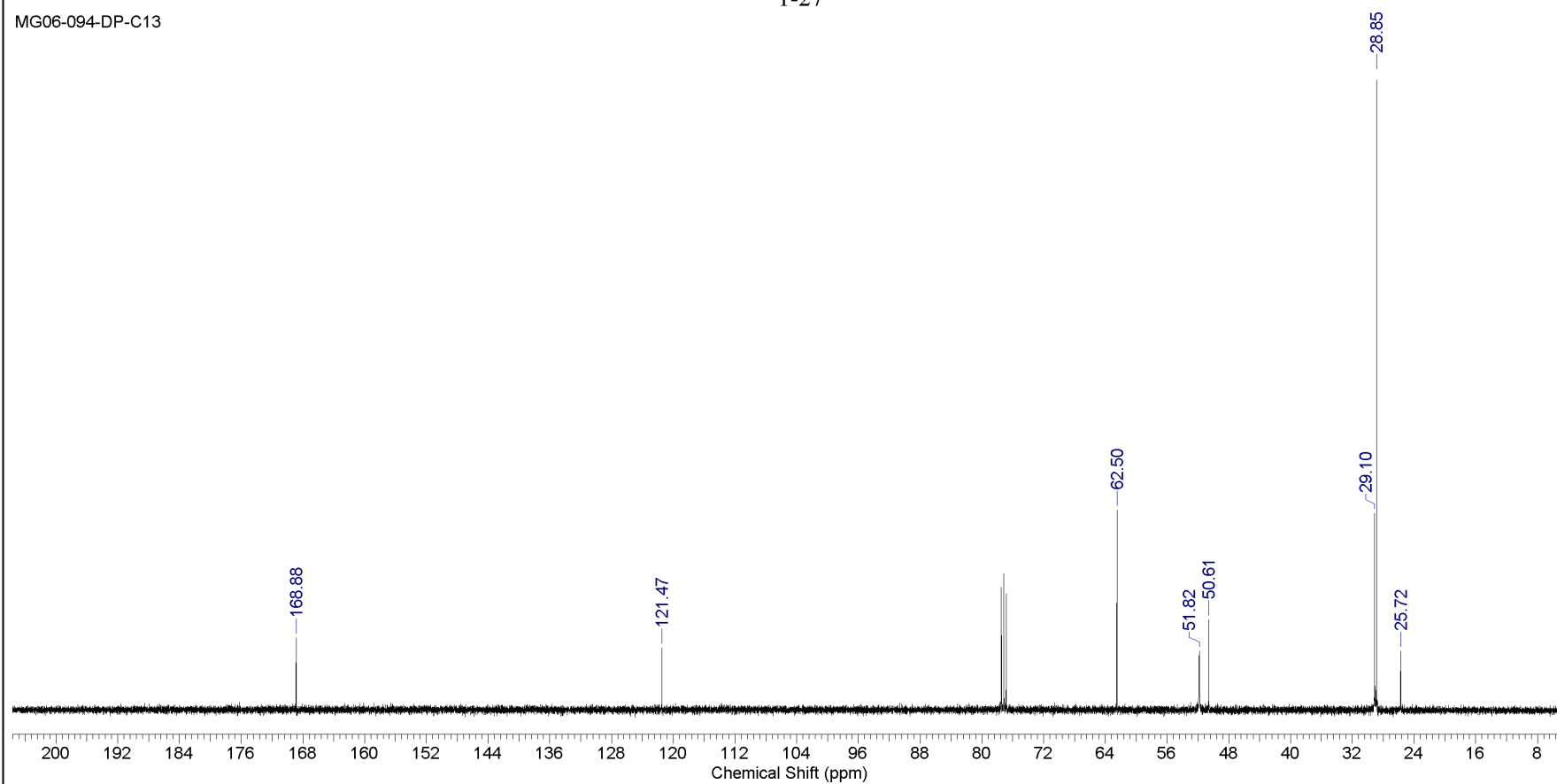
This report was created by ACD/NMR Processor Academic Edition. For more information go to www.acdlabs.com/nmrproc/

Formula	C ₁₂ H ₂₁ N ₃ O	FW	223.3146
----------------	--	-----------	----------



1-27

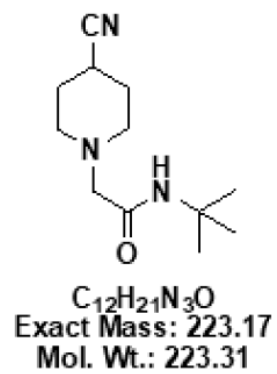
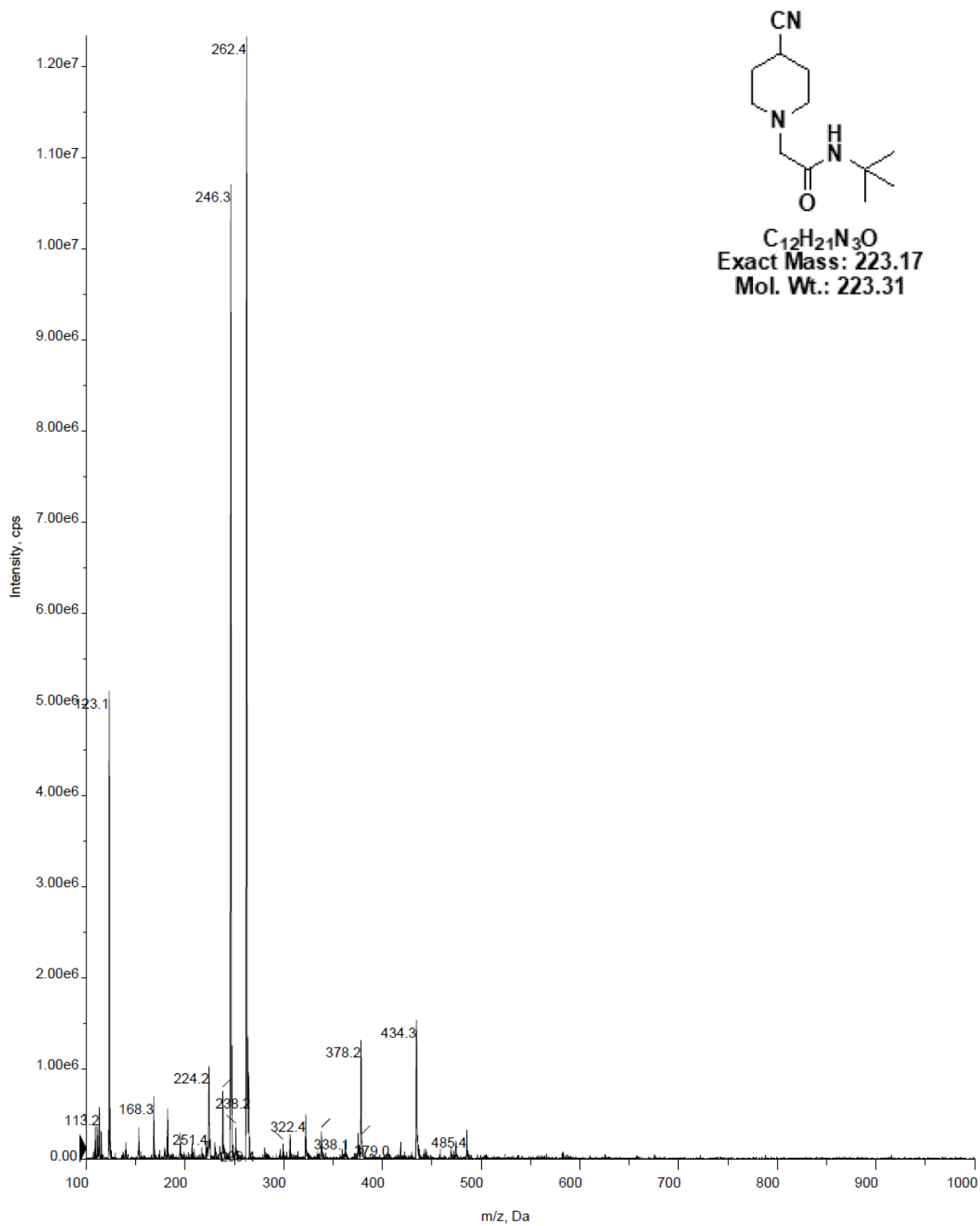
MG06-094-DP-C13



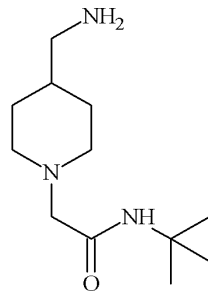
J:\T-TYPE CALCIUM CHANNEL\NMR\1-27\MG06-094-DP-C13

■ +Q1: 19 MCA scans from Sample 1 (TuneSampleID) of MT20141014190638.wiff (Turbo Spray)

Max. 1.2e7 cps.

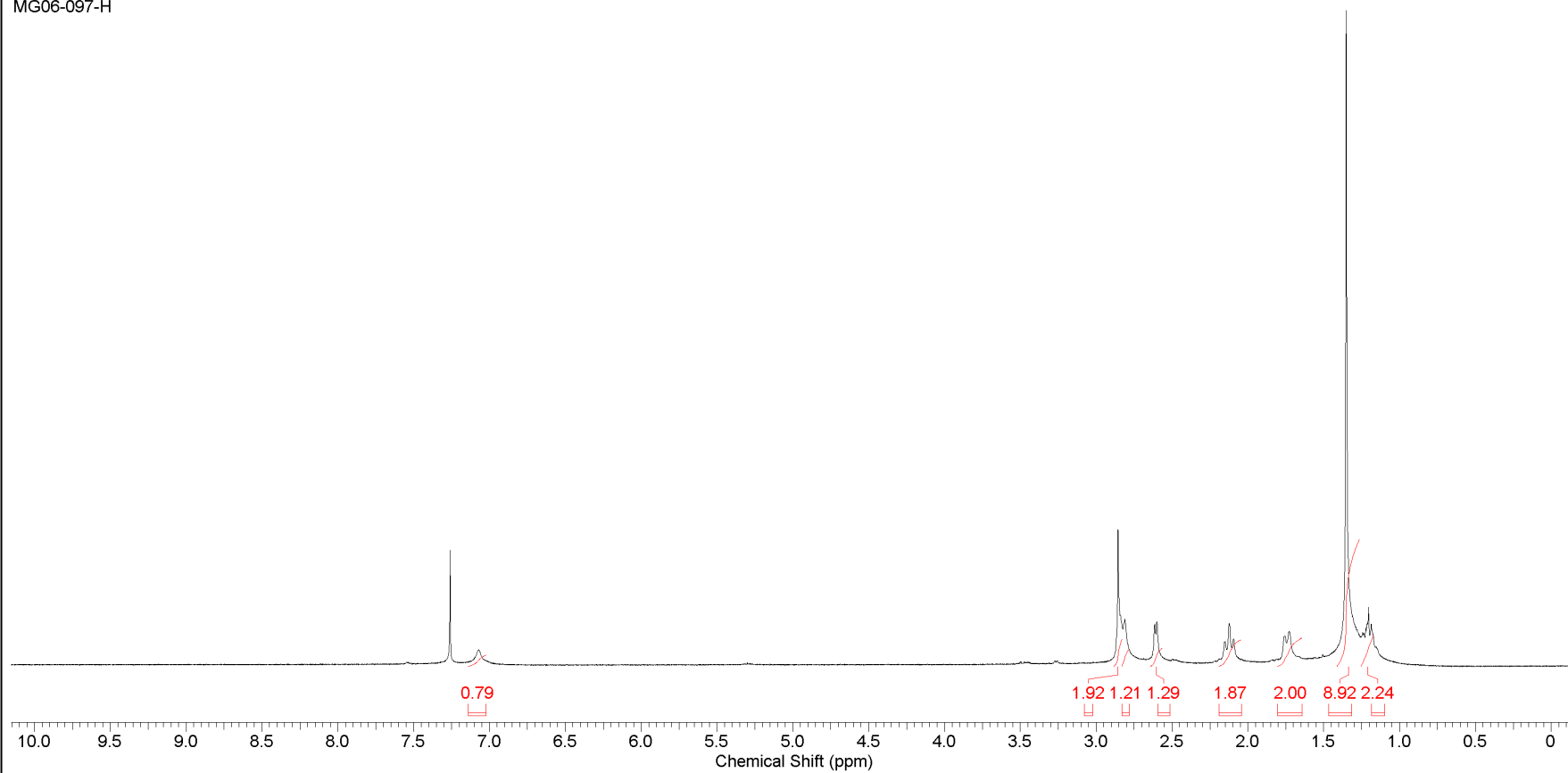


Formula C₁₂H₂₅N₃O FW 227.3464



1-28

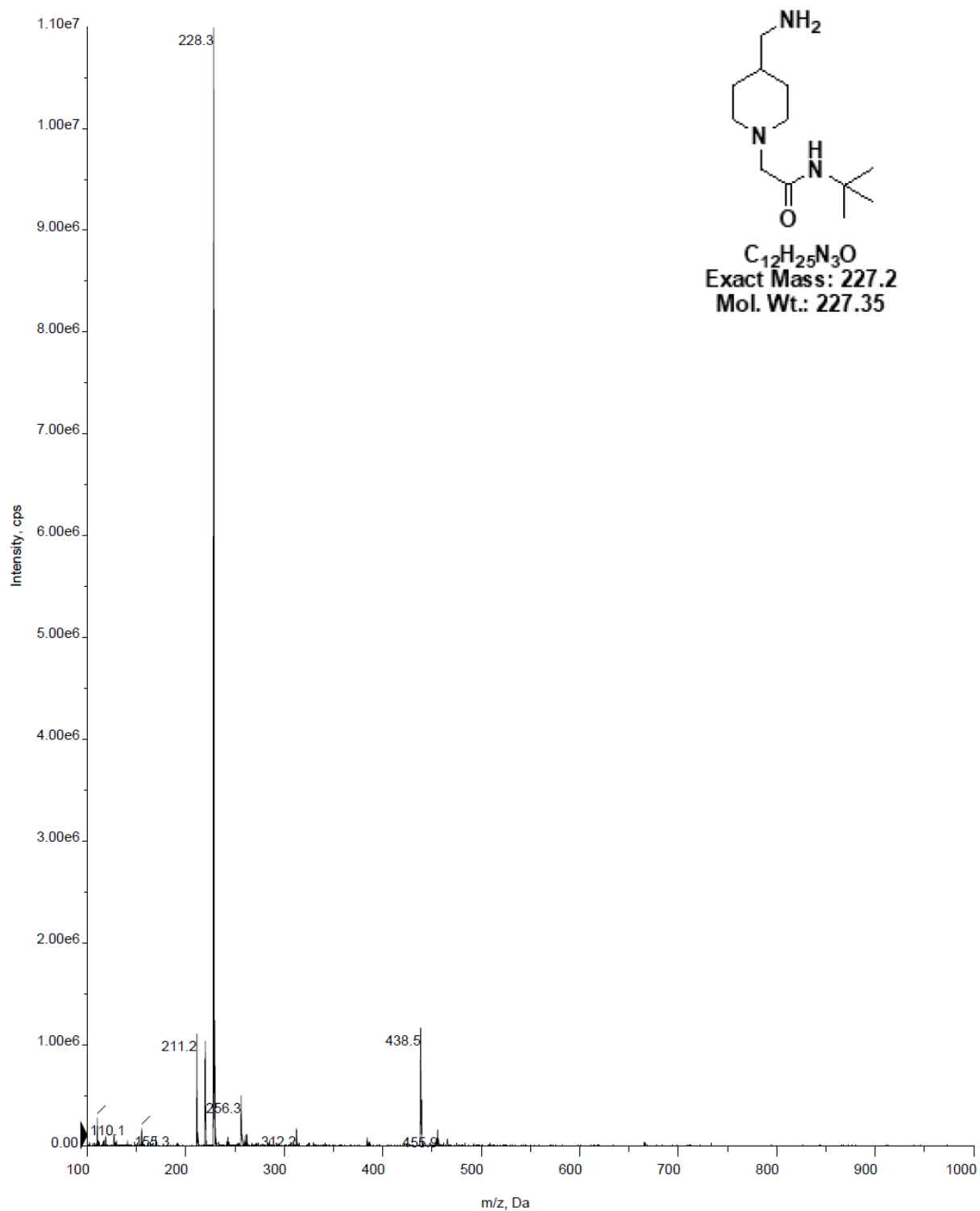
MG06-097-H



J:\NOTEBOOK6\MG06-097-H

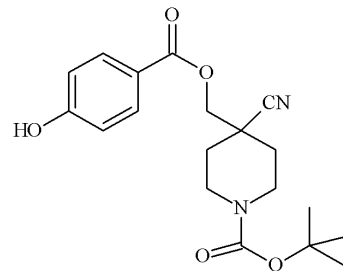
■ +Q1: 5 MCA scans from Sample 1 (TuneSampleID) of MT20141023181334.wiff (Turbo Spray)

Max. 1.1e7 cps.



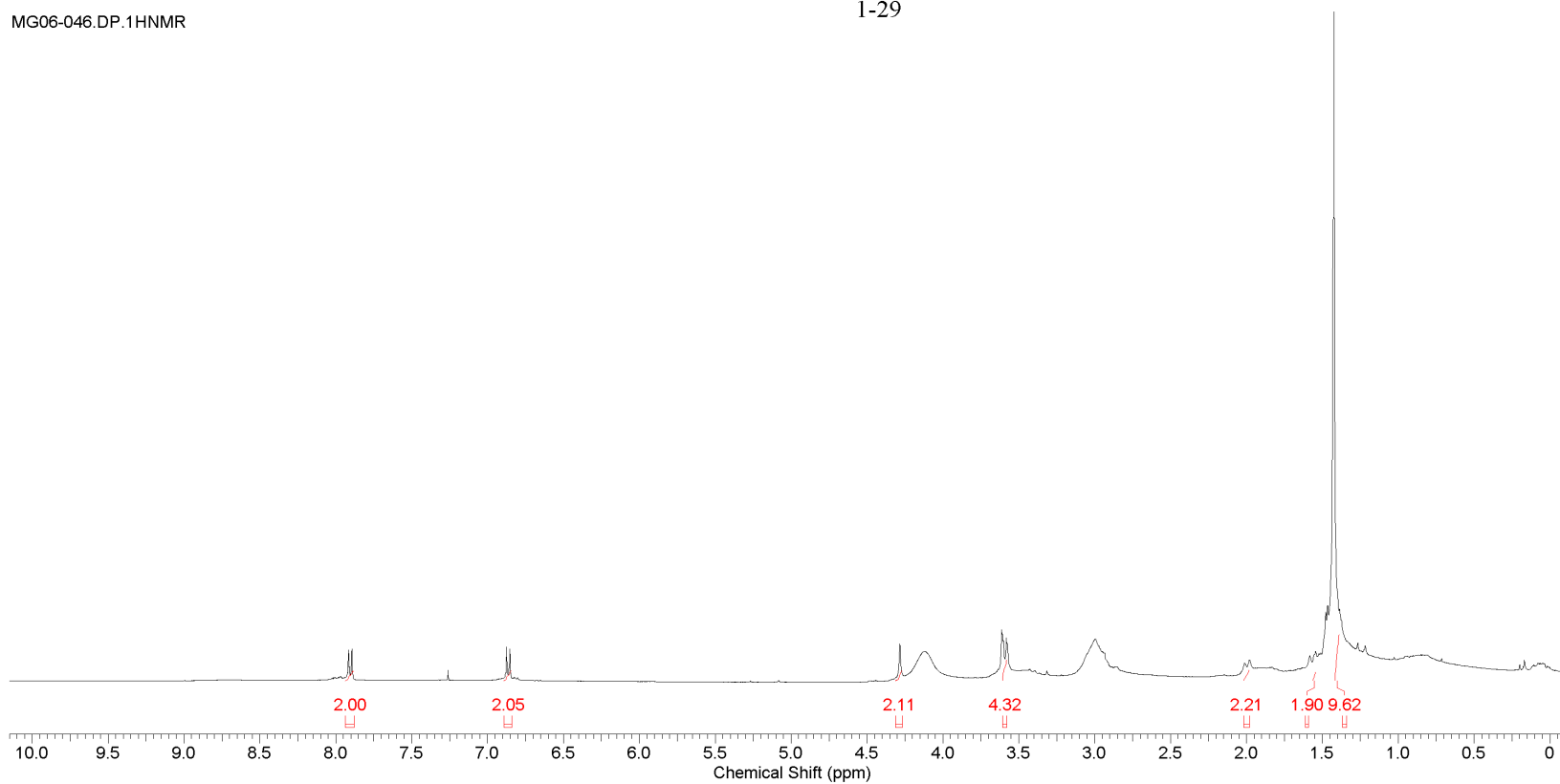
This report was created by ACD/NMR Processor Academic Edition. For more information go to www.acdlabs.com/nmrproc/

Formula C₁₉H₂₄N₂O₅ FW 360.4043



1-29

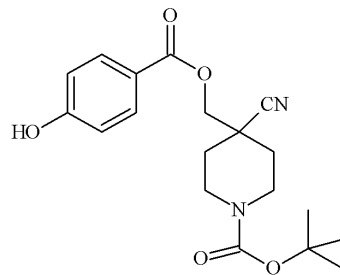
MG06-046.DP.1HNMR



J:\NOTEBOOK6\MG06-046.DP.1HNMR

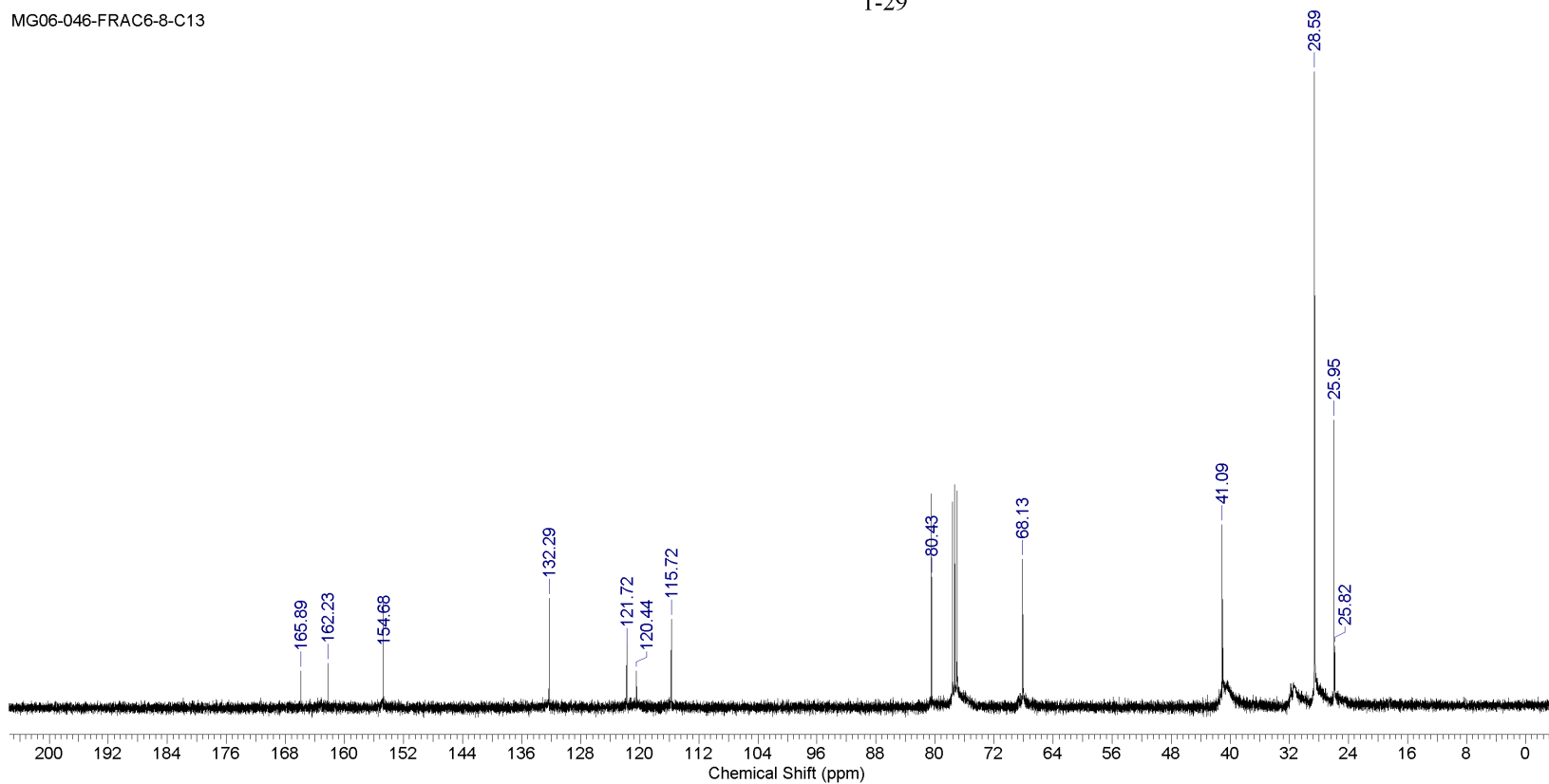
This report was created by ACD/NMR Processor Academic Edition. For more information go to www.acdlabs.com/nmrproc/

Formula C₁₉H₂₄N₂O₅ FW 360.4043



1-29

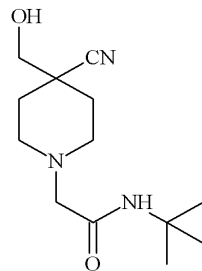
MG06-046-FRAC6-8-C13



J:MG06-046-FRAC6-8-C13

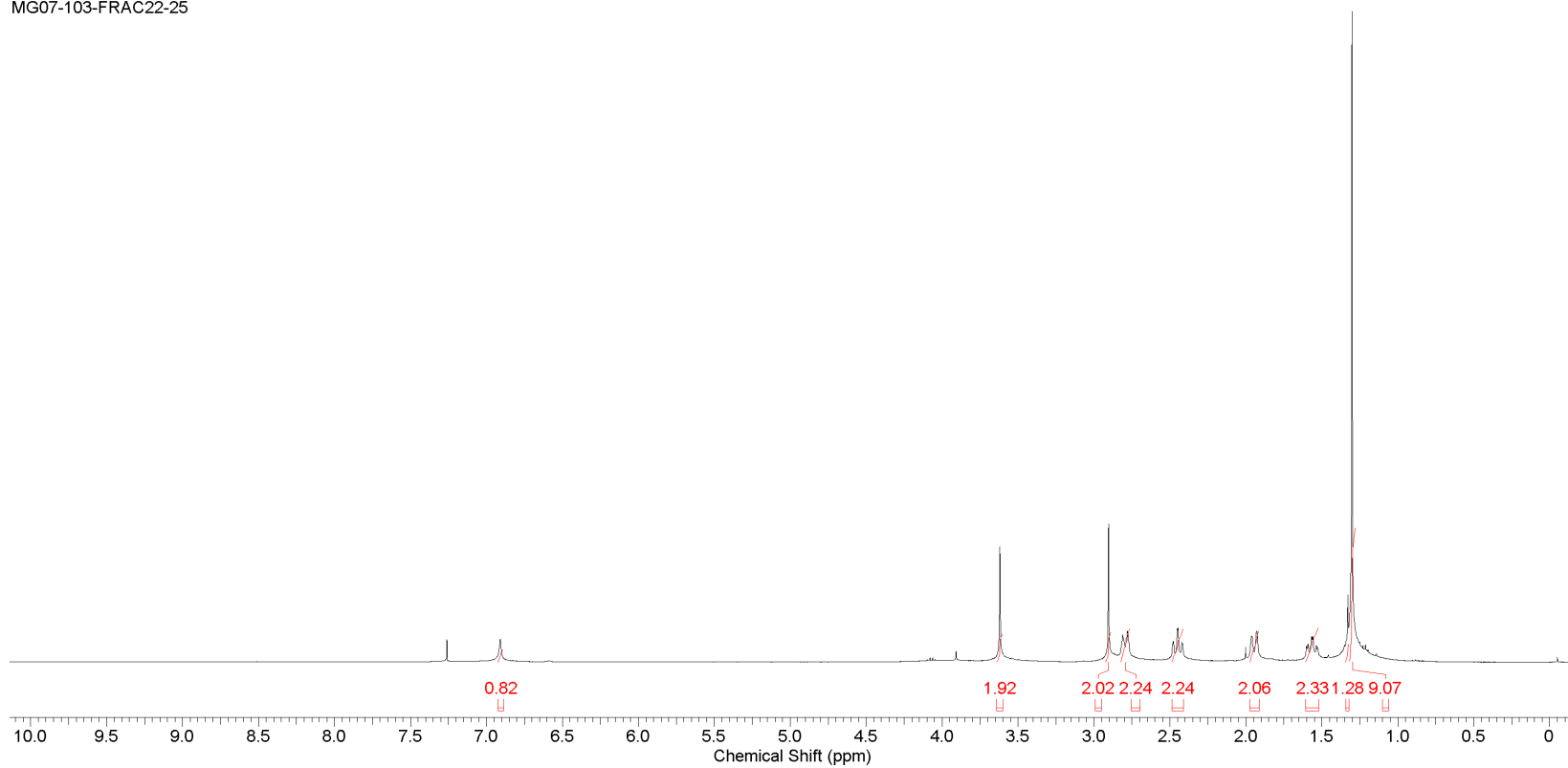
This report was created by ACD/NMR Processor Academic Edition. For more information go to www.acdlabs.com/nmrproc/

Formula C₁₃H₂₃N₃O₂ **FW** 253.3406



1-34

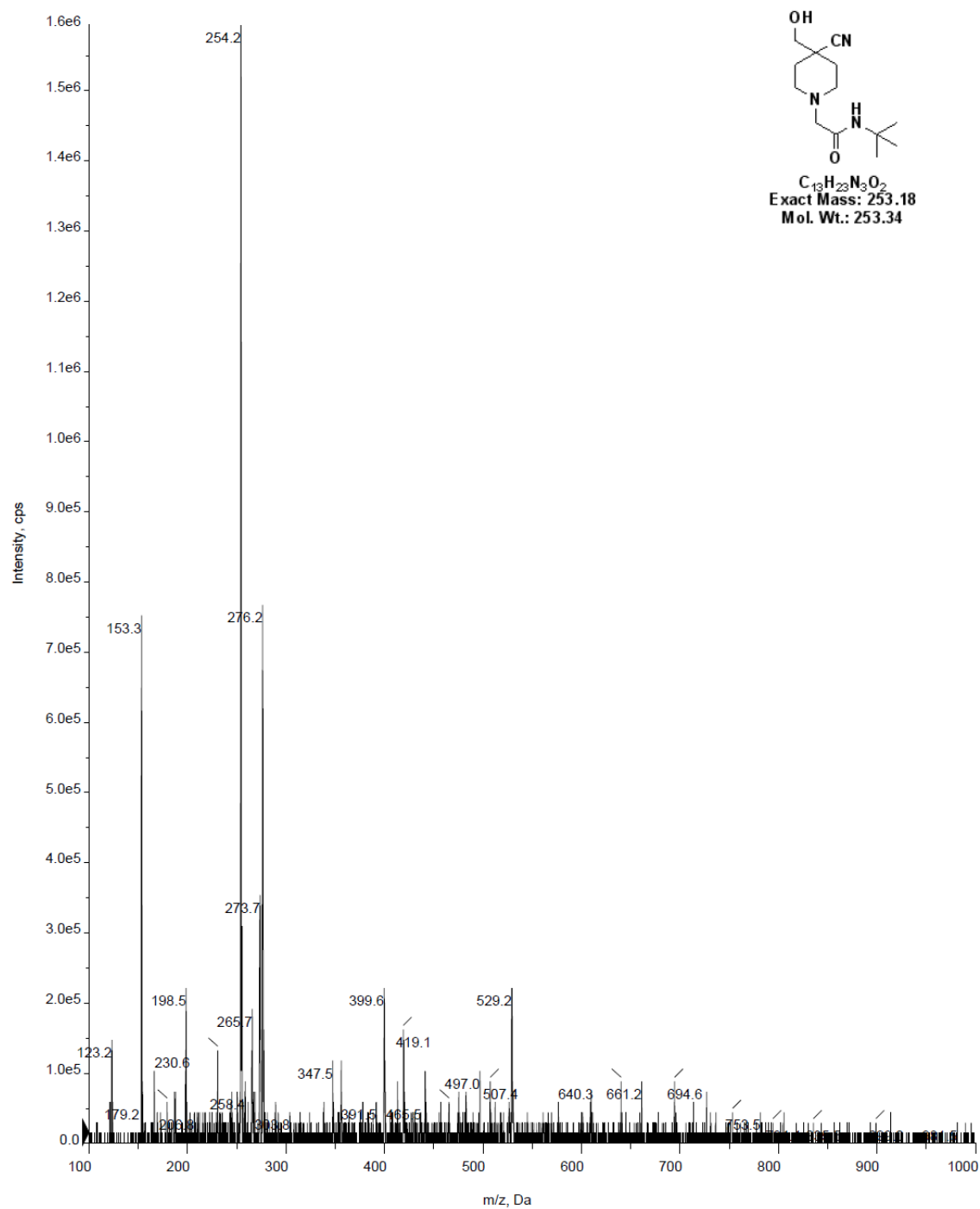
MG07-103-FRAC22-25



J:\PDI\NMR\MG07-103-FRAC22-25

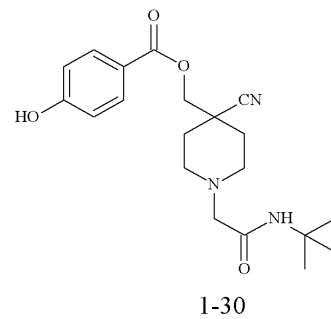
■ +Q1: 5 MCA scans from Sample 1 (TuneSampleID) of MT20150513115302.wiff (Turbo Spray)

Max. 1.6e6 cps.

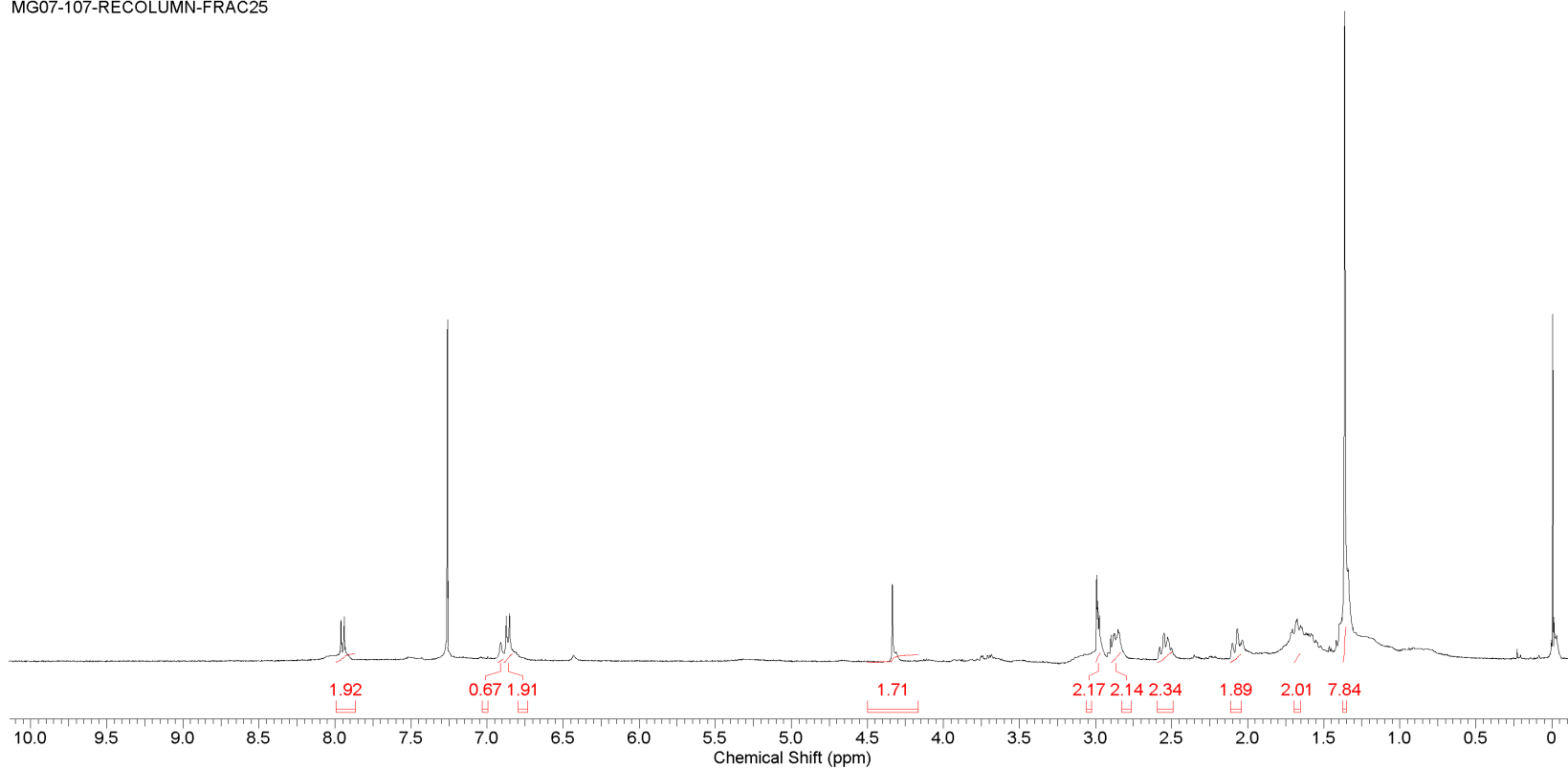


This report was created by ACD/NMR Processor Academic Edition. For more information go to www.acdlabs.com/nmrproc/

Formula C₂₀H₂₇N₃O₄ FW 373.4461



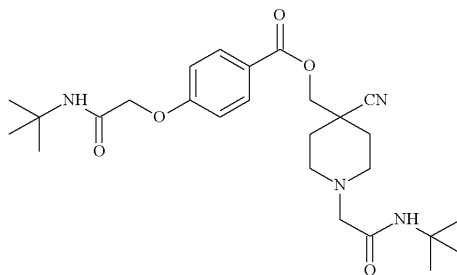
MG07-107-RECOLUMN-FRAC25



J:\NOTEBOOK7\MG07-107-RECOLUMN-FRAC25

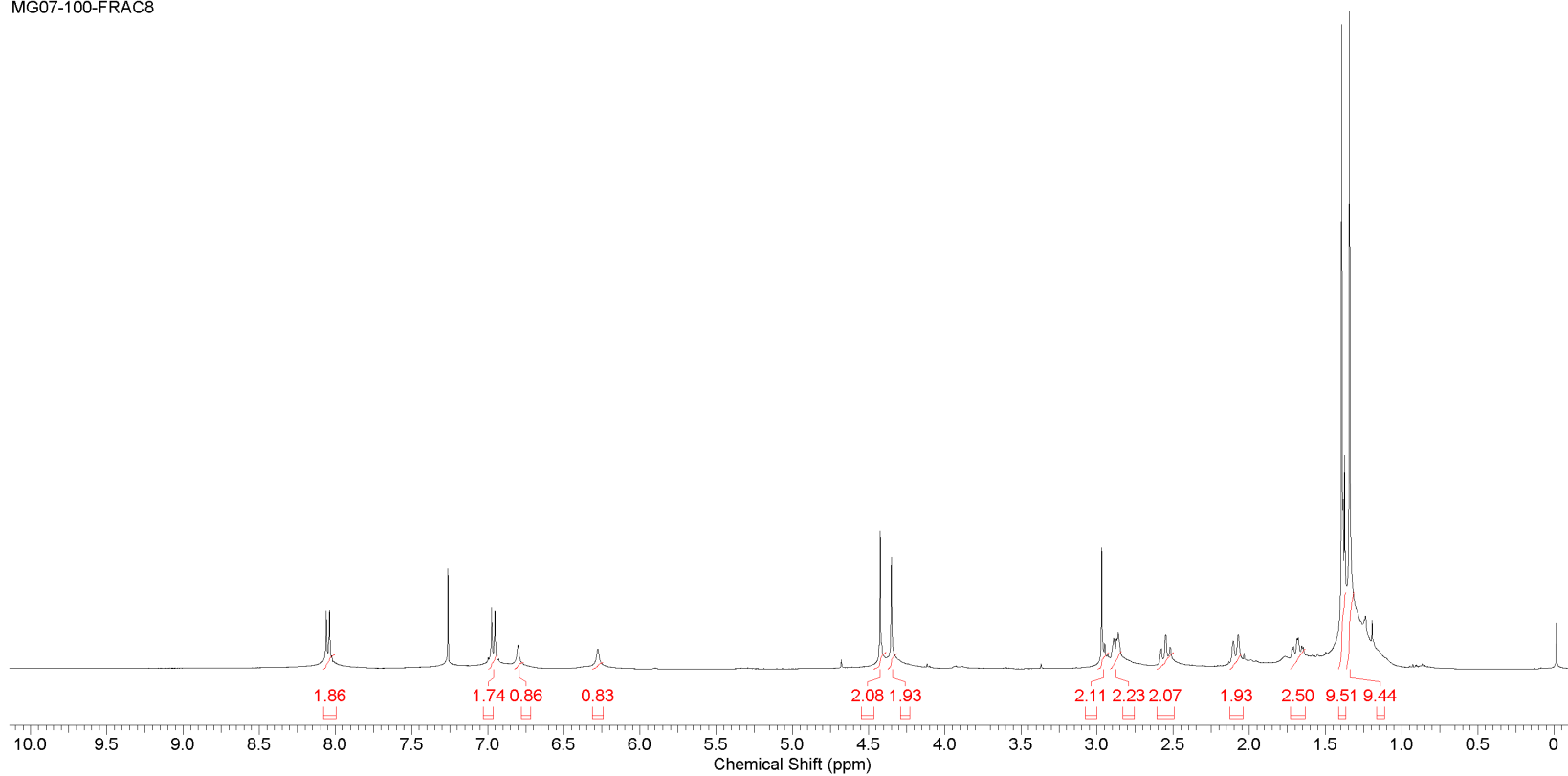
This report was created by ACD/NMR Processor Academic Edition. For more information go to www.acdlabs.com/nmrproc/

Formula $C_{26}H_{38}N_4O_5$ FW 486.6037



1-31

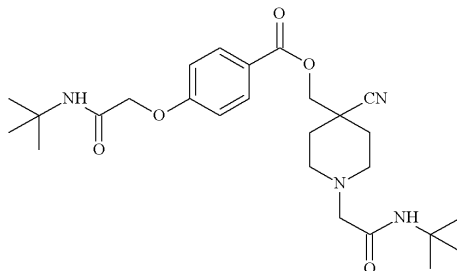
MG07-100-FRAC8



J:\NOTEBOOK7\MG07-100-FRAC8

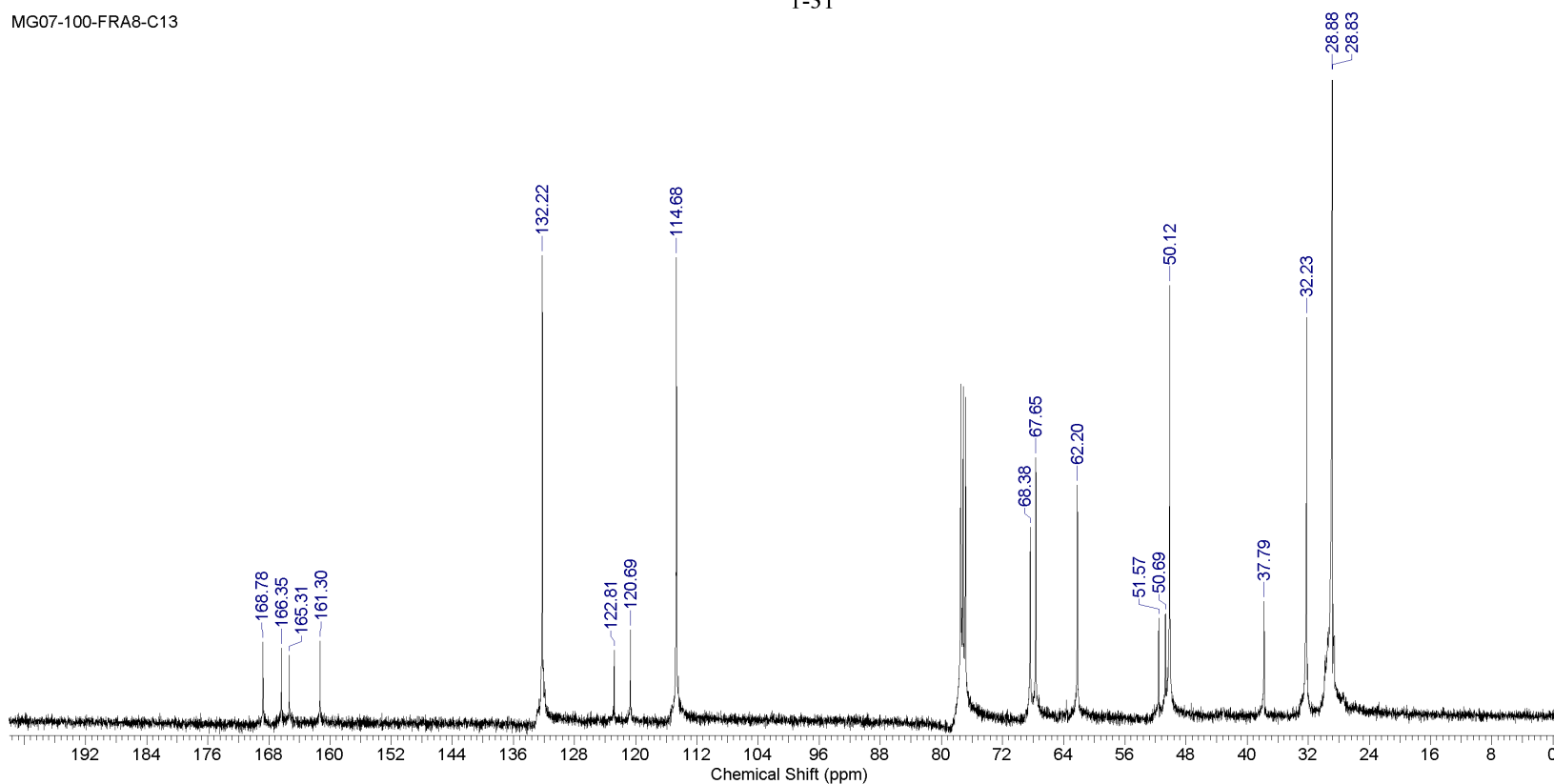
This report was created by ACD/NMR Processor Academic Edition. For more information go to www.acdlabs.com/nmrproc/

Formula C₂₆H₃₈N₄O₅ FW 486.6037



1-31

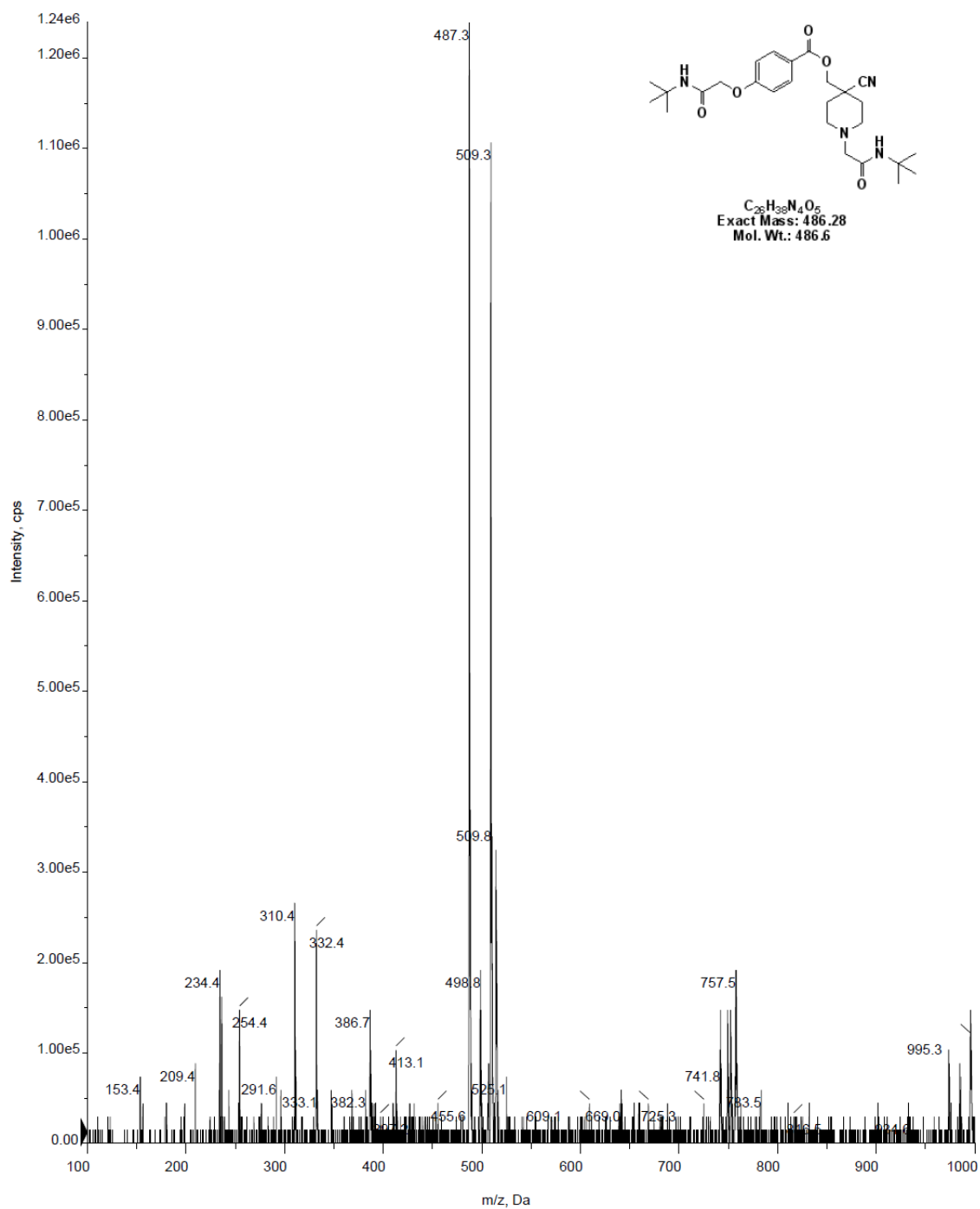
MG07-100-FRA8-C13



J:\NOTEBOOK7\MG07-100-FRA8-C13

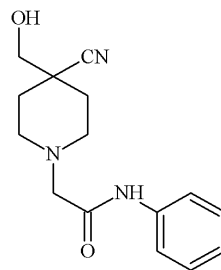
■ +Q1: 8 MCA scans from Sample 1 (TuneSampleID) of MT20150513214710.wiff (Turbo Spray)

Max. 1.2e6 cps.



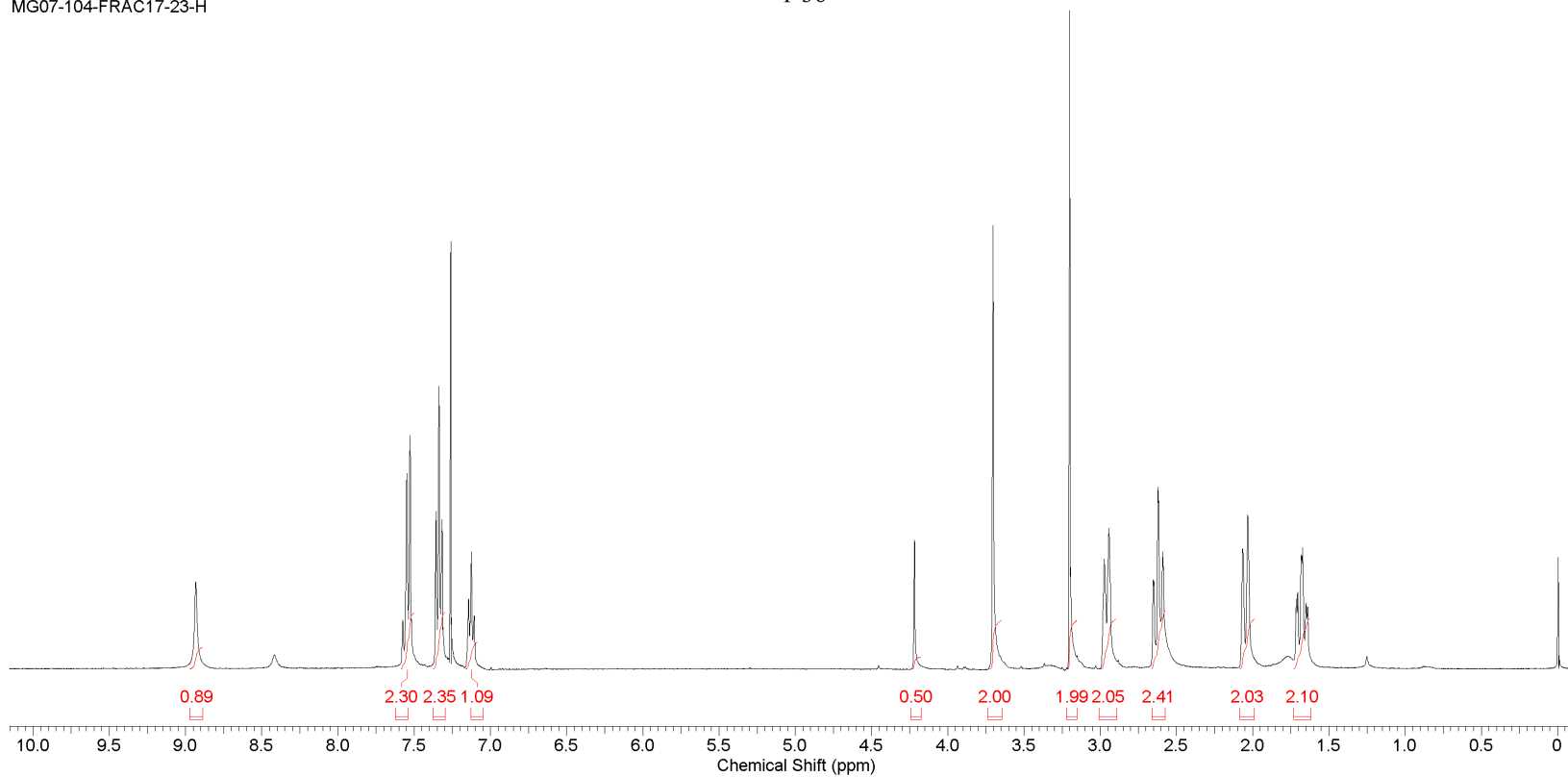
This report was created by ACD/NMR Processor Academic Edition. For more information go to www.acdlabs.com/nmrproc/

Formula C₁₅H₁₉N₃O₂ FW 273.3303



1-36

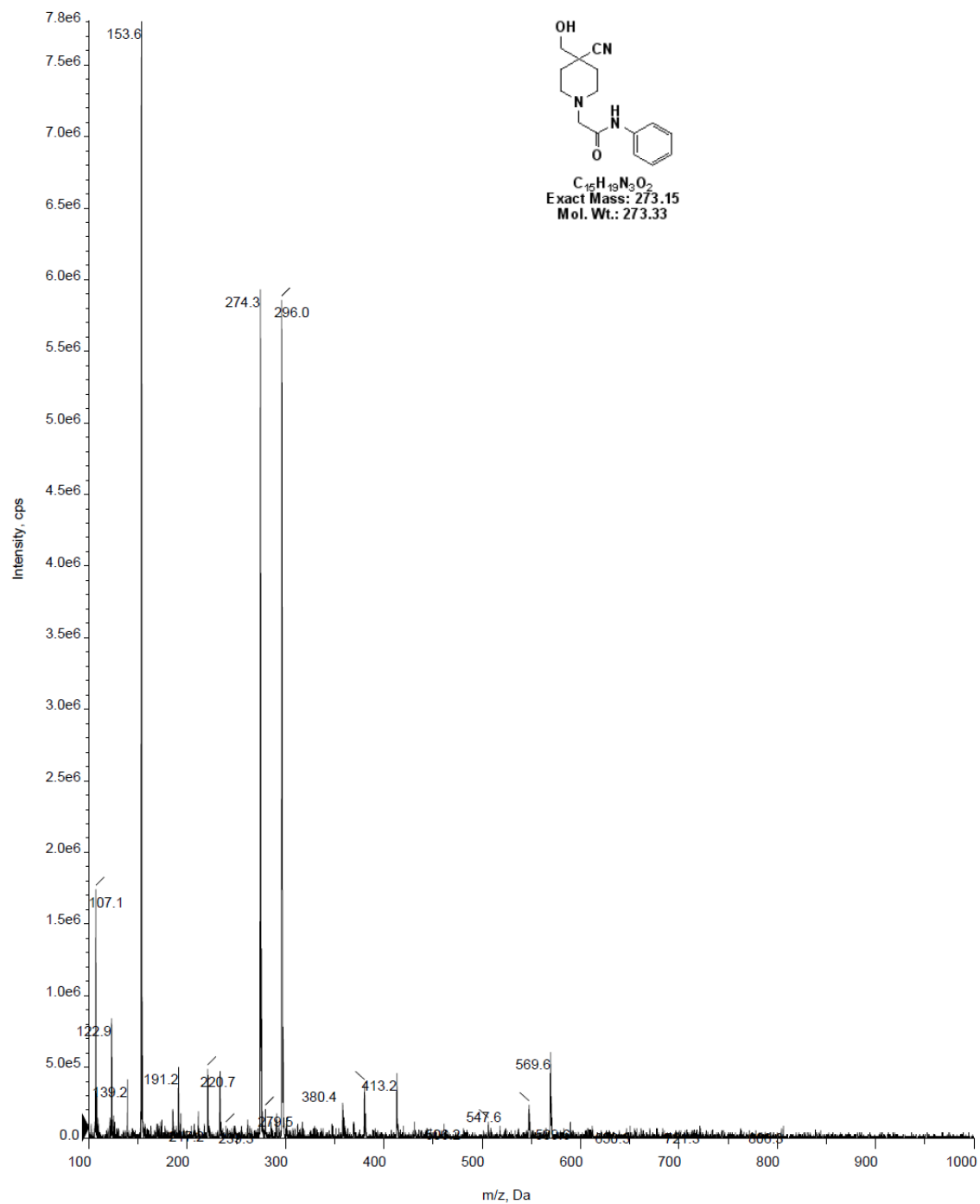
MG07-104-FRAC17-23-H



J:\NOTEBOOK7\MG07-104-FRAC17-23-H

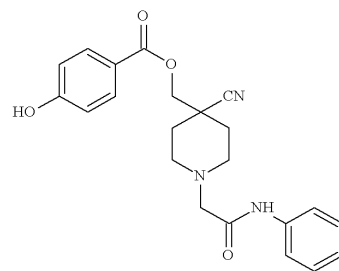
+Q1: 10 MCA scans from Sample 1 (TuneSampleID) of MT20150505162313.wiff (Turbo Spray)

Max. 7.8e6 cps.



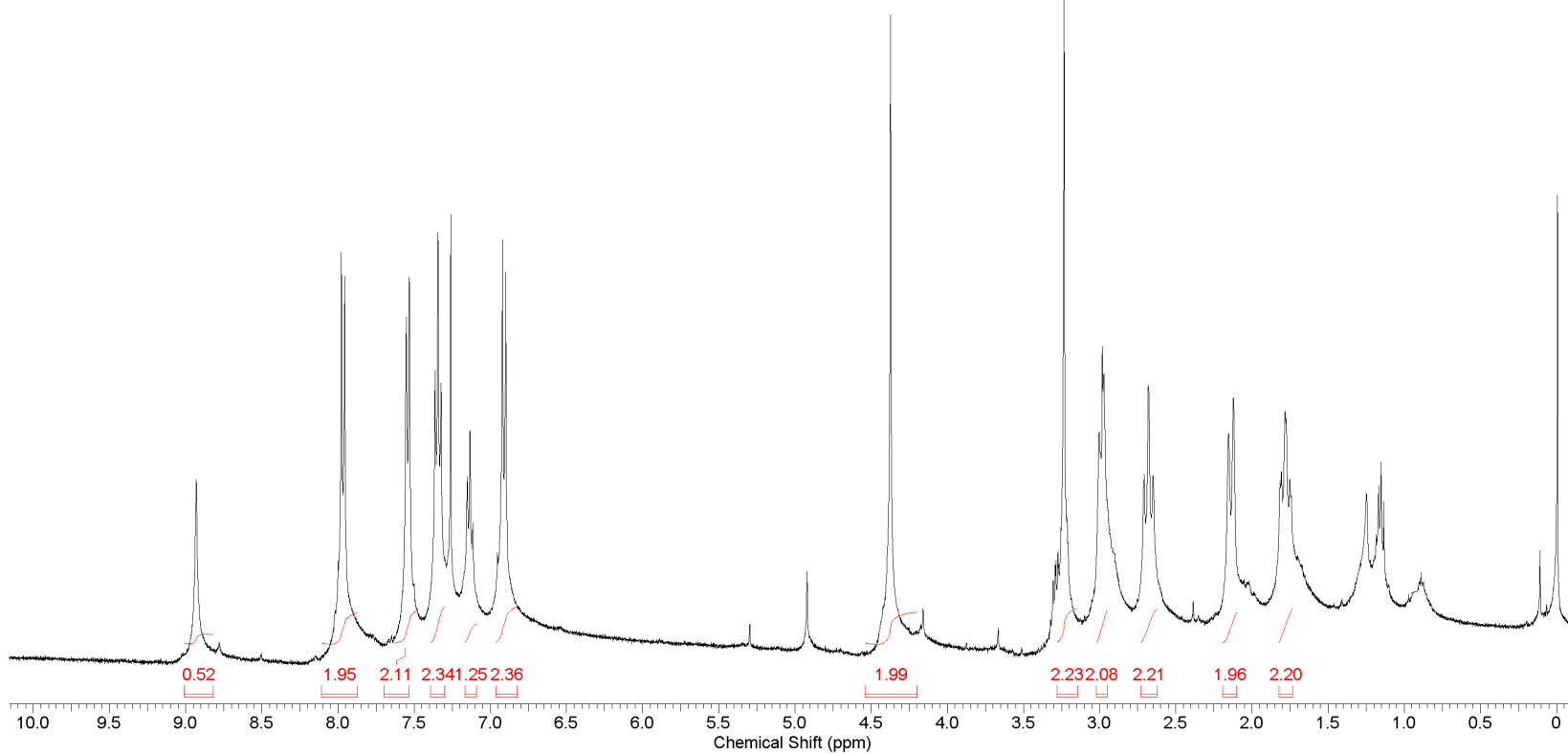
This report was created by ACD/NMR Processor Academic Edition. For more information go to www.acdlabs.com/nmrproc/

Formula C₂₂H₂₃N₃O₄ FW 393.4357



1-32

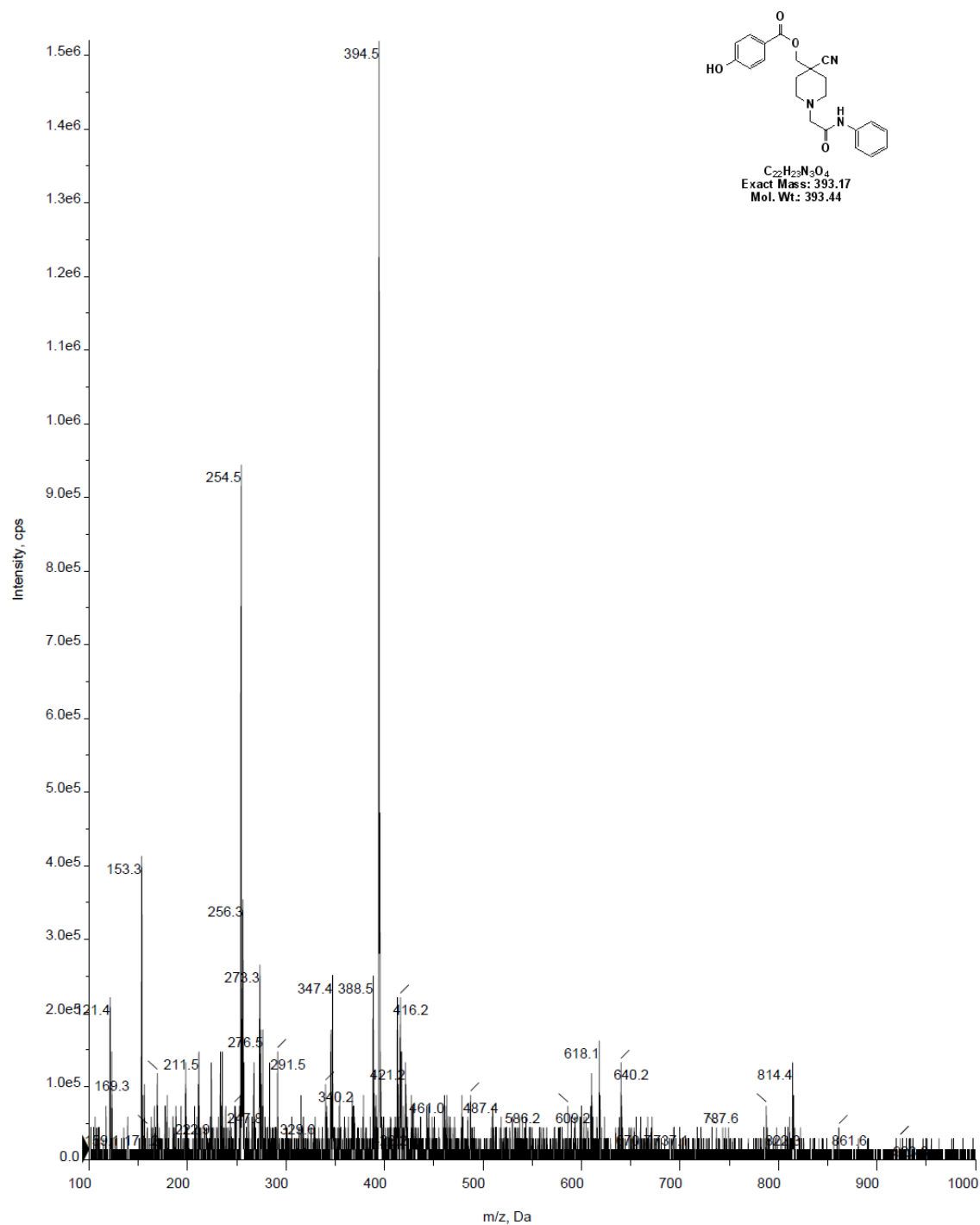
MG07-105-FRAC15-PURE

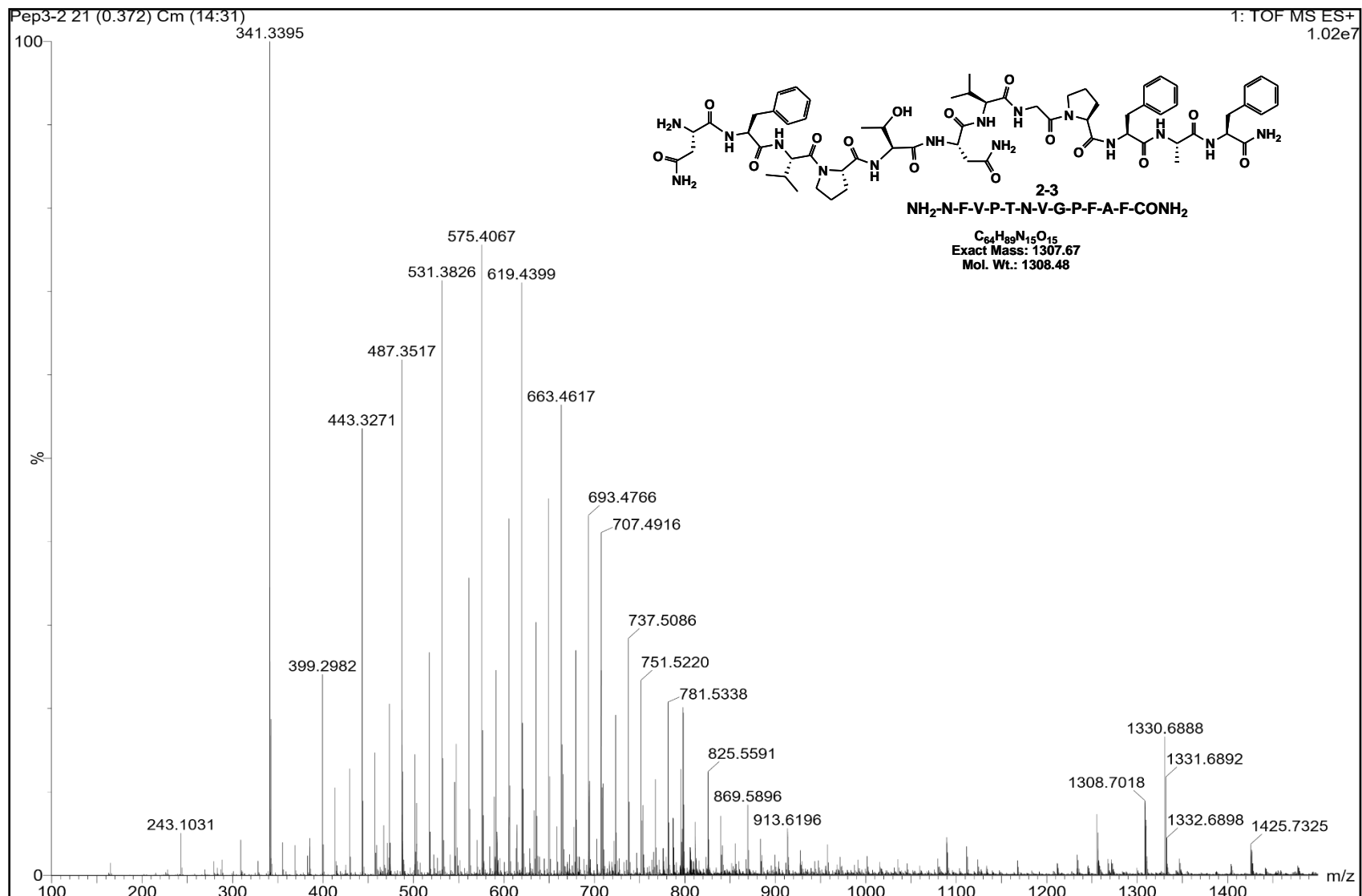


J:\PD1\NMR\MG07-105-FRAC15-PURE

+Q1: 24 MCA scans from Sample 1 (TuneSampleID) of MT20150514131715.wiff (Turbo Spray)

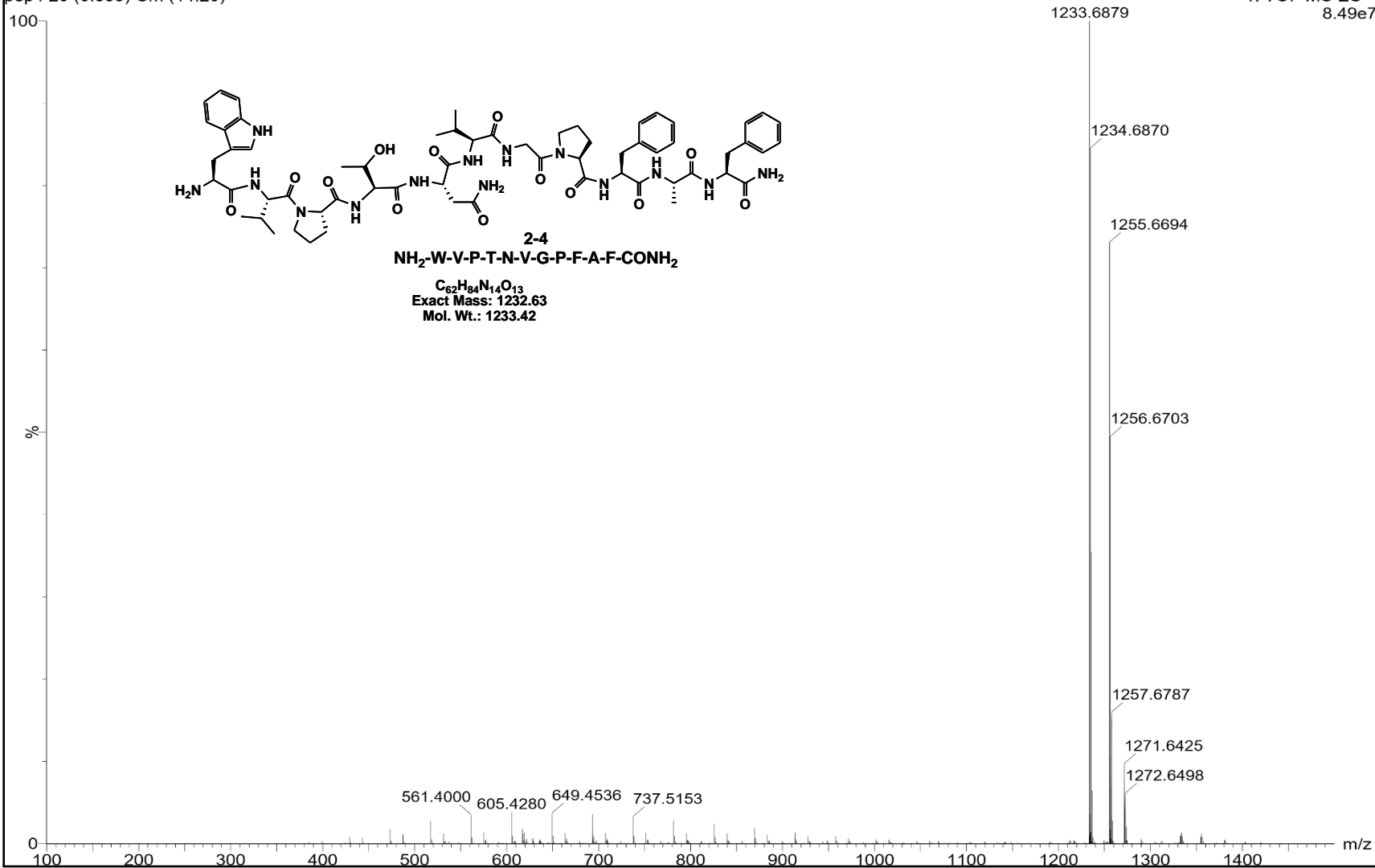
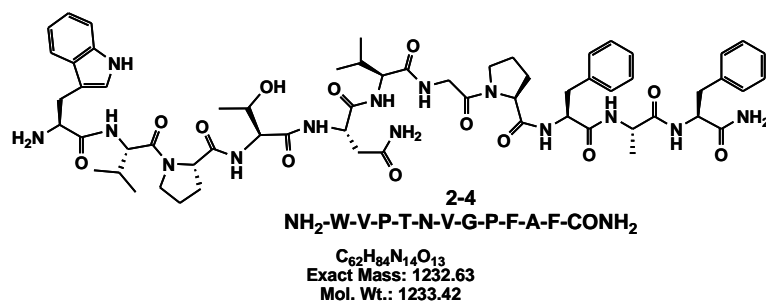
Max. 1.5e6 cps.





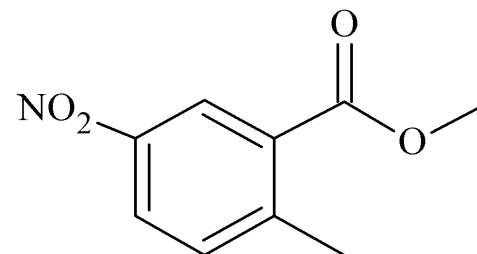
pep4 20 (0.355) Cm (14:20)

1: TOF MS ES+
8.49e7

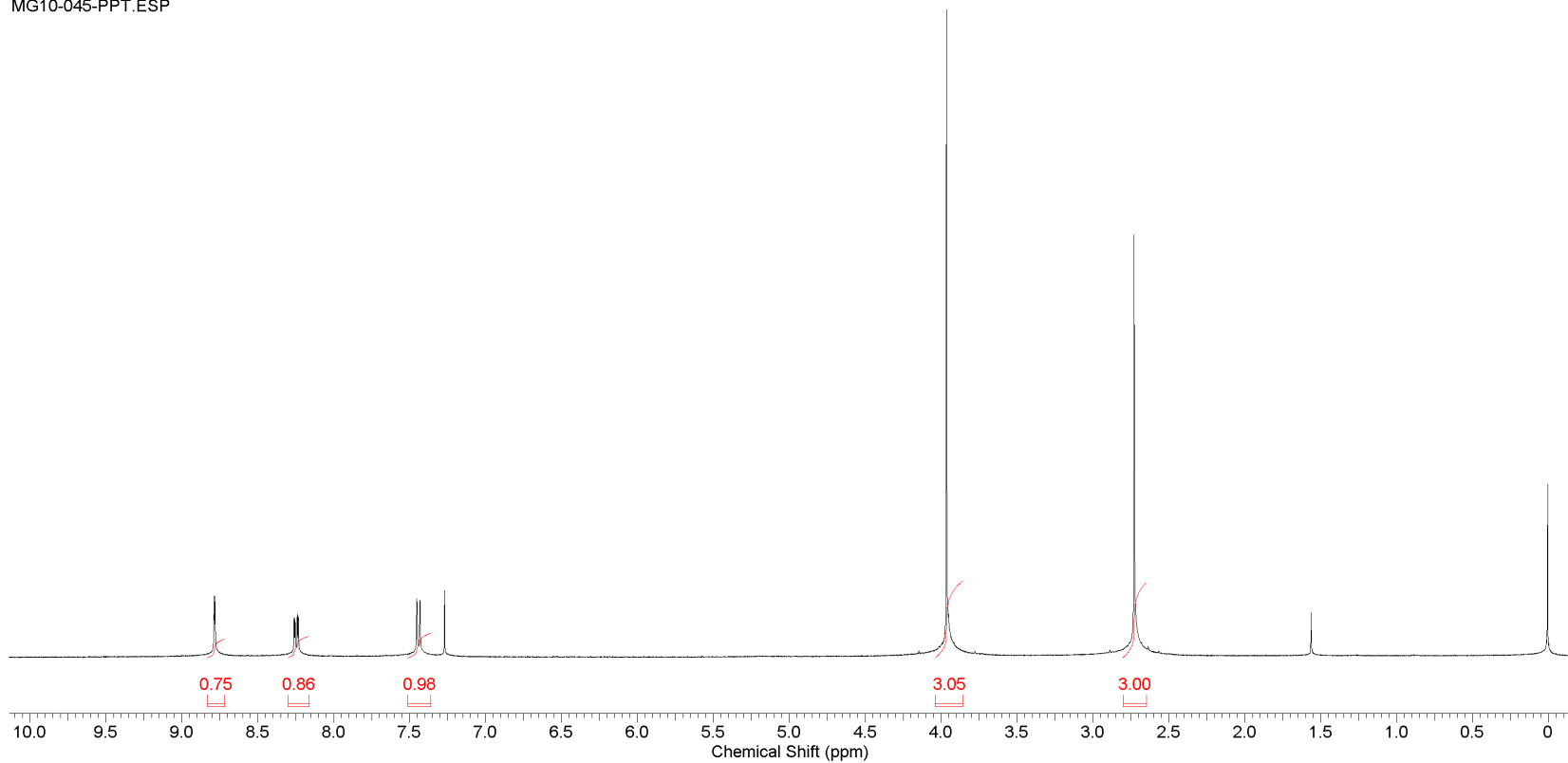


This report was created by ACD/NMR Processor Academic Edition. For more information go to www.acdlabs.com/nmrproc/

Formula C₉H₉NO₄ FW 195.1721



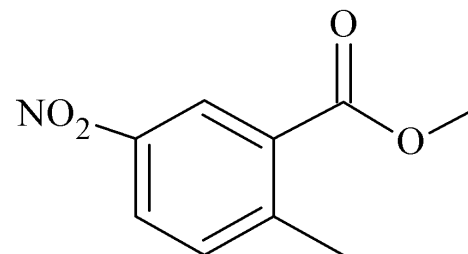
MG10-045-PPT.ESP



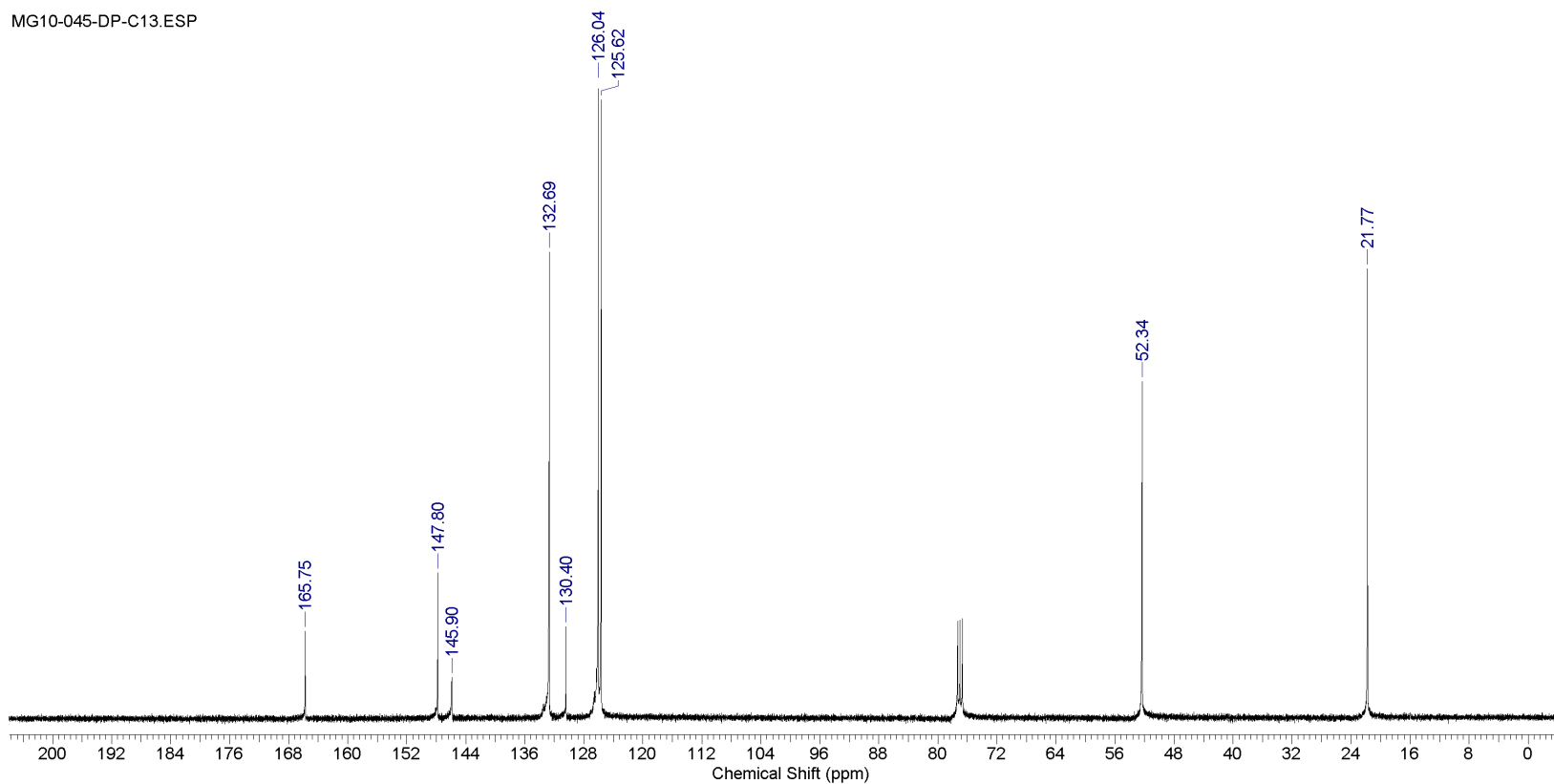
J:\JAPANESE PROJECT\NMR-MASS\JAPANESE PROJECT\COMPOUND2-METHYL 2-METHYL-5-NITROBENZOATE\MG10-045-PPT.ESP

This report was created by ACD/NMR Processor Academic Edition. For more information go to www.acdlabs.com/nmrproc/

Formula	C ₉ H ₉ NO ₄	FW	195.1721
---------	---	----	----------



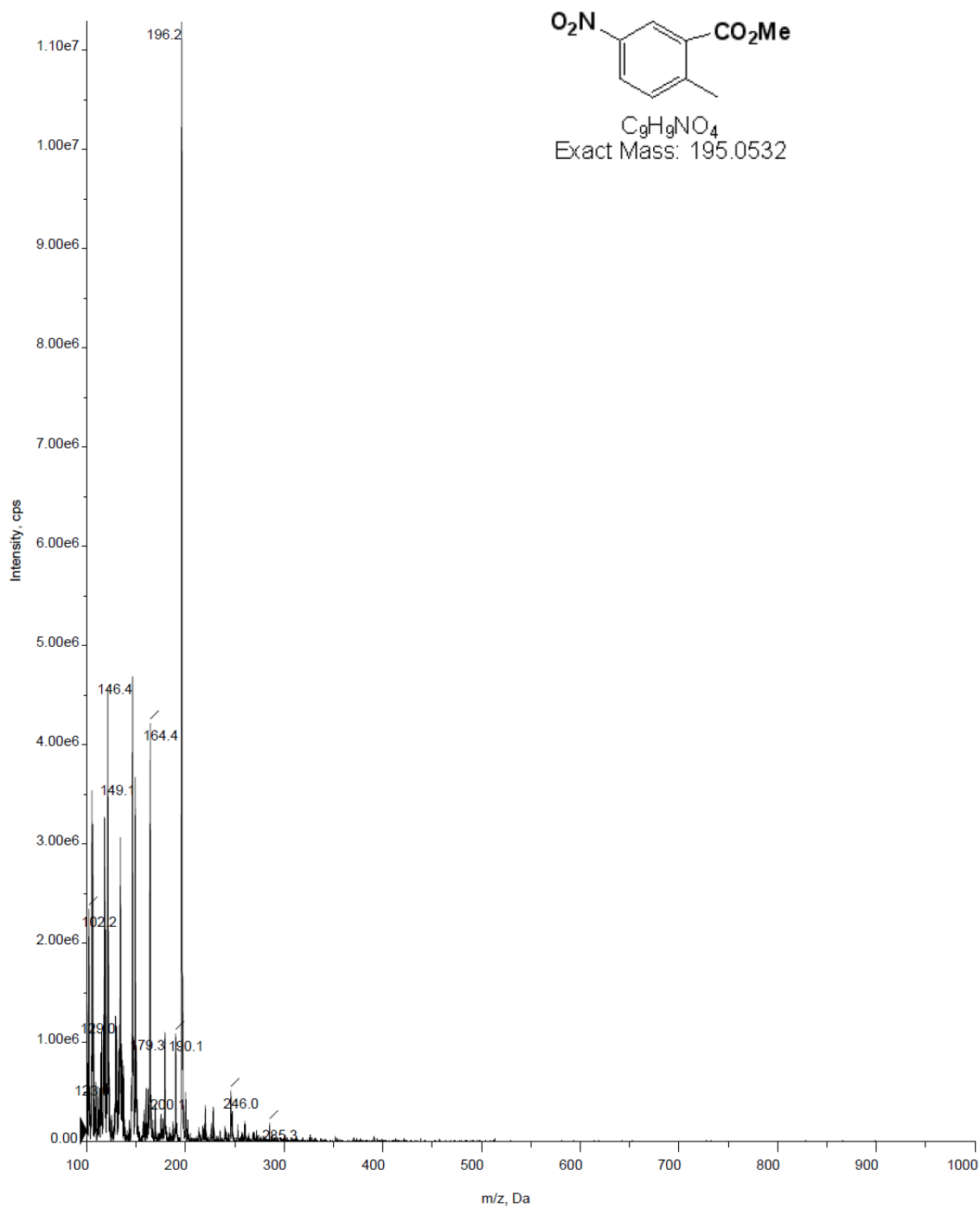
MG10-045-DP-C13.ESP



J:\JAPANESE PROJECT\NMR-MASS\JAPANESE PROJECT\COMPOUND2-METHYL 2-METHYL-5-NITROBENZOATE\MG10-045-DP-C13.ESP

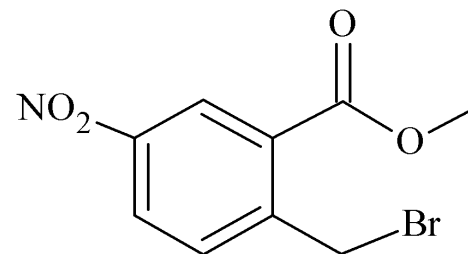
+Q1: 8 MCA scans from Sample 1 (TuneSampleID) of MT20170807142739.wiff (Turbo Spray)

Max. 1.1e7 cps.

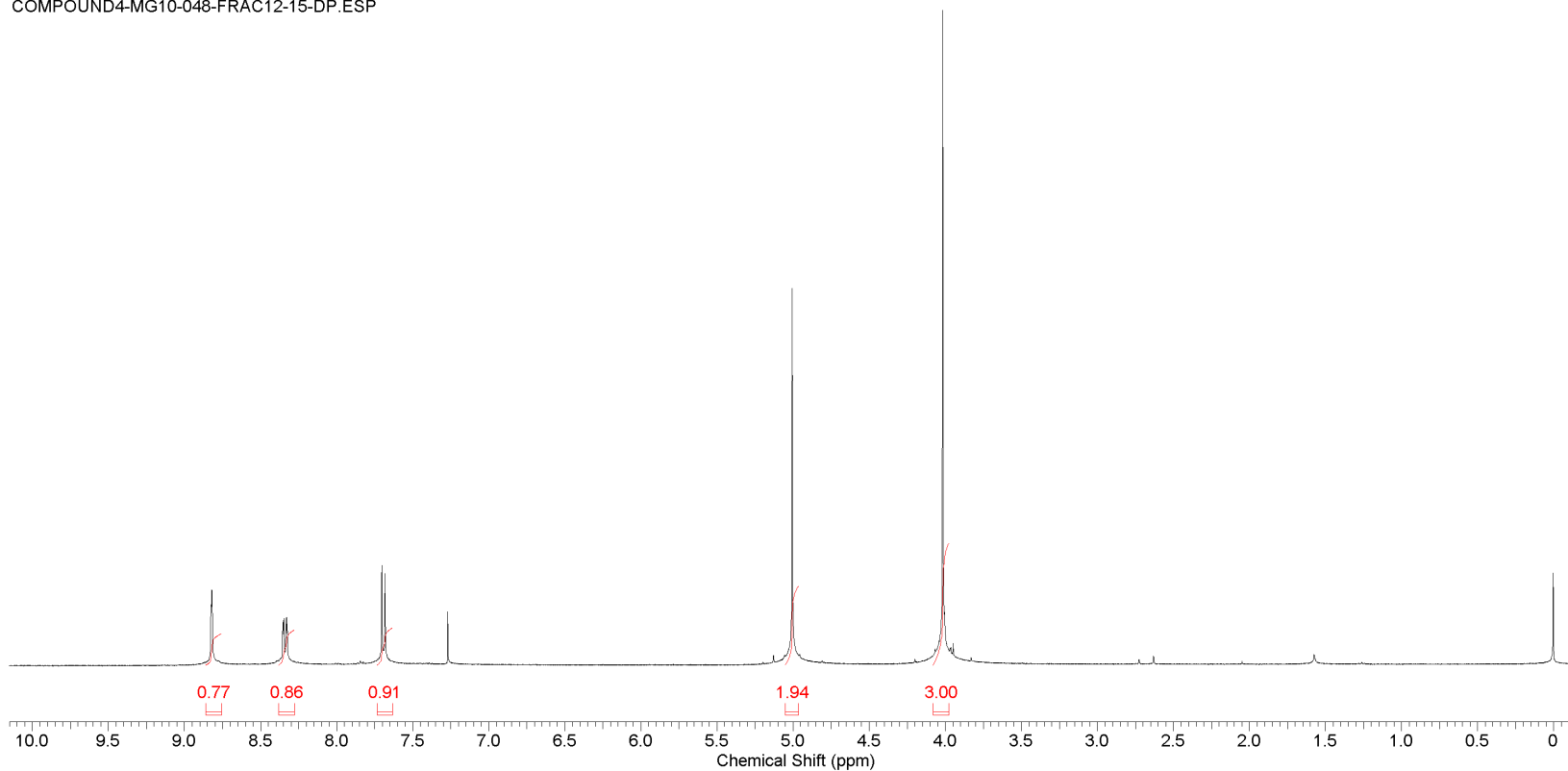


This report was created by ACD/NMR Processor Academic Edition. For more information go to www.acdlabs.com/nmrproc/

Formula C₉H₆BrNO₄ FW 274.0681



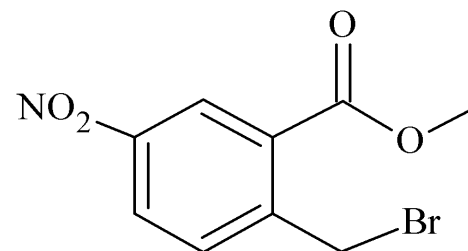
COMPOUND4-MG10-048-FRAC12-15-DP.ESP



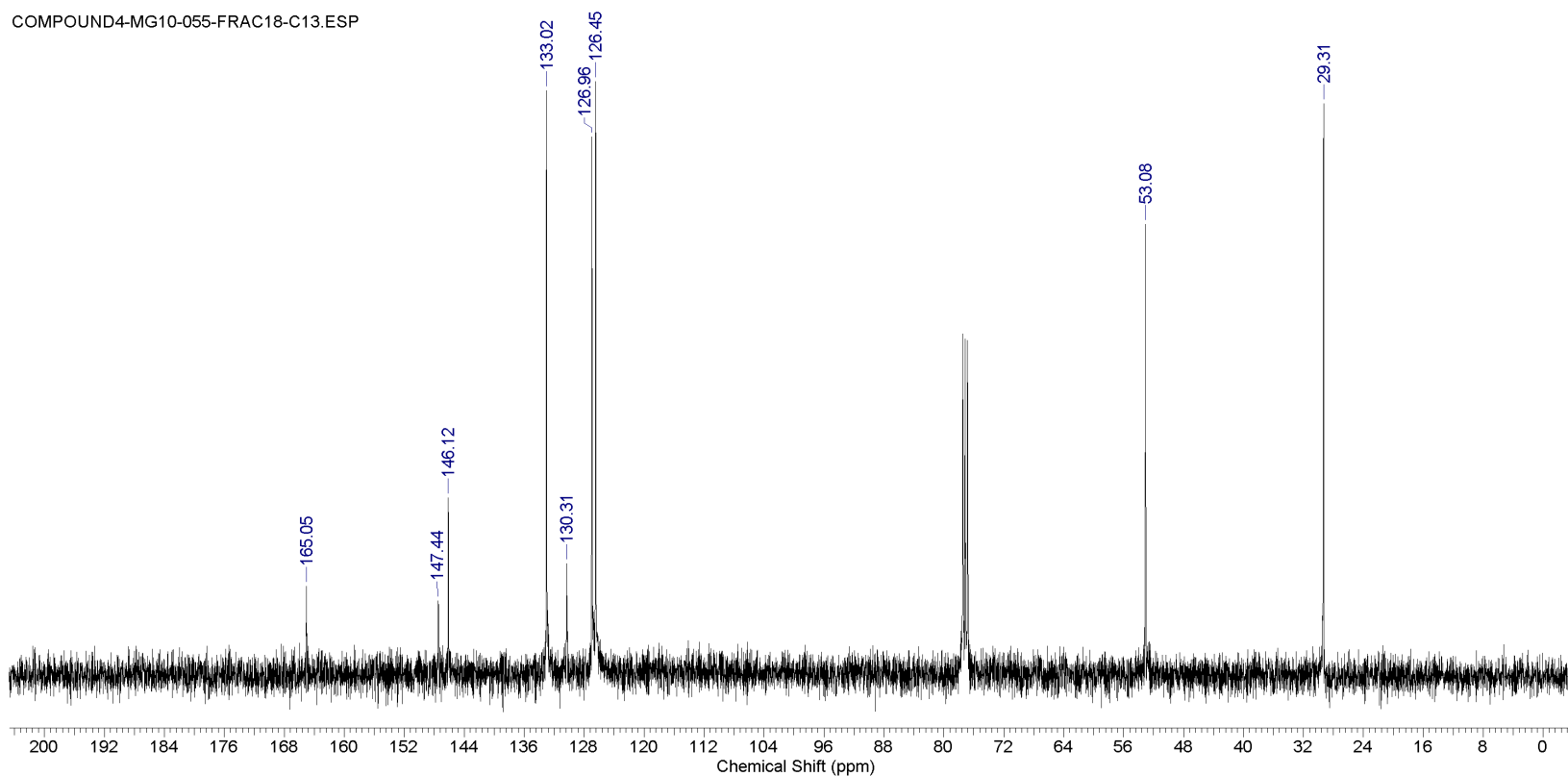
J:\JAPANESE PROJECT\NMR-MASS\JAPANESE PROJECT\COMPOUND4-METHYL 2-(BROMOMETHYL)-5-NITROBENZOATE\COMPOUND4-MG10-048-FRAC12-15-DP.ESP

This report was created by ACD/NMR Processor Academic Edition. For more information go to www.acdlabs.com/nmrproc/

Formula C₉H₈BrNO₄ FW 274.0681



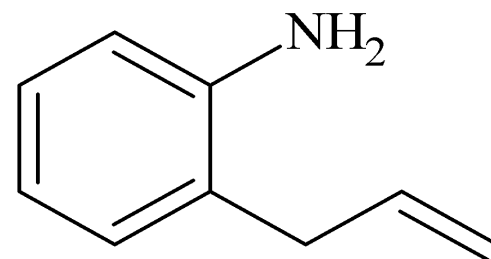
COMPOUND4-MG10-055-FRAC18-C13.ESP



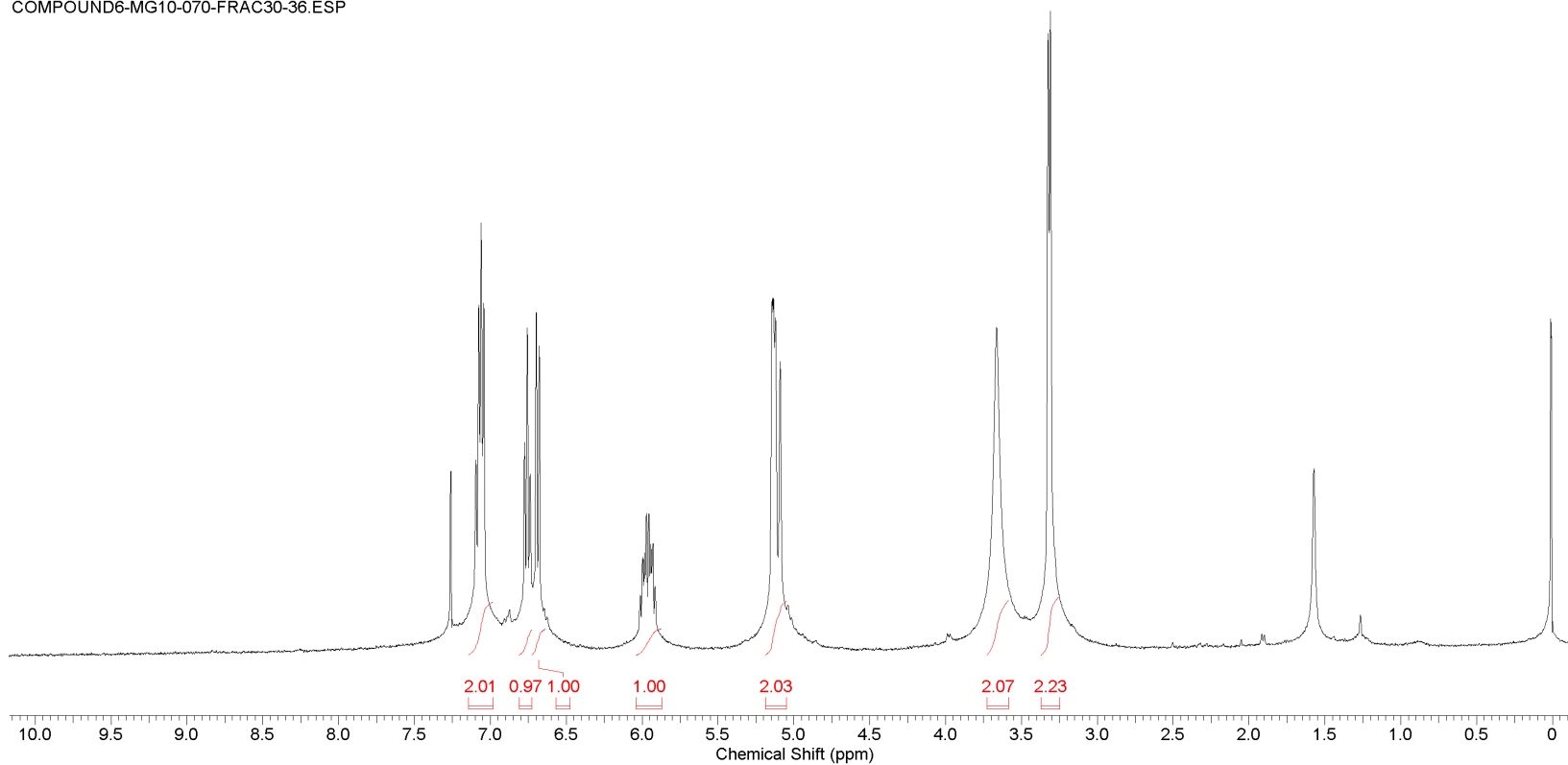
J:\JAPANESE PROJECT\NMR-MASS\JAPANESE PROJECT\COMPOUND4-METHYL 2-(BROMOMETHYL)-5-NITROBENZOATE\COMPOUND4-MG10-055-FRAC18-C13.ESP

This report was created by ACD/NMR Processor Academic Edition. For more information go to www.acdlabs.com/nmrproc/

Formula C₉H₁₁N FW 133.1903



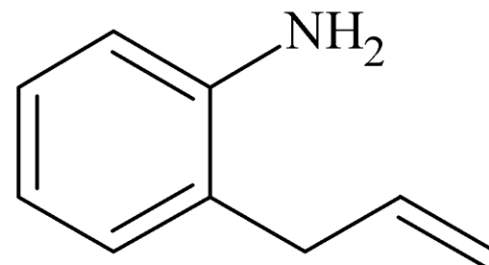
COMPOUND6-MG10-070-FRAC30-36.ESP



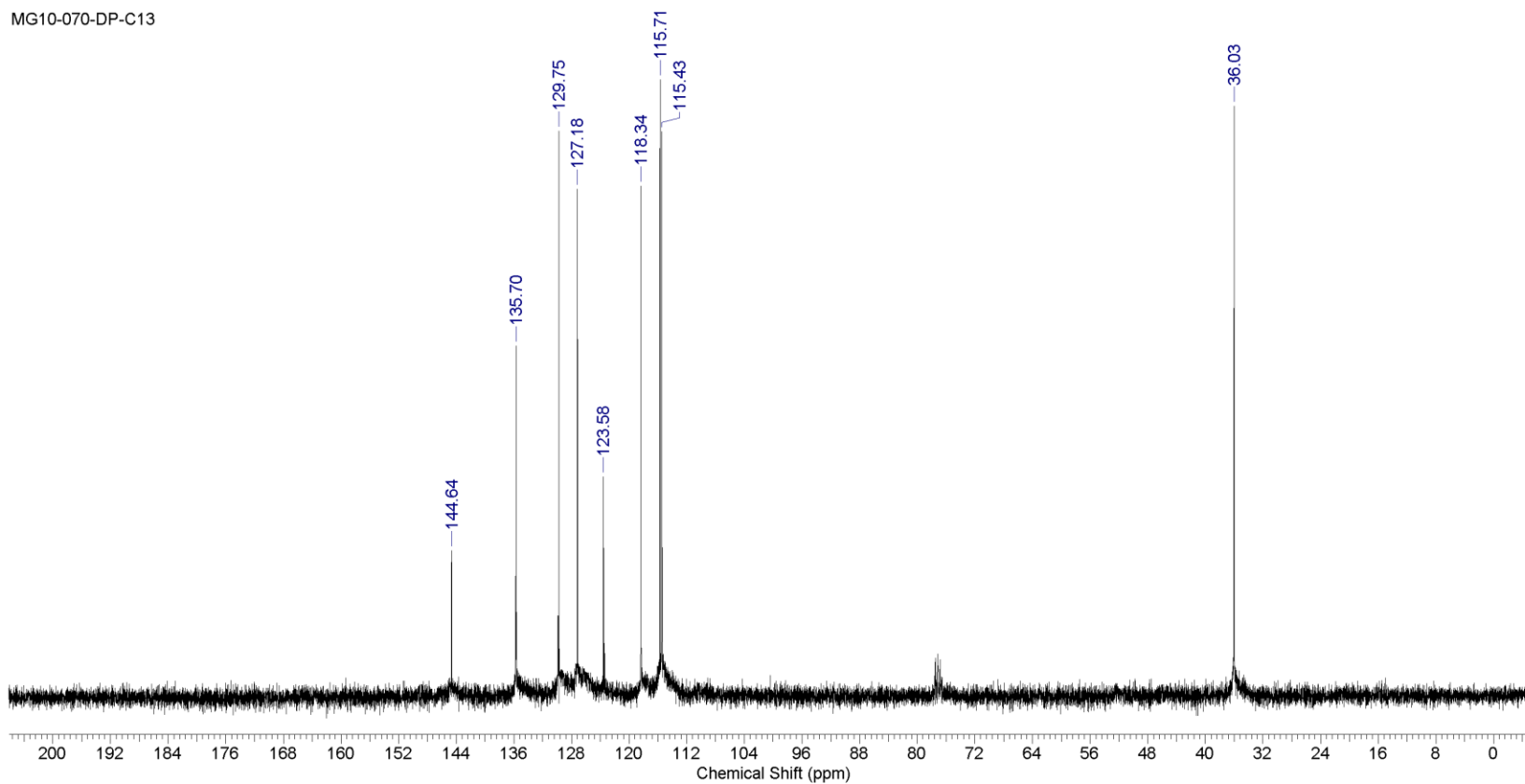
J:\JAPANESE PROJECT\NMR-MASS\JAPANESE PROJECT\COMPOUND6-2-ALLYLANILINE\COMPOUND6-MG10-070-FRAC30-36.ESP

This report was created by ACD/NMR Processor Academic Edition. For more information go to www.acdlabs.com/nmrproc/

Formula	C ₉ H ₁₁ N	FW	133.1903
---------	----------------------------------	----	----------



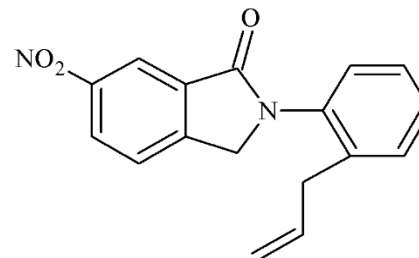
MG10-070-DP-C13



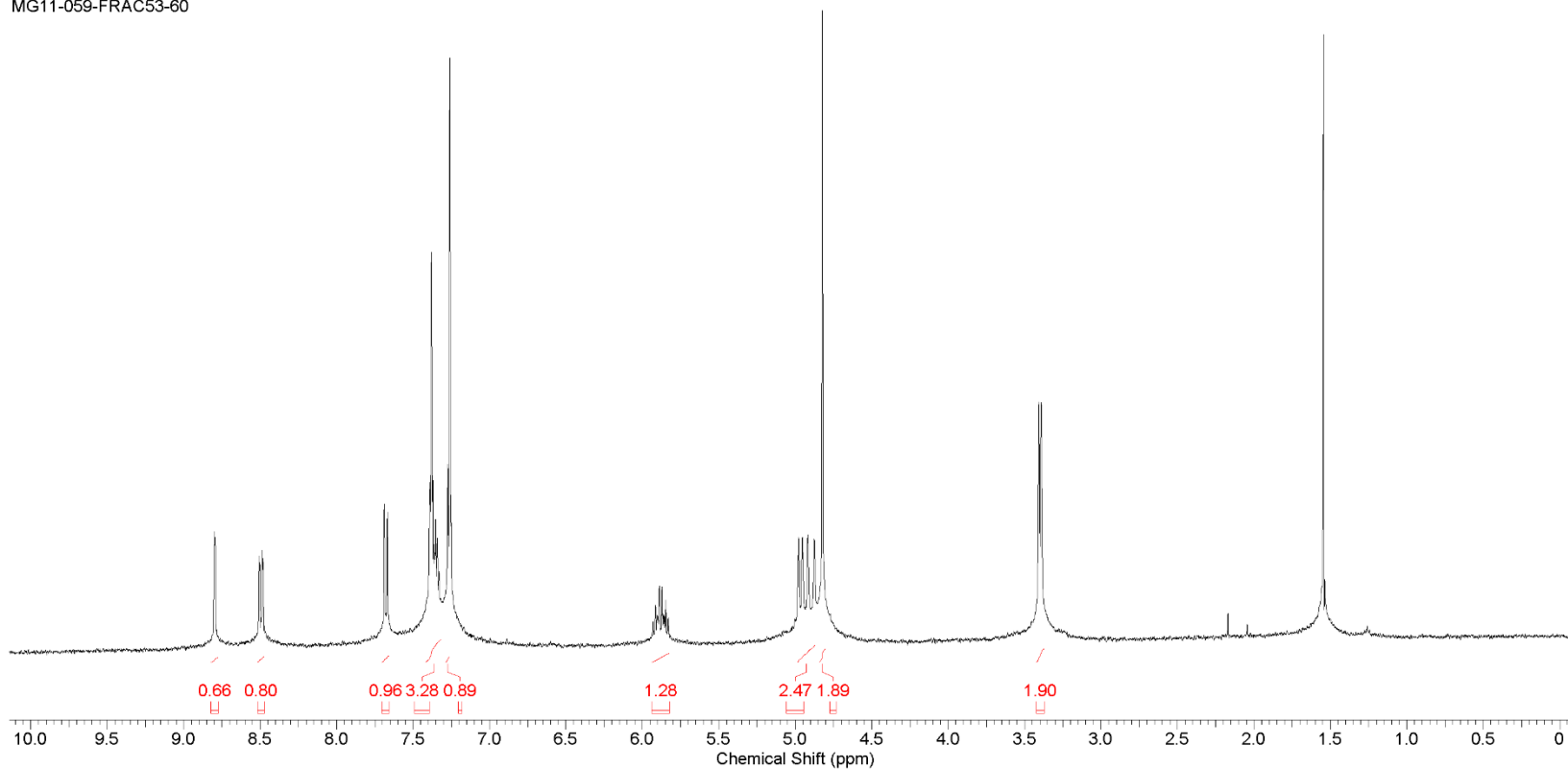
J:\JAPANESE PROJECT\NMR-MASS\JAPANESE PROJECT\COMPOUND6-2-ALLYLANILINE\MG10-070-DP-C13

This report was created by ACD/NMR Processor Academic Edition. For more information go to www.acdlabs.com/nmrproc/

Formula C₁₇H₁₄N₂O₃ FW 294.3047



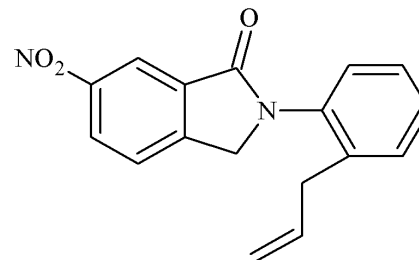
MG11-059-FRAC53-60



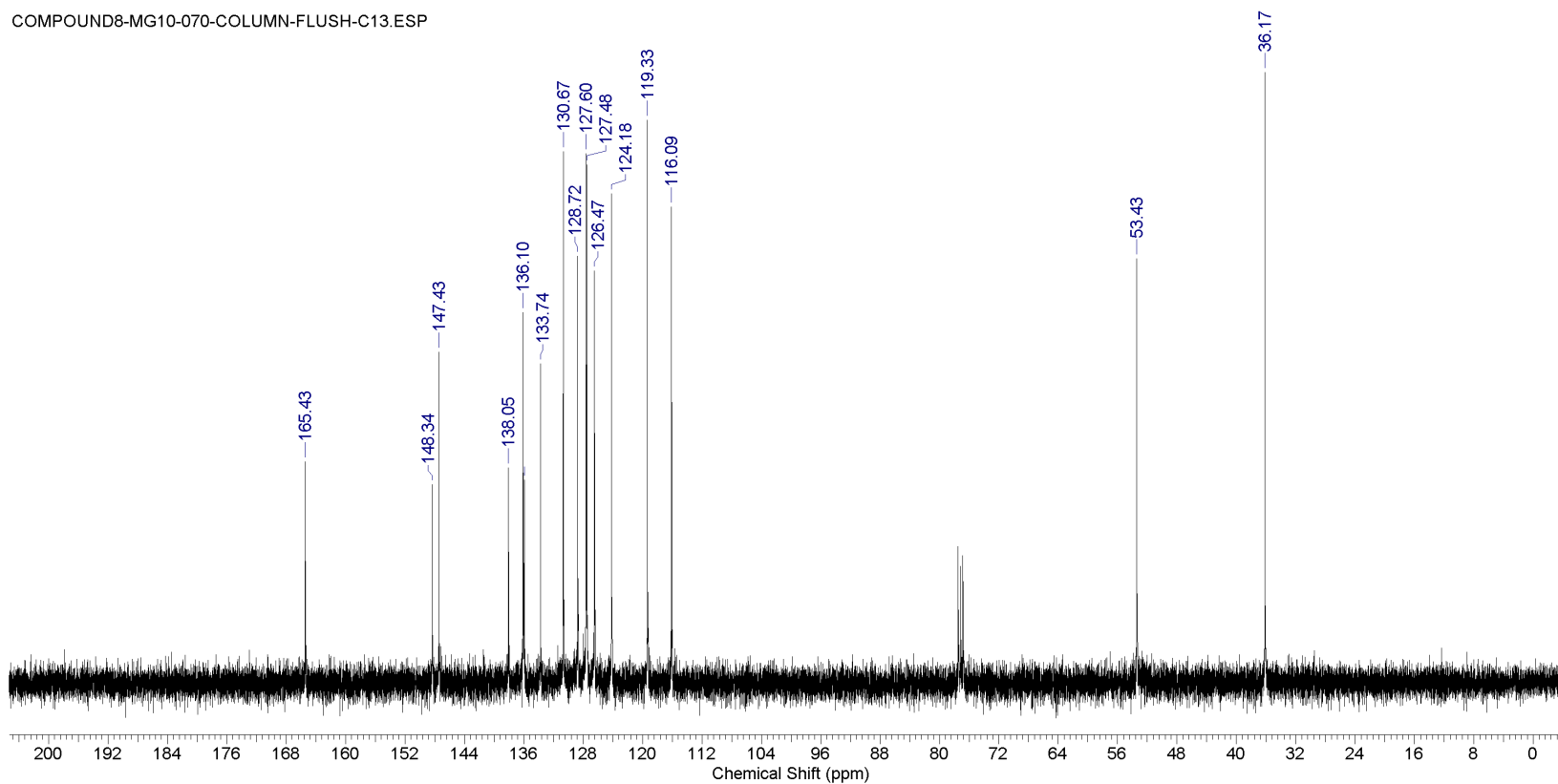
J:\JAPANESE PROJECT\NMR-MASS\JAPANESE PROJECT\COMPOUND8-2-(2-ALLYL-PHENYL)-6-NITRO-2,3-DIHYDRO-ISOINDOL-1-ONE\MG11-059-FRAC53-60

This report was created by ACD/NMR Processor Academic Edition. For more information go to www.acdlabs.com/nmrproc/

Formula C₁₇H₁₄N₂O₃ FW 294.3047



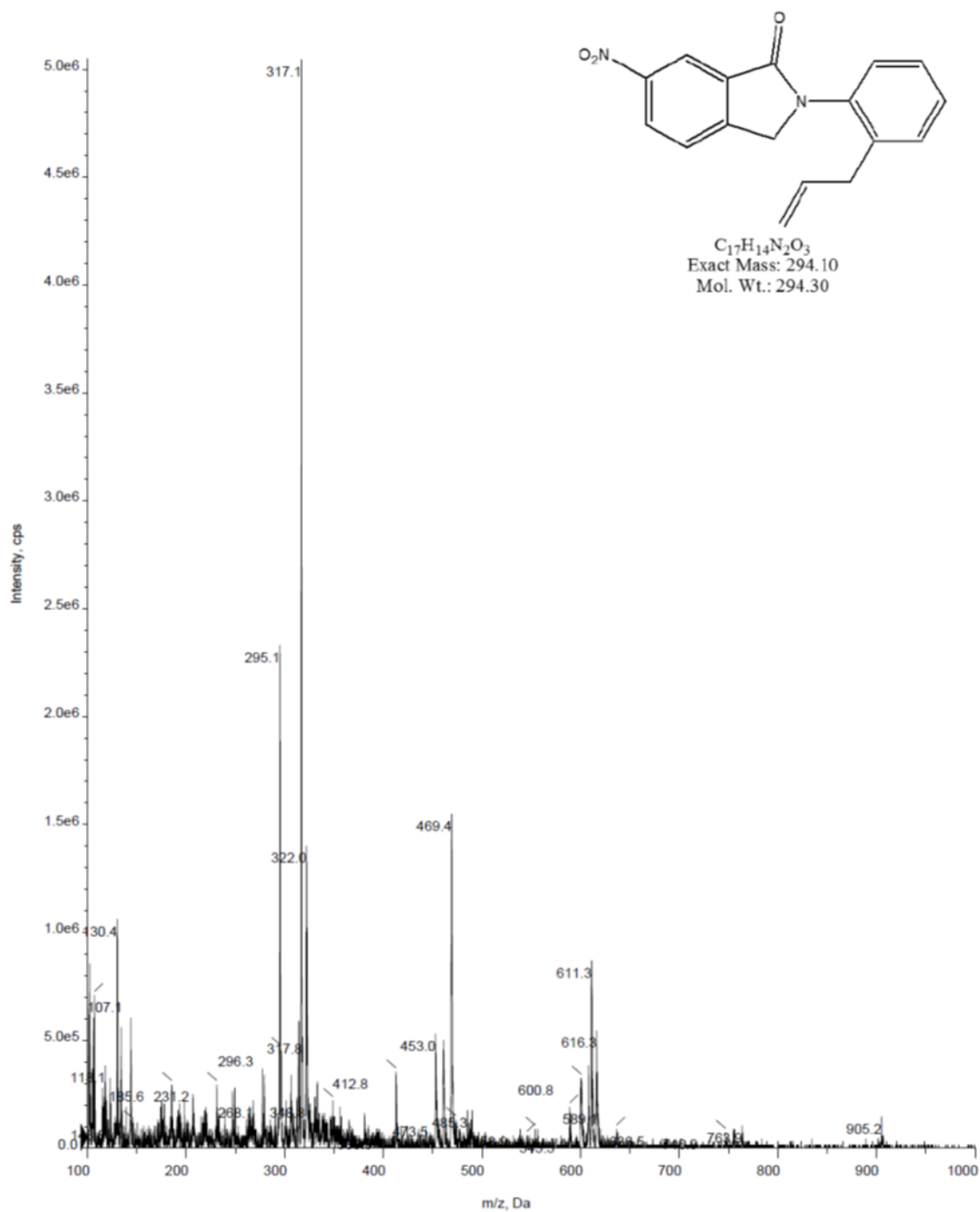
COMPOUND8-MG10-070-COLUMN-FLUSH-C13.ESP



J:\JAPANESE PROJECT\NMR-MASS\JAPANESE PROJECT\COMPOUND8-2-(2-ALLYL-PHENYL)-6-NITRO-2,3-DIHYDRO-ISOINDOL-1-ONE\COMPOUND8-MG10-070-COLUMN-FLUSH-C13.ESP

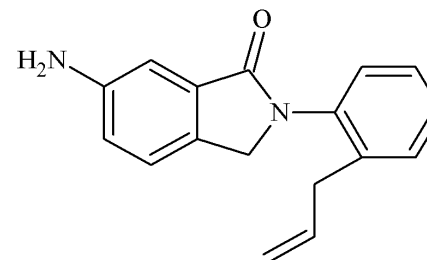
+Q1: 5 MCA scans from Sample 1 (TuneSampleID) of MT20161108101956.wiff (Turbo Spray)

Max. 5.0e6 cps.

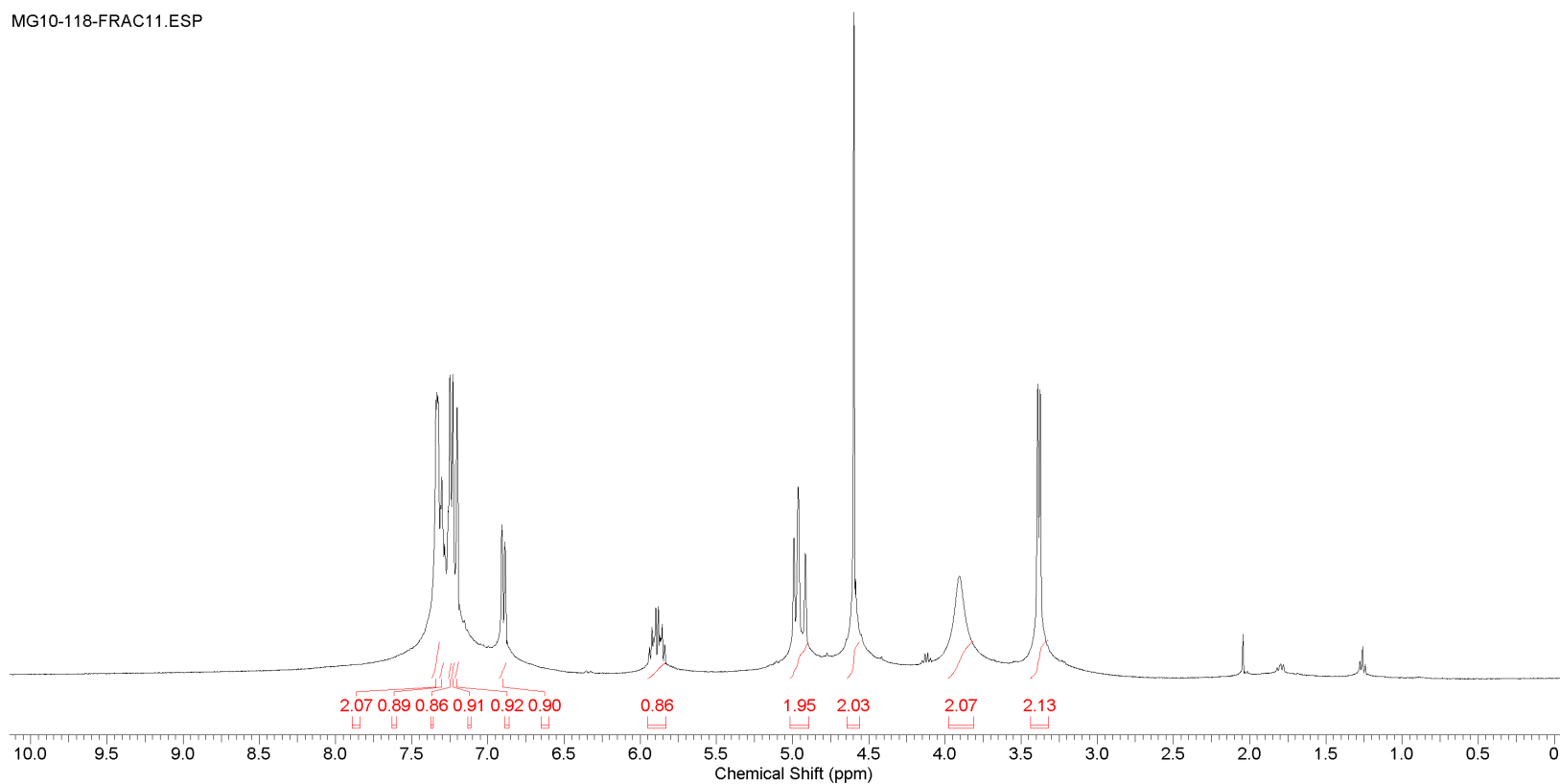


This report was created by ACD/NMR Processor Academic Edition. For more information go to www.acdlabs.com/nmrproc/

Formula C₁₇H₁₆N₂O FW 264.3217



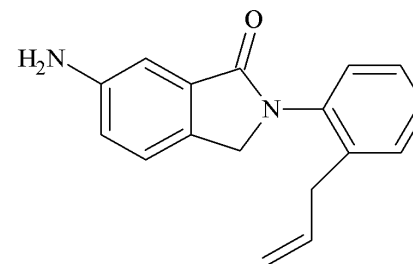
MG10-118-FRAC11.ESP



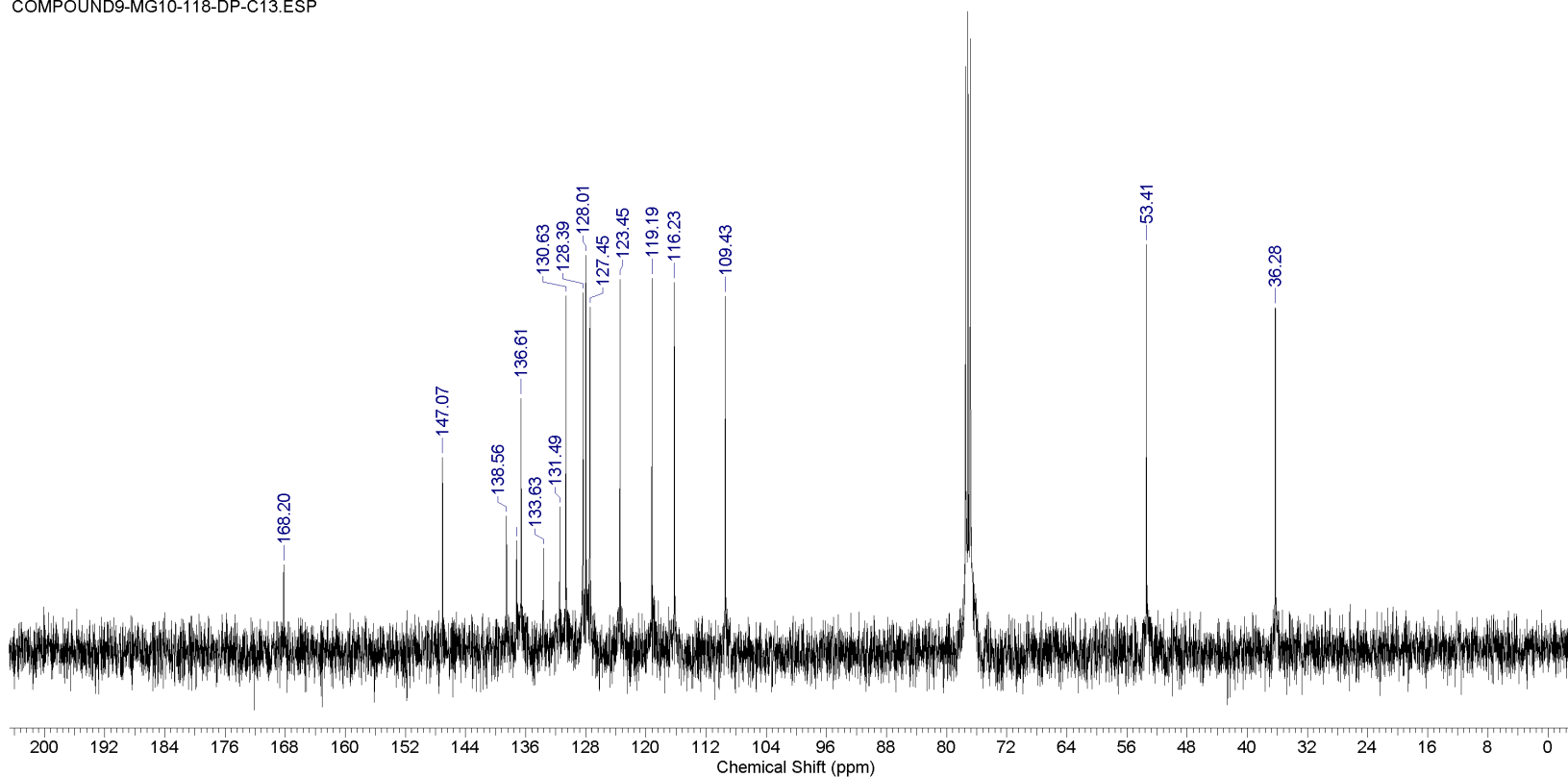
J:\JAPANESE PROJECT\NMR-MASS\JAPANESE PROJECT\COMPOUND9-2-(2-ALLYLPHENYL)-6-AMINOINDOLIN-1-ONE\MG10-118-FRAC11.ESP

This report was created by ACD/NMR Processor Academic Edition. For more information go to www.acdlabs.com/nmrproc/

Formula C₁₇H₁₆N₂O FW 264.3217



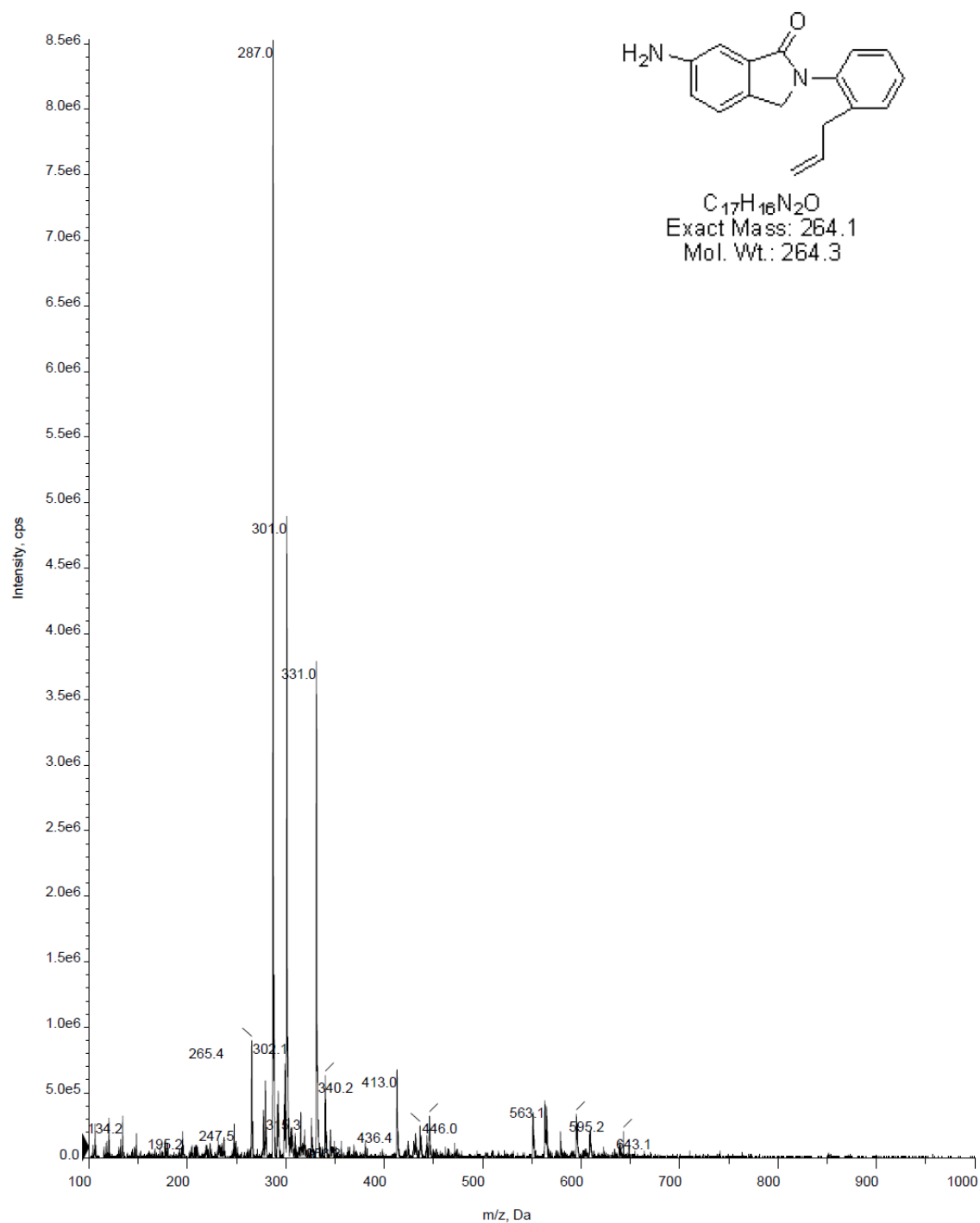
COMPOUND9-MG10-118-DP-C13.ESP



J:\JAPANESE PROJECT\NMR-MASS\JAPANESE PROJECT\COMPOUND9-2-(2-ALLYLPHENYL)-6-AMINOISOINDOLIN-1-ONE\COMPOUND9-MG10-118-DP-C13.ESP

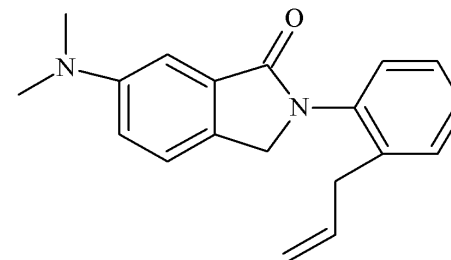
+Q1: 16 MCA scans from Sample 1 (TuneSampleID) of MT20170108124050.wiff (Turbo Spray)

Max. 8.5e6 cps.

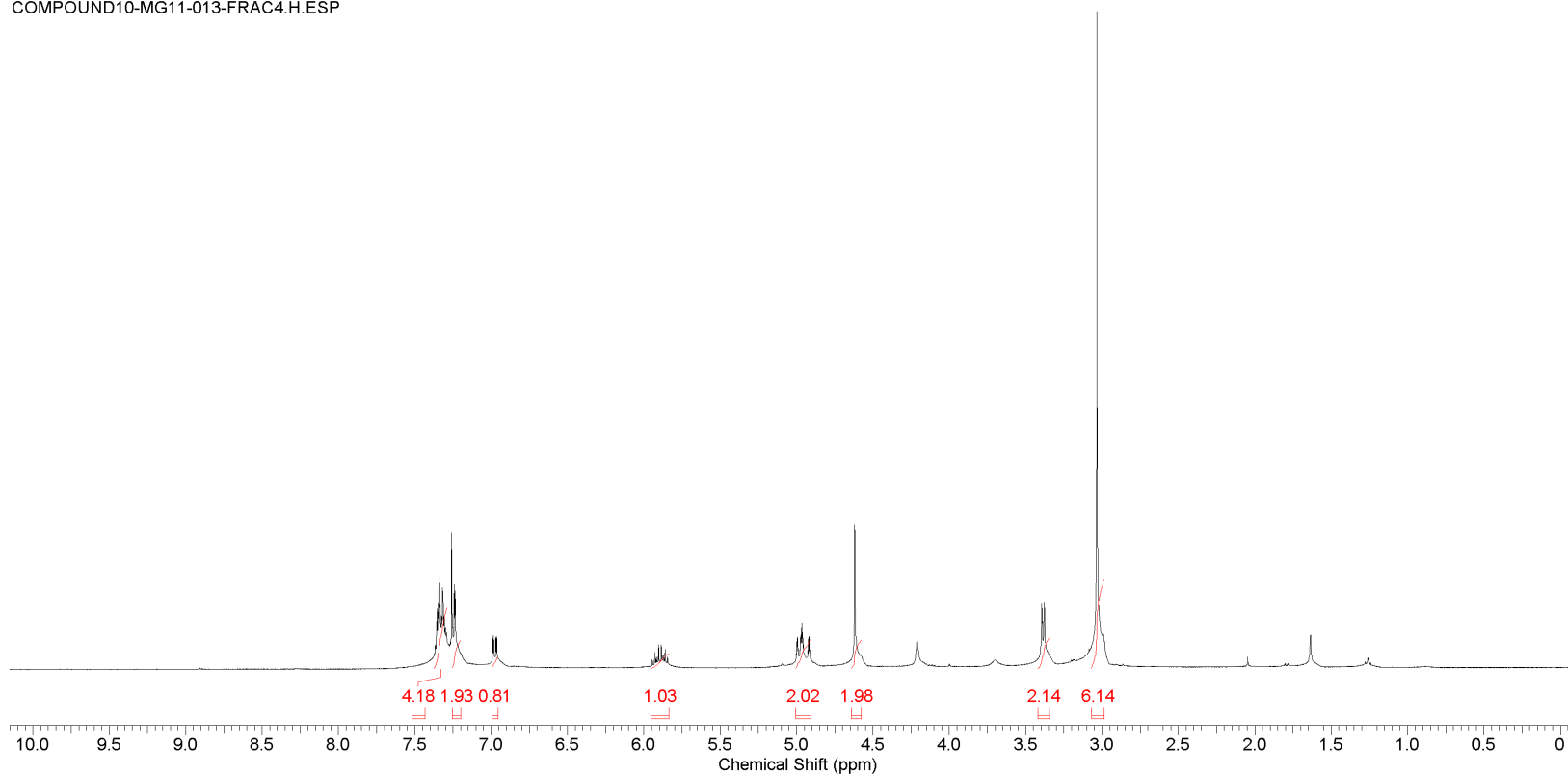


This report was created by ACD/NMR Processor Academic Edition. For more information go to www.acdlabs.com/nmrproc/

Formula C₁₉H₂₀N₂O FW 292.3749



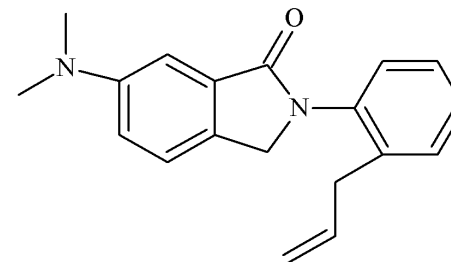
COMPOUND10-MG11-013-FRAC4.H.ESP



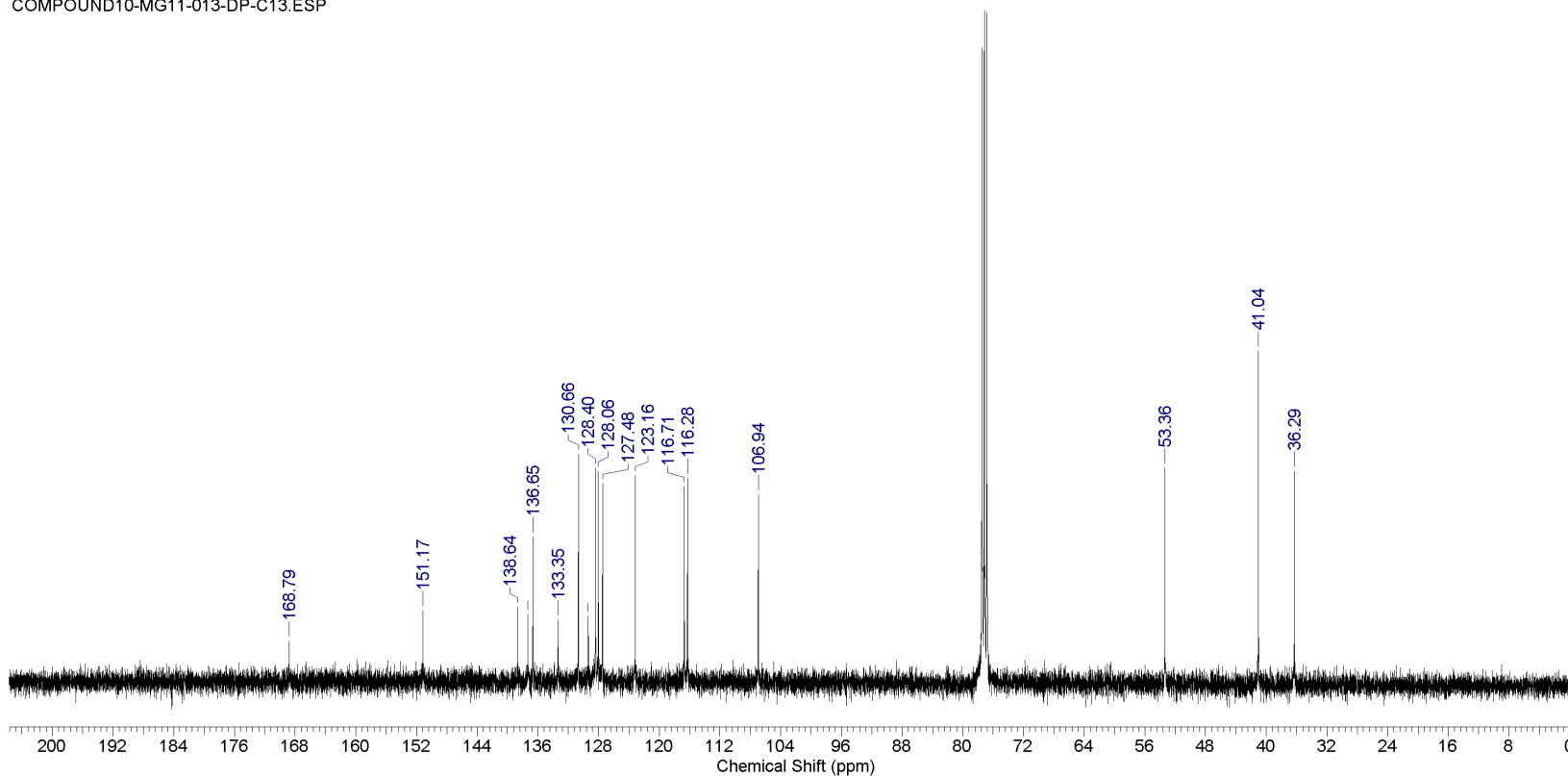
J:\JAPANESE PROJECT\NMR-MASS\JAPANESE PROJECT\COMPOUND10\COMPOUND10-MG11-013-FRAC4.H.ESP

This report was created by ACD/NMR Processor Academic Edition. For more information go to www.acdlabs.com/nmrproc/

Formula C₁₉H₂₀N₂O FW 292.3749



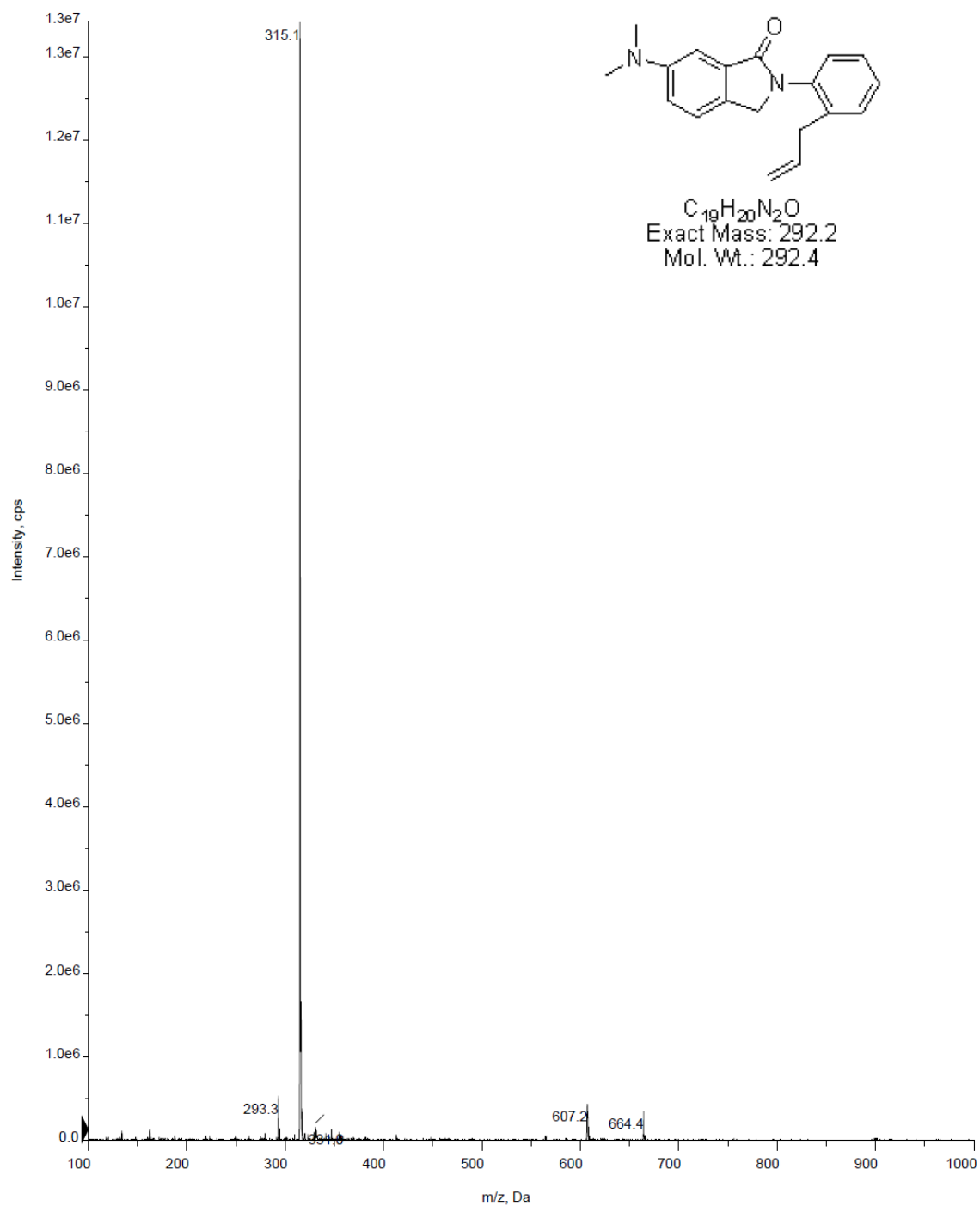
COMPOUND10-MG11-013-DP-C13.ESP



J:\JAPANESE PROJECT\NMR-MASS\JAPANESE PROJECT\COMPOUND10\COMPOUND10-MG11-013-DP-C13.ESP

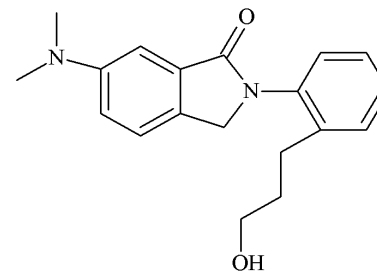
■ +Q1: 4 MCA scans from Sample 1 (TuneSampleID) of MT20170108113929.wiff (Turbo Spray)

Max. 1.3e7 cps.

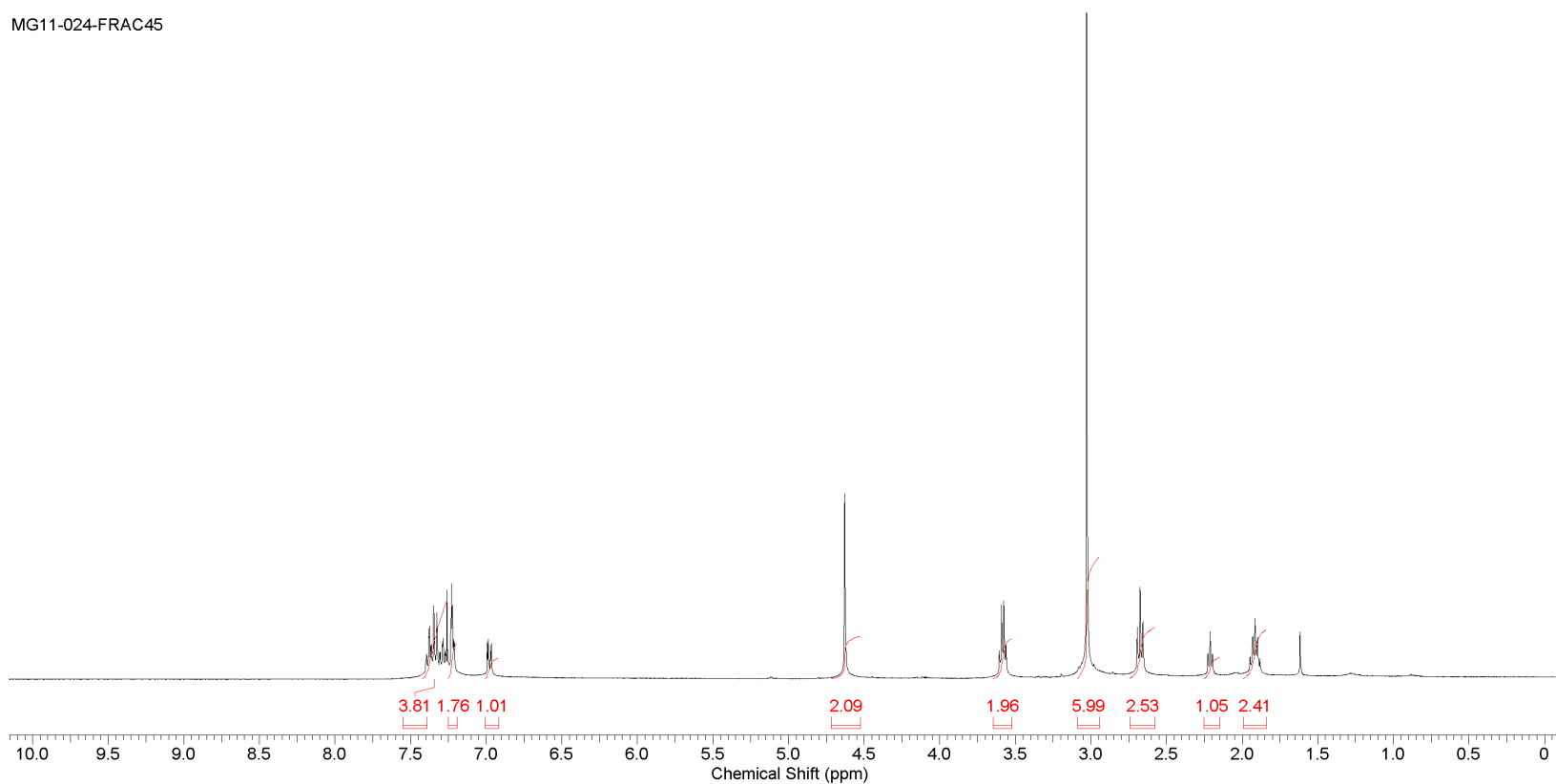


This report was created by ACD/NMR Processor Academic Edition. For more information go to www.acdlabs.com/nmrproc/

Formula C₁₉H₂₂N₂O₂ FW 310.3902

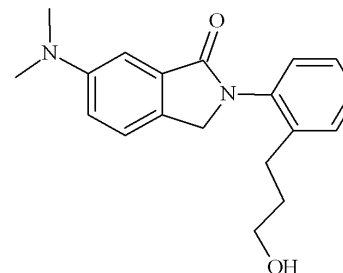


MG11-024-FRAC45



I:\NOTEBOOK11\MG11-024-FRAC45

Formula C ₁₉ H ₂₂ N ₂ O ₂	FW 310.3902
--	--------------------

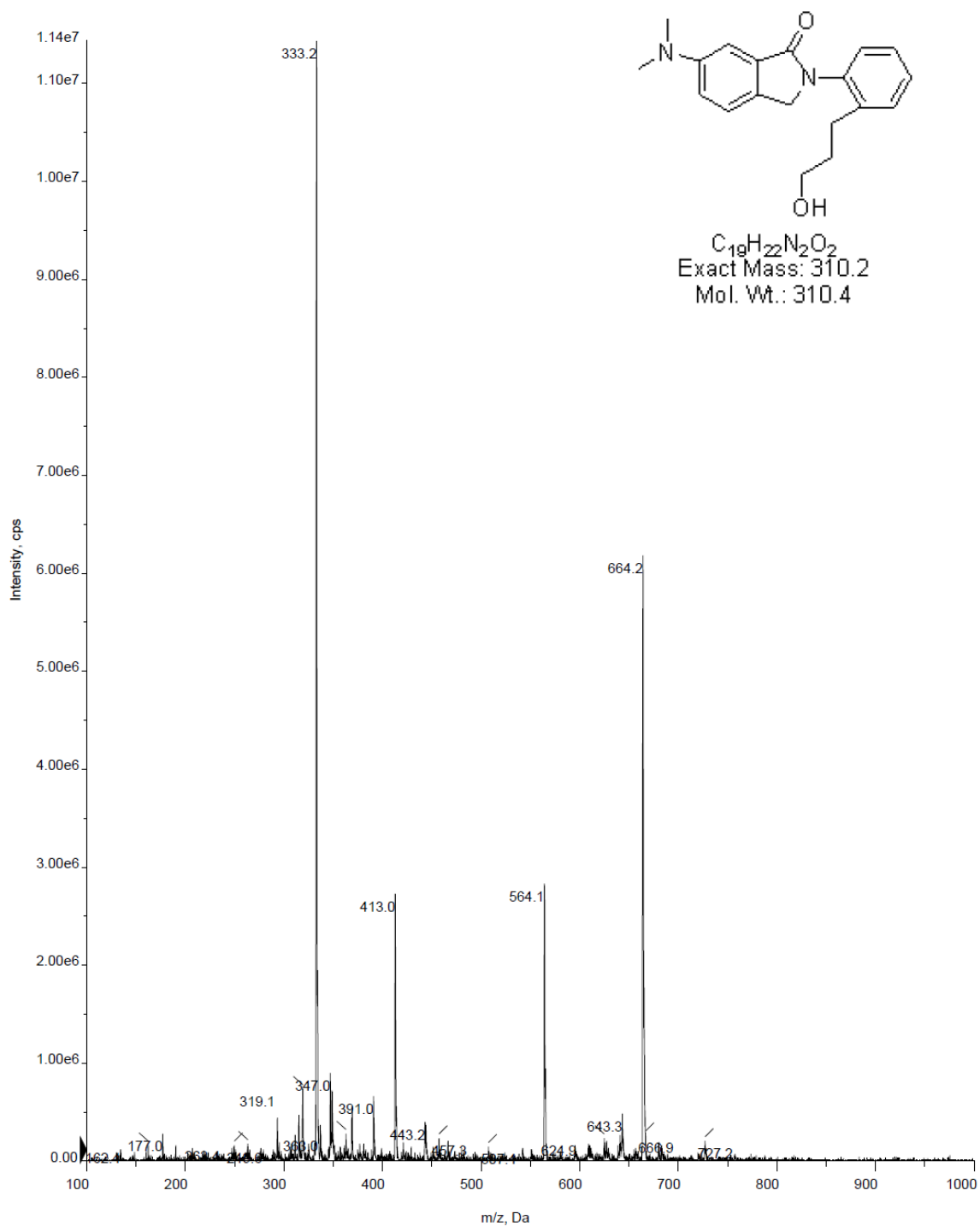


¹³C NMR spectrum (CDCl₃) of compound 10a. The spectrum displays 17 distinct peaks, with chemical shifts (ppm) labeled above each peak: 169.40, 151.17, 140.22, 137.28, 133.19, 129.84, 128.21, 127.08, 123.18, 116.79, 106.92, 77.00 (triplet, CDCl₃ solvent), 61.56, 53.71, 40.99, 32.71, and 26.81.

J:\JAPANESE PROJECT\SPECTRA\JAPANESE PROJECT\COMPOUND11\MG11-024-DP-C13.ESP

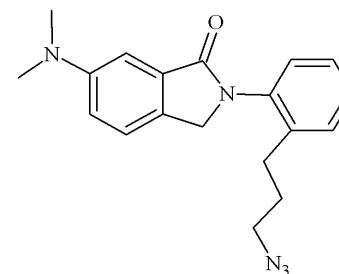
■ +Q1: 11 MCA scans from Sample 1 (TuneSampleID) of MT20170108114842.wiff (Turbo Spray)

Max. 1.1e7 cps.

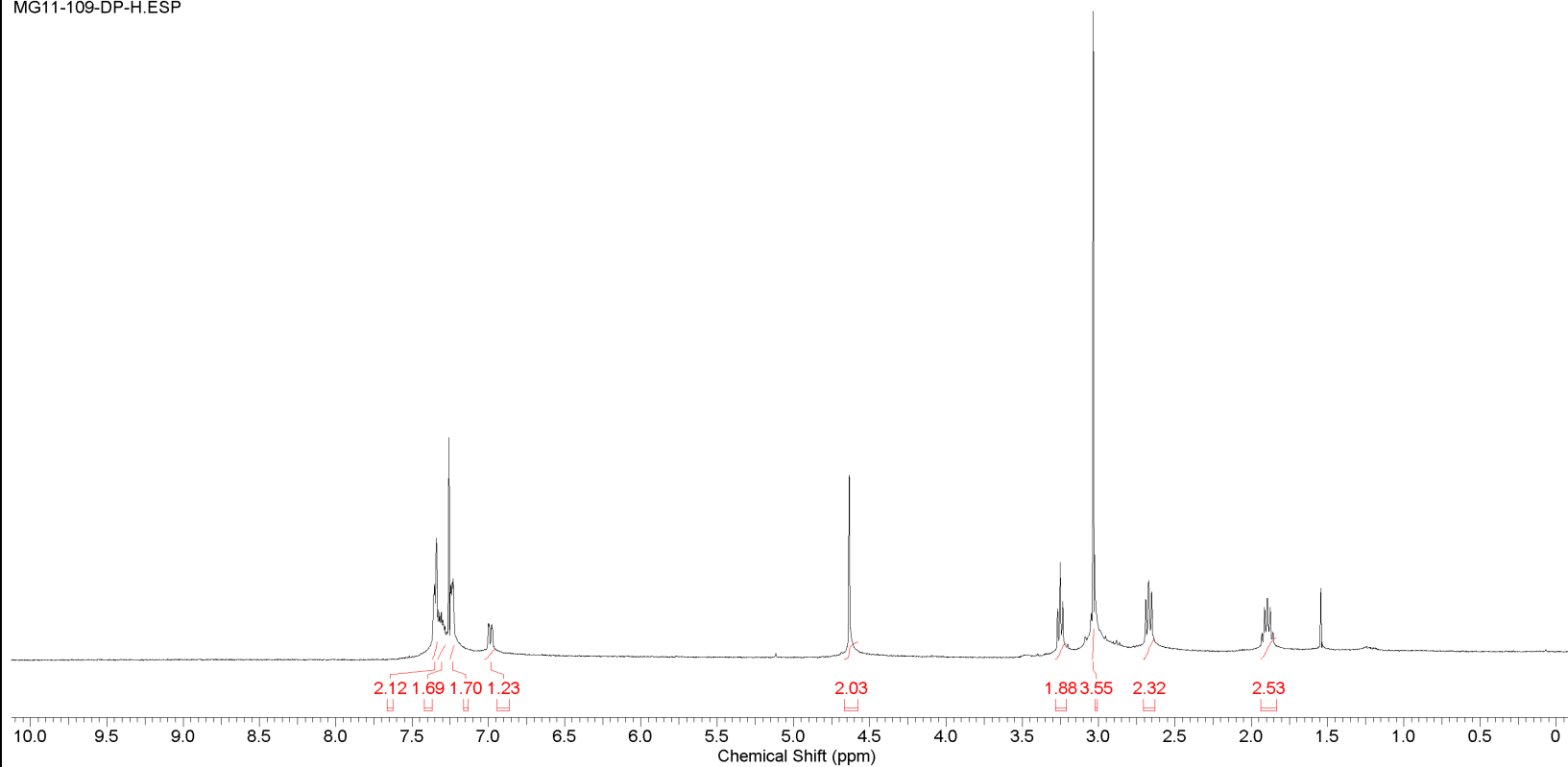


This report was created by ACD/NMR Processor Academic Edition. For more information go to www.acdlabs.com/nmrproc/

Formula C₁₉H₂₁N₅O **FW** 335.4029



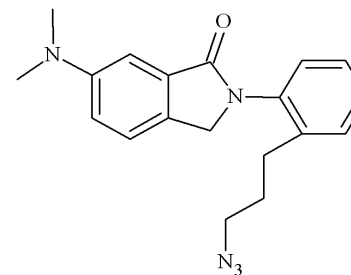
MG11-109-DP-H.ESP



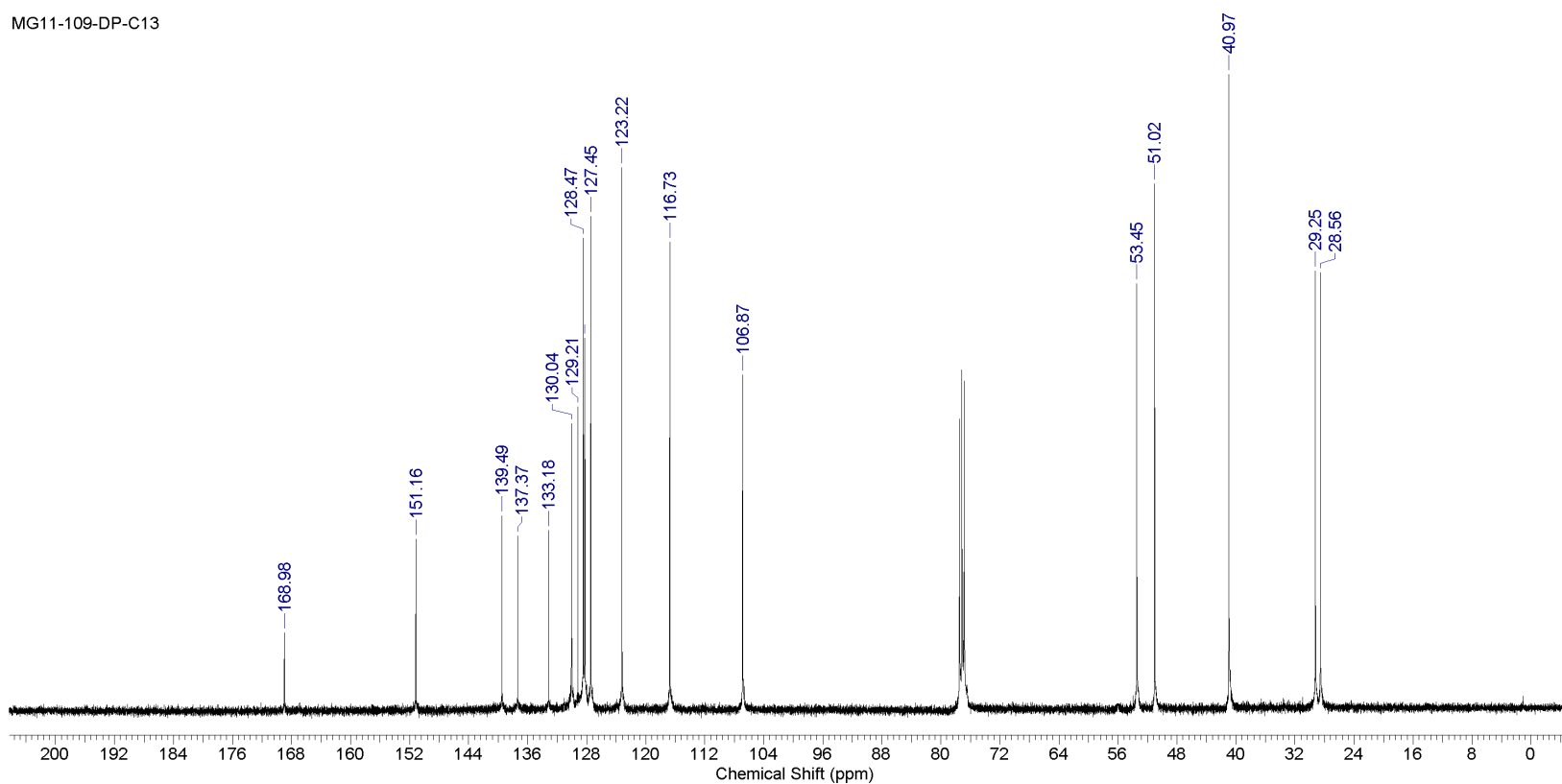
J:\JAPANESE PROJECT\NMR-MASS\JAPANESE PROJECT\MOLECULE B\MG11-109-DP-H.ESP

This report was created by ACD/NMR Processor Academic Edition. For more information go to www.acdlabs.com/nmrproc/

Formula C₁₉H₂₁N₅O FW 335.4029



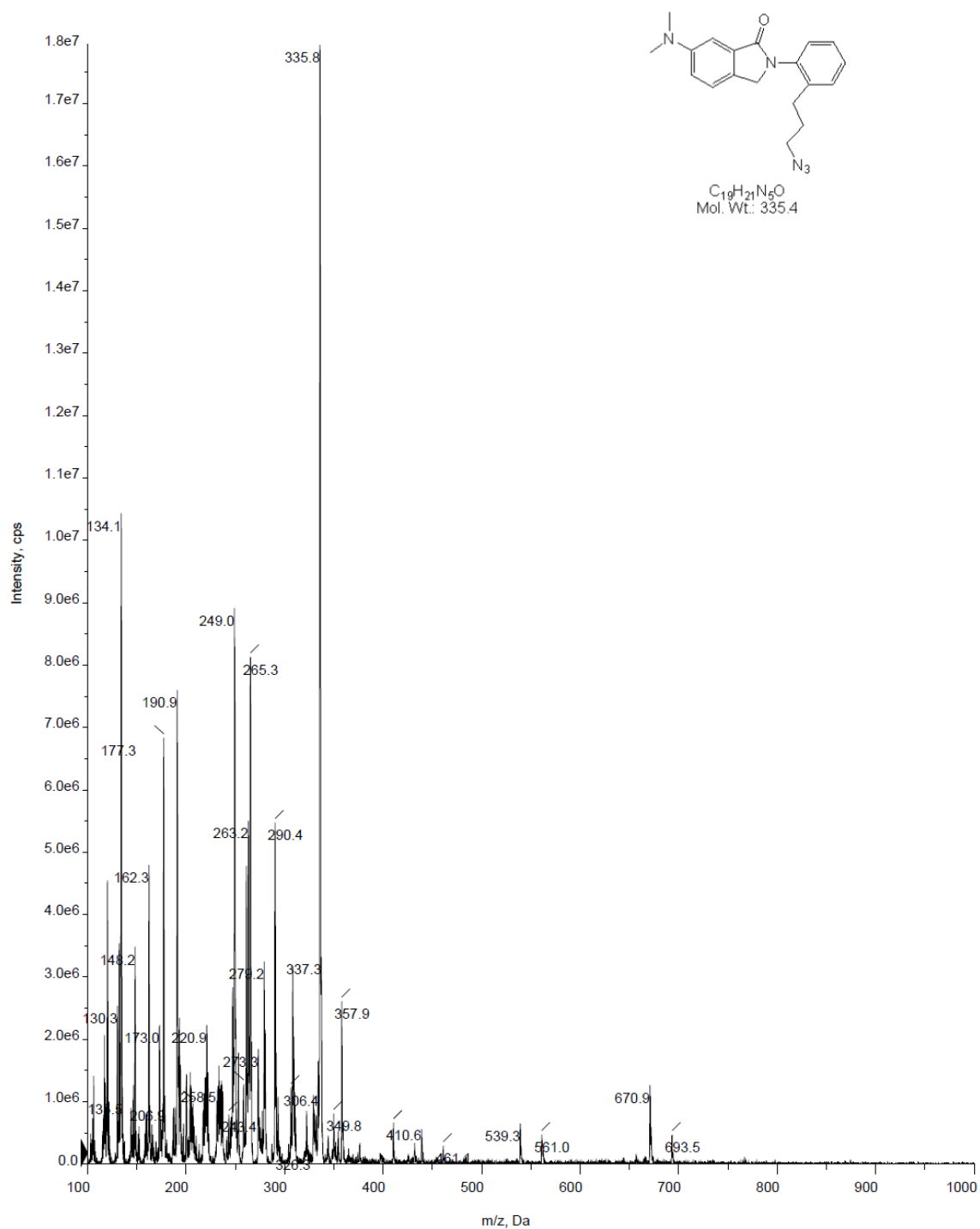
MG11-109-DP-C13



J:\JAPANESE PROJECT\NMR-MASS\JAPANESE PROJECT\MOLECULE B\MG11-109-DP-C13

■ +Q1: 6 MCA scans from Sample 1 (TuneSampleID) of MT20170318162543.wiff (Turbo Spray)

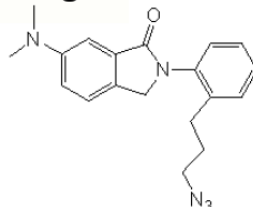
Max. 1.8e7 cps.



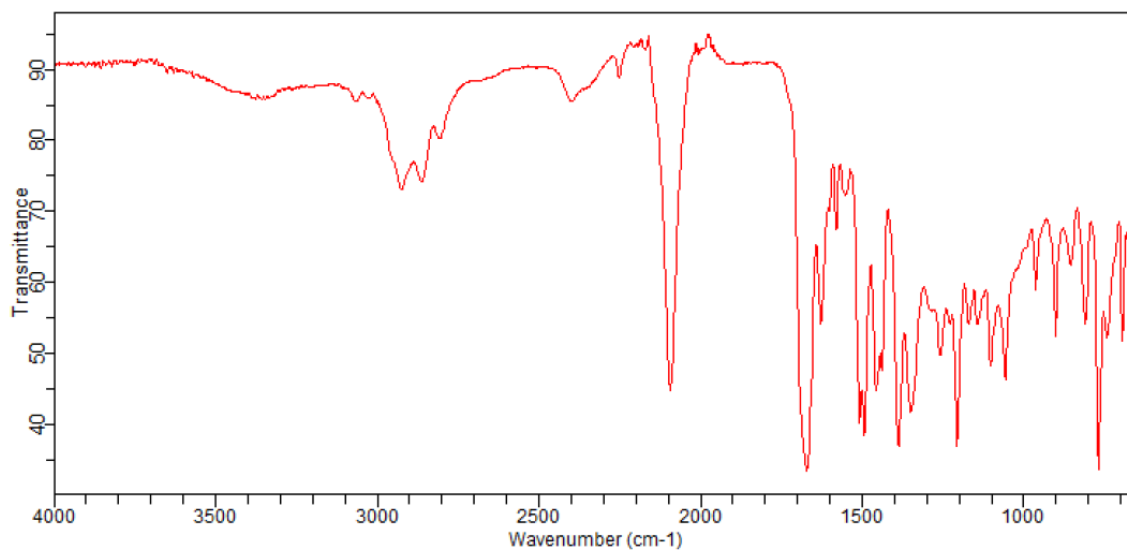


Agilent Technologies

Sample ID: mg11-104-DP
Sample Scans: 64
Background Scans: 64
Resolution: 4 cm⁻¹
System Status: Good
File Location: C:\Program Files\Agilent\MicroLab PC\Results\mg11-104-DP_2017-03-06T16-13-28.a2r

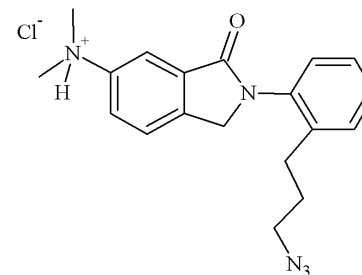


Method Name: ATR
User: Hua
Date/Time: 3/6/2017 4:10:45PM
Range: 4,000.00 - 650.00
Apodization: Happ-Genzel

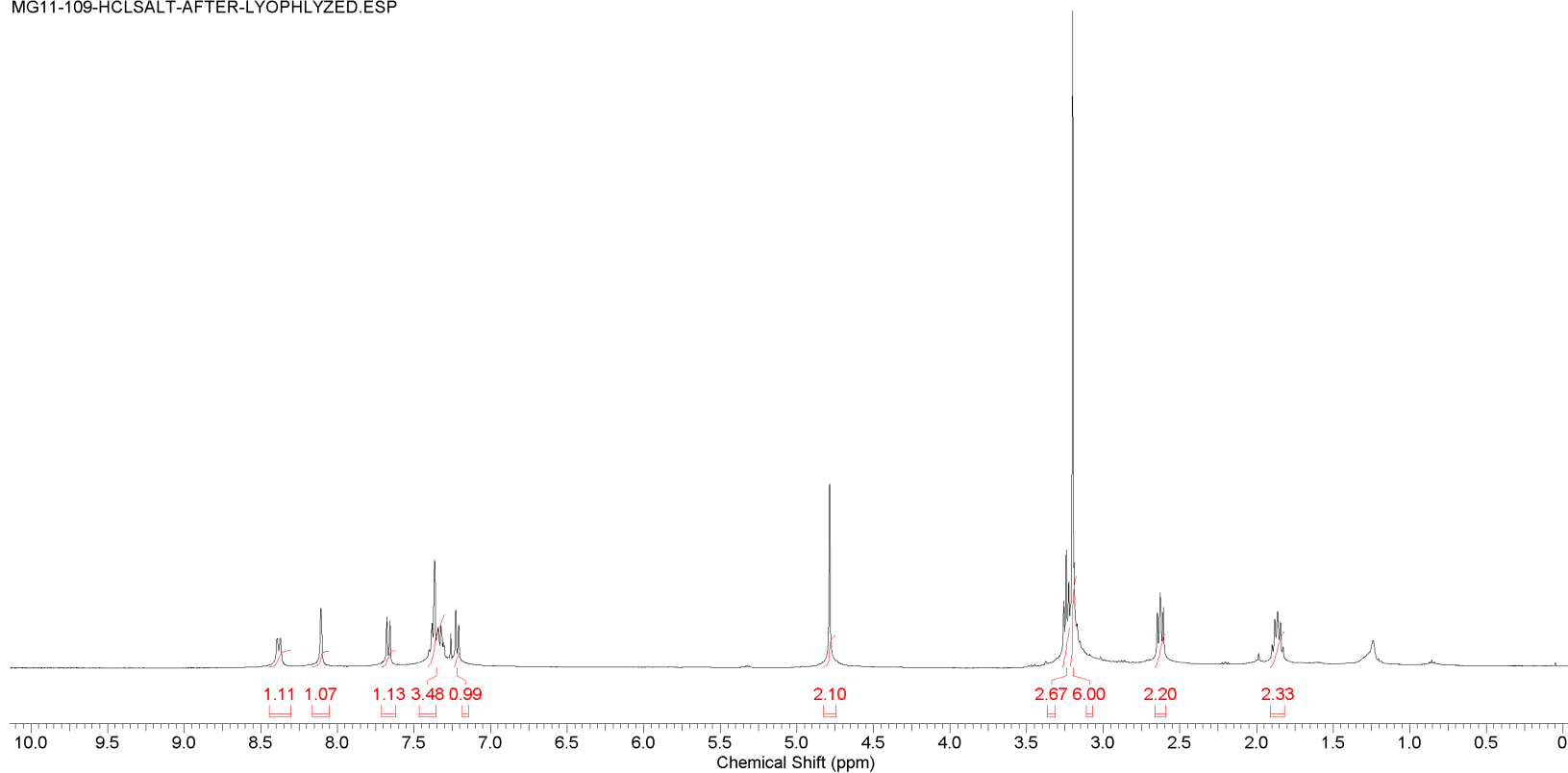


This report was created by ACD/NMR Processor Academic Edition. For more information go to www.acdlabs.com/nmrproc/

Formula C ₁₉ H ₂₂ ClN ₅ O	FW 371.8639 (336.4103+35.4535)
---	---------------------------------------



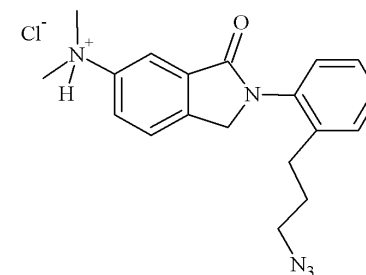
MG11-109-HCLSALT-AFTER-LYOPHYLIZED.ESP



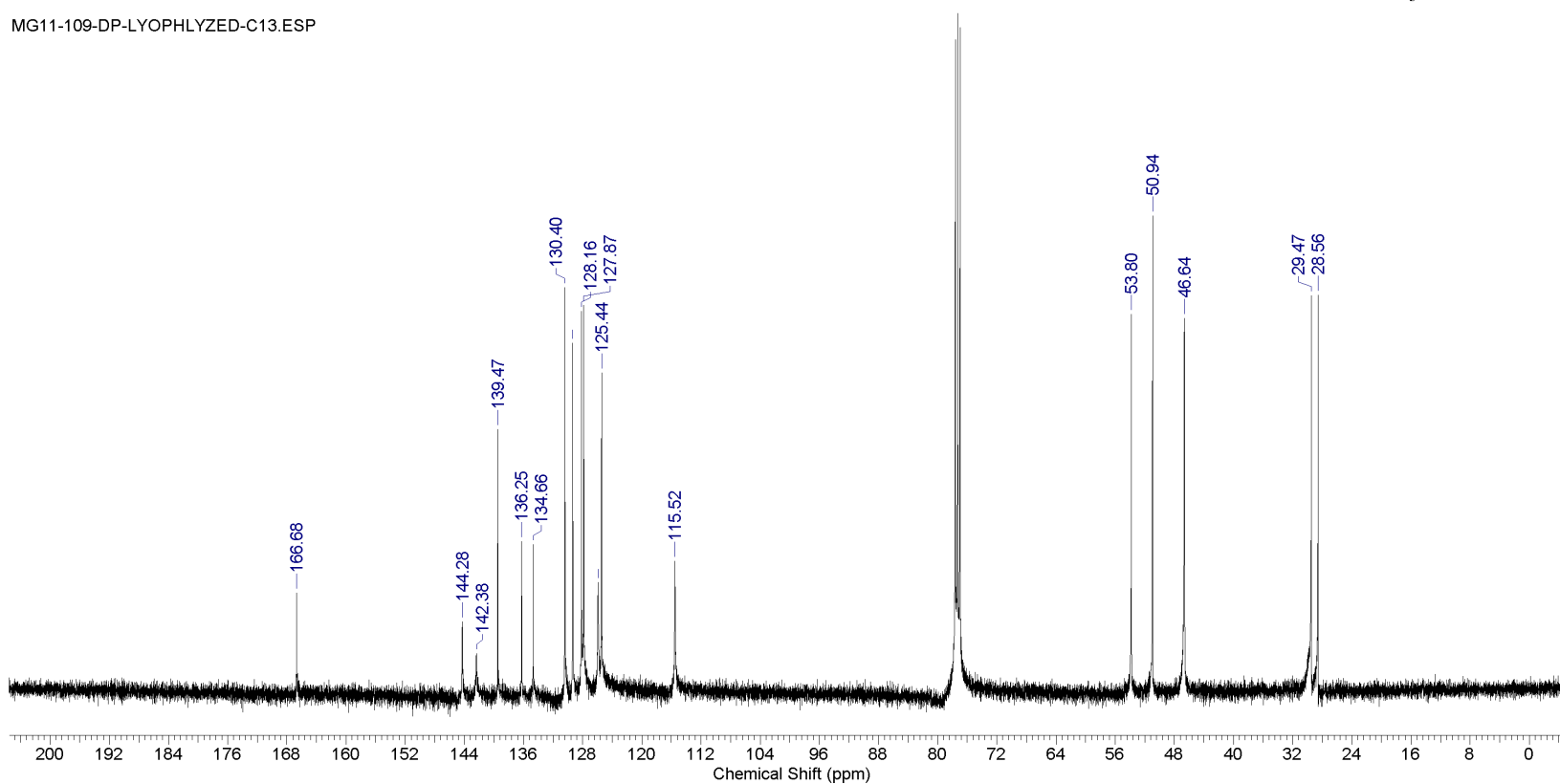
J:\JAPANESE PROJECT\NMR-MASS\JAPANESE PROJECT\MOLECULE B\MG11-109-HCLSALT-AFTER-LYOPHYLIZED.ESP

This report was created by ACD/NMR Processor Academic Edition. For more information go to www.acdlabs.com/nmrproc/

Formula C ₁₉ H ₂₂ ClN ₅ O	FW 371.8639 (336.4103+35.4535)
---	---------------------------------------



MG11-109-DP-LYOPHLYZED-C13.ESP



J:\JAPANESE PROJECT\NMR-MASS\JAPANESE PROJECT\MOLECULE B\MG11-109-DP-LYOPHLYZED-C13.ESP

